UNIVERSITEIT VAN PRETORIA
UNIVERSITY OF PRETORIA
YUNIBESITHI YA PRETORIA

Metals from K2 and Mapungubwe: A technological study of early second millennium material culture, with an emphasis on conservation

by

Farahnaz Koleini

A thesis submitted in partial fulfilment of the requirements for the degree

DPhil Archaeology

in the Department of Anthropology and Archaeology at the

UNIVERSITY OF PRETORIA
FACULTY OF HUMANITIES

SUPERVISOR: Dr Alex Schoeman
CO-SUPERVISOR: Prof Innocent Pikirayi
                       Dr Shadreck Cherikure

February 2013

To my husband

Abstract

This thesis focuses on the conservation of iron and copper objects that mostly belong to the Iron-Age sites of K2 and Mapungubwe (825-1290 AD), the two most prominent archaeological settlements in the middle Limpopo valley area of northern South Africa. For the purpose of conservation three main objectives were considered during this study which consisted of revealing the material and methods of fabrication, evaluating physical and chemical stability, and preservation. The selected objects were in four main categories, namely round wire, strip, plate and implements, and were in various states of preservation, from heavily to low corroded. This thesis consists of seven chapters that are based on these objectives.

Chapter 1, introduction, provides a short introduction to the study, presents the study objectives, a brief history of the investigation of the sites, some archaeological interpretations and a discussion on the metallurgy of the objects made by the inhabitants.

Chapter 2, methodology, contains analytical methods and principles which were used in gathering and management of the data.

Chapters 3 and 4 present a discussion of the methods of manufacture of the selected artefacts as well as their physical stability. In these chapters the iron and copper artefacts were respectively studied by the use of non-destructive methods such as neutron tomography and microscopy. Here, a new quantitative technique in estimating the corrosion percentage by utilizing neutron tomograms and IMAGEJ software was introduced. Some of the objects with ambiguity in their fabrication, such as iron hoes or copper bangles with a central longitudinal void, were sampled destructively for metallography examination and further chemical analyses. In the case of the manufacture of native objects the outcomes confirmed the results of previous researches. Meanwhile new light was shed regarding signs of a new technique used in the production of some type of round wire on Mapungubwe Hill (strip-drawing). In the case of the round wires that were used in the manufacture of the bangles finding the definite method of manufacture was problematic.

In Chapter 5 the chemical stability and the deterioration process of the artefacts were studied with consideration of both the corrosion composition as well as the effects of environmental conditions on their formation. It indicated hydroxyl (OH^-) was the prominent ions in the corrosion of iron although a high amount of soluble chloride ions were detected in the burial environment in K2. In the case of copper artefacts, both chloride and hydroxyl ions were effective in corrosion and the objects were mostly subjected to severe bronze disease.

This information was gathered using analytical techniques such as Raman spectroscopy, XRD and SEM-EDS.

In Chapter 6 the suitable and practical conservation methods were presented. These methods consisted of both interventive and preventive conservation and were designed on the basis of the chemical and physical stability of the objects and environmental condition in the museum and in the storage facility.

In chapter 7 (conclusion) a summary and the results of the study was presented which formed the final part of the thesis.

Table of Contents

CHAPTER 1   INTRODUCTION

CHAPTER 2   METHODOLOGY

CHAPTER 3   PHYSICAL STABILITY AND MANUFACTURING TECHNIQUE OF IRON ARTEFACTS

CHAPTER 4   PHYSICAL STABILITY AND MANUFACTURING TECHNIQUE OF COPPER ARTEFACTS

CHAPTER 5   CHEMICAL STABILITY AND DETERIORATION PROCESS

CHAPTER 6   CLEANING AND PRESERVATION

CHAPTER 7   CONCLUSION

x

List of figures in appendix B

List of figures in Appendix C

xvi

List of tables

xix

Chapter 1

Introduction

1.1. About this thesis

1.1.1. Background to the study

The poor condition of excavated metal artefacts from Mapungubwe and Bambandyanalo (K2) which were mostly in a state of complete disintegration was the main reason behind this study. Both K2 and Mapungubwe belong to a cluster of sites in the middle Limpopo River valley which attest to a significant culture and technological development associated with the middle or later Iron Age in southern Africa (Meyer 1998; Huffman 2007). During this time, gold, lead, brass and bronze appeared in the metallurgy of southern Africa. Significant numbers of metal objects were unearthed during past decades by archaeologists (Fouché 1937; Gardner 1963; Meyer 1998) while few of them were preserved and are displayed in some museums for public viewing.

Due to the paucity of written records from the pre-Portuguese era in regard to the history and culture of the communities that were living in southern Africa, uncovering the manufacturing methods of excavated handicrafts was one of the main objectives of archaeologists in revealing historical information about this period. In fact, the technical study of artefacts led researchers to a greater knowledge about the technological achievements and bilateral trade of these societies with contiguous and non-contiguous areas during this period. This approach led to more intensive research on the manufacture methods of the metallic objects while the lack of research on the causes of deterioration of the artefacts is obvious. This research is essential as the results are helpful in the preservation of the archaeological objects as well as the knowledge about how to prevent further degradation.

The metal artefacts that were found at K2 and Mapungubwe are in varying states of degradation, from low to heavily corroded. Some of them have been completely reduced to a corroded mass of corrosion and have completely lost their form and their physical integrity. The disintegration of each artefact is equal to the loss of significant amounts of information about a culture that is gone forever. Except for the chemical deterioration, sampling in some cases resulted in losing the physical integrity of the objects. This situation fired my enthusiasm to study about the conservation of the artefacts and finding out about the appropriate methods of preserving them from further degradation.

1.1.2. Aims and objectives of the study

This thesis focuses on the conservation of a number of iron and copper objects from Mapungubwe and K2. Conservation was defined by the European Confederation of Conservator-Restorers' Organizations (E.C.C.O.) as a direct action carried out on cultural heritage with the aim of stabilizing condition and retarding further deterioration. This is achieved through the study of material, method of manufacture and process of deterioration which provide essential data to select an appropriate method in either treatment or preservation so as to reduce, minimize or forestall further degradation. These categories are the main objectives of this study which can be numerated as follows:

1

1. Finding material composition and method of manufacture.

2. Evaluation physical and chemical stability of the artefacts and explanation of the process of degradation in the objects.

3. Introducing the suitable methods in preservation of the objects.

Finding the manufacture method refers to uncovering the techniques that were used in the past to form certain particular raw materials such as pure metals or alloys, to produce the objects. Each technique has particular effects on the macro and microstructure of metal. These traces assist in recognizing the historical method of manufacture of the objects. Scientific analyses can clarify some of this evidence. Recognizing these techniques and the material constituents, based on scientific study, would form a primary basis to decide on the appropriate preservation methods while showing the level of technology a society had achieved. Previous studies in this field by Fouché (1937), Stanley (1937), Becker (1979), Oddy (1991) and Miller (2001) revealed that mostly simple techniques were utilized in producing the objects. This background knowledge confined this part of study to those objects that had some ambiguous aspects in their manufacture, origin or function such as the bangles, hoes and funnels respectively.

The estimation of physical stability of the objects is possible by visualizing the internal structure and elucidating the physical defects in them. Assessing physical stability provides essential information about the endurance of metal objects towards different kinds of chemicals or mechanical pressure that may be encountered during treatment. All the objects were examined with neutron tomography in this regard.

Evaluating the chemical stability of the metal artefacts and study of the deterioration process refers to the recognition of the corrosion composition and relevant chemical reactions that result in the loss of material and physical integrity of the objects. Most of archaeological artefacts lost their original physical and mechanical properties during burial. The presence of humidity, oxygen and dissoluble salts in the soil starts the process of corrosion that accompanies the loss of material constituents through the formation of corrosion products. This process continues after excavation until the object either attains natural stability within the environment or is manually preserved from chemical deterioration. Besides the characteristics of the metalwork itself and the burial context, environmental conditions after excavation also have an important effect on the process of corrosion. High oxygen concentration and fluctuation in humidity after excavation increase the rate of corrosion that had been in a state of equilibrium during a long term burial. These processes may gradually degrade the metal artefacts.

 All the corrosion processes are not the same and have different effects on the stability of the artefacts. Some of the corrosion products may produce severe problems for the metal stability and some could remain dormant until specific environmental conditions activate them again. For example, nantokite can remain dormant during burial but with enough oxygen and humidity present after excavation this product could easily be subjected to a cycling corrosion with formation of hydrochloric

acid and copper trihydroxychloride. This corrosion reaction is known as bronze disease (Scott 1990). Corrosion products are not always harmful and a few of these products can noticeably halt the corrosion process such as cuprite in cupreous artefacts (Scott 2002). Consequently, corrosion composition and stratification on the objects as well as knowledge of the processes involved in their formation are important factors in estimating chemical stability and the further stabilization of metal artefacts in a specific environment. In this thesis, to evaluate the chemical stability of the objects, corrosion composition was identified by chemical analysis. Here also the formation process of the identified products was discussed briefly to elucidate the chemical and environmental factors that were part of their formation.

For better interpretation of corrosion products, their stratification and their mechanism of formation the objects' burial environment was also studied. Through this study the severe corrosion in the majority of the artefacts might be explained logically. To achieve this goal, soil samples from K2 were studied although some restrictions lessened the accuracy of the results. These restrictions mostly arose due to the long exposure after excavation, which affected soil properties such as electrical conductivity and pH.

On the basis of information gained through part of this study, it is also possible to retrace the history of the metal artefacts, from the time of discarding in the soil until the present time. Corrosion, composition and stratification as well as environmental conditions during burial and after excavation, is the basic information that can assist in revealing the history of the archaeological metals after deposition. Composition of the corrosion crust depends on the chemical characteristics of a substance (metal) and the burial environment, while the stability of corrosion products and their stratification are only subjected to environmental conditions. Each corrosion product has a specific range of stability in the environment as can be seen in Eh-pH diagrams. Consequently the existence of one product gives useful information about the environmental conditions the object was placed in.

Treatment and preservation mainly focused on revealing the original form of the object at some point in the past as well as halting the corrosion process through the utilization of passive and/or non-passive techniques. Conservation of corroded metals usually involves the removal of harmful corrosion products to reveal the original surface (cleaning) while keeping the patina intact as a sign of their age and for aesthetic reasons. In heavily corroded objects it is difficult to find an undamaged surface which shows the details of the original form of the object. In archaeological metals the original surface is mostly deformed and, if it is retained, its pseudomorphic structure would be under different layers of corrosion and soil contaminants. In this part of study appropriate cleaning methods based on the chemical and structural characteristics of the corrosion are recommended. These characteristics also were used as the main guide towards providing applicable methods for halting the corrosion. Halting or reducing the rate of corrosion is possible by removing the harmful corrosion or converting them to the stable and harmless ones with the use of the appropriate chemicals. To carry out preventive conservation, before and after treatment, a knowledge of the range of stability of the corrosion products and monitoring of the environment are essential. In this part of the study

temperature and relative humidity (RH) of the environment as the main factors in increasing the rate of corrosion of the metals was monitored at storage facilities and showcases in the museum. These data, put together, elucidated the undesirable environmental conditions in the museum and the storage facility in which the metal artefacts are kept.

1.1.3. Chapter summary

This thesis was submitted in 7 chapters as follows:

Chapter 1 is an introduction to the thesis and presents the study objectives, a brief history of the investigation of the sites, some archaeological interpretations and a discussion on the metallurgy of the objects made by the inhabitants. In this chapter the corrosion phenomenon was also briefly explained .

Chapter 2, methodology, provides the principles which give a discipline to this study such as conservation ethics and the factors that had effects on selection of the objects of the study. Scientific instruments and analytical methods that were used in the identification of the metal and corrosion compositions were introduced in this chapter.

Chapters 3 and 4, physical stability and manufacturing technique, present the study of metal compositions, fabrication methods and traces of usage on the iron and copper objects respectively. In this section, the physical stability of the metal objects was also estimated.

Chapter 5, chemical stability and deterioration process, provides the study of corrosion composition and stratification on the iron and copper artefacts. In this chapter, the corrosion processes involved in the disintegration of the metals are explained.

Chapter 6, preservation, presents the appropriate methods of cleaning and treatment of the objects. In this section, both the passive and non-passive techniques for reducing the rate of corrosion by means of chemicals and controlling the environment are provided.

Chapter 7, conclusion, presents the outcomes of the research. Some limitations, which prevent to achieve to desired results were mentioned in this section.

1.2. Archaeological background

1.2.1. K2 and Mapungubwe

K2 (Bambandyanalo) and Mapungubwe are Iron-Age sites situated in the middle Limpopo valley area of northern South Africa, just south of the confluence of the Limpopo and Shashe rivers (Fig.1.1). K2 is situated some kilometres away to the south-west of Mapungubwe Hill (Fig.1.1) (Meyer 1998). On the basis of calibrated radiocarbon dates by Vogel (1998) this site was inhabited approximately between 825-1220 AD that shows it predated the main occupation on and around Mapungubwe Hill (1220-1290 AD) settlement. Mapungubwe is a steep-sided, flat-topped sandstone hill, which was substantially occupied soon after K2. In the southwest of the Hill is a related settlement, the Southern Terrace, which was occupied during the middle of 11th century and coincides

with the last phase of the settlement at K2 (Huffman 1986, 1996, 2007; Pikirayi 2001). On the basis of archaeological data, it appears that the ordinary people lived on the Southern Terrace and on a low plateau to the north while the elite or high-ranking community members occupied the hilltop area (Meyer 1998; Huffman 2000; Smith 2005).
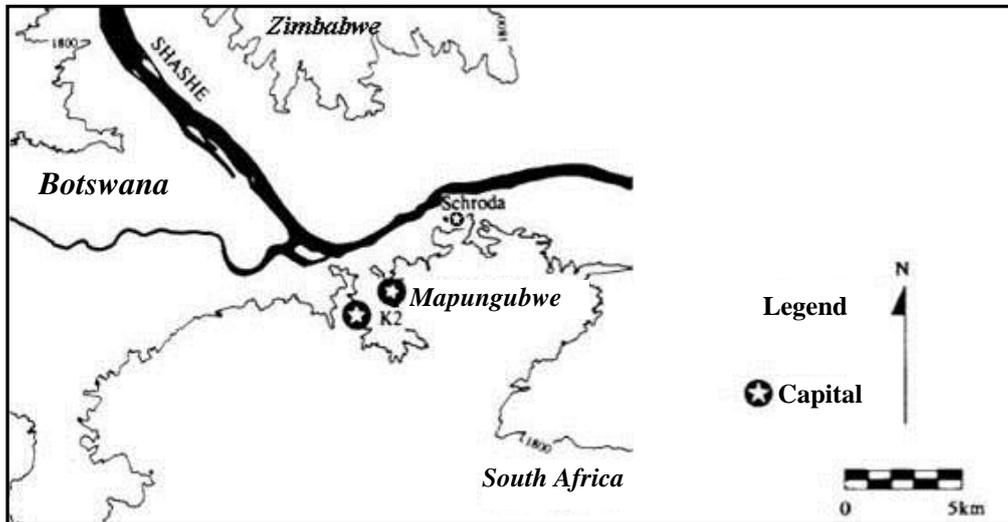
Figure 1.1. Locations of K2 and Mapungubwe, near the Shashe and Limpopo confluence. *Adapted from Huffman (2000).*

1.2.1.1. Phases of settlement at Mapungubwe

According to available radiocarbon dates (Huffman 2000, 2007), Mapungubwe was occupied for just under a century. Systematic excavations by Meyer (1998) have identified four phases of occupation, some of which predating the main occupation of the Hill. Phase One that delivered only a small number of early Iron Age potsherds, Happy Rest ceramics, that is assumed to be evidence of a small settlement preceding the main occupation of K2, and Mapungubwe (Meyer 1998). Phase Two of the settlement is dated between 1030 AD and 1220 AD, which includes the bottom layers on the Southern Terrace and Mapungubwe Hill (Meyer 1998). This phase consists of the remnants of the burnt old village, which had existed during the heyday of K2 (Smith 2005; Huffman 2007). Phase Three of the settlement lasted from 1220 AD to about 1250 AD (Meyer 1998). It is the remnant of the new settlement, which succeeded K2 (Smith 2005; Huffman 2007). Settlement Phase Four on Mapungubwe is dated to the period between 1250 AD and 1290 AD (Meyer 1998). The gold-bearing burials on Mapungubwe Hill may have been associated with this phase (Vogel 1998; Miller 2001). The first appearance of metalwork was reported from phase two (Eloff 1979; Miller 2001) and subsequent phases. The gold artefacts were discovered from phase three onwards (Miller 2001).

5

1.2.1.2. Social life at K2 and Mapungubwe

Research by Huffman (1986, 2000, 2007) shows the transition from K2 to Mapungubwe represented a significant stage in the development of socio-political complexity in southern Africa. Mapungubwe became the first capital of a state society that was established in much of the middle Limpopo valley and adjoining areas of what are now Zimbabwe, Botswana and northern South Africa. Continuity of K2 ceramic style in this area shows that the occupants of Mapungubwe, who are identified by a ceramic tradition called Leopard Kopje had the same culture as the inhabitants of K2. The only difference was the spatial shift from K2 to a new location, the Mapungubwe Hill (Huffman 2000). In fact the shift of people from K2 to Mapungubwe was an *in situ* social and political change from a chiefdom capital to a state capital (Huffman 1986, 2000; Smith 2005) as a result of increasing wealth and political power that was gained mostly due to trading with overseas merchants. Segregation of the elite from the rest of the society and settlement to a more secluded hilltop location was the outcome of this process, which, according to Huffman (2000, 2007) is defined as the Zimbabwe Culture Pattern. This marks the origins of sacred leadership and class distinction in southern Africa (Huffman 1986). In this pattern sacred seclusion and prestige of the elite were emphasized by stone walling which was constructed around their elaborate settlement on the slope of the Hill and on the summit (Huffman 2000). Before this date Leopard Kopje people organized their settlements according to the principals of the central cattle pattern (Huffman 2000). Thus development around K2 and Mapungubwe represent a significant transformation in the settlement pattern as the result of changes in the ideology of the site occupants.

K2 and Mapungubwe societies depended on farming and herding as well as participating in trading and economic activities with societies in the region as well as overseas merchants (Mitchell 2002). The presence of rare Chinese pottery, cowries and other Indian seashells, and numerous glass beads is evidence of their connections (Miller 2001, 2002; Mitchell 2002) with the East African-based Swahili traders (Axleson 1973; Voigt 1983; Miller, Desai & Lee-Throp 2000 ; Smith 2005). Before the rise of K2 and Mpungubwe, trading was also practiced among the farming societies of the Gokomere Tradition, represented in the middle Limpopo valley by Zhizo phase pottery between 900 and 1010 AD but only in the K2 and Mapungubwe phase did trading come under the centralized control of the elite and this control was intensified more in the latter (Huffman 1972, 2000). Pikirayi (2001) suggested trading or transforming raw material to a real wealth needed special ability that only belonged to the elites. He argued that gold and ivory which were the main trading items in the Shashe-Limpopo basin (Freeman-Grenville 1975) and made a great impact on the economy and foreign market did not have immediate subsistence value. These items had to be gathered, worked and finally traded which was only possible through the supervision of a capable person. The skill of controlling this process brought wealth to the owner while distinguishing him from the common people.

Trading was a natural response to probable agricultural failure caused by drought that occurred from time to time in this area. In fact, the farming communities for their livelihood in drought periods needed to produce surpluses and exchange them for their other needs through an interior (sub-continental trade network) or transoceanic (Indian Ocean) trade (Beach 1977; Maggs 1982; Swan 2007). Exploitation of Metals was one of the industries that had a significant role in production of surplus to exchange for the people necessities. Metals were beneficial products, which were used for both interior and exterior trade (Swan 2007). Gold, copper and iron were predominant metals for trade. Among them, gold had a very important role in the external trade and the economy of the region (southern Africa). Iron never had a prominent role in long-distance trade but it had a good regional market (Pikirayi 2001).

The most important factors contributing towards the rise of Mapungubwe as an urban and regional centre of political power were control over agricultural resources, coordination of networks of trade and contact, and efficient management of wealth such as gold production and its trade with societies in eastern Africa (Pikirayi 1993; Miller 1995). Two hypotheses have been proposed for the abandonment of the settlement. The first one claims that climatic changes could be the reason for the decline or demise of Mapungubwe near 1290 AD. The shift to a cooler, drier climate in the late 1200s might have been one of them (Huffman 1996; Mitchel 2002; Smith 2005). These changes could have had a direct influence on agricultural crops. Some other environmental changes could have been caused by human activities and have also been suggested as a reason for the decline of major settlements such as Mapungubwe. Pikirayi (2001:37) noted '*Some centers of state power were over populated, overgrazed, and farmed to the point of lowered productivity, elsewhere, woodlands were reduced to Savanna grassland and some places were extensively mined'*. These activities could cause loss of the natural resources that were significant for the survival of the occupants in these areas. The second hypothesis which was argued by Voigt (1983), Huffman (1996) and Smith (2005) refers to a change of the trade routes towards the north and areas that were closer to the east African coast. They argued that the exterior trade depended on the east African coast and the people to the north, who were closer to the coast, excluded Mapungubwe from the trade network. There was also the possibility that Swahili traders themselves preferred to ignore Mapungubwe and started exchanging commercial items with a closer site. The result was Mapungubwe's demise and the trade moved to Great Zimbabwe (Huffman 1996).

1.2.1.3. *Rituals in smelting and symbolic roles of metal*

Metalworking needed special skills and particular kin ties, which were monopolised by particular groups (Cline 1937; Herbert 1984; Childs& Killick 1993). This activity was closely linked to ritual. During the second Millennium AD, iron and sometimes copper smelting in southern Africa carried metaphors of impregnation, gestation, and parturition, requiring various forms of seclusion and the

observance of extensive rituals (Herbert 1993, 1996; Miller 2002). In this process, male metalworkers would bring the metal into the world by allocating the reproductive power of women to the furnace (Childs & Killick 1993). During smelting a male metalworker had to be fully available and faithful to his furnace. Based on these metaphors, smelting took place outside the confines of the village where no female, except post-menopause women, could be present (Herbert 1984). That is why scholars argue that both iron and copper smelting were not practiced at Mapungubwe and the adjacent Southern Terrace (Miller 2001). For a successful smelting and production of valuable metal the metalworker must satisfy the ancestral spirit by enforcing a sexual taboo and some kind of sorcery. For instance, the metalworker prepared medicine or a charm from different ingredients and put it in or around the furnace or even the mine and the forge. In this way he prevented spells to be cast by envious people or placated the ancestors. (Tessman 1913; Van der Merwe & Avery 1987; Killick 1990; Childs & Killick 1993.)

In addition to smelting, some stages of metalworking like mining and smithing required special precautions and rituals in sub-Saharan Africa (Cline 1937; Childs & Killick 1993). The ritual attributed to the process of smithing was somehow different from smelting. These activities, unlike smelting, were more public (de Maret 1980, 1985; Childs & Killick 1993) which could be carried out in residential areas. Scientific studies by Miller (2001) on residuals of metal working activities confirmed this arguement and indicated that both copper and iron smithing were practiced at K2 and Mapungubwe.

Three characteristics of metals were noted by Herbert (1984) that made them receptive to acquiring a symbolic role in the social life of sub-Saharan people. The first one refers to the scarcity of some metals such as copper and gold as the main reason for making them valuable and expensive. Therefore, copper and gold could be an indicator or symbol of wealth and the high status of the owner. The second one refers to the physical characteristics of metals such as colour, luminosity, malleability and storability which not only has an influence on their function but can also assign a symbolic role to them. The third one ascribes to unexplained transformation from ore to metal which was a metaphor of gestation and parturition that were symbols of fertility and productivity. (Childs& Killick 1993.)

1.2.1.4. Metal technology at K2 and Mapungubwe

1.2.1.4.1. Smelting

The development of metallurgy in the Shashe-Limpopo region, a part of sub-Saharan Africa, is different to that of Mediterranean North Africa, the Nile Valley, and the Red Sea coast in terms of its chronology, technology and mechanisms of indigenous metal production (Van der Merwe 1980; Miller & Van der Merwe 1994). While the advent of metallurgy in the Nile Valley occurred about 5000 - 4000 B.C with the use of copper (Tylecote 1976; Miller & Van der Merwe 1994), in sub-Saharan Africa the appearance of copper and iron seems to have been simultaneous and there are no

signs of prior copper metallurgy or a former Bronze Age period in this region (Tylecote 1976; Van der Merwe 1980; Miller & Van der Merwe 1994). The technology of copper and iron smelting introduced in southern Africa possibly via separate eastern and western routes in the first millennium AD (Denbow 1990) and by 500 AD the production of iron was widespread (Miller & Van der Merwe 1994). During the first millennium AD iron and copper were in use (Miller 1995; Miller 2002). Present archaeological evidence shows that, only after 1100 AD, gold and bronze were utilized in metalworking in southern Africa (Killick 2009).

The excavated objects in K2 (825-1220 AD) show that the inhabitants were not familiar with gold, tin and bronze (an alloy of tin and copper) or had no enthusiasm in utilizing them in production of ornaments. This lack of interest could be due to a strong cultural preference for the redness of copper over the yellow of gold and bronze throughout sub-Saharan Africa before the Islamic era (Herbert 1984; Killick 2009). Mapungubwe, a post K2 settlement, was one of the first sites from where the appearance of gold and bronze was reported (Miller 2001).

The advent of tin exploitation and possible bronze production in southern Africa are very poorly understood (Miller 1995). The earliest bronze finds belong to the thirteen century AD (Miller 2002) while the earliest well-provenanced tin ingot, which was found at Great Zimbabwe, dated between 1450 and 1550 cal CE (Chirikure *et al.* 2010). The only known pre-colonial tin mine in eastern and southern Africa is Rooiberg (Recknagel 1908; Killick 2009). The tin production at the Rooiberg mine has been dated to 1436-1650 cal AD and 1426-1633 cal AD on the basis of radiocarbon dating on charcoal embedded in a tin ingot and on a wooden pit prop from a prehistoric mine respectively (Hall 1981; Grant 1990; Chirikure *et al*. 2007; Killick 2009). These dates are quite later than the thriving period of Mapungubwe where some of the earliest bronze objects were found there (1220-1290). On the other hand, the recent study of Molofsky (2009) on the lead isotope ratio in one of the Mapungubwe bronze objects, in addition to some other objects from Zimbabwe and Bosutswe, indicated the source of tin in these objects to be from Rooiberg. On the basis of isotopic evidence, Killick (2009) pushed back the tin exploitation and the bronze production in Rooiberg to around the thirteenth century AD. He also believes that traders from the Indian Ocean had a great impact on the advent of gold and tin metallurgy in southern Africa. Regarding this he noted '*…the first use of tin and bronze, like the first use of gold, was prompted by the recognition of the mineral deposits by traders coming inland from the Indian Ocean'* (Killick 2009:411). Before isotopic study of the bronze object from Mapungubwe, the uniformity in the composition of the bronze artefacts was considered as a reason for a probable exotic origin of them (Miller 2001).

The earliest appearance of brass (an alloy of copper and zinc) was also reported in the local archaeological record of Mapungubwe (Miller 2002). This assemblage consisted of a single irregular casting spill with a composition of 66% copper, 25% lead, 6% zinc and 3% tin by weight. Since there is no evidence of indigenous zinc and lead production in southern Africa it is supposed that the brass was an imported item via the east coast trade but cast and worked at the site (Miller 2001, 2002).

9

The study of archaeological slags that were found on K2, Mapungubwe Hill and the Southern Terrace by Miller (2001) indicated that iron and copper smelting were not practiced there. Lack of large quantities of associated smelting slags and/or their small size were suggested as the main reasons. In the case of copper, the unearthed slag nodules mostly adhered to copper prills that were primary raw materials of smithing. In the case of iron, although numerous slags were found on K2, their small size indicated that they belong to a smiting process rather than smelting. Contrary to K2, very few iron slags were found on Mapungubwe and the Southern Terrace. Iron and copper used for smithing might have come from the adjacent areas but their exact origins were not identified (Miller 2001). Miller (2002) also refers to another form of copper smelting which might have been practiced at Mapungubwe. In this method, possibly more pure malachite ore was smelted directly in ceramic crucibles. Malachite stains on the slagged crucible that were recovered from the dumps by Calabrese (2000) led to his conclusion. Numerous slagged crucibles that have been recovered from the dumps by Calabrese (2000) have malachite stains or prills of copper embedded in the glassy slag (Miller 2001). Miller (2002) also suggested that these crucibles were probably used for the resmelting of smelted copper for secondary casting.

In southern Africa, as in the other parts of sub-Saharan Africa, a wide variety of minerals were mined or collected for use as iron ore (Miller & Van der Merwe 1994; Miller 1995). The chemical diversity of iron ores resulted in various bloomery processes in different types of furnaces (Miller 1995). These minerals include ferruginous laterites, goethite, and magnetite (Van der Merwe & Killick 1979; Miller 1995). These iron ores which were mostly exploited by indigenous miners contained high levels of impurities. These ores could be processed at relatively low temperatures, and enabled early smelters to produce bloomery iron of high purity with a carbon content ranging up to those of medium steel (Miller 1995). Although during this kind of smelting nodules of cast iron could be produced (David *et al.* 1989; Miller 2002), no intentional production of cast iron was reported in southern Africa (Miller 2002). This bloomery iron also contained unburned charcoal fuel, unreacted nodules of ore, and bits of furnace lining and small pieces of slag (Miller 1997, 2002).

The minerals that were used as sources in the extraction of copper by indigenous smelters mostly consist of hydrated carbonate ore like malachite and azurite (Miller & Van der Merwe 1994; Miller 1995). The main copper mines in South Africa were Messina (De Vaal 1952; Hanisch 1974; Wilson 1989; Miller 1995) and Phalaborwa (More 1974; Schwellnus 1937; Van der Merwe & Scully 1971; Verwoerd 1956; Miller 1995), although small indigenous copper mines were also reported in numerous locations in the Transvaal (Evers & Van den Berg 1974; Friede 1980; Mason 1974, 1982; Steel 1974, 1980; Miller 1995). The miner could also exploit weathered superficial ores. This means that copper ore was more widely available than would appear from present location of copper mines (Miller 2002).

There is not a lot of information about copper smelting in southern Africa (Miller 1995; Swan 2007). In this process, like iron smelting, different kinds of furnaces were employed (Miller 2000). In

some instances the smelters roasted the surficial oxidized ores to remove the water before smelting. In this process fragments of sulphide trapped in the ore could be incidentally oxidized although the systematic roasting of sulphide ores for extraction of copper was not practiced before colonial times (Herbert 1984; Miller & Van der Merwe 1994). Herbert (1984) argued that sufficient amounts of surficial carbonate ores made them an easy access source for local usage while deeply seated sulphides made it un-minable. In the process of copper smelting, iron oxide was occasionally used as flux (Miller & Van der Merwe 1994) but the possible addition of other fluxes such as lime in the form of shells or calcrete is debatable (Herbert 1984). The origin of some percentages of iron in slag inclusions within the copper artefacts could be the added flux during smelting (Miller 2002) or the presence of iron oxides in the ore (self fluxing ores) such as the copper deposits from Phalaborwa mine which contain magnetite (Dawson & Hinton 2003). Miller (2002) also refers to the presence of sulphide inclusions in cuprous objects and concluded that it must have originated from small amounts of unweathered sulphide that generally exists within carbonate ores as impurities. Copper smelting produced either nodular copper prills that were embedded in slag or dish ingot that was solidified at the bottom of the furnace.

1.2.1.4.2. *Fabrication methods of iron objects*

Locally manufactured iron arrowheads, both barbed and unbarbed, spear blades, hoes, adze, chisels, solid rings and coiled wire are found in K2 and Mapunbugwe assemblage (Meyer 1998; Miller 2001). Metallographic analyses of available iron artefacts by Miller (2001) show that fabrication methods of iron during this period were similar to the first millennium metalworking experience in southern Africa and only had a small progress. The blooms that were used to produce artefacts had materially no distinguishable difference in Early and Late Iron Age and were inhomogeneous in carbon content. This variation has been directly transferred to the objects. The carbon content of iron was varied in a range from 0.1% to 0.8 wt% that can even be seen in one object. There was no sign of systematic selection of iron with a different carbon content to produce special characteristics in an artefact by welding.

Miller & Van der Merwe (1994) argued that hot forging of bloomery iron such as elsewhere in sub-Saharan Africa was the main fabrication method in southern Africa. In this process the raw metal, bloomery iron, was heated above 900ºC in an open hearth in oxidizing condition to reduce the carbon content of inhomogeneous bloom and forged to expel the slag (Miller & Van der Merwe 1994; Miller 2002). Along with the cycling process of hot-working, the bloomery iron was converted to a condensed shape and subsequently to the desire tool or jewellery with low carbon content. The objects were mostly left in a full annealed or partially cold working condition. During this process the remaining slags within the bloom were elongated (Miller 2002) in parallel with the worked surfaces. A little evidence of cold working in iron implements from K2 and Mapungubwe was reported which can

be due to an act of corrosion (Miller 2001). This evidence is in the form of grain distortion and is mostly observable near the surfaces of the metal which can be easily lost by corrosion during burial or after excavation.

Helically wound wire was also fabricated in the same way as it was done in other parts of southern Africa. For making this wire, which was used for the fabrication of bangles, necklaces and rings, a hammered iron sheet was cut by a sharp tool into strips and wound around a fibrous core (Miller, 2002). No sign of iron wire drawing was reported by Miller (2001). Miller (2002) suggested that corrosion of round delicate drawn wires could be the reason. Hot welding for enhancing the physical property of the objects was also not reported by Miller (2001).

An increase in volume of iron production is the only difference between iron technology in this period and the first millennium AD although the presence of many large iron artefacts was not reported from K2 and Mapungubwe (Miller 2001). Recycling of large iron objects, because of their intrinsic value to produce smaller items, and their disintegration due to intensive corrosion during interment, were suggested as two possible reasons for their low numbers by Miller (2002). Since the chance of survival of larger iron objects in the same environment is higher than smaller ones, the first reason seems to be more correct.

1.2.1.4.3. *Fabrication methods of copper objects*

Globules, rods and strips helically wound wire, rings and bangles were the main cuprous artefacts that were recovered from K2 and Mapungubwe (Meyer 1998). The microstructural study of copper artefacts by Miller (2002) shows that they were manufactured according to the same methods as the iron objects. The metal was hot and cold worked and often left in the fully annealed state. Helically wound strips that were used to produce jewellery, were fabricated in the same way as those that were made of iron. A sheet of thin copper was cut into strips, annealed and wound around flexible fibre. Soldering and welding were not used for joining. Casting molten metal was limited to the production of small copper bars that were sometimes fashioned to make a bangle (Miller 2001). For casting, prills of copper or pieces of metal that were cut off from a dish ingot, melted in a ceramic crucible in the forging hearth and poured into a one-piece mould (Miller 2002). No evidence for copper wire drawing was reported by Miller (2001). As the metallurgical evidence showed, the only development in manufacturing of copper artefacts, compared with the first millennium AD, is confined to the casting.

The bronze artefacts consisted of a curved bar, shaped like a bucket handle, that was found at the Southern Terrace and a few helically wound bangle fragments (Miller 2002). These are all 6% tin in copper and have a gold colour in polished form (Miller 2002). The fragments of wound strips, found at elite burials, shows that bronze might have had the same symbolic role as gold. All of these bronze artefacts underwent final annealing after considerable hot and cold working and contain inclusions that probably were copper sulphide (Miller 2001). A single length of fine brass wire has also been found at

Mapungubwe Hill but it is probably an intrusive object which was brought to the site later (Miller 2002).

1.3. Corrosion, definition and its behaviour in aerobic condition in general

Most of the metals are in the form of mineral compounds in the nature that are recognized as ores. Extracting pure metal from ore and separating it from gangue with consideration of the diversity of ores necessarily involves different procedures. During the process of smelting a large amount of energy is consumed to reduce the metallic ores to form pure metals. This energy is stored in the chemical structure of purified metal. In fact, the Gibbs free energy (ΔG) of the reduction reactions that are involved in the extraction of pure metal, are positive (see Thompson (1924) and Ellingham-Richardson diagram for metal oxides formation). Based on thermodynamic rules the products of these reactions, due to their higher free energy, are unstable (Vining 2011). These products always have a tendency to reduce this energy and be converted to a lower energy composition. Corrosion is a natural process via it a pure metal reacts with active agents in an environment. In this process metal is converted to its chemically stable compounds which are present in the nature.

Since corrosion in metals is mostly coupled with loss of material this phenomenon is known as an undesirable process. Vanishing evidence of usage and fabrication as well as disfiguration in meal artefacts are the main results of corrosion. Despite this belief corrosion is not always harmful. With respect to the historical and archaeological metal objects, corrosion can be quite favourable by adding aesthetic and age value to them. Sometimes corrosion products with their various and attractive colours add aesthetic value to an object and hold the attention of viewers. Age value and authenticity in historical metal objects also have a close association with the corrosion phenomenon and stratification of corrosion products on metals, especially in the case cuprous artefacts. These desirable aspects of corrosion only take place in particular conditions and result in the formation of a corrosion crust that is known as *noble patina*. *Noble patina* refers to a continuous and dense corrosion crust on metal objects that not only reduces the rate of corrosion but also contains historical evidence and aesthetic value. This kind of corrosion mainly forms slowly in a moderate environment with a low amount of aggressive elements such as chlorine. Reactions that contribute to the process of corrosion basically were divided into two, chemical and electrochemical groups (Scott 2002) which can be described as follows:

1.3.1. Chemical reaction

This type of reaction involves the transfer of an electrical charge (electron) locally between atoms without any conductor (Scott 2002). The common corrosions of this kind are direct reactions between metal and oxygen (Cronyn 1990) or water (Walker 1982).

1.3.2. Electrochemical reaction

In these reactions an electrical charge (electron) is transferred between atoms by means of a conductor that connects anodic and cathodic regions. For electrochemical reaction the presence of three factors is essential (Walker 1982). They are:

a) Anodic and cathodic areas (metallic couple)

b) A metallic circuit between anodic and cathodic regions

c) An electrolyte in which anode and cathode are in contact.

Electrochemical reaction is almost always the main reason for the corrosion of archaeological metals; since cathodic and anodic regions, together with enough humidity (an electrolyte) are mostly present (Scott 2002; Cronyn 1990). The potential difference between cathode and anode is the main factor for the transfer of electrons via a metallic circuit. This potential difference may produce easily with the connection of two different metals (galvanic corrosion) or even on the surface of one metal substance. However anodic and cathodic sites are mostly situated on one metal base. In this case, physical and chemical inhomogeneity in metal or corrosive environment defines the position of cathode and anode on the metal surface (Brasunas *et al.* 1984).

Chemical impurity in metal as one of the factors in electrochemical corrosion might be produced deliberately by making an alloy, or accidentally during the smelting process by the formation of unwanted metallic elements. Physical inhomogeneity in metals can be due to the shape of the object or formed by mechanical stress during fabrication and later usage. These stresses result in acceleration of corrosion along with stress lines (Hamilton 2000).

Inhomogeneity in the environment can be formed by a different concentration of ions or oxygen in adjacent to the metal surface which by producing a concentration cell defines the region of electrodes (Brasunas *et al.* 1984). In addition to these, the effect of different temperatures and pH on the metal surface also has been reported as other factors that have an influence on location of the anodic and cathodic areas on the metal surface (Hamilton 2000).

In anodic areas electrons are produced through an oxidation reaction (Cronyn 1990) and start their movement towards the chatodic areas within the metallic phase. The unique oxidation reaction that occurs in anode is (Brasunas *et al.* 1984):

$$M \rightarrow M^{n+} + n\ e^{-} \qquad\qquad (1.1)$$

This process results in the dissolution of metal in the electrolyte. In alloys which contain dissimilar metallic elements, metal dissolution through oxidation reaction can occur for all of them (Brasunas *et al.* 1984). In the cathodic area electrons are consumed by reduction reactions that occur there (Cronyn 1990). Reduction reactions in the cathode mostly consist of the following reactions in aerobic conditions (Brasunas *et al.* 1984; Walker 1982; Turgoose 1982*a*):

Oxygen Reduction $O_2 + 4H^+ + 4\ e^- \rightarrow 2H_2O$ (1.2)

(Acid solution)

$$O_2 + 2H^+ + 4e^- \rightarrow 2(OH)^-$$ (1.3)

Oxygen Reduction $O_2\ (g) + 2H_2O + 4\ e^- \rightarrow 4OH^-(aq)$ (1.4)

(Neutral and alkaline solution)
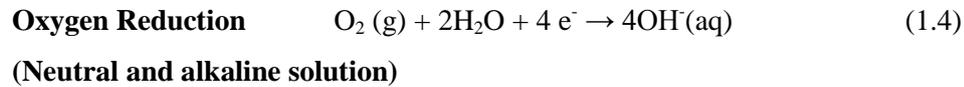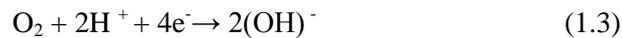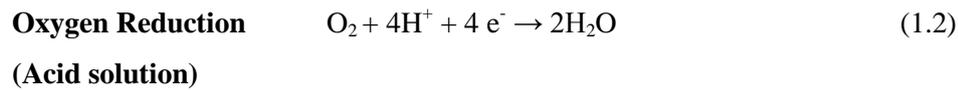
The combination of products of anodic and cathodic reactions forms corrosion products (Brasunas *et al*. 1984). Meanwhile, the other present soluble anions in the burial environment such as chloride and carbonate ions can also participate in subsequent reactions with dissolved metallic ions to form different kinds of mineral products (Cronyn 1990). Some of the corrosion products are insoluble and adhere perfectly to their substrate. These products can reduce or stop the rate of corrosion in a stable and non-acidic environment such as cuprite and malachite do in cupreous metals. On the contrary, some of them are harmful, unstable or participate in the cyclic corrosion process. Corrosion can develop an even and uniform surface on metals or act locally and produce ones that are uneven and non-uniform. The latter can cause a lot of damage to the structure and appearance of the metal artefact.

Chapter 2

Methodology

2.1. Codes of ethics in conservation

This study was conducted within the framework provided by the codes of ethics in conservation. The codes of ethics are a combination of moral principles and values that provides a framework by which conservators can operate and make a correct decision (Keene 1994a; Edson 1997; Caple 2000). These codes of ethics were issued by professional conservation associations or committees such as American Institute for Conservation (AIC), The United Kingdom Institute for Conservation (UKIC), Canadian Association of Conservation (CAC) and the conservation committee of The International Council of Museum (ICOM). The issued codes by the different associations have considerable similarities together and considered different ethical aspects of a complete procedure in the conservation of historical objects. Ethical codes that were issued by the principal AIC (American Institute for Conservation) (1994) maintain that the primary goal of conservation practice is preservation and stabilization of material culture preferably through preventive conservation. These ethics also consider the necessity of use, investigation and understanding of the cultural properties (Caple 2000). In these ethics any interventive conservation should be performed with consideration of the uniqueness of the material constituent of the objects while attaining the highest available standards for conservation restoration procedures (AIC 1994) as well as utilizing the methods or materials that do not affect adversely on an object or its future examination (AIC 1994). On the other hand, the materials that are utilized in conservation should be reversible (ICOM 2006). These materials should present no health hazards to the conservator and the associated environment (AIC 1994). One of the most important ethical codes is the recording of the objects and all procedures of conservation. Documentation of artistic–historic properties before any conservation activities helps to preserve the historical evidence that might have been missed during the time, for example by corrosion or subsequent conservation (Caple 2000). The documentation should be continued during treatment and preservation to retain the evidence for later treatment or research. Conservators must provide guidelines for continuing care, recommend appropriate environmental condition for storage and exhibition, and proper procedure for handling, package and transport of the objects (AIC 1994) to secure their stability for a longer time. A conservator should be aware of the limitations of individual knowledge, competence and facilities (AIC 1994) while considering and respecting other related expertise and the rights of other professions (AIC 1994).

2.2. The objects of this study

Choosing a few objects for this project was the preliminary step in starting the investigation. Mapungubwe and the K2 metal assemblage of the University of Pretoria consists of a huge number of artefacts that are mostly fragmented or completely corroded and unstable. These pieces mostly belong to more delicate ornaments like helically wound wires that were previously in the form of necklaces, bangles or rings. Small heavily corroded bars or rods that could respectively be a part of a hoe shank

16

or arrowhead are seen among them. It was impossible to find fragments that belong to one object. Only a few of the objects kept their original form and are in a better condition. These metal objects are kept in storage and few of them were placed in display cases at the Mapungubwe museum. From these 38 artefacts were selected. The following four main factors influenced this selection:

1. The selected objects have mainly kept their original form although some of them have parts missing and are heavily corroded. The reason for this decision is due to the fact that the preliminary investigation and the subsequent conservation are a time and resource consuming processes. Consequently those objects with physical integrity which contain important historical or aesthetic value are in priority for conservation.

2. The objects were mostly selected from the artefacts which are kept in the storage facility. These artefacts are in a worse condition compared to those that are in the Museum display. The storage facility environment is damp with about 73-75% relative humidity (RH) during a rainy season which can increase the rate of corrosion in the metal artefacts. The objects on display are robust and their condition is monitored from time to time. This category encouraged me to select from storage all artefacts that were susceptible to corrosion and further degradation. Only one hoe from the Mapungubwe museum display case was added to this list because of uncertainty about its manufacture provenance.

3. From 38 selected objects 35 were chosen for the purpose of conservation. Three of the objects from K2 (KC5, KC4 and KI6) were selected only for investigation about the effect of burial conditions on corrosion to increase the number of objects from K2.

4. The objects are divided into two main categories on the basis of their archaeological context. The first are those which have their original identification tag with exact archaeological provenance. The second are those with poor provenance, and included two categories. The first category consisted of discarded objects from the waste in the Mapungubwe northern dump. The second one included those where the documents only refer to the area they were found and no additional information or sign is available to show the exact place or layer they were found, such as MI2, MI7 and MI9.

2.3. Documentation

Primary records of this assemblage that indicate their identity details and condition at the time this research was started are presented in **Appendix A**. In this record each object was presented in one table under a particular title that was used as the identity code in this thesis. The first letter refers to the name of the site the object was found; the second one indicates the material constituent of the object and the last letter refers to its particular context in the assemblage. Then **MI1** indicates an **I**ron object from Mapungubwe which has been placed at the top of the list of the assemblage. In these records general information with regard to the physical description and damage of the objects was gathered by

17

naked eye. Weight, dimension and photographs of all objects were also brought in this part. The photographs are in colour and consist of images of both sides of an object in addition to close-up images of damage. Photographs were taken in natural light.

2.4. Sampling

For purposes of identification, the composition of metals, characterization of corrosion products and establishing the method of manufacture through metallographic examination, some of the objects were sampled, mostly transversally to the original surface, using a jeweller's saw. These objects consisted of hoes (MI2, MI7, MI9, and MI10), hook (MI4), drill (KI5) and bangles (KC1, MC10, MC11 and MC12), ingot (MC9) and pin (MC8) with ambiguity in their manufacture or composition, and funnels (MC7) of which the function was unclear. Some of the objects only had study value and the sample was removed mostly for the study of corrosion composition and stratification such as KC4 and KC5. A few of the objects were fragmented as a result of corrosion or sampling during previous studies. In these objects such as MI5 and SI1 the fragments were used instead of sampled.

The dimension of the samples ranged mostly from 1 mm to 3 mm^3. These samples were embedded in resin and ground with silicon carbide paper up to grade 1100, and then polished with diamond paste down to grade 1 micron with an ethanol based lubricant to prevent compositional alteration of the corrosion products.

2.5. Instrumentation

2.5.1. Stereo microscope

For a more accurate study, and to reveal the probable microscopic evidence on the surface, apart from visual observation, a stereo microscope was also used. Four types of visual evidence can be observed on the surface of historical objects: manufacture, use, decay and conservation (Caple 2000). Most of the artefacts of this assemblage have been covered with a thick layer of corrosion and only show traces of decay. Only a few of the objects show traces of manufacture, usage and conservation which, in some cases, were hardly distinguishable from each other. These signs were only seen on the low corroded iron objects and those copper artefacts which were either not covered by a thick layer of green corrosion or such layer was manually removed by archaeologists to expose the metal underneath. The surfaces of all the objects in the assemblage were observed under a Nikon SMZ800 stereo microscope powered by ACT software provided by Nikon. But the results of a particular number of objects that showed some evidence of manufacture, usage and conservation were discussed in Chapter 3 and 4 of this thesis.

2.5.2. Neutron- and X-ray tomography

In this study, neutron- and X-ray tomography were chosen as two complementary non-invasive visualization techniques to study the internal structure and physical stability of the objects. Physical stability can be assessed by revealing the condition of remainder metal within corrosion, its physical shape and its continuity along the corroded metalwork. Neutron/X-ray radiography and tomography (NT, XT), two complementary and available facilities were chosen because they can reveal defects such as cracks or voids as well as the method of manufacture in metal objects. In order to compare the capability of these instruments, five representative examples of archaeological metal artefacts were examined using both techniques. Comparative studies revealed neutron tomography to be generally superior to X-ray tomography because of the enhanced penetration properties of neutrons through the metal objects. Effectiveness of these two facilities depends directly on X-ray- and neutron attenuation and imaging characteristics. On account of this result the remainder of the objects were examined by neutron tomography. Estimation of corrosion percentage in artefacts was actualized by utilizing the obtained data via neutron tomography as well as advanced image processing techniques (ImageJ). No other technique could be used to quantify the corrosion of artefacts as these methods are destructive and not suitable for this type of investigation on precious samples.

Neutron/X-ray radiography and tomography studies of the metal objects were performed at the South African Neutron/X-ray radiography (SANRAD) facility, which is located on the beam port floor of the SAFARI-1 nuclear research reactor at beam port No. 2 based at The South African Nuclear Energy Corporation (Necsa), near Pretoria. The neutron and gamma beams produced by the fission reaction in SAFARI-1 are filtered by a Bismuth crystal and the scattered neutrons and gamma rays are collimated towards the sample and detector. The result is a 93% thermal neutron beam that passes onto and through the sample. A 100 kV X-ray tube can be installed at the exit of the collimator to replace the neutron beam delivery with X-rays. It affords the opportunity to use and compare the result of two penetrating radiation types in the study of metal objects.

The samples were positioned on a rotary table between the radiation source and the scintillator screen detector. To minimize the second and higher order detrimental scattered neutrons (unwanted background) from the samples, they were placed more than 80mm from the detector. For high spatial resolution results, the samples were placed as near to the detector as possible. Scintillator screens used for neutron and X-ray detection are ^{6}LiF/ZnS: Cu, Al, Au and Gd_2O_2S respectively. The optical images from the scintillator are reflected via a 45° mirror onto a lens system (SMC-Pentax lenses) that focuses the image onto a Peltier-cooled CCD camera (Andor type) with a 1024 -1024 pixel array and 16-bit image output device at 2μm/pixel. The camera chip is cooled to -45°C to minimize dark current and thermal noise. Projections were recorded by incremental rotation of the sample through an angular interval of, $\Delta\theta = 0.96°$ from 0° to 360°. This yields a total of 375 projections for each

tomogram. Octopus reconstruction software was used to post-process the data into 2D axial slices. A full description of the facility can be found in de Beer (2005).

After reconstruction a full 3-D virtual image of the object is available. IMAGEJ visualization software which is available on the (http://www.ansci.wisc.edu/equine/parrihs/imagejpc.zip) allows extraction of both qualitative and quantitative information regarding the distribution of features in the image in any desired slice through the object such as corrosion percentage.

Physical characteristics of the objects in addition to the specific attenuation coefficient of X-ray and neutron for different kinds of materials result in a contrast in images which is informative in terms of the interpretation of physical defects.

2.5.2.1. *X-Ray- and neutron attenuation and imaging characteristics*

Imaging of the complete three-dimensional (3D) object is made possible through penetrating radiation. To form a proper visualization of the interior of the object two conditions need to be met. The first is that the radiation must be able to pass through the interior. The second is that, in this process, sufficient interaction must occur on different scales with the structures in the interior of the object to provide sufficient contrast and to enable visualization. This means that the radiation must be able to penetrate the object but that the object must not be fully transparent to the radiation. This condition is used to perform some quantitative estimates of the imaging power of X-rays and neutrons respectively for different types of materials.

Equation (2.1) below describes attenuation for the special case where a parallel beam with intensity I_0 impinges upon a slab of material. It provides a formula for the remaining intensity I after penetration through a thickness x *(cm)* of material of density ρ *(g/cm^3)* and mass attenuation coefficient μ *(cm^2/g)*.

$$I = I_0 exp(-\mu\rho x) \qquad (2.1)$$

Although strictly speaking it is accurate only for parallel geometry, the equation can be used to estimate depth of penetration into real objects with more complicated geometry. It shows that the intensity drops off exponentially with distance into the object and that the factors influencing the attenuation of the incident radiation beam are the attenuation coefficient (radiation type dependent) and the material density and the thickness (object dependent only) (Kardjilov *et al*. 2006). The same general relation applies for X-rays and neutrons, the only difference being in the mass absorption properties (μ -values) for interaction of X-rays and neutrons with the different kinds of materials in the object. This depends on the fundamental properties of the two types of radiation. X-rays interact with the electron cloud around the atom and neutrons interact with the nuclei (Deschler-Erb *et al*. 2004). Equation (2.1) can be rearranged to explicitly estimate the thickness of material, which will attenuate the original intensity I_0 by 99 %, say. The resultant formula is:

$$x = \frac{4.6}{\rho\mu} \, cm$$

(2.2)

Only 1% of the radiation manages to penetrate deeper than this value and one can thus safely assume that this constitutes a good estimate for "absolute" visualization depth.

For X-rays there exists a direct relation between the mass attenuation coefficient and the effective atomic number of an element or compound, also known as Moseley's law. The high atomic number of heavy metals thus result in them having larger μ values, which in combination with their high densities (ρ –values) limits penetration only to the surface regions of the objects as predicted by equation (2.2). This is especially true for low energy X-rays (<100 kV). For instance, for 60 keV X-rays on iron, $\rho = 7.86 \, g.cm^{-3}$, $\mu = 1.2 \, cm^2.g^{-1}$ and thus $x = 0.5 \, cm$. Objects with characteristic size larger than this become opaque to the X-ray beam and cannot be visualized in their interior. The opposite extreme of low-Z materials and low density predicts "transparent objects" that again leads to ineffective or negligible visualization capability. X-rays are therefore generally not well suited to study objects exclusively containing materials made of light elements, or large objects containing heavy metals such as iron, lead, copper, silver and gold. The latter are of course materials of choice for artefact construction.

Fortunately neutrons afford a means to study these objects. Neutron attenuation shows no systematic relationship with atomic number, such as with X-rays (See Appendix D: Table 2.1). In particular neutrons can penetrate the heavy metals readily and can also visualize material containing low atomic number elements such as H, B, C, O, Al, etc. These properties of the neutrons in radiography make it possible to detect organic materials inside metal objects, a function that cannot be achieved with X-rays. This becomes of particular interest to conservation management as the majority of corrosion products have hydrogen in their composition. At the same time the high penetration ability of neutrons through metal objects renders it a suitable technique in retracing manufacture methods in archaeological metal artefacts.

For proper interpretation of radiographs and tomogram slices provided later in this thesis, it must be remembered that slices contain only the image information contained in the plane of the slice itself. A radiograph, on the other hand contains all the image information projected onto a plane of observation (the scintillator screen) for a particular orientation of the object in the beam. Due to the very large number of electronic "cuts" or slices that can be made into the tomograms of each sample through open source image analytical software package, IMAGEJ, it is impossible to include all possible slices. In the analysis of each of the artefacts in the paragraphs below, the figures included represent the best slice which describes the condition of the specific artefact the best. The corrosion products are represented in white in the B&W figures while the metal core is normally represented by a grey mass.

2.5.2.2. The method in estimating corrosion percentage

When there is a simple invariant or symmetry of the corrosion structure, it becomes easy to estimate volume fraction of corrosion via direct estimation of area fraction along any representative slice. In Illustration 2.1 (a) below we depict a cylindrical object with an annular corrosion product layer of approximately constant thickness along its length axis.
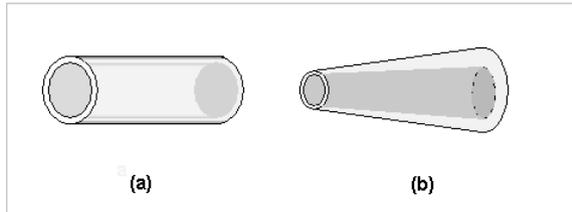
Figure 2.1. A schematic illustration of two corrosion scenarios.

In such a simple case (Fig.2.1a) any single axial slice will provide sufficient information to estimate the volume corrosion percentage of the whole object. In fact the volume percentage becomes equivalent to the area percentage in the slice:

$$C\% = \frac{A_{corroded}}{A_{total}} \times 100 \qquad (2.3)$$

By adjusting contrast and brightness (ImageJ open source analytical software) the corrosion region in the slice can be contrasted and identified more clearly to improve accuracy. In (Fig.2.2) we have such a scenario for the shaft region of a real object (the spatula also shown in (Appendix A. Table SI1). Using the software tools it becomes possible to isolate the corroded region as shown in (Fig. 2.2a). The area of the corroded part as well as the total object area can then be sensitively determined. The exact units are irrelevant as we are only interested in the dimensionless ratio as defined by equation (2.3).
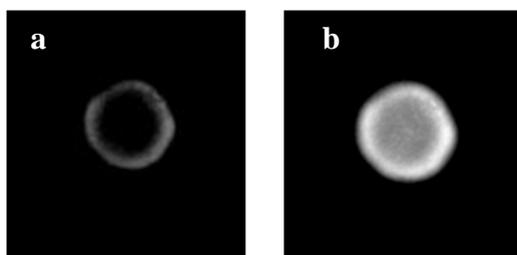
Figure 2.2. Slice perpendicular to the spatula (SI1) shaft axis with adjusted contrast to show: (a) the corrosion ring alone; and (b) the metal core in grey and corrosion in white.

For more complicated scenarios, such as in (Fig.2.1b), a single slice will not suffice to estimate volume percentage as each axial slice now clearly yields a different area fraction of corrosion. For relatively simple geometries volume fractions can still be estimated from a finite number of axial

22

slices, say N, of known length each, which constitutes a distance along which the corrosion properties remain constant or approximately so. The estimated average volume percentage of corrosion can then become:

$$\%C = \frac{100}{N}\sum_{i=1}^{N}R_i d_i$$

(2.4)

Here R_i is the area corrosion fraction of section i, and d_i is the length of that section. When a simple geometry, like the cases illustrated, does not apply, the determination of corrosion percentage becomes difficult unless advanced image processing techniques (such as available in ImageJ) are applied to integrate slices along the object analogous to what is shown by equation (2.4).

2.5.3. Scanning electron microscope energy dispersive spectroscopy (SEM-EDS)

For quantitative elemental identification of metallic phase, corrosion products and a detailed study on phase distribution in the corrosion crust a Jeol 5800 Scanning Electron Microscope coupled with a Thermo scientific Energy Dispersive X-ray micro-analysis system (SEM-EDS) with a Nano Trace Si(Li) detector was utilized. The analyses were performed under an accelerating voltage of 20 kV and mostly in raster mode on well polished mounted samples which were coated with a thin layer of carbon to prevent electrical charge. In this mode the area analysed varied and depended on the size of the phases. The live time was 100s to improve background to a peak signal. The SEM images of corrosion study are given in Appendix C.

2.5.4. X-ray diffraction (XRD)

To elucidate the exact crystalline structure of corrosion products, XRD analysis was performed qualitatively using a PANalytical X'Pert Pro powder diffractometer with X'Celerator detector. The sample was scanned at the required 2θ angle ranges from 5 to 90 (°) with step size (°) 0.0084. The radiation was Fe-filtered CoKα radiation in order to eliminate fluorescence which would cause, high background and poor peak to background ratio. The phases were identified using X'Pert Highscore plus software. For routine phase identification a particle size of less than 50 μm is required, which was achieved by hand grinding in an agate mortar, and then top loaded onto a zero-background holder due to small sample size. Two copper (KC2 and MC11) along with two iron objects (KI1 and MI6) as two representative samples from the sites of K2 and Mapungubwe were sampled superficially (micro-destructively) by scalpel and the powder was analyzed qualitatively by the device. This method was also utilized in respect of the one copper artefact (MC7) with unusual anaerobic corrosion products.

2.5.5. Raman Spectroscopy

The Raman spectra were recorded with a T64000 micro-Raman spectrometer from HORIBA Scientific, Jobin Yvon Technology (Villeneuve d'Ascq, France). The Raman spectra were excited with either the 514.5 or 647.1 nm lines of a Krypton Argon mixed gas laser (Coherent, Innova 70c) with laser power less than 1mW on the surface of the samples. A 50x objective on an Olympus microscope was used to focus the laser beam (spot size ~ 12 μm) on the samples and also collected the backscattered Raman signal. An integrated triple spectrometer was used in the double subtractive mode to reject Rayleigh scattering and dispersed the light onto a liquid nitrogen cooled Symphony CCD detector. The spectrometer was calibrated with the silicon phonon mode at 520 cm^{-1} before performing the analysis.

2.5.6. Metallography

Metallography was performed on the mounted samples to determine the microstructure of the metal phase and to elucidate the manufacture method. This was achieved by utilizing a Nikon EClIPSE ME600 metallography microscope under bright field illumination. Iron samples were etched with natal (2%). Copper and copper base alloys were etched with ferric chloride solution in ethanol and hydrochloric acid in different concentrations on the basis of the results. Vickers microhardness of the samples was measured with a fm-FUTURE TECH microhardness tester with varied loads of 50 to 100g depended on the sample size. The micrographs were used to estimate the grain size and carbon content in iron-carbon alloys. The carbon content was estimated in a qualitative way by comparing volume fraction of pearlitic zones in micrographs of the samples to reference data with the same magnification published in Samuels (1980). The grain size was established by using the standard Heyn method which is a lineal Intercept Procedure (ASTM E112). The images of metallographic study on the samples are given in Appendix B.

2.5.7. Controlling the relative humidity and temperature

Measurement of the dampness in the air is done by monitoring the relative humidity (RH). RH is the ratio of the actual quantity of water present in the air (AH) to the maximum quantity of water the air could hold before condensation takes place (SH) at a constant temperature (Cronyn 1990):

$$RH(\%) = AH/SH * 100$$

Fluctuation of the RH is under effect of the temperature. Raising the temperature results in a decrease in the environmental RH and vice versa. For this reason the temperature along with RH was monitored in the storage area and the showcase.

Relative humidity (RH) and temperature were monitored by utilizing a hygrometer and thermometer respectively. For estimating RH% two kinds of hygrometer – the hair hygrometer and the digital hygrometer were placed in the display case and in the storage facility respectively. Before that the two hygrometers were placed together in the same damp environment to estimate the difference between the RH % that is registered by them. The digital hygrometer was together with a thermometer while a separate thermometer was used to measure the temperature in the museum display case.

Two main reasons prevented of the measuring of RH% and temperature throughout 12 months of a year. The copper and iron objects display case does not have a specific place in the museum. This display case is relocated every few months in different galleries. This relocation could result in fluctuation of RH and temperature in the display case environment which is directly the effect of the surrounding environment. For this reason the RH% and temperature were registered during those months that the display case was kept in the same place. Flooding of the storage area, which was not a natural occurrence, impeded the monitoring process of the RH% and temperature there.

2.6. Soil Analysis

To determine the soil properties that affect corrosion such as particle size, pH, organic material, electrical conductivity and soluble anions, available soil samples from K2 were analysed. The only soil sample available in Mapungubwe Research Facility (MRF) belongs to excavation (TS 1968). Four layers of this profile have been taken in different depth for analysis to submit a representative physical and chemical composition of the excavation area.

Soil analyses were performed at the Department of Plant Production and Soil Science at the University of Pretoria and were based on formulary of the AGRI Laboratory Association of Southern Africa (AGRI LASA). The carbonate content of the soil was measured separately, based on preliminary steps in volumetric method 7 (SA07), ISO 10693.

For an estimation of soil aggressiveness AWWA, standard C105-72 was used although could not be systematically applied here. Calculating the amount of soil resistivity and pH based on ASTM in this formula must be applied *in situ* or shortly after sampling which is not possible with consideration of present soil samples in this study which date to1968. In this formula soil resistivity and pH are the main factors in estimating the corrosivity of the soil among other characteristics of soil such as Redox potential, sulphides and moisture content (Palmer, 1989). With consideration of these limitations the result in respect to aggressiveness of K2 soil can have less accuracy whereby the submitted data about electrical conductivity (EC) and pH here are not exactly based on ASTM rules. AWWA formula is used about ferrous metal (piping) but based on what is suggested by Myers and Cohen (1984) the soil

parameters having an effect on the rate of corrosion of copper are mostly the same. Any difference in the influence range of these parameters on corrosion of copper is discussed in Chapter 5.

For an estimation of soil effects on corrosion eight metal artefacts, iron and copper, were chosen that were found during Gardner's excavation (1935-1940) at K2 adjacent to TS 1968. One copper object (KC3) belongs to excavation TS4 1976. Figure 2.3 shows the location of excavation TS 1968 and Gardner (1935-40). The objects belong to a different depth of the Block 1, 2 and from different sections. These objects are relevant to each soil layer. Except KI4 the other objects are almost similar with respect to their shape and volume. The archaeological data of these artefacts are given in Appendix D: Table 2.2.
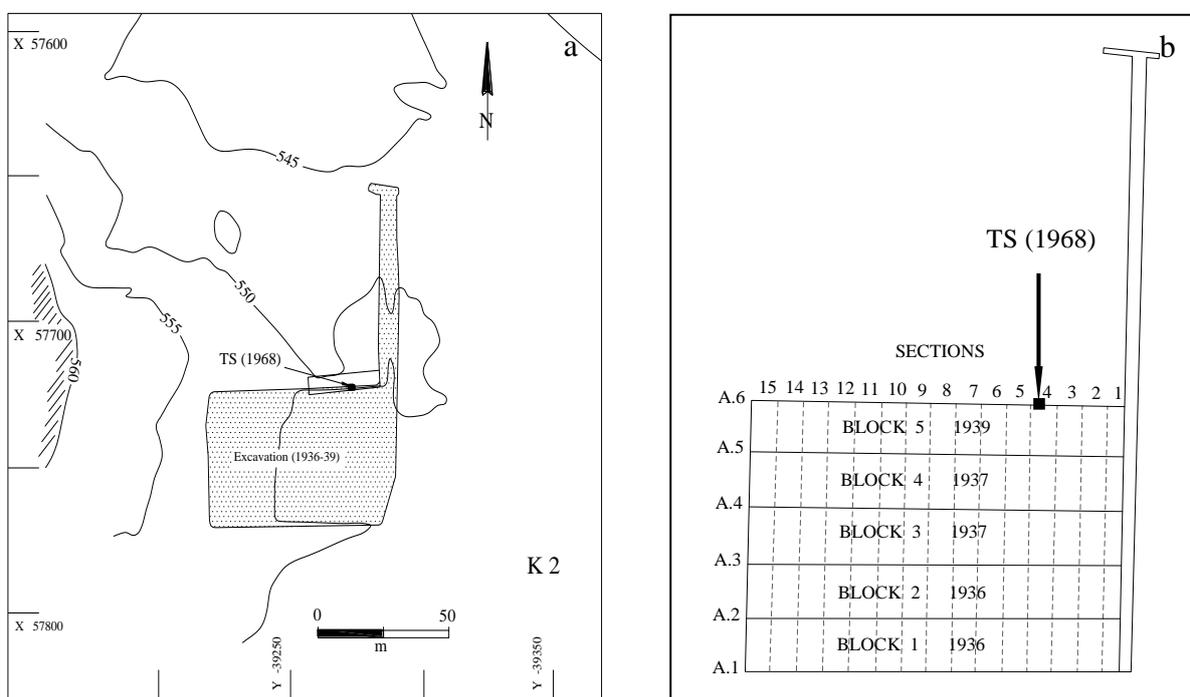
Figure 2.3. a) Location of TS 1968 in relation to Gardner excavation. b) It is adjacent to square 4 in block 5. (Images are respectively adopted from Meyer 1998 and Gardner 1963.)

2.7. Appendices

For convenience of the readers of this thesis all the cluster images of the objects or metallographic samples, as well as the tables, are provided in 4 separate appendices A, B, C and D.

26

Chapter 3

Physical stability and manufacturing technique of iron artefacts

3.1. Introduction

Material and manufacture technology of metal artefacts from *Greefswald* produced during the first three centuries of the second millennium were successively studied by previous researchers (Fouché 1937; Stanley 1937; Becker 1979; Pienaar 1979; Oddy 1991; Miller 2001) but the unique properties of each artefact, from a conservation point of view, made another technical study necessary in order to obtain a more comprehensive view of this assemblage before any treatment. The selected iron artefacts mostly comprised of utilitarian objects such as a rod, spatula, arrowhead and hoes, which a few of them are poorly provenance in archaeological context (Appendix A. Tables: KI3, KI5, MI1, MI2, MI3, MI4, MI7, MI8, and MI9). Some of these objects were found in the excavations dumps from the 1930s and 1940s, and a number of objects were labelled only with the name of the site of origin. The state of preservation of some of these artefacts indicated they might belong to a more recent date than the heyday of Mapungubwe (1220-1290 CE).

In this chapter, in a systematic technical study, all the historical evidence on the surface and interior structure of the iron objects were first examined by means of non-destructive techniques such as microscopic observation of the surface, and neutron tomography. The outcomes of this study indicated which of the objects needed more detailed study to clarify ambiguous aspects in their manufacture and origin. Further technical study on these specific objects was conducted by means of metallography of the mounted samples. Objects of which sampling might result in losing their physical integrity were not studied in detail. These objects included the heavily corroded artefacts such as MI1 and MI3. Some of the objects with clear provenance were not sampled such as KI4, MI5, SI3 and SI2 which the latter was examined by Miller (2001). In this chapter, I discuss the data relating to the manufacture of the artefacts, and use this data to identify the objects that belong to later date. In addition, I estimated the physical stability of the objects by revealing physical defects and estimating corrosion percentage in them. This is one of the basic components in further conservation of the objects.

3.2. Survey of surface characterizations, neutron tomograms and microstructure of the iron objects

3.2.1. Rods

KI1

This iron bar was found at K2 at a depth of 30.5 mm from the surface (Appendix A. Table: KI1). The bar has a simple rectangular shape with a square cross section. The object is heavily corroded and a calcareous deposit is observable on the surface. Except for trace of decay no other evidence was found on its surface.

Neutron tomograms show that except in its broken point, the metal core (light grey) is solid along the bar. The metal core is not rigid towards the broken part and shows several cracks which were filled

with corrosion products (white lines) (Fig.3.1). Based on evaluation of the axial slices, 53% of the object contains corrosion products. The total sample is covered by a thin corrosion layer which has penetrated more or less in metal core and made an uneven surface. A summary of the neutron tomography result of the object was given in Appendix D. Table: 3.1.
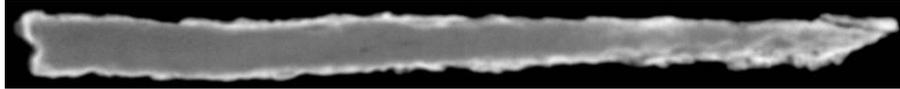
Figure 3.1. Neutron tomogram of KI1. Sagittal slice. Metal core was weakened by penetration of cracks and corrosion products toward broken part of iron bar at the tip.

EDS analysis of the iron bar revealed a small amount of silicon (0.1%) in the bulk of metal which was the result of probable dispersed fine silicate inclusions that have crystallized out of the ferrite solution as it was cooling (Miller 1996) (Appendix D. Table3.2: analysis KI1). In transverse section two distinctive kinds of inclusions were observable. There was a low number of small (<50μm) two-phase inclusions, consisting of light grey wüstite in the form of dendrite or globule (Appendix D. Table3.2: analysis KI1a1 and b1) in a dark matrix of slag (Appendix D. Table3.2: analysis KI1a and b). This kind of inclusion is typical in bloomery iron (Appendix B. Fig.1, 2). The largest (>100μm) were oxide and slag inclusion which consisted of two different compositions of iron oxides (Appendix D. Table3.2: analysis KI1c and c1) accompanied by a transversely fractured glassy phase (Appendix D. Table3.2: analysis KI1c2) (Appendix B. Fig.3). These are probably formed during corrosion due to the probable connection of glassy phase with the surface. There were also numerous elongated amorphous glassy inclusions. These inclusions are dispersed in various parts mostly in stringers parallel to the worked surface with more accumulation around the large one (Appendix B. Fig.3). A low amount of detected calcium (0.3 – 7.3%wt) in slag inclusions (Appendix D. Table3.2: analysis KI1a,b ,c, c1, c2) indicated the use of iron ore with a lime content (Tylecote 1962) or a fuel with high Ca content.

Metallography of the sample shows the bar was made of hypoeutectoid steel with an inhomogeneous carbon content of between 0.08 and 0.2% in different zones. The microstructure consists of mostly irregular ferrite grains with a degenerated pearlite island. The lowest carbon content region is associated with large polygonal ferrite grains with average ASTM grain size number 4 which were spread out in a restricted area parallel to the metal surface. This small area was mostly surrounded with fine irregular ferrite grains in higher carbon content zones (Appendix B. Fig.4). These large polygonal ferrite grains contain numerous etch pitting within the grains and grain boundaries. The fine ferritic grains had an average grain size of ASTM 10. The microhardness is varied between 170 H_V in the area with coarse grains and 243 H_V in areas with fine grains and a higher carbon content. This structure as Samuels (1980) described might be formed by working at a temperature lower than the A3 temperature followed by normalizing. Then it was annealed at subcritical temperature lower

28

than the A1 temperature which resulted in both critical growth of cold worked ferrite grains, formation of degenerated pearlite islands and precipitation hardening in large grains of ferrite.

KI6

This iron rod was found at K2 at a depth of 122cm from the surface in 1936. The rod has a simple shape with annular cross section. The rod is gradually tapered toward one point which was slightly bent. Except for trace of decay no other evidence was found on its surface (Appendix A. Table: KI6).

Neutron tomography shows that this iron rod has a crumbly metal core (Fig.3.2). The sharp point has a lamellar structure with no traces of metal. At the thick point of the rod the metal core has a fractured structure. A deep crack, filled with corrosion products, is seen along the entire length of the object. Based on frontal slices, 64% of the object consists of corrosion products. The original surface is damaged. A summary of the neutron tomography result of the object was given in Appendix D. Table: 3.1.

a   b
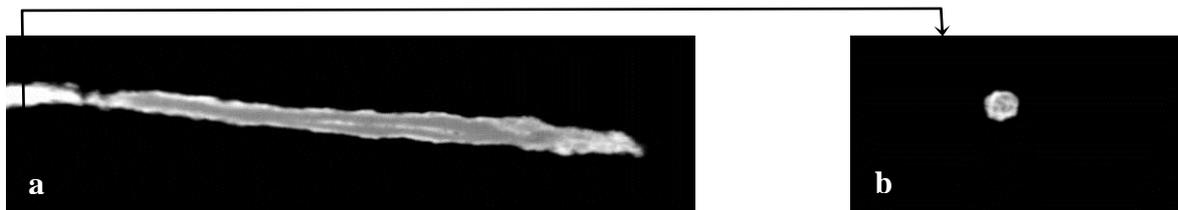
Figure 3.2. Neutron tomograms of KI6. a) Sagittal slice. Longitudinal crack spread among the object. b) Axial slice. Cracular structure of metal core with penetration of corrosion products can be observed.

MI6

MI6 was found on Mapungubwe Hill at a depth of 122cm from the surface. The rod has a round cross section and is tapered toward the one end. Except for trace of decay no other evidence was found on its surface (Appendix A. Table: MI6).

Neutron tomography shows that this iron rod has a continuous weak metal core. In one section along the rod, almost to the middle, the diameter of the metal core is really low which could cause brittleness in the object (Fig.3.3). Based on axial slices 62% of the object consists of corrosion products. The original surface is intact in between the corrosion. A Summary of the neutron tomography result of the object was given in Appendix D. Table: 3.1.

Figure 3.3. Neutron tomogram of MI6. Axial slice. Lean metal core leads to brittleness of the object.

The rod was heavily corroded and a small remainder of the metallic core is only visible within the removed cross section (Appendix B. Fig.5). Microscopic study of the section revealed that the structure of the metal phase was almost kept within the corrosion products and showing inhomogeneity in terms of distribution and dimensions of remnant inclusions within the sample. The inclusions in the metal phase are quite small and low in numbers while larger ones in high compactness are concentrated among corroded parts. There were two types of inclusions. These consisted of small angular or stringers of glass (Appendix D. Table3.2: analysis MI6a) (Appendix B. Fig.6) and particles of lime which were mostly embedded in large voids (Appendix D. Table3.2: analysis MI6b) (Appendix B. Fig.7, 8). Tylecote (1962) argued that this happens when the amount of lime is more than 15% and the furnace temperature is not high enough to cause an efficient reaction between the lime and other impurities in the ore to form calcium silicate content slag. This reaction takes place in a temperature of about 1600°C in a modern blast furnace as was suggested by Tylecote (1962). Consequently, a high amount of lime that might have been added deliberately or accidentally during smelting in addition to a low temperature of the bloomery furnace are the main reasons for the existence of detected particles of unreacted lime in the form of inclusion. There were also fine cracks within the metal phase which were also visible in fossilized form within the corrosion structure (Appendix B. Fig.9).

The etched transverse section shows that the metal is homogeneous in its microstructure. The microstructure consists of former austenite grains with ASTM 10 and cementite grain boundaries (Appendix B. Fig.10). Eutectoid cementite particles are mostly found in a compact form in a plate shape or partially spheroidized in a matrix of ferrite within the former austenite grains. The microhardness is about 230 H_V and is uniform in different parts of the metal phase. All these characteristics formed a complex microstructure which can hardly be interpreted or was made impossible to estimate the carbon content on the basis of volume fraction of cementite. Hypothetically, this structure, however, could have been formed by annealing of hypoeutectoid steel with a composition close to eutectoid in a temperature slightly above the A1 temperature which caused precipitating of cementite at grain boundaries and prevented formation of pearlite in slow cooling (Samuels 1980). Formation of cementite film at grain boundaries prevented grain growth while it kept a continuous easy fracture line in these areas resulting in the formation of cracks and its propagation within the metallic core (Appendix B. Fig.9) (Samuels 1980).

3.2.2. Spatulas (Pendants)

KI2

This delicate spatula was found in K2 at a depth of 61 cm from the surface in 1936 (Appendix A. Table: KI2). The object has a triangle blade with a narrow long shaft with circular cross section. The triangular missing part in the blade is due to sampling in the past (Appendix A. Table: KI2). Except

for trace of decay no other evidence was found on its surface

Neutron tomogram slices of this spatula show that only a small amount of the metal core has remained. The remainder metallic phase is mostly concentrated in the handle. The blade has a weak structure with dispersed metal zones, if any, toward the edges. A crack is visible along the handle which is filled by corrosion products (white line). A sagittal slice of spatula clearly exhibits the weak condition of the object (Fig.3.4). Based on axial slices 58% of the whole object contains corrosion products. A Summary of the neutron tomography result of the object was given in Appendix D. Table: 3.1.
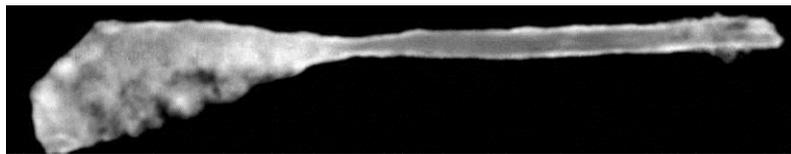
Figure 3.4. Neutron tomogram of KI2. Sagittal slice. Remnant weak metal core is seen in the shaft and mostly in thin sheets among the blade.

MI3

MI3 was found within the discarded archaeological deposit in the northern dump at Mapungubwe Hill (Appendix A. Table: MI3). Except for trace of decay no other evidence was found on its surface. The unstable physical structure of the object in the junction point between the shaft and the blade with a narrow weak metal core, prevented sampling this object.

Neutron tomography shows that this spoon-like artefact has a continuous metal core, although the edges of the blade in some parts are structurally weak. At the edges of the blade corrosion has decreased the thickness of the metal to the extent that, in some places, no metal has remained. (Fig.3.5a). Investigative cleaning is needed to establish whether the original surface has remained in these areas. A crack which is filled with corrosion products can be observed in the shaft (Fig.3.5b). Based on axial slices, 66% of the object consists of corrosion products. A Summary of the neutron tomography result of the object was given in Appendix D. Table: 3.1.
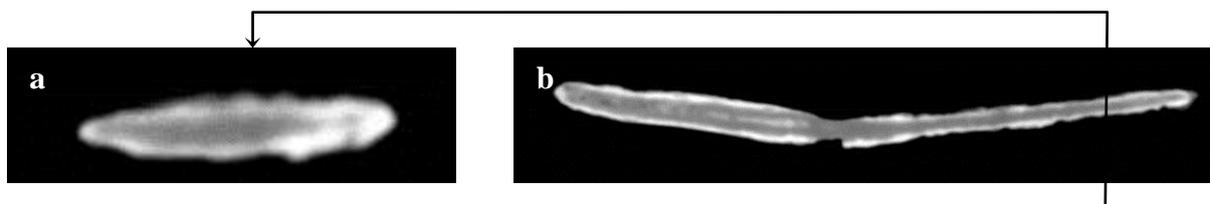
Figure 3.5. Neutron tomograms of MI3. a) Axial slice. Demolishing of metal at the edge of blade is observed. b) Sagittal slice of the object. Longitudinal crack among the shaft is revealed.

31

MI5

The spatulas were found during the excavation of MK1 in layer 11 on Mapungubwe Hill in 1973. This layer has been dated to a period from 1243 AD to 1252 AD on the basis of calibrated radiocarbon dating (Vogel 1998). This date is related to phase three of the settlement i.e. the period between 1220 and 1250 AD. The spatulas were encrusted together inside a mixture of soil, corrosion products and charcoal that formed a bulky mass. Neutron radiography revealed the spatulas to be in an unstable physical condition but could in fact allow virtual separation. Visualization revealed that one spatula has an intact shaft with part of the blade missing while in the other one the end part of the shaft is missing. Both the objects have kept their original shape inside the crust. The area where the two spatulas are in close contact appears bright gray in (Fig.3.6a) while the darker regions indicate the presence of an intrusion of a mixture of soil and corrosion products between them.

The remaining shaft has a delicate loop at one end (Fig.3.6b). A thin wire is twisted along the length forming a screw-like feature (Fig.3.6b, c). The thinness of the wire indicates it was not manufactured by simple hammering although the corroded structure of it prevents revealing the exact method of manufacture. This technique of manufacture is similar to another spatula (SI1) which was found in the same chronological layer at Southern Terrace.

The low interaction of neutrons with unconsolidated soil allowed the structures inside the crusted clump to be studied in detail, revealing the structure of the corroded artefacts. Only a small amount of metal core has remained in the shaft, while within the blades no remnant of metal is detected (Fig.3.6c). A reliable estimation of the corrosion percentage was unsuccessful in this case due to a large variation in thickness, particularly in the joint part. A summary of the neutron tomography result of the object was given in Appendix D. Table: 3.1.
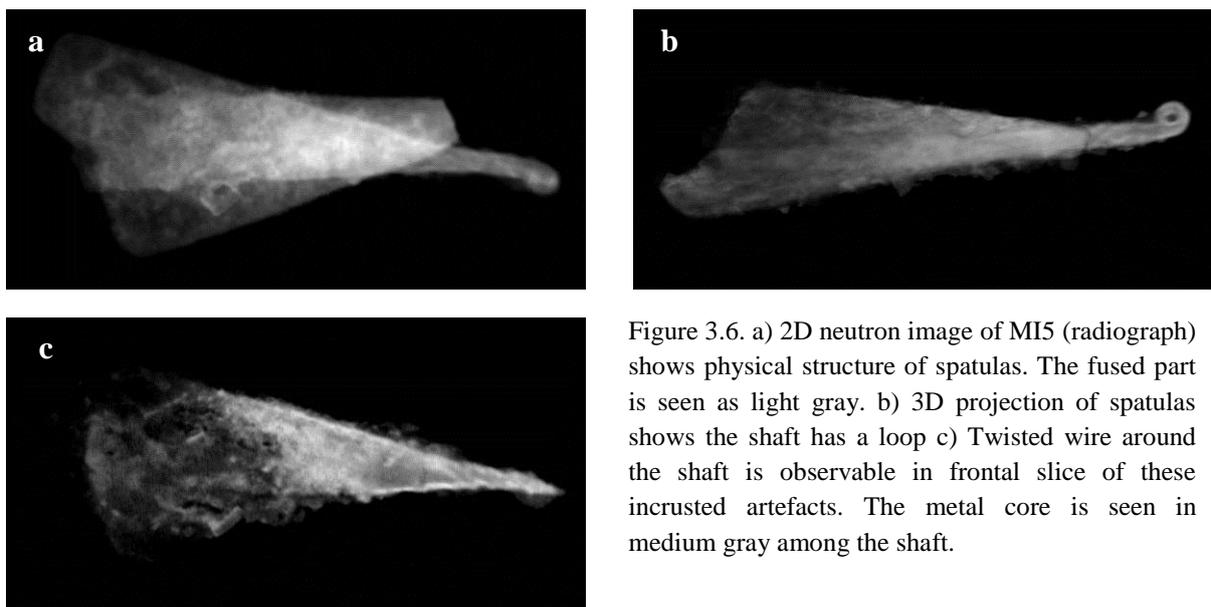
Figure 3.6. a) 2D neutron image of MI5 (radiograph) shows physical structure of spatulas. The fused part is seen as light gray. b) 3D projection of spatulas shows the shaft has a loop c) Twisted wire around the shaft is observable in frontal slice of these incrusted artefacts. The metal core is seen in medium gray among the shaft.

SI1

This small, delicate iron object appears to have been used as a pendant (Appendix A. Table: SI1). It was found southwest of Mapungubwe Hill (Southern Terrace) during the excavation of K8 in 1971, at a depth of 45 cm, in a layer of loose sand and was dated to 1284 AD (Meyer 1998; Vogel 1998). It has an integral long shaft that was bent to form an eye for suspension (the separate globular part). The edge of the shaft appears serrated. This feature, details of which are difficult to see by the naked eye, appears to be the remnants of a thin iron wire that was wound around the shaft and that became completely corroded, flaked and had partially disintegrated. It was fractured into two parts that might have been the result of destructive sampling in the past since the breakage surface is completely even.

This particular item is not similar to earlier pendants with twisted shafts that were found in southern Africa at Divuyu (550-760 AD) and Nqoma (660-1090AD), two early Iron Age sites in northwestern Botswana. The shafts of these pendants were bent and twisted around itself to form an eye at the top (Fig.3.7). The thin iron wire around the shaft of SI1 appears to have been made by a technique such as wire drawing although the completely corroded structure hampers any conclusion as to the method of manufacture.

a   **b**

1cm
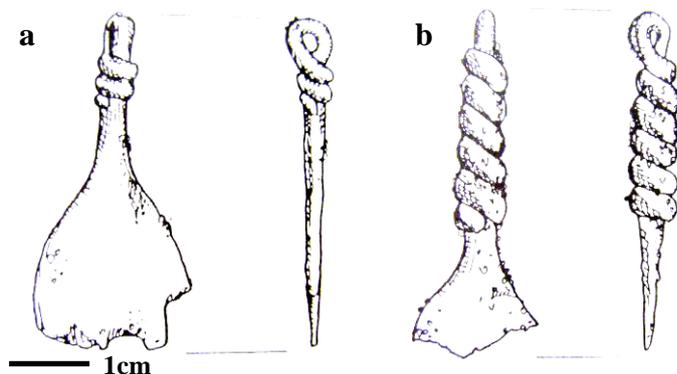
Figure 3.7. a) Pendant from Divuyu b) Pendant from Nqoma. Adapted from Miller (1996)

Neutron- and X-ray tomography was performed successfully on this small sample. Figure.3.8a shows a 2D neutron transmission radiograph of the spatula. Due to the high penetrability of neutrons through the metal it is not possible to clearly distinguish between the remaining metal core and corroded material in this image. A survey of tomogram slices, however, provides more detail about the extension of the corroded area. The particular sagittal slice near the mid plane of the object, shown in Figure.3.8b, is a good illustration of this. The higher contrast region around the edge is now more visible and represents the corrosion products on the outside. The high contrast of the surface corroded area is the result of the presence of hydrogen, which has a high neutron attenuation coefficient, in the chemical composition of corrosion products. While it remains difficult to assign a specific part as belonging to intact metal, features become visible in Figure.3.8b that may be attributed to a combination of factors such as a different composition of corrosion products, lamination and flaking

(darker "hollow" areas). A survey of axial slices provides further details about the presence of flaking and lamination (Fig.3.8c, d). Lamination is visible as a longitudinal grey line and flaking as dark areas, indicating loss of material.

As expected for small metallic samples (see Section 2.5.2.1) the X-ray 2D image (Fig.3.8e) reveals the metal core with a much higher contrast in the shaft area than is possible with neutrons, making the exact position of the metal core more recognizable than in the neutron image. This is the result of a high interaction of X-rays with metals in general. A gradual decrease in corrosion density towards the tip of the blade is visible in the X-ray image. This small spatula was the only object in this assemblage where X-ray tomography with 100 kV energy provided better results for recognition of the remaining metal core. This is due to the relatively small corroded part (not usually seen by X-rays), high contrast of the metal part (best seen by X-rays on small objects) and the small size of the object (allowing X-ray penetration through the object).

However, the wire twisted around the shaft is seen with greater clarity in the neutron images (Fig.3.8a, b). The fact that the wire feature stands out more clearly in the neutron images, suggest that the original iron has become almost completely corroded. Based on the neutron tomography axial slices, approximately 59% of the object consists of corrosion products, which are mostly concentrated in the blade. A Summary of the neutron tomography result of the object was given in Appendix D. Table: 3.1.
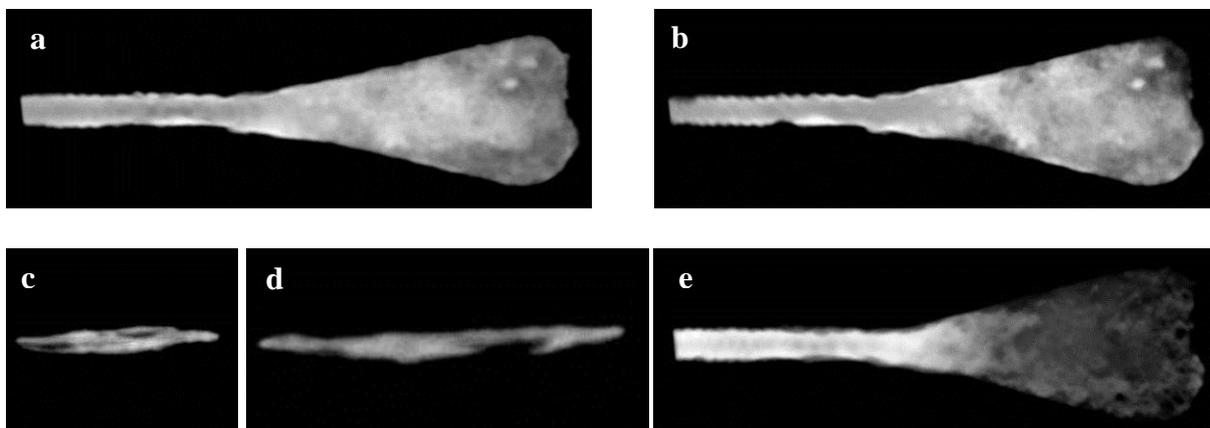
Figure 3.8. a) Neutron 2D image of SI1. b) Sagittal tomogram slice near the mid plane showing detachment of corroded metal in the blade as dark areas. c, d) Neutron tomogram axial slices illustrating lamination and flaking in the blade. e) X-ray 2D image showing the metal core in the same zone as in the neutron sagittal slice.

EDS analysis of the metal phase shows except for Si (0.1%) no traces of other impurities are present. The metal phase contains numerous inclusions in three different types which were scattered inhomogeneously (Appendix B. Fig.11). The numerous ones are elongated stringers of dark-grey glass surrounding the light dendrite or globule phase of wüstite (Appendix D. Table3.2: analysis SI1a and a1) (Appendix B. Fig.12). Dispersed elongated inclusions consisted of plain glass (Appendix D.

34

Table3.2: analysis SI1b) (Appendix B. Fig.13) and angular inclusions of dark-grey glass with high amounts of Si (>33%) were also detected (Appendix D. Table3.2: analysis SI1c and d).

The etched cross section of the pendant in its lobe shows a carburized structure (Appendix B. Fig.14) with a gradient between the maximum carbon content of 0.7-0.8 wt% on the exterior surface of the lobe (case) and the minimum of 0.2-0.4wt% in the middle (core). The same gradient is observable in the opposite direction between the maximum amount of 0.6 wt% at the interior surface towards the middle. The microstructure consists of allotriomorphs grain boundaries of ferrite with Widmanstätten intragranular and side plates morphologies at former austenite grains with eutectoid pearlite (Appendix B. Fig.15). The former austenite has ASTM grain size number 4 towards the inside and 6 at the outermost of the lobe. The microhardness is varied from the maximum of 230 H_V in dark zones and the minimum of 125 H_V in areas with low carbon content in the middle. This structure was formed by carburizing of the object in temperatures above the A3 temperature followed by fairly rapid cooling in air (normalizing).

SI3

This object that was identified by the archaeologists as a spatula, found in MST during the excavation of K8 in 1971 (Appendix A. Table: SI3). It has a triangular blade with a short shaft. The shaft has a round cross section with a spherical end. Except for trace of decay no other evidence of manufacture, wear or usage was found on its surface.

Neutron tomography of the object shows that it is not robust. The metal core is severely corroded and in some parts it has completely vanished. The original surface is uneven and extremely pitted. Low density corrosion products cover the entire surface area. The shaft has a loop in the top which was filled by corrosion products and seems such as a sphere now (Fig.3.9). A summary of the neutron tomography result of the object was given in Appendix D. Table: 3.1.
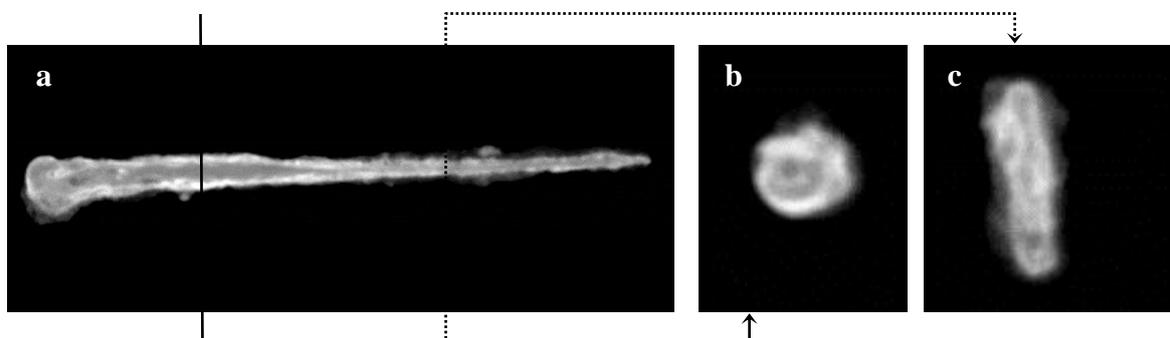
Figure 3.9. Neutron tomograms of SI3. a) Axial slice of the shaft. The penetration of corrosion into the metal core in this part has weakened the shaft. b) Axial slice of the blade. The remnant of original surface is uneven. c) Frontal slice. The sweat scraper has a looped shaft which is not clear among the corrosion.

35

3.2.3. Adzes

KI3

This adze is poorly provenance in archaeological context. The attached tag to the object shows it was found at K2 in 1971 but the excavation and the layer that the object was found are not clear. Except for trace of decay no other evidence of manufacture, wear or usage was found on its surface.

Neutron tomography shows that this adze has a robust continuous metal core. A thin layer of corrosion covers the surface of the object. A few flakes which are surrounded by corrosion are observed on the surface. In parts of the blade the corrosion penetrated the metal core and damaged the original surface thereby volume expansion of the corrosion products. (Fig.3.10). Based on axial slices, 37% of the object was corroded. A summary of the neutron tomography result of the object was given in Appendix D. Table: 3.1.
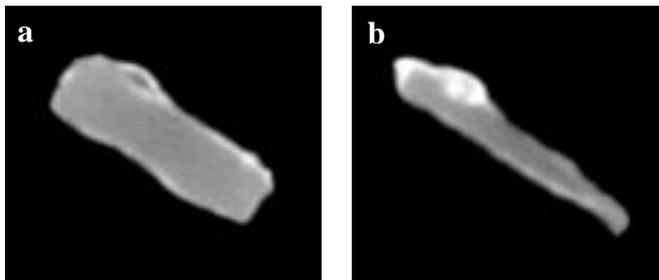
Figure 3.10. Neutron tomograms of KI3. Axial slices. a) Corrosion produced flakes on the surface of the object. b) Penetration of corrosion in the metal core caused defects on the original surface.

EDS analysis on the cross section of the adze that cut off from the narrow point of the shaft revealed a small amount of silicon (0.2%) in the bulk of metal as an impurity which was probably due to the dispersed fine silicate inclusions (Appendix D. Table3.2: analysis KI3). The sample consists of numerous inclusions, most of which have an irregular shape with a dimension lower than 25μm (Appendix B. Fig.16). Few of the inclusions have elongated along worked surfaces of the artefact. There were two kinds of inclusions that were distributed within the metal phase. A low number of multiphase inclusions with granulated structure, containing different compositions of glass, which is seen as globules of light phase in the centre (Appendix D. Table3.2: analysis KI3a) within a plain dark grey matrix (Appendix D. Table3.2: analysis KI3a1) (Appendix B. Fig.17). A great number of rounded and elongated glassy slags were dispersed across the sample with different elemental proportions which resulted in a different contrast in SEM BEI images (Appendix D. Table3.2: analyses KI3b, c) (Appendix B. Fig.16, 17). Low amount of detected calcium (0.3 – 3.4 wt%) in slag inclusions (Appendix D. Table3.2: analyses KI3a1, b and c) indicative of the use of iron ore with a lime content (Tylecote 1962).

The etched cross section shows homogeneous microstructure both in terms of carbon content and effects of temperature. The sample has an approximately 0.2 wt% carbon content on the basis of volume

36

fraction of pearlite zones. The ferrite laths with ASTM 8 shows Widmanstätten morphology (Appendix B. Fig.18). The average of microhardness is about $135H_V$. This structure would be formed by working at austenitizing temperature (above the A3 temperature) with subsequent fairly rapid cooling (Samuels 1980).

KI4

The adze was found at K2 at a depth of 30.5 cm in 1936. It has an almost triangular form with a broad sharp blade tip and a narrow cubic shank (Appendix A. Table: KI4). Except for trace of decay no other evidence of manufacture, wear or usage was found on its surface.

The sagittal and frontal slices of the neutron tomogram show the adze has a continuous and robust metal core from tip toward the shank. Corrosion is present as a thin layer on the surface of the whole object. The blade shank has a lamellar structure resulting from severe corrosion in this area. The lamellas are severely corroded and only a small section of metal connects them to the rest of the metal core. Narrow cracks which have been filled with corrosion products are seen close to and along this structure. Expansion of these products may induce more pressures in these zones. Consequently, after a while, the lamellar structure would extend further toward the inside (Fig.3.11a, b). Approximately 31% of the object contains corrosion products. On the surface, flakes that contain metal core are mostly surrounded by corrosion and have no connection to the rest of the object (Fig.3.11c). Presence of flakes and laminations on the surface will reduce the chance to have an even surface after treatment. Fortunately the number of flakes is low. A summary of the neutron tomography result of the object was given in Appendix D. Table: 3.1.
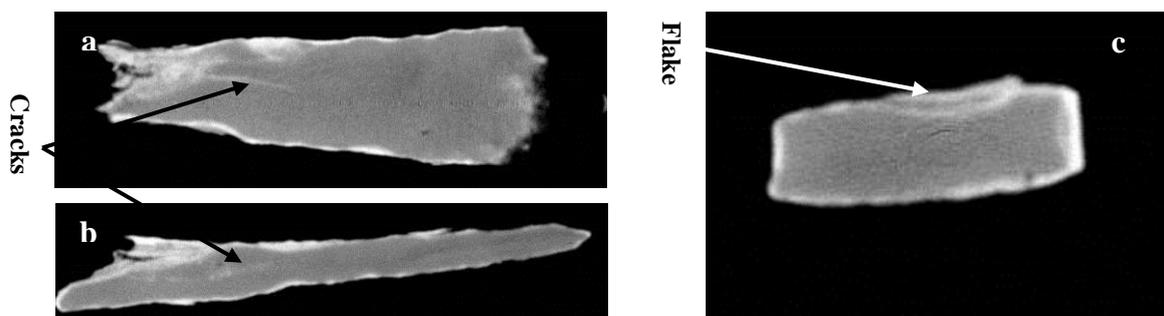
Figure 3.11. Neutron tomogram slices of KI4. a) Sagittal slice b) Frontal slice c) Axial slice.

SI2

This adze was found at the Mapungubwe Southern Terrace at a depth of 150-170cm below the surface during the excavation H5 in 1971. This adze (SI2) is larger than KI4 but has a similar shape. It has an almost triangular form with a broad sharp blade tip and a narrow cubic shank (Appendix A. Table: SI2). The object was sampled in the past and two big missing parts are visible both in the blade

tip and the shank. Examination of the two opposite broad sides of the object shows that the porous external corrosion layer was removed close to the area where a square sample was previously cut off (Appendix A. Table: SI2, Fig.3.12). It appears that the corrosion layer was removed by the stress formed during removal of the sample. The iron corrosion has a low cohesion to the metal substrate, especially the porous external layer which mostly consists of alkaline iron(III) products. These products have higher volume than the iron itself. Volume increasing in corrosion results in formation of cracks and porosity within corrosion layer. Consequently, the exerted force to the metal surface during sampling, especially by using Buehler wafering machine can result in peeling the corroded layer from the surface. A thick layer of rust can be seen on the rest of the object.

Neutron tomography result shows that the adze has a robust continuous metal core. Based on axial slices, 43% of the sample consists of corrosion products. A summary of the neutron tomography result of the object was given in Appendix D. Table: 3.1.

Figure 3.12. Neutron tomogram of SI2. Axial slice. Corrosion layer is only seen on two narrow edges of the object.

3.2.4. Chisel

KI5

This chisel is poorly provenance in archaeological context and has no exact source in the chronological sequence of the settlement. The attached tag to the object only shows it was found at K2. Except for trace of decay no other evidence of manufacture, wear or usage was found on its surface. The low corroded structure of the object indicates it might belong to a post-K2 and Mapungubwe period.

Neutron tomography result shows that this iron chisel has a continuous robust metal core. A short crack, filled by corrosion products, is seen within the tapered point of the sample (white line) (Fig.3.13a). A damaged part is also seen at the end of the shaft which is more obvious in the axial slices (Fig.3.13b). Here a flake of metal is completely surrounded by corrosion products. In the case of treatment of the object in chemical solution, this part may be removed and results in damaging of the object. Except in this case, corrosion is only observed on the surface of the object and did not penetrate deep inside. Based on axial slices, 15% of the object contains corrosion products. A summary of the neutron tomography result of the object was given in Appendix D. Table: 3.1.
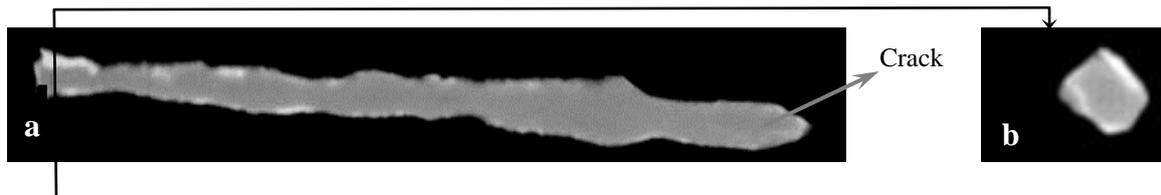
Figure 3.13. Neutron tomogram of KI5. a) Frontal slice. Small crack is seen along the sharp point. b) Axial slice of end point of shaft at the position of the line, shows presence of a flake.

EDS analysis of the drill revealed a small amount of silicon (0.1%) in the bulk of metal as an impurity which is probably due to finely dispersed silicate inclusions (Appendix D. Table3.2: analysis KI5a). The metal phase also contains 0.7 wt% nickel as the only metallic impurity. The sample contains four types of inclusions in low numbers. The inclusions mostly have a small spherical form (<10μm) with a fayalite composition (Appendix D. Table3.2: analysis KI5a) (Appendix B. Fig.19). The second and third types consisted of a few larger and more complex inclusions (>50μm) with irregular shape. These consist of two-phase of light wüstite dendrites in dark grey fayalite (Appendix B. Fig.20) (Appendix D. Table3.2: analysis KI5b and b1) and iron oxide. The inclusion of primary iron oxide contains angular sand grains and has located almost parallel to the surface (Appendix B. Fig.21). This indicates it was included during forging by entrapping surface oxide. There were also secondary iron oxide inclusions which were formed during penetration of corrosion in the metal phase. The fourth type of inclusion consists of irregular shaped glassy slag which was randomly detected in the metal matrix (Appendix D. Table3.2: analysis KI5c).

After etching, the sample showed inhomogeneity in terms of carbon content in a banded structure with a lesser lower amount towards the surface (~0.1 wt%) and around the poor parallel weld (Appendix B. Fig.21) which was induced by decarburization during forging in oxidizing condition (Appendix B. Fig.22) and 0.2wt% in the middle. The surface consisted of irregular nonequiaxed ferrite grains with small islands of pearlite as well as cementite film at the grain boundaries. Toward the middle of the sample this structure was gradually converted to proeutectoid grain boundaries ferrite with Widmanstätten side and intragranular plates along with eutectoid fine pearlite. This structure has almost 0.2 wt% carbon (Appendix B. Fig.23). The ferrite has an average grain size of ASTM 9 on the surface and the former austenite a grain size of ASTM 4 in the middle. Vickers microhardness is almost uniform in each part with 243 H_V in the middle and a maximum of 254 H_V on the surface. This structure was formed by heating the object to full austenitized temperature (the A3 temperature) followed by fairly fast cooling in air (Samuels 1980). This process results in the formation of irregular ferrite grains in the area with lower carbon content (0.1 wt%) while in the area with higher carbon (0.2 wt%) proeutectoid ferrite with obvious Widmanstätten morphology will be formed.

39

3.2.5. Arrowhead

MI1

Only one arrowhead was found in this selected assemblage. This object is poorly provenance and the archaeological context is not clear. The attached tag to the object only shows it was found at Mapungubwe Hill. Except for trace of decay no other evidence of manufacture, wear or usage was found on its surface.

The neutron tomograms show the arrowhead does not have a robust metal core (Fig.3.14). In the shaft the metal core is denser. In the sharp point of the arrowhead only a small quantity of metal is observed in the form of a thin sheet. This sheet has no even form and has a variable thickness in different parts. It seems that the original surface kept its form within corrosion products. Based on axial slices, 51% of the object consists of corrosion products which are mostly concentrated in the point of the arrow. Investigative cleaning is needed to find out more about the physical condition of the original surface within corrosion. The weak structure of the object prevented of sampling for microstructure study. A summary of the neutron tomography result of the object was given in Appendix D. Table: 3.1.
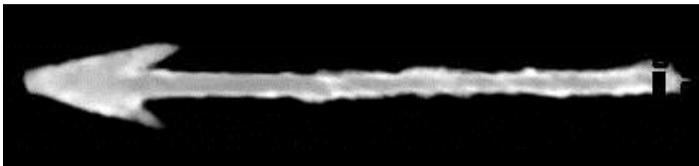
Figure 3.14. Neutron tomogram of MI1. Sagittal slice. Thin layer of iron is seen in the point of the arrowhead.

3.2.6. Hoes

3.2.6.1. Historical evidence on the surface of MI2, MI7, MI9 and MI10

Four iron hoes are present in this assemblage. Three of these hoes have a few similarities in their typology and one of them, MI2, is very different from the other three (Appendix A. Tables: MI2, MI7, MI9, MI10). Based on the state of preservation, MI2, MI7 and MI9 which are less corroded, appear to belong to a more recent date.

Although Fouché (1937) did not mention any iron hoes found during the first two archaeological expedition (1933-1935), MI9 (excavation No: 33.176) and MI10 (excavation No: 34.2) were listed in the excavation inventory (Fouché 1933). In this inventory, the hoes (MI9 and MI10) were listed as an 'iron pick' and an 'iron gad' respectively. Of these only MI10 has clear provenance that links it to the archaeological site where it was found. MI7 and MI9 were found in unknown rock shelters in the area adjacent to Mapungubwe Hill, and the provenance of MI2 is recorded as Mapungubwe in the accession register.

40

Fouché (1933) also referred to the European manufacture of MI9 due to the presence of a manufacturer's mark on it, but no additional information about the mark was recorded in this document. Consequently the specific provenance, as well as the history of MI9, is ambiguous. MI9 was found in association with glass beads, which were important items in the Indian Ocean trade network. This indicates the hoe was probably used as a trade item and exchanged with other goods from the interior.

In his account of the function of MI10 Fouché (1933) referred to it as a piece of iron (gad) that was probably intended to be an assegai. While broadening of the blade toward its tip shows the dedicated function to the object, is not commensurate with the finished shape of it. The broad blade of the object shows it most probably is a small iron hoe.

MI2 has a rectangular blade with a long semi-rectangular cross section handle which tapers toward the end (Appendix A. Table: MI2). The manufacture evidence on the surface of the hoe shows that it is incomplete. The surface of the blade was raised along the edges (burr) due to the hammering. The burrs became more obvious because the edges were forged in opposite directions. This formed a thick flat surface on these parts (Fig.3.15a, b, c).It appears that this stage was a preliminary step in several successive stages of narrowing the edges to produce a steep facet. In the next step the manufacturer would suppress the burrs by continuing forging of the blade's surface but these have remained intact.
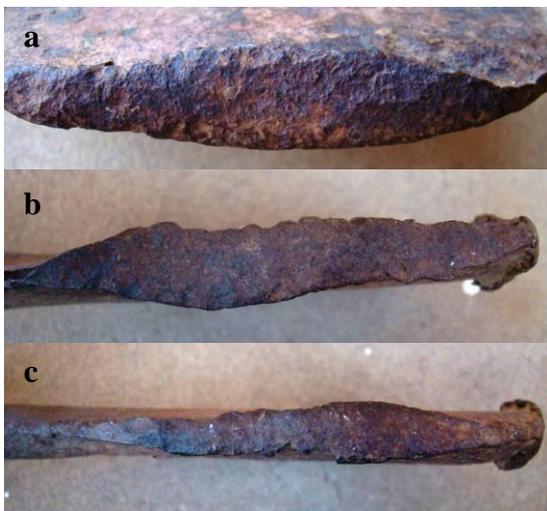
Figure 3.15. a) Thick flat surface on front edge of the hoe (MI2). b.c) Flat surface on the side edges

The manufacture of the handle appears to be more complete. The surfaces of this part, except for the traces of broad scratches that belong to a pincer-like device (Fig.3.16a) are smooth. These signs are seen in the same places on both sides of the handle and show how the inward force of hammering caused the tightly held pincers to move in opposite direction. Measurement of these impressions (~6.75 mm in broader sign) indicates that the pincer blades were narrow. The sharp edge of the marks shows that it was probably a metal tool with incised edges. In addition to these marks, the metal was

41

flaked on one side of the shaft. This flaking indicates that the hoe shaft was probably fixed to the hard surface of an anvil during hammering of the blade tip. The force of hammering resulted in sudden slipping of the hoe from the anvil. Scrubbing of the hoe handle and the hard anvil edge peeled the metal surface (Fig.3.16b). Compared to the other ones the shaft of this hoe has no sharp edges.
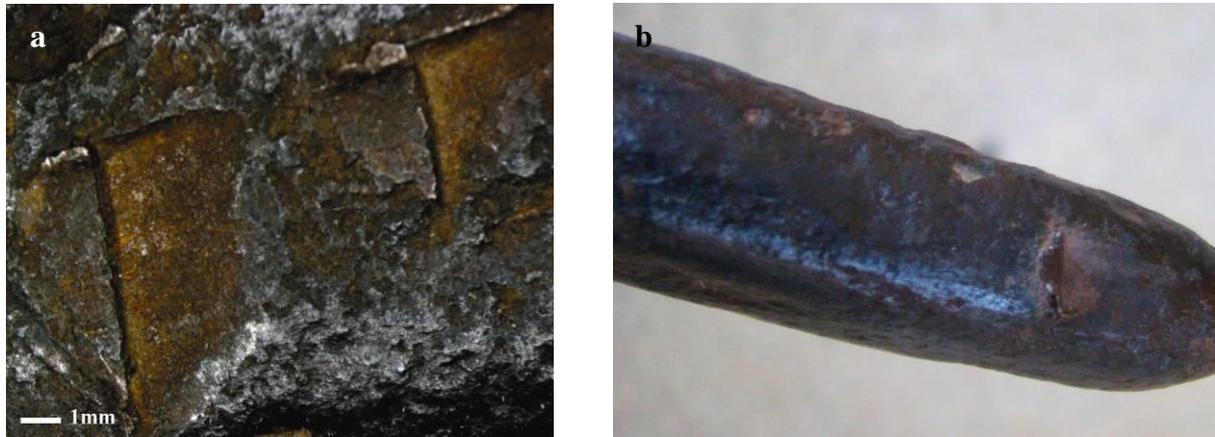
Figure 3.16. a) The broad scratch marks on the shaft of hoe (MI2). b) Foliation the metal caused by scrubbing with another hard surface probably a metal anvil.

MI7, MI9 and MI10 are more similar in their typology (Appendix A. Tables: MI7, MI9, MI10). Their blades are almost scapula-shaped and joined to the handle at an obtuse angle. They, however, are different in size. The blade tips of these hoes were completely sharpened. The signs of creasing (burr) on the edges of the MI7 and MI9 blades are due to forging (Fig.3.17a, b). These are clear to the naked eye, while the heavily corroded structure of MI10 obscured all traces of manufacture on the surface.
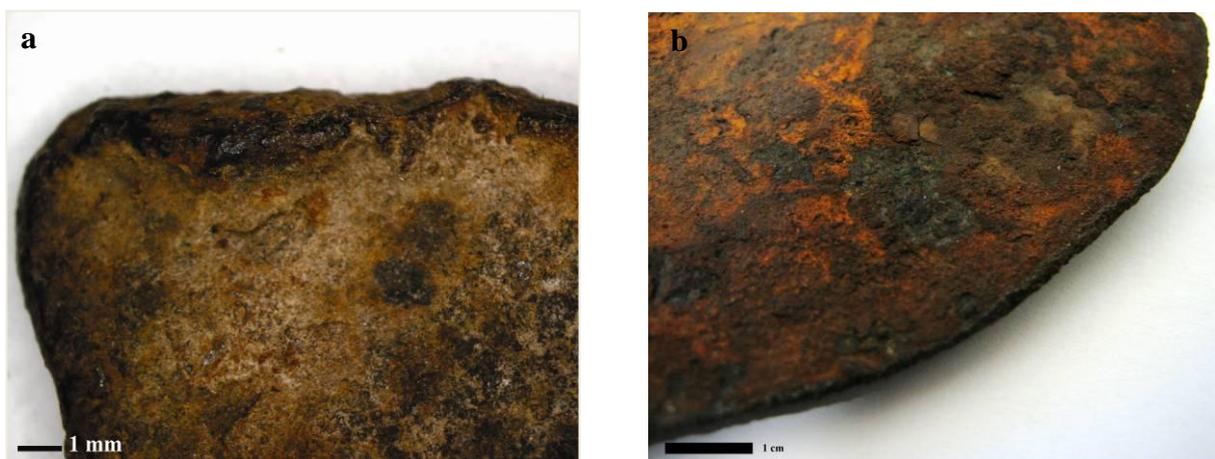
Figure 3.17. a) Creasing marks on the blade edge of MI7. These marks are seen continuously along the edge b) Creasing marks on the blade of MI9. The creases here are more delicate than MI7 and are not continuous.

42

The handles of these hoes have rectangular cross sections which taper toward the end with sharp edges. MI10 has a short narrow handle and the handles of the other two are longer and thicker. The typology of MI10 is similar to one of the iron hoes from Great Zimbabwe, which dates from the mid 14th to the mid 16th century (Fig.3.18a). There, however, is a key difference. Most of the hoes from Great Zimbabwe have a loop on the shaft (Miller 2002) which is not seen in the Mapungubwe assemblage. No abrasion lines were observable on the shaft of low corroded hoes (MI7, MI9) which indicates that hard material was not used to cover this part as a handle. It is however possible that a softer material such as a wooden cover was used to cover.

As Fouché (1937) noted, a delicate script in English is present on the handle of MI9 which is hardly discernible to the naked eye due to corrosion and calcareous deposit (Fig 3.18b). It consists of two short lines. The depth of the impression in both of the lines was reduced to the same degree from left to right which indicates that the lines were formed at one stage of the metalworking process, for example by sealing. In the first line a few of the letters are barely recognizable. Neither the naked eye nor microscope could render them legible, but the incomplete word BIRMINGHA in the second line is identifiable. It is likely that the word is Birmingham. This would indicate to a United Kingdom manufacture provenance, and the illegible first line could be the name of the manufacturer.
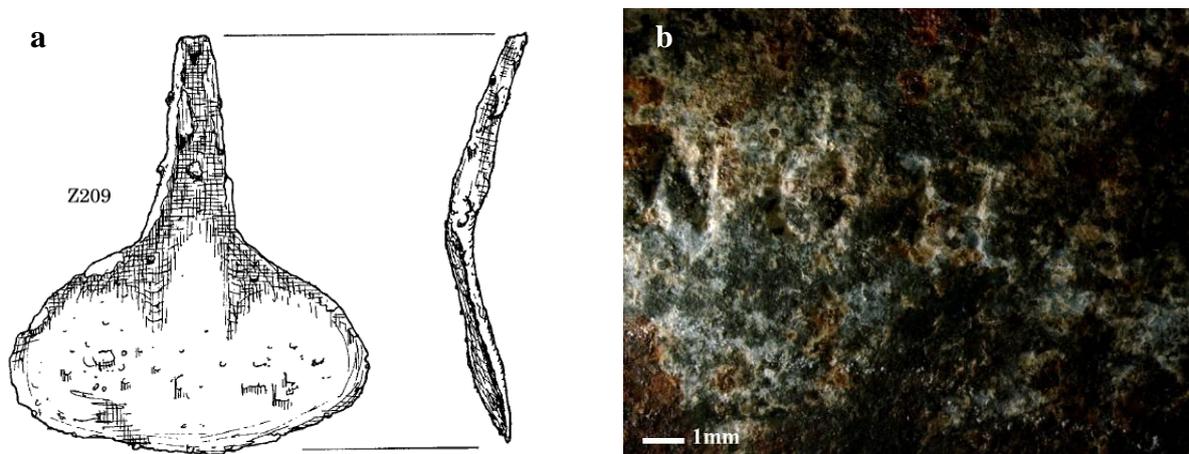
Figure 3.18. a) Iron hoe from GreatZimbabwe. Adapted from Miller (2002). b) A part of sealed script on the handle of hoe (MI9)

The presence of a script with capital English letters on the handle of MI9 may be an indicator that this long handled hoe (MI9) does not belong to the heyday of Mapungubwe during 1220 and 1290 AD. Birmingham has been a centre of metalworking in Great Britain since the 16th century (Miller, 1851), while the trading of fabricated items were only started in the 18th century and thrived during the Victorian era (Timmins 1866; Upton 1993). Consequently MI9 may simply have been brought to the site by the arrival of British traders in the late 18th to19th centuries onwards. This would not be

43

surprising as there are several historic sites in the region. These have yielded trade goods such as historic glass beads. Wood (2000, 2005) argued, based on typological grounds, that a substantial number of the beads in the Mapungubwe collection also post-date the medieval occupation.

Among these hoes only MI7 shows traces of post excavation treatment. A large, probable missing part of its, handle was filled with a white filler material like plaster.

A more precise idea about the manufacture of this assemblage, particularly in the case of (MI2, MI7), and the period of their production could only be determined by further analytical-metallographic study and comparison of the results with conventional manufacture methods in southern Africa during the Iron Age period.

3.2.6.2. *Neutron tomography and microstructural study of the iron hoes*

MI2

The neutron tomograms show that this hoe is robust with a continuous metal core. The brightness contrast of the metal core in the blade and the shaft in the neutron tomograms (Fig.3.19a, b) is related to low interaction of neutrons with iron. Consequently, a difference in thickness of the object can result in a brightness contrast in images. A summary of the neutron tomography result of the object was given in Appendix D. Table: 3.1.
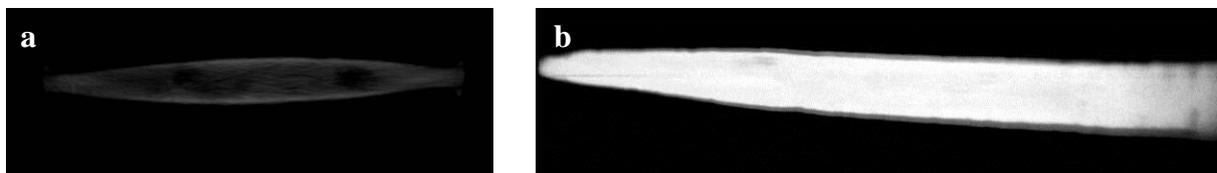
Figure 3.19. Neutron tomograms of MI2. a) Axial slice of the blade. b) Sagittal slice of the shaft.

The analysis of the metal phase indicated that, apart from carbon which cannot be detected by EDS, there were no other impurities (Appendix D. Table3.2: analysis MI2). There were numerous elongated glass inclusions parallel to the surface of the blade. These elongated inclusions have a granular structure, which was mostly surrounded by the voids (Appendix B. Fig.24, 25). The inclusions contain a high amount of calcium (13.5 wt %) which is equivalent to almost ~ 28.4 wt % CaO (Appendix D. Table3.2: analysis MI2a). The calcium content of this slag is quite high for common bloomery iron slag. Tylecote (1962) argued that the slag with a high amount of lime (lime >15 wt%) and low FeO content has a high free-running temperature and only forms when the temperature of the furnace is high enough (1600 ºC in a modern blast furnace) to allow the lime to react with other impurities in the ore. He furthermore maintains that the lime may not be absorbed by the slag in such quantities (higher than 6%) in a primitive iron smelting process with the temperature that cannot exceed 1200ºC. This indicates that the smelting temperature of the iron ore that was utilized in the production of the hoe was much higher than 1200ºC and might have been smelted in a blast furnace. There were also a few

44

iron oxide and slag inclusions close to the surface which were formed during the penetration of corrosion along the entrapped slags.

The form and distribution of the inclusions in the shaft are quite different from the blade which is due to the different orientation of the sections. Here the inclusions are visible close to the surface and in irregular form (Appendix B. Fig.26). They mostly consist of two-phase inclusions of light grey grains within a darker phase which were embedded in the voids (Appendix B. Fig.27). There were also large complex glass and oxide inclusion with transversely fractures in the glassy phase due to the hammering below transformation temperature of the glass (Appendix B. Fig.28). The transformation temperature, depending on the composition of glass, is almost in the range of 500°C to 700°C (Babcock 1977).

Etching the sample in nital revealed a spheroidized structure of cementite in a matrix of ferrite with a non uniform grain size (Appendix B. Fig.29). One of the blade's broad surface layers has irregular coarse ferritic grains with ASTM 6 while the rest consists of fine grains of ferrite with an average ASTM 10. The micro hardness is varied with a minimum amount of 108 H_V among the coarse grains which were almost decarburized, and a maximum of 163 H_V in the rest with a maximum distribution of spherical cementite particles (Appendix B. Fig.30). The carbon content of the sample, with consideration of the volume fraction of cementite compared to the reference micrographs with the same magnification that were submitted by Samuels (1980), varies between 0.2 wt% on one broad surface of the blade and 0.6 % in the other areas. This structure as described by Samuels (1980) could have been formed by forging in the partial austenitizing zone, the temperature above the A1 temperature, with subsequent annealing below but close to the A1 temperature for a prolonged time which is subordinate to the annealing temperature and the degree of prior cold work. The grain coarsening effect is possibly due to the critical growth of ferrite grains which were subjected to cold working such as when forging was completed at a temperature slightly below the A3 temperature. This temperature can also result in partial decarburizing of ferrite grains on the surface in the oxidizing environment of the forging hearths. Lack of cementite particles in the grain boundaries of the decarburized area allows the grain boundary to migrate easily without any restraining influence, and the formation of coarse grains on one of the surfaces during annealing.

The transverse section of the handle shows a compositional gradient between the maximum carbon content of 0.8 wt% on one lateral surface and almost 0.08wt% in the point of the shaft. In a higher carbon content zone most eutectoid colonies of pearlite were partially spheroidized within a former austenite grain boundary with microhardness 250 H_V (Appendix B. Fig.31). Toward the point of the shaft, carbon was reduced gradually to produce proeutectoid ferrite grains along with degenerated pearlite island and spheroidized cementite within grains with a micro hardness 204 H_V (Appendix B. Fig.32). Exactly on the point equiaxed ferrite grains with ASTM 5 and microhardness 230 H_V have inter and intragranular etch pitting. In the meantime an α-veining substructure was developed by etching of subgrain boundaries (Appendix B. Fig.33) which is due to the formation of etch pitting at

45

the walls of dislocation at the subgrain boundaries by slow cooling of a temperature below the A3 temperature (Samuels 1980).

While considering the metal microstructure in both the blade and shaft, it seems the hoe was manufactured of a close to eutectoid as normalized steel with a carbon content of between 0.6-0.8 wt%. The steel was forged in a temperature below the A3 temperature which resulted in critical grain growth on one of the surfaces during annealing. The object then fully annealed in a temperature below but close to the A1 temperature which resulted in full spheroidizing of the cementite plate in areas of intensive forging (blade) and partial spheroidzing in areas with a lower degree of reduction by cold working (shaft). The object was then air cooled.

MI7

The neutron tomograms show that MI7 has a continuous and robust metal core. The handle has a gap which was filled with plaster. A broad arrow shape which is seen beneath the filler appears to be an impression mark within the object surface. Beneath the arrow the material constituent of the object has a different composition or density (Fig.3.20a- c). A summary of the neutron tomography result of the object was given in Appendix D. Table: 3.1.

Figure 3.20. Neutron tomograms of MI7. a) Frontal slice. An arrow shape was appeared next to surface among plaster. b) Sagittal slice. The depth of the gap is observable. c) Axial slice. It seems the arrow form has placed close to the surface and among the plaster.

Material with lower contrast under the arrow mark

Cross section of arrow
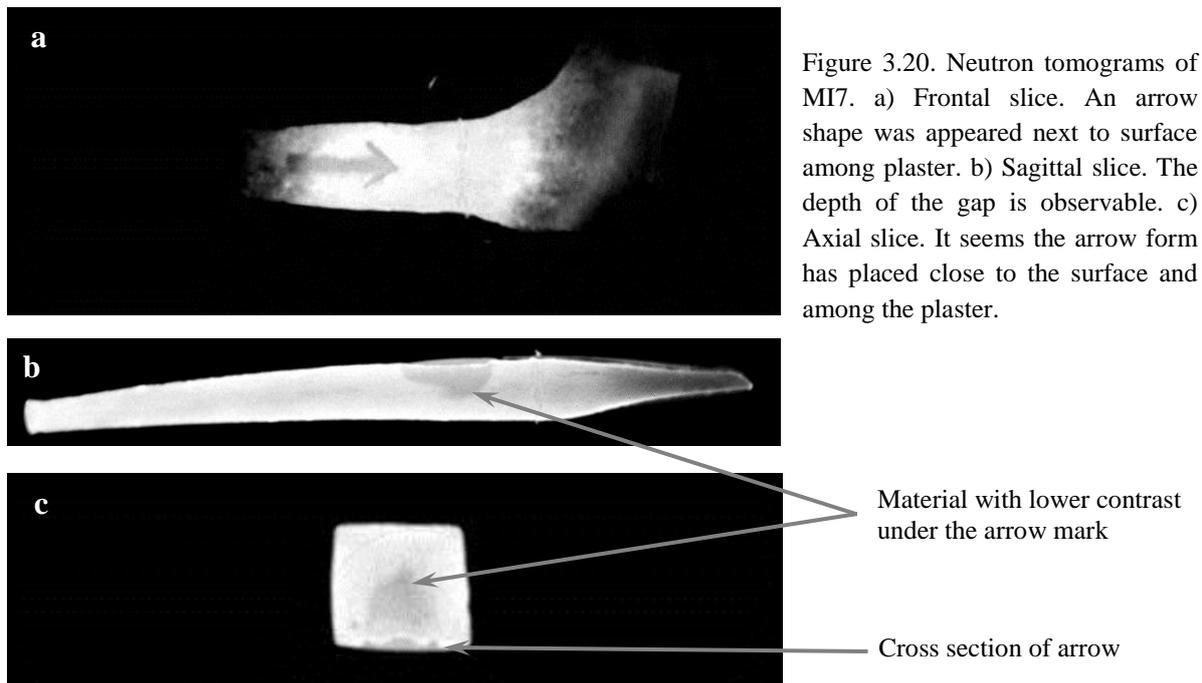
The broad arrow is the most common mark of British government ownership in Britain and its commonwealth countries such as South Africa. The mark has been imprinted on Enfield rifles, bayonets and related military kit alone, above or between letters. The arrangement of the mark alone or among the letters has various concepts while the accompanying letters give more information about the history and origin of the object. Here the sole arrow is only a government acceptance mark which

means the hoe passed quality control and was accepted into service. This hoe might be a part of military equipment and probably dates to before the formation of Union of South Africa (1909 AD). After this date the broad arrow was emerged within the U.

The result of EDS analysis revealed low amounts of Si and P (0.1%) as impurities in the metal matrix (Appendix D. Table3.2: analysis MI7). There were numerous elongated slag stringers parallel to the heavily forged surfaces (Appendix B. Fig.34). These inclusions contain globules or dendrite of wüstite (Appendix D. Table3.2: analysis MI7a1) that precipitated in a dark-grey matrix of glassy phase (Appendix D. Table3.2: analysis MI7a1). The inclusions were distributed homogeneously along the sample. Cross section of the handle showed that, unlike the blade, the inclusions have angular forms with a fractured structure within (Appendix B. Fig.35). The difference in general form of inclusions in blade and shaft is generally due to difference in cutting orientation. There were numerous inclusions in different size with the maximum length of 300μm. It appears that the inclusions have the same composition as the blade.

The etched sections of the blade and handle revealed that the hoe was manufactured of a low-carbon steel (0.08 wt%) with an almost homogeneous microstructure consisting of equiaxed ferrite grains with a thin grain boundaries film of cementite (Appendix B. Fig.36). The ferrite grains contain tiny precipitates, probably carbide or nitride (Samuels 1980). Towards the blade tip and handle point, shear bands within the ferrite grains are indicative of deformation, probably by cold working after final heat treatment or even utilizing the hoe. The ferrite has an ASTM grain size number 6 and a microhardness of 133 H_V in the middle of the blade while towards the tip the grain size dropped to 8 and microhardness rose to 247 H_V. This structure was formed by forging followed by annealing in a temperature slightly above the A1 temperature which resulted in the formation of a thin film of cementite at the ferritic grain boundaries while the grain size is still small and microhardness is high. Reducing the grain size and increasing the microhardness at the blade tip is due to later cold working. It appears that the dark zone under the arrow mark (Fig.3.20) on the handle was formed by forging a seal in this area which caused some deformation in the ferrite grains structure which was not eliminated by final heat treatment.

MI9

The neutron tomograms show that MI9 is completely robust. The metal core is unceasing along the length of the hoe (Fig.3.21). The first line of the sealed script on the handle is also illegible when using tomography, since the depth of the impression on the surface was too low and corrosion completely deformed a few of the letters. Consequently the neutron slices that belong to this part of the object also did not reveal the imprints of the words. The contrast between the blade and handle is related to their different thickness. A summary of the neutron tomography result of the object was given in Appendix D. Table: 3.1.
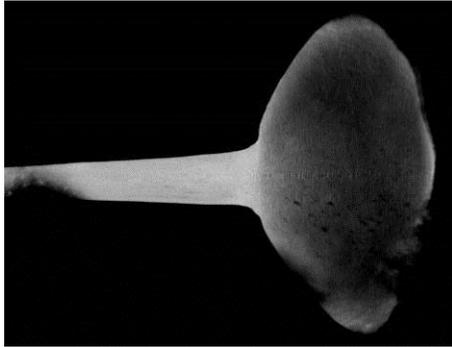
Figure 3.21. Neutron tomogram of MI9. Frontal slice. Voids are obvious in half part of blade.

The EDS analysis result revealed about 0.3% phosphorus as impurity in the metal phase (Appendix D. Table3.2: analysis MI9). The longitudinal sample of the hoe blade contains numerous elongated and more or less spherical inclusions. Elongated slag stringers were placed along the length of the heavily worked surfaces in a banding structure. Some of these included dendrite of wüstite within a matrix of dark-grey glass (Appendix D. Table3.2: analysis MI9a and a1) and a few completely contained glassy phase (Appendix B. Fig.37). There were also complex inclusions of iron oxide and slag that were formed by the penetration of corrosion along the slag in the metal phase (Appendix B. Fig.38). Cross section of the shaft shows two kinds of inclusions. Several angular inclusions along with lower numbers of elongated ones contained dendrite of wüstite in a matrix of the glassy phase. Some of these inclusions were completely fractured.

The etched section of the blade shows the metal is hypoeutectoid steel with almost 0.08 wt% carbon content. The microstructure consists of massed equiaxed ferrite with ASTM grain size 6.5 and microhardness 260 H_V. The grains are coarser toward the surface and in the middle with ASTM 3 (Appendix B. Fig.39). Cementite is present as a thin film at the grain boundaries whereas in the small zone in the middle, particles of cementite are also seen within the grains and around the inclusions. In this area the microhardness fell to about 165 H_V and revealed lower amounts of carbon remaining in the solution in the ferrite (Samuels 1980). On the basis of evidence presented by Samuels (1980) this structure was formed due to forging at lower, but close to the A3 temperature (850°C), followed by annealing at a temperature slightly above the A1 temperature which resulted in the formation of cementite grain boundaries as well as critical growth of ferrite grains on the surface and in the middle due to the presence of a certain degree of deformation. The high microhardness of the blade can be partly due to a low amount of phosphorus in solution in ferrite. Microstructure in the transverse section of the shaft with ferrite ASTM grain size 8-11 is the same as the blade while plastic deformation of grains towards one lateral surface with shear banding is an indication of cold working after the final annealing (Appendix B. Fig.40). Here the microhardness is about 297 H_V which is higher than that of blade which could be as a result of finer grain size and final cold working.

MI10

The neutron tomograms show that this iron hoe has a thin weak blade. The metal core has completely disintegrated on the two opposite sides of the blade. The blade has such a thin structure near the edges, that the low interaction of neutrons in these areas produced an image from which these parts are absent (Fig. 3.22). Consequently, the missing areas in the neutron image appear more extensive than in the object itself. A summary of the neutron tomography result of the object was given in Appendix D. Table: 3.1.
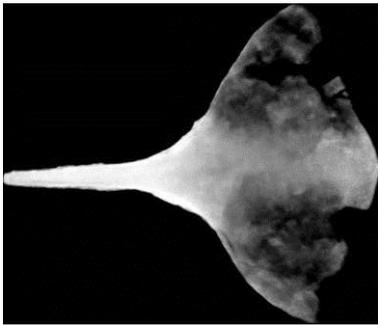
Figure 3.22. Neutron 2D image (radiograph) of MI10. Physically unstable blade is observable in this image. The missing parts in this image are larger than its documented photos. It is as the result of low interaction of neutrons with low thickness parts.

The EDS analysis shows that the iron, without consideration of carbon content, is pure (Appendix D. Table 2.4: analysis MI10). The cross section of the blade shows that low numbers of two different types of inclusions were dispersed within the sample. There was an oxide inclusion that contains two different iron oxides with fossilized sign of grain boundaries (Appendix D. Table3.2: analyses MI10a and a1) (Appendix B. Fig.41).There were also fine elongated stringers of glassy slag with prominent difference in their Ca content (Appendix D. Table3.2: analysis MI10b and c) passing along the forged surfaces (Appendix B. Fig.42). MI10b shows a high amount of Ca content (10.9 wt%) equal to almost 15.2 wt% CaO which is higher than the maximum reported amount in primitive bloomery slags (6 wt% CaO) formed in the smelting of iron ore with lime content (Tylecote 1962). This evidence indicates lime was probably entered unintentionally in smelting of the iron in a proportion close to the maximum amount (15 wt%) that was capable of reducing the melting point by about 50°C (Tylecote 1962). In the shaft the inclusions have a higher concentration than in the blade. There were elongated and more or less spherical forms of almost the entire glass inclusion together with a wüstite-like globule in an intermediate of dark-grey glass (Appendix B. Fig.43).

The etched section of blade shows slightly inhomogeneous hypoeutectoid steel with a gradient in carbon content of between the minimum amount of 0.4% in the middle and the maximum of 0.6 wt% towards the surface (Appendix B. Fig.44). The microstructure consists of grain boundaries allotriomorphs of ferrite along with Widmanstätten side and intragranular plates at former austenite grains with microhardness 168-189 H_V and ASTM grain size of 6 (Appendix B. Fig.45). The etched cross section of shaft also revealed inhomogeneity in term of carbon content with a gradient from

almost 0.08 (pure iron) to 0.2 wt% towards opposite lateral surface (Appendix B.Fig.46). The pure iron zone consists of equiaxed ferrite grains with thin film of cementite at grain boundaries and tiny precipitated particles of probably carbide or nitride at grain boundaries and within the grains (Samuels 1980) (Appendix B. Fig.47). Here the ferrite grains have ASTM grain size number 6 and the microhardness 95 H_V. This structure is gradually converted to irregular ferrite grains with eutectoid pearlite islands which have ASTM grain size number 5 and microhardness 145 H_V.

High carbon content of the thin blade with slight increasing in its weight percentage toward the surface can be a sign of carburization. This structure was formed by carburizing of almost pure iron in full austenitizing temperature (above A3 temperature) in the reducing condition of the hearth followed by fairly rapidly cooling which led to formation of ferrite grain boundaries with Widmanstätten structure in the blade and irregular ferrite grains with the same structure in the zones with 0.2wt% carbon content in the shaft. A low amount of carbon content in the shaft indicates the blade was intentionally subjected to the carburization.

3.2.7. Wires

MI4

MI4 was found within the discarded archaeological deposit in the northern dump at Mapungubwe Hill (Appendix A. Table: MI4). This artefact is a hook which was manufactured from a piece of round wire with a sharp point at one end. The wire was bent in the opposite directions to form a hook in one side and a loop in the other side. Except for trace of decay no other evidence was found on its surface. The neutron tomograms show the object is robust with a continuous metal core. Rust is only seen on the surface and appears almost parallel to the metal core. In two different places corrosion crust has been flaked from the surface (Fig.3.23a, b). Here the original surface is damaged. Based on axial slices, 35% of the object contains corrosion products. A summary of the neutron tomography result of the object was given in Appendix D. Table: 3.1.
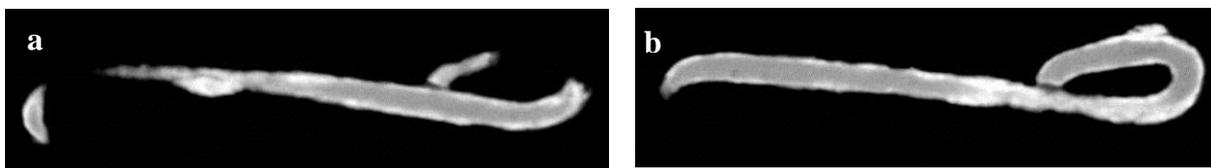
Figure 3.23. Neutron tomograms of MI4. Sagittal slices. a,b) lamination of corrosion products from the surface.

The EDS analysis of the iron hook identified small amounts of silicon and phosphorus (0.1%) in the bulk of the metal as impurities. Silicon can be due to probable dispersed fine silicate containing

50

inclusions (Appendix D. Table3.2: analysis MI4a). Phosphorus might have been derived from ore, flux, ceramic refractory or fuel was used in smelting. In this process phosphorus containing compounds are reduced to phosphorus vapour and absorbed by the metallic phase (Schmidt 1997). The iron also contains a low amount of nickel (0.3 wt%) as impurity that in this quantity might have originated from ore (Tylecote 1962). The cross section revealed numerous fine stringers of glassy slag elongated parallel to the surface (Appendix D. Table3.2: analysis MI4a) (Appendix B. Fig.48). Angular glassy inclusions (Appendix D. Table3.2: analysis MI4b) were also detected (Appendix B. Fig.49). The sample also contains oxide and slag inclusion which was formed due to the penetration of corrosion along the entrapped slag.

The etched transverse section shows the sample as inhomogeneous in terms of carbon content in the range of 0.1 wt% in peripheral as well as around the poor weld in the middle (Appendix B. Fig.50) and 0.2 wt% in a restricted lateral band zone which was bent toward the middle (Appendix B. Fig.51). The low carbon area consists of laths of recrystallised ferrite with ASTM 11 and pearlite islands. Meanwhile the ferrite is in the form of grain boundaries allotriomorphs with Widmanstätten intragranular plates and side plates at former austenite grains with ASTM 7 in zones with a higher carbon content. Microhardness varies between the maximum of 279 H_V in areas with Widmanstätten structure and the minimum of 266 H_V in decarburized zones. It seems the object was fabricated from 0.2 wt% carbon steel which was decarburized partially during forging in oxidizing condition. In the final stage the object was fully austenitized at temperatures above the A3 temperature and cooled fairly rapidly. This heat treatment resulted in the formation of ferrite boundaries with Widmanstätten intragranular and side plates morphology on former austenite grain boundaries in areas with almost 0.2 wt% carbon (Samuels 1980) (Appendix B. Fig.51). In the meantime in decarburized zones, laths of recrystallised ferrite and pearlite islands were formed.

MI8

This piece of block- twisted strip is poorly provenance in archaeological context and has no exact source in the chronological sequence of the settlement. The provenance of MI8 is recorded as Mapungubwe Hill in the accession register. This artefact is manufactured from a strip of iron with the width of 6.25mm and the thickness of 1.76mm. The strip was twisted about its axis to take a spiral shape that is seen in Appendix A. Table: MI8. This process is the first step in production of solid wire with constant diameter along the length. Oddy (1977) as well as Newbury and Notis (2004) mentioned that the twisted strip is then converted to wire by rolling it between two flat surfaces such as two flat pieces of hard wood. The block- twisted strip from Mapungubwe did not go through the second step of this method. This means it could be a piece of a strand of block-twisted wire which was broken during its manufacture.

51

The neutron tomograms show that the strip has a robust metal core with a thin layer of corrosion products on the surface (Fig.3.24). Based on frontal slices 22% of the sample consists of corrosion products. A summary of the neutron tomography result of the object was given in Appendix D. Table: 3.1.
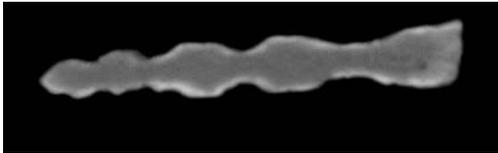
Figure 3.24. Neutron tomogram of MI8. Frontal slice.

The EDS analysis revealed no trace of impurity, apart from carbon that cannot be detected by this technique in the metal phase (Appendix D. Table3.2: analysis MI8). The cross section of the block twisting wire shows numerous scatter inclusions some of them elongated across the heavily worked surface (Appendix B. Fig.52). There were two types of inclusions mostly plain glassy slag (Appendix D. Table3.2: analysis MI8b) or in lower number the glassy phase accompanied by globule of wüstite (Appendix D. Table3.2: analysis MI8a and a1) (Appendix B. Fig.53). Few of the glassy inclusions, mostly toward the surface, were transversally fractured which indicates the object was forged in temperatures below glass transformation temperature which is in the range of 500-700°C (Babcock 1977). The sample also revealed the existence of fine cracks within the metal phase (Appendix B. Fig.54). It can be due to both tension and residual stress that were formed by the wire method of manufacture.

The etched cross section revealed that the metal is hypereutectoid steel with almost 1.1-1.2 wt% carbon content which was decarburized in a restricted zone around an entrapped oxide inclusion during forging (Appendix B. Fig.55). The structure consists of eutectoid coarse pearlite with thin cementite allotriomorphs grain boundaries at former austenite grains with microhardness 292 H_V. Disorder among cementite grain boundaries and coarse pearlite prevented estimating the grain size in this sample. In decarburized area the carbon content is about 0.1-0.4wt% from the margin toward the internal zone with a higher carbon content (Appendix B. Fig.56). Here the microstructure consists of eutectoid pearlite islands and laths of ferrite with ASTM 11. The microhardness is only slightly lower than the hypereutectoid zone with 287 H_V. This structure was formed by austenitizing the object above the A_1 temperature followed by slow-cooling (annealing) as the final heat treatment. The hard and brittle cementite phase which was formed at former austenite grain boundaries in this process reduced the steel ductility and gave rise to formation of cracks along grain boundaries during utilizing the object and/or in an interment environment.

3.3. Summary and conclusion

3.3.1. Classification of the exposed physical signs of manufacture

The exposed signs of manufacture, use, and wear on the surface or within internal structure of the iron objects which were revealed by observation of the surface and neutron tomography can be summarized as follows:

1. Scratch marks

Broad scratches are seen on the surface of the hoe shaft (MI2). These scratches have been formed during the manufacturing process of the objects. These marks are the traces of tongs used for gripping the hoe during forging.

2. Crease (burr)

Crease marks are seen on the blades of the iron hoes (MI2, MI7, and MI9) and are a direct result of forging.

3. Impression

The impression marks were found on the handle of the iron hoes (MI2 and MI9) in the form of a broad arrow and a Manufacturer's inscription respectively. This is evidence that these hoes belong to a later period (late 18th century and later) long after the heyday of Mapungubwe.

3.3.2. Composition, microstructure and manufacture methods

A summary of the microstructural description of the iron artefacts on the basis of metallography results is submitted in Appendix D. Table3.3.

3.3.2.1. Metal composition

The iron artefacts were mostly pure in terms of external metallic elements and only alloyed by carbon in various proportions in the ranges of pure iron (0.08 wt% carbon) to high carbon steel (1.2 wt% carbon).Two of the objects (KI5, MI4) contain low amounts of nickel, 0.7 and 0.3 wt% respectively as metallic impurity. Tylecote (1962) argued that iron ores, with few exceptions, contain less than 0.2% Ni. This means that this low amount of Ni, with possibility, might have originated from iron ores. Considering that no trace of Ni was detected within the indigenous iron artefacts with authentic provenance in K2 and Mapungubwe, it is possible that these two artefacts were fabricated elsewhere by means of a different ore composition. Typology and the well preserved structure of the

53

two objects reinforce this hypothesis that these two artefacts belong to a later date and were left on the sites.

Phosphorous is a non-metallic impurity that was detected in low amounts of 0.1- 0.3wt% in MI4, MI7 and MI9. Its origin might be ore, fuel, flux or even ceramic refractory or tuyeres (Schmidt 1997). In the cases of MI7 and MI9, as will be discussed later, the origin of phosphorus may not be the tuyere.

The objects are mostly uneven in terms of carbon content. Three of the four iron artefacts with precise provenance (KI1, SI1 and MI10) in addition to those that were re-excavated in Mapungubwe dump (MI4 and MI8), and some of the well preserved objects (KI5, MI2) with dissimilar typology from the indigenous ones are in this category. It seems this inhomogeneity is mostly due to unintentionally carburizing or decarburizing in the course of forging in the hearth. Two of the iron hoes (MI7 and MI9) have the lowest amount of carbon in comparison with the indigenous iron artefacts from K2 and Mapungubwe. These were fabricated of homogeneous pure iron (almost 0.08 wt% C) with numerous inclusions contain wüstite in dark glass. This microstructure is quite similar to the produced wrought iron in the puddling process which was a development in the refining of pig iron in the late 18th to 19th centuries in Europe (Samuels 1980). This criterion, in addition to other typology characteristics mentioned before in section 3.2.6, indicates that the hoes belong to a period (late 18th to 19th century), much later than Mapungubwe (1220-1290 AD).

Both hypereutectoid steel (C>0.8%) and hypoeutectoid steel (C<0.8%) were utilized in manufacture of the artefacts. MI8 was fabricated of hypereutectoid steel with 1.2 wt% carbon content. The microstructure of this artefact with cementite allotriomorph grain boundaries is not a desired structure in metalworking and results in brittleness along these lines of weakness. Grain boundaries of cementite were also discovered at MI6 with the same fractures along lines of weakness although it seems the microstructure was rather formed by annealing of hypoeutectoid steel with carbon content near eutectoid slightly above the A1 temperature. In such a case (MI6), estimating the exact carbon content could be helpful to better interpret the microstructure while the small size of the samples restricted the use of such an analyzing method in this study.

3.3.2.2. Inclusions

All the artefacts have numerous inclusions that, on the basis of composition and structure, were classified as follows:

1. *Iron rust inclusion*. These inclusions mostly contain different compositions of iron oxides or oxyhydroxides on the basis of various contrasts they have in SEM BSE images. In some cases (KI1, KI5, MI2, MI4 and MI9) iron rust is accompanied by dark glassy slag which could be formed by penetration of corrosion along the slag phases during interment (secondary iron oxide) or together with the glassy phase they are a remnant of un-expelled slag during forging. In one case

54

(KI5) entrapped iron corrosion within the metal phase is also seen parallel to the surface together with quartz grains which were formed during forging (primary iron oxides) and probably by folding of the shaft rim over the forged surface. MI10 contains a two phase iron oxide inclusion in the metal phase with ghost signs of former grain boundaries which indicates that it was formed as a result of corrosion during burial or even later while in storage.

2. *Glassy slags*. All the samples contain angular or stringers of glassy inclusion with different proportions of elemental constituents in an amorphous structure. The elongated inclusions were generally parallel to the worked surface and frequently had transverse fractures (KI1, MI2, MI7, MI8, MI9) due to forging below the transformation temperature of the glassy phase which is variable with composition (Babcock 1977). Most of the glass inclusions in iron artefacts (KI3, KI5, MI4, MI8, SI1) contain calcium in a range between 0.2 and 4.5 wt% which is the ordinary composition in primitive bloomery slag that was produced by the smelting of iron ores that contained lime (Tylecote 1962). The source of lime in these proportions could also be fuel ash and refractory ceramic (Blakelock *et al*. 2009). In three artefacts this amount is higher in some of the glassy inclusions within the metal phase (KI1, MI10) or in all of them (MI2). Inclusions with lower than 15 wt% CaO in KI1 and MI10 led to the hypothesis that lime was probably added unintentionally for example in the composition of the fuel. Considering that, lime as a flux hardly can be effective in smelting of iron in the bloomery process confirms this hypothesis. Tylecote (1962) suggested up to about 12% lime can only decrease the melting point of slag by about 50°C which would not be of much benefit to the process. The amounts higher than 15% increase the melting point of slag. The amount of lime was so high in the case of MI6 which did not react with other impurities in the ore to form calcium silicate content slag. This lime remained unreacted in the form of particles within voids in the bloomery process. This phenomenon raises the question about the exact source of high lime in this artefact. To get a precise idea about the source and high concentration of Ca in glassy inclusions, it is necessary to know more about the calcium content of the iron ores that were utilized in the smelting process. It is also necessary to know the composition of ceramic refractory and fuel ash which was derived from burning charcoal in the furnace as one of the sources of the Ca in the bloomery slag. Glassy inclusions in MI2 show the highest amount of Ca and lowest amount of iron in comparison with the above mentioned inclusions. This composition is an amorphous compound of calcium and silicon which is formed in a desirable reaction between lime and silicate content slag in high temperature of modern blast furnaces (Tylecote 1962). This criterion indicates MI2 is a modern manufacture which was left in *Greefswald* quite later than the blooming period of K2 and Mapungubwe during Iron Age.

3. *Two-phase inclusions of wüstite in silicate matrix*. Wüstite is an iron oxide with the lowest valance of iron with a non-stoichiometric composition ($Fe_{1-x}O$) which is formed in temperatures above

570°C (Samuels 1980). With these types of inclusions the wüstite phase is seen in the form of a light grey globule or dendrite embedded in a well defined crystalline silicate compound such as fayalite (Fe_2SiO_4) in the case of KI5 or an amorphous glassy phase with a different elemental compositions and weight percentage in the cases of KI1, MI7, MI8, MI9 and SI1.

4. *Alloying element segregation*. In the ferrite grains of a few of the objects (KI1, MI2, MI7, MI9) which contained lowest amount of carbon, a tiny precipitation of small plates were revealed by etching which are minor species present in alloy, probably nitride or carbide, that forms in the process of quench aging (Samuels 1980).

3.3.2.3. Manufacture method

The study of microstructure shows two main heat treatments as the final step in manufacture of the iron artefacts which are the following.

1. *Normalizing*. The majority of the artefacts (KI3, KI5, MI4, SI1 and MI10) in this assemblage were heated to above the A3 temperature and fairly rapidly cooled by air. This process results in the formation of ferrite grain boundaries with Widmanstätten morphology on pearlitic former austenite grains in areas with 0.2-0.4wt% carbon content (KI5, MI4, MI10 and SI1) and irregular non-equiaxed ferrite grains with pearlite islands in zones with carbon content lesser than 0.2 wt% (KI3, KI5, MI4, MI10 and SI1) (Samuels 1980).

2. *Annealing*. The annealed objects were heated above or below the A1 temperature and cooled slowly. Two definitely extraneous artefacts of this assemblage (MI7 and MI9) in addition to one that was found in Mapungubwe dump (MI8) and had a known provenance (MI6), were cooled slowly from above the A1 temperature. This process gave rise to the formation of massed equiaxed ferrite grains with a thin film of cementite in hypoeutectoid steel (MI7 and MI9), which was cooled from slightly above the A1 temperature while cementite allotriomorph grain boundaries on pearlitic former austenite grains were the result of hypereutectoid steel (MI8) (Samuels 1980). In MI6, which appears to be hypoeutectoid steel a thick grain boundary of cementite was formed on former austenite grains of ferrite with partially spheroidized eutectoid cementite. Two of the artefacts (KI1 and MI2) were annealed by heating below, but close to the A1 temperature which gave rise to formation of fully spheroidized eutectoid cementite (Samuels 1980) in MI2 and degenerated pearlite in KI1. As Samuels (1980) suggested the rate of cementite spheroidizing is subject to time, temperature and prior cold deformation. Degenerated pearlite in KI1 shows the annealing time was not sufficient enough in that specific temperature to form a fully spheroidized structure**.**

The results indicate that the iron objects were mostly air cooled from high temperature above A_3 and rarely annealed. Gradual gradient of carbon wt% from the surface toward interior of the samples shows that the uneven distribution of carbon is due to the decarburization (KI5, MI2 MI4 and MI8) or

carburization (MI10 and SI1) of the metal during forging in a different atmosphere from oxidizing to reducing. It seems the blade of MI10 was deliberately carburized contrary to carburization in the shaft of the pendant (SI1) to increase its hardness.

Evidence of cold working is only seen in the form of shear bands in two extraneous hoes (MI7 and MI9) which was probably formed after final annealing or during utilizing of the hoes. The sign of slight cold working in a partial austenitizing zone (between the A1 and A3 temperature) is observable in the form of critical grain growth (Samuels 1980) mostly towards the surface in three objects (KI1, MI2 and MI9) while only one of them (KI1) is an indigenous product which indicates that the objects from K2 and Mapungubwe were mostly forged in fully austenitized temperatures.

The objects show a variety of grain size from ASTM 4 to lower than ASTM 10. In general grain size depends on original grain size, the degree of prior cold work and final annealing temperature, and time (Rostoker & Dvorak 1977, Samuels 1980). In the annealed objects (KI1, MI2, MI9) where there was a big difference between the minimum and maximum grain size, large grains were associated with areas with a lower carbon content, etch pitting and subgrain boundaries which is a sign of cold and warm deformation before subsequent annealing (Rostoker & Dvorak 1977).

Chapter 4

Physical stability and manufacturing technique of copper artefacts

4.1. Introduction

The selected copper objects were in four main groups: wire, strip, and plate in various forms such as rod, bangle, ring, funnel and helical ornament. In this chapter, in a systematic technical study, all the historical evidence on the surface and within the internal structure of the objects were first examined by means of non-destructive techniques such as microscopic observation of the surface, and neutron tomography. The historical evidence of manufacture, usage, wear, and conservation was only detected on the surface of few artefacts (KC3, MC6, MC9, MC12, and SC2). These exposed signs were completely interpreted in this chapter. The outcomes of neutron tomography as well as microscopic study of the surface showed which of the objects required more detailed analysis to clarify ambiguous aspects in their manufacture. Further technical study on these specific objects was conducted by means of metallography of the mounted samples. Among these objects those whose sampling might result in losing their physical integrity were not studied in detail. These objects included unique artefacts (KC3, MC3) and also the heavily corroded objects (MC5, MC7 and SC1). Neutron tomography also assisted in detection of physical defects and stability of the objects. In this regard all copper artefacts were examined.

4.2. A survey of surface characterization, neutron tomograms and microstructure of the copper objects

4.2.1. Round wires

KC1

This artefact is a thick round wire in the form of an open-ended bangle. This was found at K2 at a depth of 91 cm from the surface by Gardner (1935-40) (Appendix A. Table: KC1). Except for traces of decay no other evidence was found on its surface.

Neutron tomography shows it has a thick continuous metal core although half part of the bangle is more corroded. Light powdery green corrosion products in some parts penetrate further inside the metal core. In these parts the original surface has been damaged and the metal core pitted (Fig.4.1). The pitted surface which was exposed in the neutron tomograms, shows the aggressive nature of this kind of corrosion. It seems that the bangle is infected by bronze disease. The affected surface, relative to the rest of the object is not extensive and an appropriate treatment can prevent further damage to the bangle. Approximately 34% of the sample consists of corrosion products. In this type of encrusted object investigative cleaning will be helpful to reveal the exact position of the original surface. A summary of the neutron tomography result of the object was given in Appendix D. Table: 4.1.

Figure 4.1. Neutron tomograph. Axial slice of KC1.

EDS analysis shows that the bangle was made of pure copper with low amounts of silicon (0.4 wt%) and oxygen (1.7 wt%) as impurities within the metallic phase (Appendix D. Table 4.2: analysis KC1a). The silicon and oxygen can be due to the presence of fine dispersed inclusions in the metal.

The inclusions within the transverse section of the bangle have a banded structure of numerous globules that possess two different oxide compositions (Appendix B. Fig.57). The first category consists of small rounded inclusions (1.25-5μm) near the surface and in the centre containing oxides of copper with oxygen content in proportion close to cuprite (Appendix D. Table 4.2: analysis KC1b). In the second category the amount of oxygen is higher than the predicted oxygen content in cuprite with a stoicheiometric composition of Cu_2O (Appendix D. Table 4.2: analysis KC1c). These inclusions probably contain an admixture of tenorite (CuO) and cuprite together. The presence of copper oxide inclusions is an evidence of remelting of copper in an oxidizing condition (Tylecote 1962, Scott 1991, Miller 2001) which indicates a cast article, probably a rod, was utilized in the manufacture of the bangle. According to the Cu-O binary phase diagram these eutectic reactions occur from 1091°C for an oxygen content higher than 33.3 at.% to form tenorite, while this product is stable at a lower temperature of 1066°C which resulting in the formation of cuprite for an oxygen content lower than 33.3 at.% (Neumann *et al.* 1984). It may be a sign of a non-equilibrium melting condition in a crucible with higher oxygen in access toward the surface of the molten metal.

The etched transverse section revealed recrystallised angular grains of copper with annealing twins resulting from either prior cold-working with subsequent annealing or a direct hot-working (Appendix B. Fig.57). The inclusion banding in the metallic phase confirm the second method of manufacture. The microstructure is homogeneous with average microhardness 107 H_V and average ASTM grain size 7.

KC3

This ornament is a unique artefact from K2 (Appendix A. Table: KC3) the usage of which has not yet been determined. It consists of two symmetric spiral shapes which were formed from a single thick copper wire. A similar incomplete form was found at Mapungubwe with one spiral only (Fig.4.2a). The latter was found by Gardner in 1939 during excavation of block 2, section 4 at a depth of 91.44 cm from the debris above a hut floor. Due to corrosion the original form of this ornament had practically disintegrated and it is impossible to ascertain whether it had the same shape as KC3. However, the evidence indicates that this type of spiral was used in manufacturing of some kind of unknown ornaments at both sites although very few of these were found.

59

The contamination was previously removed manually from two parts of the KC3. As a result, scratched lines became visible underneath (Fig.4.2b). Although delicate parallel lines appear on the surface along the bare wire, the presence of a band of lines running in a different direction than what was produced above this part with a similar texture can be inconsistent with wire drawing as a method of manufacture of this artefact. These lines are only seen on one side and nothing is observed on the other surface.
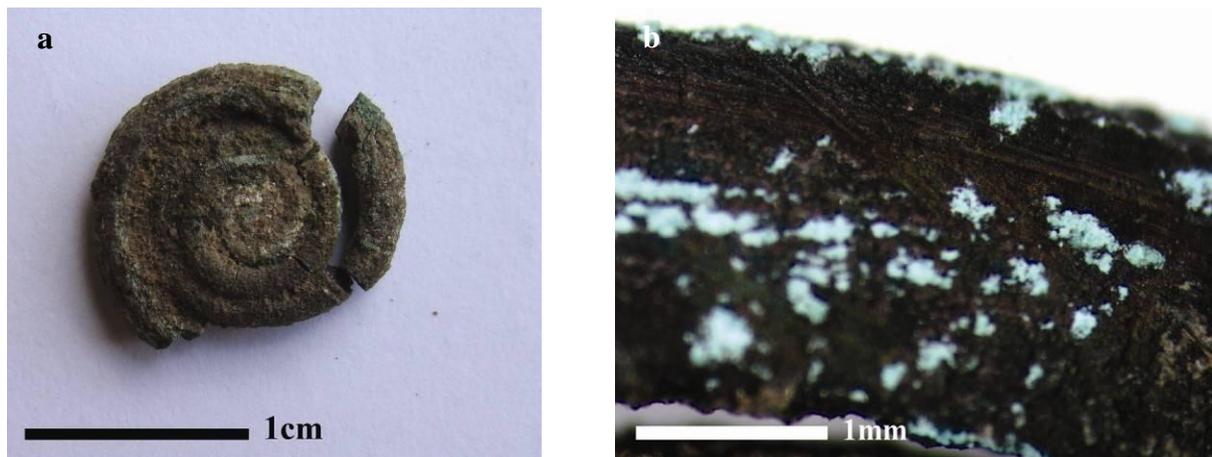
Figure 4.2. a) Spiral wire from Mapungubwe. b) Abrasion lines on KC3

The neutron tomogram slices show that this symmetric helically-wound wire is completely robust and that the metal core extends continuously along it. Corrosion products with a hydrogen content did not penetrate into the metal. The exterior corroded layer which mostly consists of cuprite is not visible in the tomograms. This invisibility may be the result of the low thickness of the layer or close attenuation coefficient of copper and cuprite. The wire diameter is uneven along the length and in some places has faceted surfaces which are characteristic of hammered wire (Fig.4.3a). In almost half of the object an interior hollow is seen along the wire whereas in the other part it is completely solid (Fig.4.3b, c). Parallel striation, which was referred to above, is seen on the surface of this solid part. A summary of the neutron tomography result of the object was given in Appendix D. Table: 4.1.

The presence of faceted surfaces along with the interior hollow and parallel striation on the surface of the wire makes it difficult to interpret the exact method of manufacture. The presence of the hollow within the wire can be an indicator of strip-drawing in the manufacture of the ornament. This technique which is known as 'the Egyptian wire-making' method was described extensively by Williams (1924). Based on the above observations it appears that the wire was manufactured from a ribbon of copper. The ribbon was gradually converted to a tubular and solid wire by passing it successively through of a number of drawing dies with diminishing diameters although in some parts the interior hollow remained intact. Williams (1924) suggested continuous drawing of the strip through dies can eliminate the hollow by curling it upon itself. Here the strip of metal was not passed

60

through the dies enough to entirely diminish the hollow. It is also possible that hammering of drawn wire diminished the central hollow in some parts. The thick drawn wire was hammered to take its symmetric spiral form in the final step of its manufacture. The faceted surfaces which are seen in some parts of wire can be the result of this hammering.

In order to fully understand the manufacturing technology of this artefact, further scientific study would be needed. Sampling was not possible due to the uniqueness of the artefact on the basis of the ethics of conservation.

Figure 4.3. a) Frontal slice of KC3 shows faceted surfaces of wire. b) Sagittal slice of KC3. Internal hollow. c) A part of subsequent sagittal slice which shows discontinuity of hollow along wire.

Interior hollow   Faceted surface
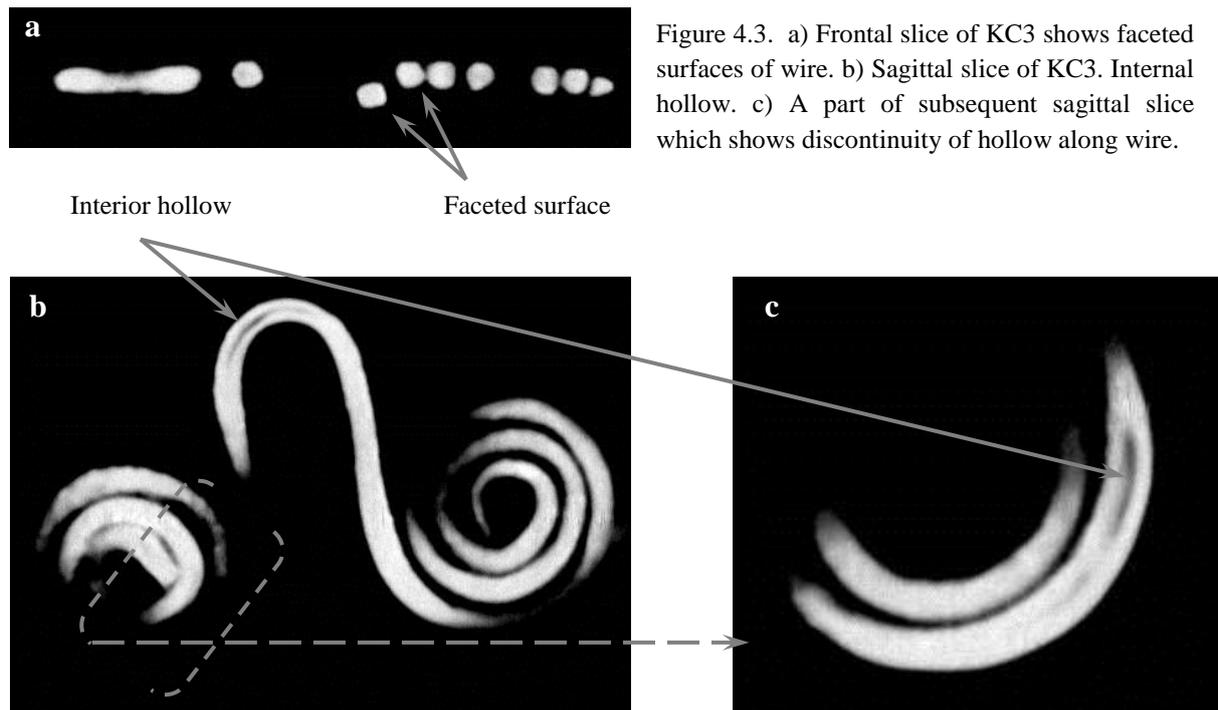
KC5

This bent copper wire was found at a depth of 30 cm from the surface at K2 in 1936 (Appendix A. Table: KC5). This round wire is probably a piece of a fragmented bangle. The fractured surface is straight and uneven while the other end is oblique and smooth. The object has research value and was added to this assemblage for the study of corrosion composition and stratification as well as microstructure. Except for traces of decay no other evidence was found on the surface of the object.

Neutron tomography shows the object has a robust continuous metal core. A hollow is seen within half part of the wire (Fig.4.4). A summary of the neutron tomography result of the object was given in Appendix D. Table: 4.1.

Figure 4.4. Neutron tomogram of KC5. Sagittal slice. A hollow is observable within the wire.

EDS analysis shows it was made of pure copper (Appendix D. Table 4.2: analysis KC5a). SEM image of the transverse section shows a large elongated central void (Appendix B. Fig.59) which consisted of copper oxide with a low amount of chlorine in its peripheral (Appendix D. Table 4.2: analysis KC5b). The chlorine content of the corrosion inside the void is almost similar in quantity to the corrosion products in the outer layer (Table 3.2: analysis KC5 L2). It appears to have been part of the central void seen in the tomograms. The void is in vertical position to the surface. The corrosion could have been formed later during burial due to penetration of corrosive elements via probable tiny open crevices that are connected to the void. There were numerous globular inclusions dispersed randomly throughout the sample in different sizes between 1.5 and 5μm with a blue reflection under plane polarized light (Appendix B. Fig.60). EDS analysis indicated the inclusions consisted of copper and oxygen as the main elements with composition close to cuprite (Talbe 4.2: analysis KC5c). The metal consisted of recrystallised grains with angular annealing twins with ASTM grain size 5.5 and average microhardness 97 H_V in an even microstructure (Appendix B. Fig.60). The object was formed by hammering a cast rod then annealed in temperature around 250°C. The annealed microstructure of the bangle hampers any conclusion as to the method of manufacture that resulted in the formation of longitudinal voids within the wire.

MC1

This delicate coiled wire was found at a depth of 3.35 m from the surface on Mapungubwe Hill. Except for traces of decay no other evidence was found on the surface of the object.

Neutron tomography shows it has a continuous metal core. A frontal neutron tomogram slice revealed a discontinuous line within the wire strand (Fig.4.5a). A sagittal neutron tomogram slice (Fig.4.5b) shows a corrosion layer with a lamellar structure. The corrosion layer can clearly be distinguished from the metal as a result of different neutron attenuation coefficients and density. Although aggressive corrosion disintegrated the original surface, it remained intact in most parts within corrosion. Based on axial tomography slices, 34% of the sample consists of corrosion products. A summary of the neutron tomography result of the object was given in Appendix D. Table: 4.1.

62
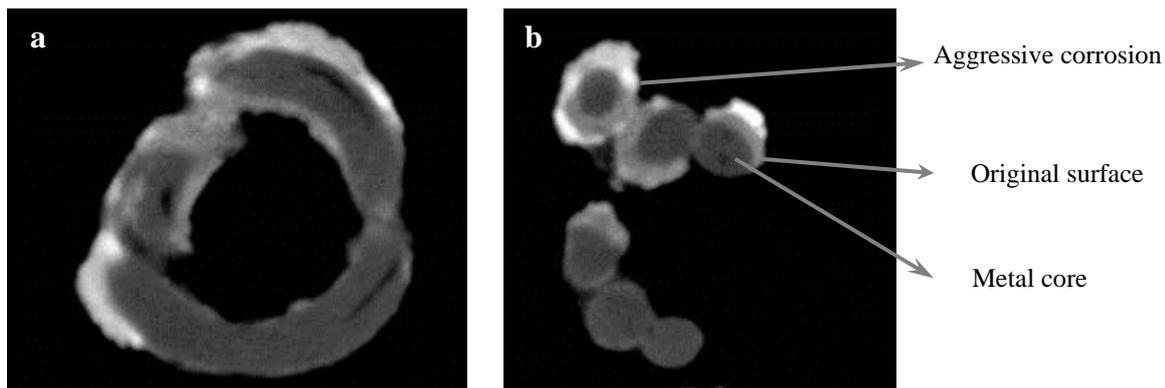
Figure 4.5. Neutron tomograms of MC1. a) Frontal slice b) sagittal slice shows how aggressive corrosion disturbed the original surface.

Discontinuous longitudinal void within the wire shows that this ring might have been manufactured by strip drawing in addition to simple hammering. Notwithstanding this ambiguous aspect in the manufacture of the ring the object was not sampled due to its shape. Sampling could damage its physical integrity.

MC2

This copper bangle was found at a depth of 1.5 m from the surface on Mapungubwe Hill by Gardner (1935-40) (Appendix A. Table: MC2). The bangle was made from a bent round wire with an un-fused joint. Except for traces of decay no other evidence was found on the surface of the object.

The neutron tomograms show that this bangle has a deep transverse crack almost in the middle of its length. It appears to have been produced by external stress which bent the bangle in this area (Fig.4.6a). In some parts corrosion has penetrated the metal core although the original surface mostly retained its form. Based on the frontal slices, 31% of the object consists of corrosion products. A longitudinal interior hollow is visible in both side of the wire (Fig.4.6b). A summary of the neutron tomography result of the object was given in Appendix D. Table: 4.1.

EDS analysis of the metal indicated the bangle was fabricated of pure copper (Appendix D. Table 4.2: analysis MC2a). The metallic phase contains numerous inclusions of one kind with globular form, with composition approaching cuprite (Appendix D. Table 4.2: analysis MC2b), and which were arranged in a banded structure (Appendix B. Fig.61). Low amounts of sulphur (0.1 wt%) in the inclusion could have originated from the sulphate content of oxidized copper ore (Tylecote 1962) that was generally used in metallurgy in southern Africa (Miller & van der Merwe 1994, Miller 2002). The microstructure of the sample mainly consists of recrystalised angular grains of copper with annealing twins (Appendix B. Fig.61) while in a restricted area, close to the surface, the grains have a flattened structure with preferred orientation and distorted twin lines (Appendix B. Fig.62). The mean grain size in fully annealed areas is about ASTM 7. The microhardness is varied between the

63

minimum amount of 117 H_V in a fully recrystallised area and maximum of 139 H_V on cold worked surface which is almost around the microhardness than that reported for cold worked pure copper (Scott 1991). Composition of the inclusion shows the bangle was fabricated from a primary casted object such as a rod. The other metallographic evidence indicates that the cast rod was first forged and then followed by final annealing around recrytallizing temperature of pure copper. The flattened grains on the surface indicate the object was subjected to light cold working after final annealing. The annealed microstructure of the bangle hampers any conclusion as to the method of manufacture that resulted in the formation of longitudinal voids within the wire.
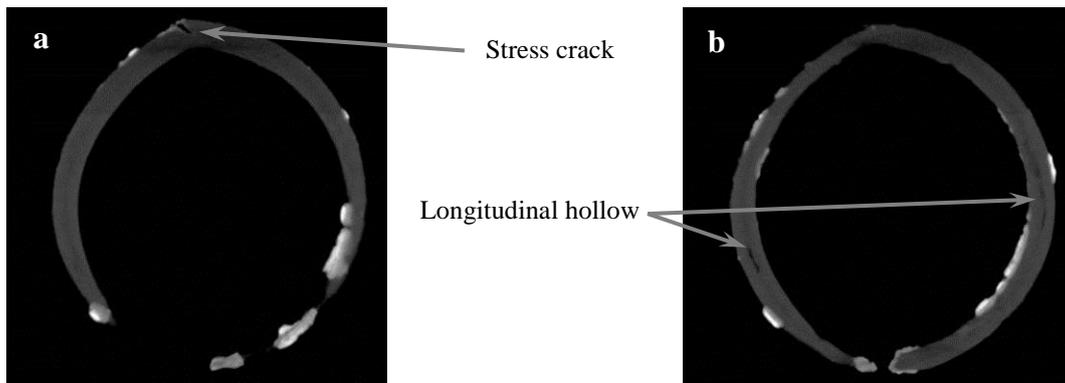
Figure 4.6. Neutron tomograms of MC2. a) Frontal slice. Deformation of the bangle almost in the middle resulted in a crack in this zone. b) Frontal slice. Two longitudinal hollows are observable along and within the wire. The original surface is seen within the corrosion products in some places.

MC10

This copper ring was found at a depth of 1.2m from the surface on Mapungubwe Hill in 1937. It was manufactured from a round wire. A piece of round wire was bent to form a circular small loop with an open end. The circular shape of the ring was distorted (Appendix A. Table: MC10). Except for traces of decay no other evidence was found on the surface of the object.

Neutron tomography of the copper ring shows it has a continuous metal core. The neutron axial slices indicate the metal core has a circular cross section with variation in its diameter along the length. Faceted surfaces are seen as the result of hammering along the wire (Fig.4.7a). A discontinuous longitudinal hollow is apparent within the wire (Fig.4.7b-d). This kind of hollow can be formed by strip-drawing. A more accurate result would necessitate further metallographic investigation. Although the original surface was disturbed by corrosion in some places it remained mostly intact. 36% of the sample consists of corrosion products. A summary of the neutron tomography result of the object was given in Appendix D. Table: 4.1.

64
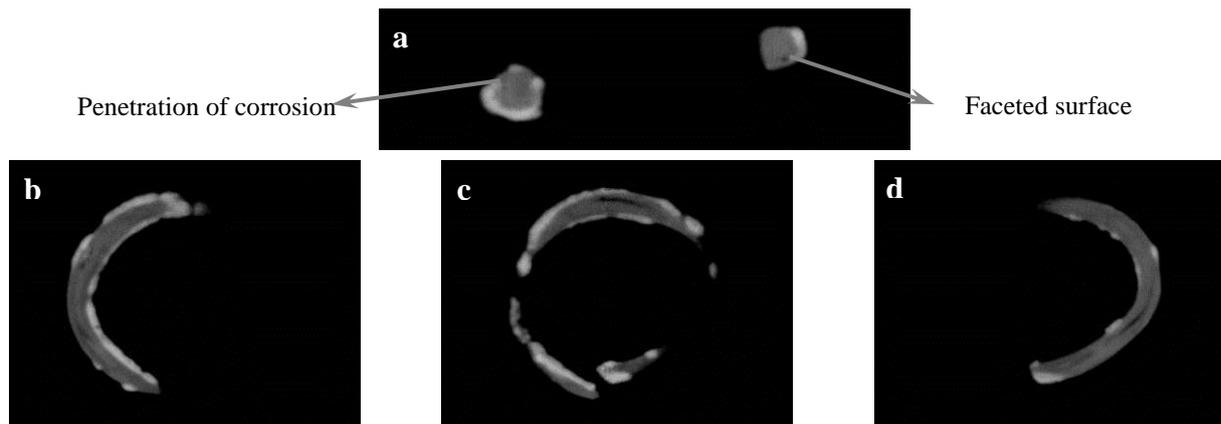
Figure 4.7. Neutron tomograms of MC10. a) Axial slice. b,c,d) Sequence of frontal slices. Internal hollow is seen along the length.

EDS analysis of the metal phase revealed that the small loop (nose ring) was manufactured from pure copper (Appendix D. Table 4.2: analysis MC10a). The metallic matrix contains a high numbers of inclusions with a composition approaching cuprite (Appendix D. Table 4.2: analysis MC10b). The inclusions had a globular form with dimensions approximately from 0.6 to 3.3 μm which were decorated in a banding structure parallel to the worked surface (Appendix B. Fig.63).

The etcheched transverse section of the ring shows recrystallised angular grains of copper with straight annealing twins (Appendix B. Fig.64). The grains have an average ASTM grain size of 5.5 and microhardness 75 H_V. The evidence indicates that the ring was manufactured from a cast piece of copper, probably a rod, by forging which resulted in the formation of annealing twins. The hollow within the thick wire (Fig. 4.7) was probably formed during forging when the artisan tried to achieve a cylindrical form of the rod. The annealed microstructure of the bangle hampers any conclusion as to the method of manufacture that resulted in the formation of longitudinal voids within the wire.

MC11

This bangle was found at a depth of 1.2m from the surface on Mapungubwe Hill in 1940 (Appendix A. Table: MC11). The bangle was manufactured from a round wire. The wire was bent to form a ring with an open end. Except for traces of decay no other evidence of manufacture, wear or usage was found on the surface of the object.

The neutron tomograms show that this bangle is completely robust with a sound metal core. Its faceted cross section in most parts indicates that it was hammered (Fig.4.8). No central void observed within this wire. Metallography of the cross section of MC11 could provide more information about the manufacturing of this object. A summary of the neutron tomography result of the object was given in Appendix D. Table: 4.1.

EDS analysis of metal phase shows that the bangle was made from pure copper (Appendix D. Table 4.2: analysis MC11a). Even without etching, the microstructure of the sample is quite apparent

65

and shows it was formed of two distinctive phases of α-pure copper and (α + cuprite) eutectic (Appendix D. Table 4.2: analysis MC11b) in a dendritic structure. The metal phase also consists of numerous voids with more concentration toward one of the surfaces, probably the rough surface (Appendix B. Fig.65). The number of dendrite nucleation within the metallic phase is considerably higher than in the case of the ingot (MC9). It is evident in micrographs with the same magnification (Appendix B. Fig.66, 82) which means the rate of solidification of the molten copper in MC11 was higher than the ingot. It could be the result of the low volume and thickness of the utilized mould in the manufacturing process of the bangle. Few of the dendrites close to the surface have straight twining lines (Appendix B. Fig.67, 68). The microhardness in this area is 120 H_V in mean which is quite high for a cast structure. On the rough surface where the large voids are present and the number of dendrite nucleation decreases due to slow solidification, the microhardness dropped to 84 H_V. It appears that the bangle was manufactured from a cast rod which was shaped to a loop by slight hammering and final annealing or slightly forged without further annealing. The annealing time or temperature was not sufficient to change the dendrites to a fully granular equilibrium structure which is in the least energy requirement (Scott 1991).

Figure 4.8. Neutron axial slice of MC11 shows the bangle has a faceted surface as the result of hammering.

MC12

This copper bangle was found at a depth of 2.4m from the surface on Mapungubwe Hill by Gardner (1935-40). It has been manufactured from a round wire. A piece of round wire was bent to form a circular bangle with an open end (Appendix A. Table: MC12). Corrosion was removed from a small longitudinal surface of this copper bangle. Scratch lines are visible underneath. The lines are not completely parallel and comprise of different sets of lines in various directions. Figure 4.9a shows the details of these scratches. It is difficult to establish whether these lines are the result of abrasive material used by archaeologists to reveal the metal type, or are traces of manufacture. The presence of brown and black corrosion in this area, with the lines running under the green corrosion layer around this part (Fig.4.9b), supports the latter line of thinking. Although the composition of the black layer has not yet been identified, the red-brown continuous layer on this part could in all probability be cuprite. Cuprite is known as a marker layer that often preserves important details of the original surface of an object (Organ 1963; Chase 1994; Scott 2002).

The result of neutron tomography of the bangle shows that it has a robust metal core. Corrosion is only seen on the surface, and except for a few places, has not penetrated inside the metal core. Based on the frontal slices 9% of the object consists of corrosion products. A hollow is visible in both sides

of the wire (Fig.4.10a-c). This kind of hollow can be the result of strip drawing. A summary of the neutron tomography result of the object was given in Appendix D. Table: 4.1.
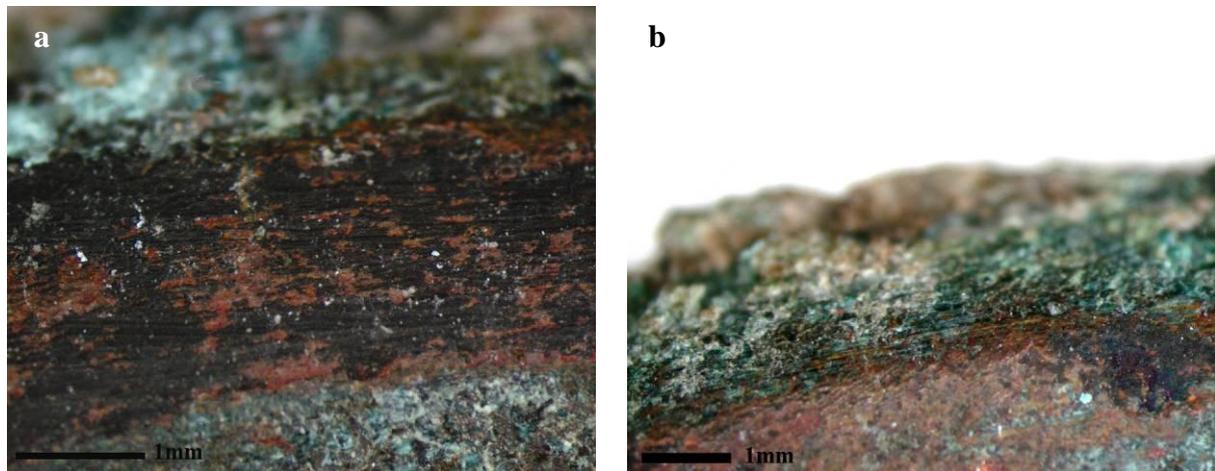
Figure 4.9. a) Unparallel abrasion lines on the surface of copper bangle (MC12) which covered partly with red and black corrosion products. b) Continuity of abrasion lines under green corrosion layer.
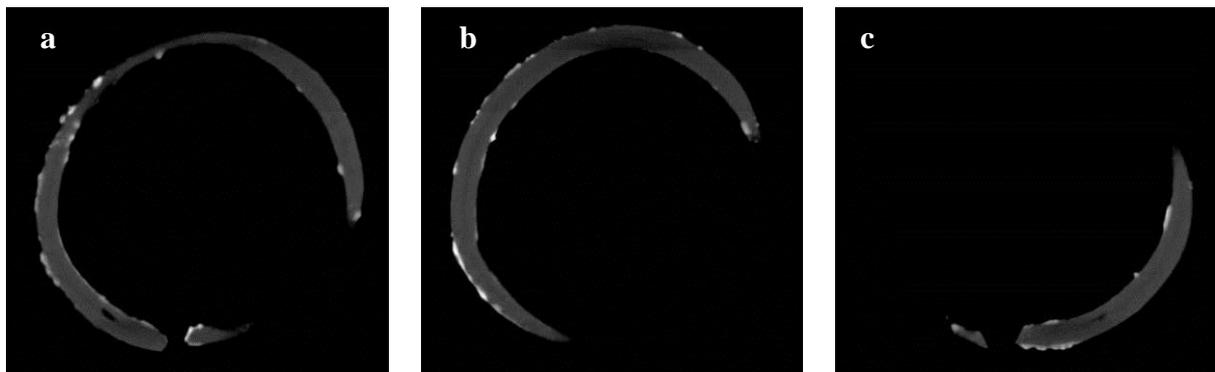
Figure 4.10. Neutron tomograms of MC12. a, b, c) Successive frontal slices show presence of hollow within both sides of the bangle.

EDS analysis of the metal phase revealed that the bangle was fabricated of pure copper (Appendix D. Table 4.2: analysis MC12a). There were numerous globular inclusions with elemental proportion close to cuprite (Appendix D. Table 4.2: analysis MC12b) and dimensions around 0.5-5 μm. The cuprite inclusions are seen in a banded structure which is a sign of hot working. There was also a large two-phase inclusion entrapped within the metal (Appendix B. Fig.69). Elemental analysis shows that it was formed by penetration of corrosion along the fissure that was formed in the manufacture procedure. In peripheral it contains cuprite (Appendix D. Table 4.2: analysis MC12c) while in the central part it was filled with a composition consisting of a high amount of oxygen, copper and traces of soil elements (Appendix D. Table 4.2: analysis MC12d).

67

The metallic phase consisted of angular recrystallised grains of copper with distorted annealing twins (Appendix B. Fig.70). The average gain size number is ASTM 7 and microhardness as 117 H_V in mean. The metallography evidence indicates the bangle was manufactured from a cast piece of copper, probably a rod. The rod was forged with a final annealing operation. In the final stage the bangle was lightly hammered which caused distortion in annealing twins and increasing the microhardness. The annealed microstructure of the bangle hampers any conclusion as to the method of manufacture that resulted in the formation of longitudinal voids within the wire.

4.2.2. Rods

KC2

This artefact is a short rod which was bent in the middle. It was found at a depth of 91cm from the surface by Gardner at K2 (Appendix A. Table: KC2). Except for traces of decay no other evidence was found on the surface of the object.

The neutron tomogram slices indicate that the copper rod has a continuous metal core with a disparate cross section, circular in some places and almost rectangular in others which could be the result of hammering (Fig.4.11a, b). Although in one part aggressive corrosion has penetrated and damaged the metal core, it has remained robust and would withstand later treatment (Fig.4.11c). Almost 33% of the object consists of corrosion products. A summary of the neutron tomography result of the object was given in Appendix D. Table: 4.1.
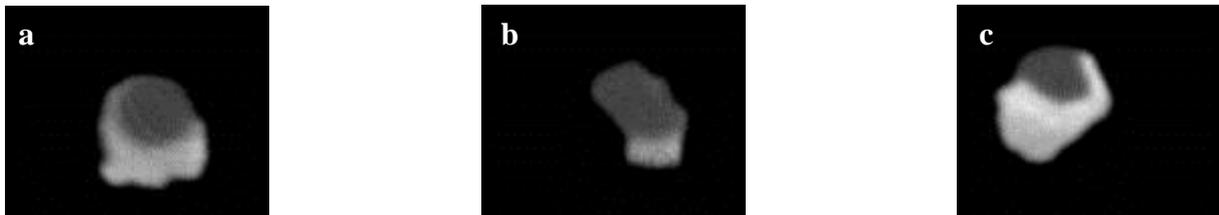
Figure 4.11. Neutron tomogram axial slices of KC2 a. b) Round and rectangular cross section of the rod in opposite side. c) Penetration of corrosion products in metal core almost to the middle of rod.

The rod was made from pure copper (Appendix D. Table 4.2: analysis KC2a) with numerous globular inclusions which were dispersed randomly within the metallic phase with composition approaching cuprite (Appendix D. Table 4.2: analysis KC2b). The inclusions have various sizes from the maximum of 7 μm to lower diameters. The metal is homogeneous and consists of recrystallized copper grains with average ASTM grain size 8 and microhardness 109 H_V. The grains are twined (Appendix B. Fig.71). The rod was shaped by hammering of a remelted piece of pure copper followed by final annealing.

MC4

This copper rod has poor provenance in the archaeological context. Museum inventory only refers that it was found at Mapungubwe (Appendix A. Table: MC4). Except for traces of decay no other evidence was found on the surface of the object.

Neutron tomography shows the rod has a square cross section which converts to an annular form toward the end points. The rod has a continuous metal core but in its curved narrow point the metal core is almost weak because of penetrating corrosion (Fig.4.12a, b). In some parts the original surface was deformed and destroyed by corrosion while in other parts it kept its form within the corrosion products. Based on the axial slices, 34% of the sample consists of corrosion. Investigative cleaning can assist to find the limit of the original surface on the artefact. A summary of the neutron tomography result of the object was given in Appendix D. Table: 4.1.
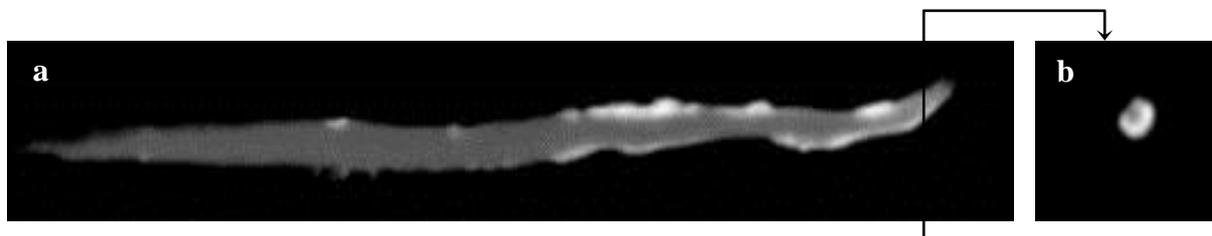
Figure 4.12. Neutron tomogram of MC4. a) Frontal slice. This slice shows half part of the object toward its narrow point. b) Axial slice. The low thickness of the remnant metal core in narrow end of the peg is observable.

The SEM image of the polished cross section shows that the rod was manufactured by folding over a narrow plate to achieve a desired thickness (Appendix B. Fig.72). The gap between these two parts was completely filled with corrosion products. MC4 is the only copper artefact in this assemblage which has 0.5wt% iron as impurity in the metallic phase (Appendix D. Table 4.2: analysis MC4a) in the presence of oxygen. It shows that no iron is present as a pure metallic phase in copper and that the detected iron belongs to the fine dispersed inclusions. Low numbers of angular inclusions were randomly dispersed in the metal (Appendix B. Fig.73) that mainly consisted of iron and copper oxides together with a similar proportion to mixtures of magnetite and cuprite (Appendix D. Table 4.2: analysis MC4b, c). The composition of the iron oxide within the inclusion was identified due to the oxygen weight percentage that each iron oxide can take in its chemical formula. The goal was achieved by using a standard conversion number of each element and taking into account the oxygen and iron wt% that were reported in EDS results. Magnetite is a common constituent of smelting slag and shows these inclusions are entrapped slags which were formed during smelting within the metallic phase. Copper sulphides ores were not in use in Iron Age metallurgy in southern Africa (Miller & van der Merwe 1994, Miller 2002) and the source of this iron might be the flux or copper deposits from an oxidation zone. The lack of individual cuprite inclusions show the copper was not

69

remelted and is a direct product of smelting which means a piece of smelted ingot was used in the manufacture of this rod.

The microstructure of the rod consisted of angular grains of copper with mean ASTM grain size 8 and average microhardness 105 H_V. Annealing twins are seen within the grain with slight distortion in some of them toward the sides (Appendix B. Fig.74). In these areas the microhardness increases to 117 H_V in mean. The evidences indicate the rod was made by forging or even cold working and final annealing. The object was then subjected to slight cold working which could also have been formed later during usage.

4.2.3. Copper plates and strips

KC4

This copper plate was found at a depth of 61cm from the surface by Gardner at K2 (Apendix Appendix A. Table: KC4). The plate that only has study value, was added to this assemblage to study corrosion stratification and composition to reveal the effects of the burial environment on corrosion. Except for traces of decay no other evidence was found on the surface of the object.

Neutron tomography shows this copper plate is robust with a continuous metal core. Corrosion is only seen on the surface (Fig.4.13). Based on axial slices 39% of the bulk of object contains corrosion products. A summary of the neutron tomography result of the object was given in Appendix D. Table: 4.1.
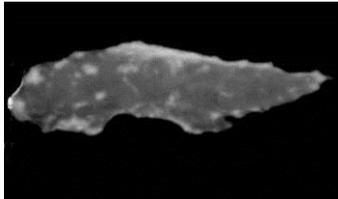
Figure 4.13. 2D neutron image (radiograph) of KC4. The metal core is seen in grey while corrosion product is in white.

Polished transverse section of the plate shows it was folded over to form a thicker section for a later manufacture process. The plate has an unequal thickness from approximately 0.1 to 0.3 mm in its opposite sides (Appendix C. Fig.18). Analytical results show that the plate was made of pure copper with a low amount of silicon as impurity (Appendix D. Table 4.2: analysis KC4a). Numerous inclusions in globular form with a diversity in size from a maximum of 8 μm to lower diameters have decorated the metallic phase in a banding structure parallel to direction of the working surface. Formation of banded structure resulted from hot-working (Miller 1996, 2001). The inclusions generally consisted of cuprite with a blue appearance within the metallic phase (Appendix D. Table 4.2: analysis KC4b, c).

70

The microstructure is almost homogeneous with recrystallised angular grains of copper and annealing twins (Appendix B. Fig.75). The average grain size in this area is about ASTM 8 and microhardness is about 88 H_V which is around to usual Vickers microhardness reported for worked and annealed pure copper (Scott 1991). The grains have flattened with a preferred orientation along the worked surface around an oblique cut in the thicker side of the plate (Appendix B. Fig.76). Distorted annealing twins are seen in this area as well. In this zone the microhardness is 117 H_V in mean. The evidence shows the plate was shaped by forging a remelted piece of copper with a final cold-working toward one of the edges which was probably formed by cutting off this part from the rest of a sheet.

MC3

This copper ring was found at a depth of 1.8m from the surface by Gardner (1940) on Mapungubwe Hill. It was manufactured from a wide, thick strip of copper. The strip was bent to form a ring with an open joint. The edges of the strip are not straight which resulted in irregularity in width of the ring. The strip also has a continuous burr toward the outside which indicates it was cut from a plate of copper by a sharp tool such as a chisel (Appendix A. Table: MC3). Stanley (1937) suggested this kind of plate was made by hammering out the metal into thin sheets.

Neutron tomography shows that the ring has a continuous robust metal core. Although in some parts corrosion has penetrated inside the metal core the original surface has kept its form within corrosion (Fig.4.14). Based on the axial slices, 16% of the sample consists of corrosion products. The ring was not sampled for microstructural study because of its simple method of manufacture. A summary of the neutron tomography result of the object was given in Appendix D. Table: 4.1.
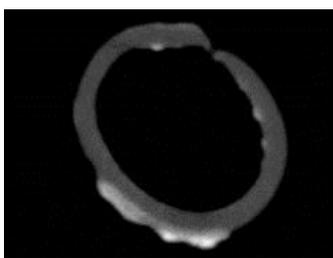
Figure 4.14. Neutron tomogram of MC3. Sagital slice. Original surface is observable among corrosion products.

MC5, MC6 and MC7

Three small, funnel-shaped copper objects -MC5, MC6, MC7-, were found within the discarded archaeological deposit from the earliest excavations (1935-1940) by Gardner at Mapungubwe Hill. Specifically, they were found on the western and northern dumps (Appendix A. Table: MC5, 6 and 7). Although the exact source of these funnels in the chronological sequence of the settlement is not clear,

the funnels could belong to the phases associated with metalworking. Only one of the funnels in the Mapungubwe museum collection is provenanced by Gardener as unearthed 2m below the surface.

The profile drawing of excavation of MK1, which was produced in 1973 of the collapsed north-western wall of Gardner's excavation revealed a depth of over 2m. This area was re-excavated in an attempt to reconstruct the site chronology. This depth would be synonymous with layer 11, which has been dated to a period from 1243 AD (PTA-1158) to 1252AD (PTA-1159) on the basis of a calibrated radiocarbon date (Vogel 1998). This date is related to the earlier component occupation at Mapungubwe a.k.a phase three of the settlement i.e. the period between 1220 and 1250 AD.

Two of the funnels, MC5 and MC7, were heavily corroded and no manufacture or wear marks are detected on the surfaces. In contrast, MC6 was less corroded than MC5 and MC7, and signs of manufacture or usage are still visible on some parts of its surface. This object is made of thin copper plate (0.64mm) which has been cut in a conical two-dimensional shape. The conical plate was rolled around its axial line to form a cone with a tight seam at the conjunction of its two straight edges. On some parts of the surface, which are not covered by contamination, the abrasion lines that run in a different direction can be seen (Fig.4.15a). It probably indicates that the surface was either polished to smooth the uneven parts resulting from manufacture and to give the artefact a shiny appearance, or was simply formed during usage of funnel.
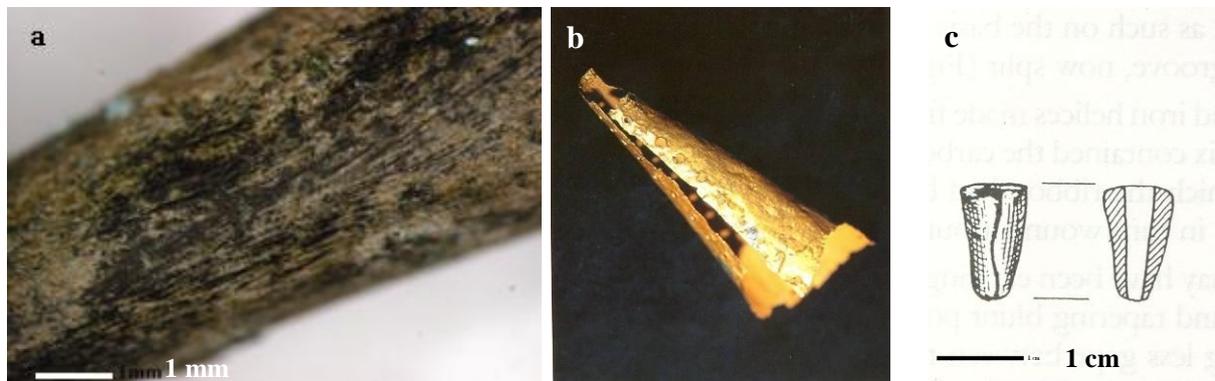
Figure 4.15. a) Abrasion lines on the surface of funnel shape copper object (MC6). b) Funnel shape golden sheet from gold assemblage of Mapungubwe. Adapted from Tiley 2004. c) Conical tube from early Iron Age site of Divuyu. Adapted from Miller 1996.

These funnel-shaped artefacts are also present in the gold assemblage from Mapungubwe (Fig. 4.15b). In the gold funnel, the presence of pinholes shows it was used to cover a wooden core as observed in some of the other gold artefacts. In contrast to the gold funnel, the cupreous items do not have pinholes and might have been used for another purpose.

An artefact with similar shape was identified by Miller (1996) among metal artefacts from the early Iron Age site of Divuyu (550-760 AD) in northwestern Botswana (Fig 4.15c). This conical tube is smaller (8.6 mm long) than the funnels from Mapungubwe and in contrast to the Mapungubwe

copper funnels, its wall thickness, tapered towards the narrow point. Miller (1996) suggested that it was made of a straight-sided wedge, possibly bent around a tapering iron point as a mandrel and then hammered, one edge over the other, to form an overlapping seam. The usage of this type of funnel artefact has not yet been determined.

Neutron tomography shows MC5 is heavily corroded. No remnant of the metal core is visible within the corrosion products. In most parts the metal was converted to dense corrosion products which have preserved the original form of the objects in such a way that the fine, interior details are clearly seen. The successive axial slices of MC5 (Fig.4.16a-d) show a thin hollow wire (pipe) on the core. The diameter of the wire was gradually decreased towards the narrow point of the funnel while the unclosed seam became a closed joint. No sign of conjunction between the funnel wall and the tube is seen. Physical evidence on the broad side of the funnel (Fig.4.16a) indicates that the wire was longer and extended outwards. It appears that corrosion completely destroyed the external part. Contrasting of the tube and the funnel wall in slices indicates both have the same linear attenuation coefficient (μ -values) property for neutrons, therefore the same composition. The neutron tomograms indicate that the manufacture of the funnel is the same as the MC6 except for an overlapping seam.
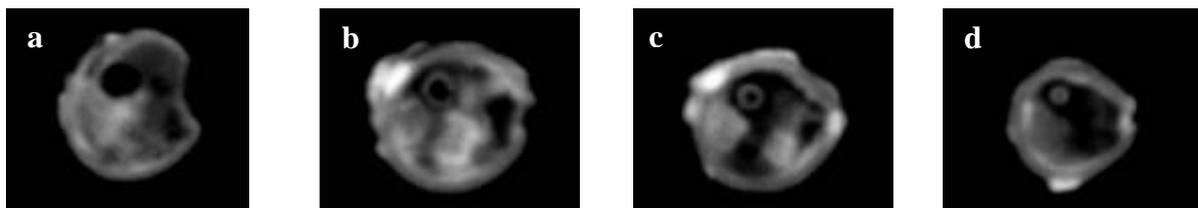
Figure 4.16. Neutron tomograms of MC5. Successive axial slices. a) Presence of a round hallow in the form of wire exactly in the same place that wire starts to appear in the axial slices. b,c,d) Presence of a narrow tube among funnel is observable. The diameter of the wire gradually decreases toward the narrow point of the funnel. In these images corroded metal core is also observable.

MC6 has a continuous metal core and low corrosion products on the surface. A strip with different composition is seen completely across the funnel which gradually folds toward the funnel narrow point to form a solid wire (Fig.4.17a-e). Here the composition of the strip differs from the funnel wall and is seen in white in axial slices due to its different linear attenuation coefficient (μ -values). These kinds of funnels might be used for strip drawing. Finding more about this structure needs further analysis.

In MC7 the dissolution of metal in the environment formed a longitudinal void in the funnel wall. Nevertheless the main form and the interior structure have remained intact among the corrosion products (Fig.4.18a). Signs of a bow strip adjacent to the funnel wall with its higher attenuation coefficient compared to the main material constituent of the funnel (copper) are recognizable in white from almost the middle (Fig.4.18b). From this point successive axial slices show with diminishing the diameter of the funnel the strip has folded as becomes narrower (Fig.4.18c-f). The folds can be seen in

73

the form of a cellular structure around a central hole or tube along the funnel in axial and frontal slices respectively (Fig.4.18a-f). The high contrast between the strip and funnel wall is mainly due to the discrepancy of material constituent of two structures with different mass absorption properties (μ - values) which a neutron beam is sensitive to. Consequently the strip must have a different composition.
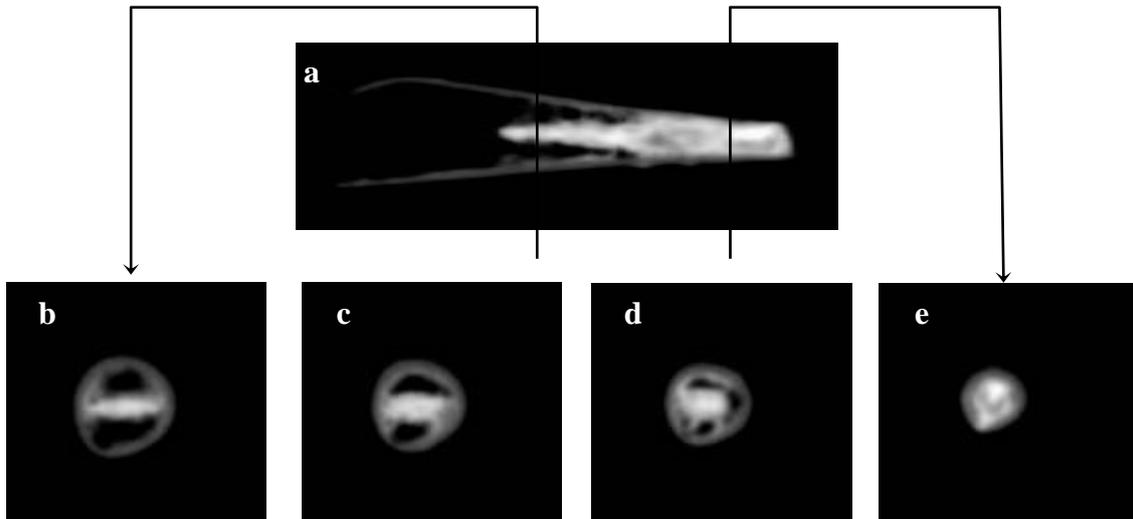
Figure 4.17. Neutron tomograms of MC6. a) Sagittal slice almost in the middle of the funnel. b,c,d,e) Successive axial slices. In white: strip. The funnel wall is in grey.

Among the funnels (MC5, MC6 and MC7), MC7 was the only one which has study value because removing the representative sample could be performed without disintegrating the entire object. The cross section of the narrow point of the funnel is seen in (Appendix B. Fig.77). Three main zones are visible in this image. Zone (a) consists of a folded strip, central tube and peripheral holes around it which were filled with corrosion products and soil contaminants. The colour of material constituent of this zone (red to reddish brown) is noticeably dissimilar to the other zone (different hue of green and purple) which indicates its composition must be quite different. Zone (b1) belongs to copper plate which corroded completely. Zone (b2) mostly consists of green copper corrosion products which have coated the surface of the funnel wall.

The thickness of copper plate in areas that increase the volume of corrosion products, has not affected its dimensions, which are about 0.4-0.5 mm. This thickness is similar to MC6 (Appendix A. Table: MC6) and shows the funnels were made with almost the same thickness of copper plate. The thickness of strip among the funnel after corrosion is lower than the funnel wall (<1/2 thickness of copper plate) although the corroded structure of the strip could not reveal the exact thickness of the strip before corrosion. The wire diameter in this place, which is almost close to the vertex of the funnel, is about 3mm.

74
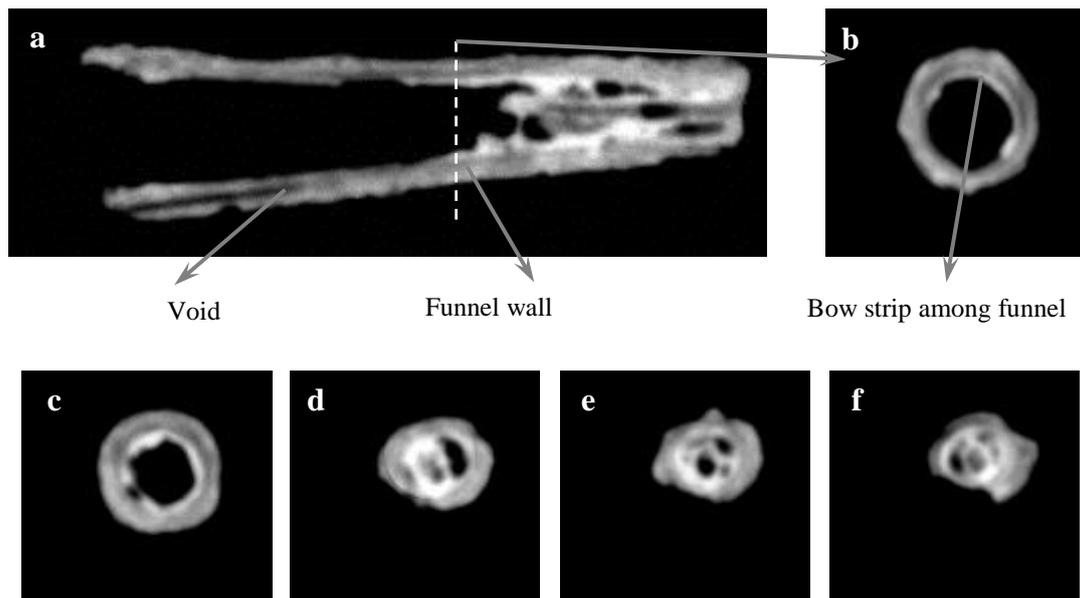
Figure 4.18. Neutron tomograms of MC7. a) Frontal slice shows almost the middle part of the funnel. Folded strip is seen in the form of longitudinal cellular structure in white and light grey among funnel while the central hollow is in dark grey and black. b,c,d,e,f,) Axial slices show the gradual folding the strip along funnel interior (in white).

Considering of EDS analytical results on the composition of different zones on the cross section of the MC7 (see section 5.2.2, MC7) it appears that the funnels were used as a die for drawing strips of iron to produce fine wire. Strip-drawing which is known as an Egyptian wire-making method was explained thoroughly by Williams (1924) with regard to the working of silver and gold. In this technique such as conventional wire-drawing decreasing the diameter of the wire, needs passing through tapered holes with gradual diminishing size. Although the corroded structure of the funnels from Mapungubwe made it difficult to determine the exact interior diameter of their tapered points, direct observation of the exterior form of the funnels indicates that the holes have different sizes (see Appendix A. tables: MC5,6 and 7).

The folded structure of the wires around a central tube among the funnels (MC6 and MC7) refers to the first pass of the iron strip (Fig.4.17, 18). Williams (1924), with regard to this stage, suggested that after the first pass the strip converts to a tube with some distortion in metal structure while subsequent passes from smaller holes steadily amended these deformations as diminishing the central hollow. Strip-drawing, contrary to wire-drawing, exerts very little strain on the drawing die, consequently dies of softer material such as copper may be practical in forming the harder one for instance iron although receiving to a definite idea in this regard needs testing the technique with the same materials and equipments practically. The structure of hollow wire among MC5 was quite different and no sign of folding was observed (Fig.4.16). It is possible that the width of the strip, relative to the other strips and compared to the funnel hole, was narrower, then lesser pressure inward

75

to it during passing through the funnel. Since there was no connection between the tube and the funnel this stage was not the first pass of the strip.

Superficial microscopic deep scratch marks on the surface of MC6 (Fig.4.15a) could be evidence of usage of the funnel in the process of strip-drawing. These scratches are seen in the form of close irregular lines which were extended towards one direction along the funnel length. These marks presumably formed during movement of the funnel as it was clamped within/on a soft immoveable base such as a wooden base. The presence of unfinished fabricated wire among the funnels indicates failure during the process of strip-drawing for instance by breaking the wire close to the exit point. In this condition the funnel was discarded.

SC1

This copper ring was found at Mapungubwe Southern Terrace (MST) in 1971. The wound wire is heavily corroded but has kept its original form in amongst the corrosion products. Visual inspection indicates that the ring was probably manufactured by helical twisting of a number of single strip twisted wires (Appendix A. Table: SC1). It is not clear, from visual inspection of the highly corroded ring, how many strand of strip twisted wire was used in the making. In a sagittal section (Fig.4.19a) the end sections of some of the strip twisted wire strands can be seen around the inner and outer perimeter (best visible around the outside perimeter). Some of the wires are cut more perpendicular to their length axis, thereby giving a roughly circular appearance with the core region visible at the centre, whilst others are cut at more oblique angles, indicating variation in winding pitch.

A core, which is a typical element of the structure of strip twisted wires, is distinguishable only inside some wires. Others appear to be hollow. The overall annular structure with a central core region however is strongly indicative of strip wire usage in its construction. In the few wires where a core seems to be present, it is visible due to a higher neutron attenuation coefficient material compared to the peripheral corroded wire but the exact material or detailed structure thereof is not identifiable (Fig.4.19b). It may be a fibrous core alone or a fibrous core with finer iron wire strands incorporated into the fibre bundle as these are two common cores in manufacture of strip twisted wires from Mapungubwe (Miller 2001). Corrosion fused all the wires together and in some parts completely destroyed the wire walls. Although no metal core has remained, the overall circular structure of the central region as revealed in (Fig.4.19b) strongly suggests the original presence of such a structure. From appearance of the neutron images alone, a general conclusion that the object is fragile with very little physical stability can nevertheless be drawn. A summary of the neutron tomography result of the object was given in Appendix D. Table: 4.1.
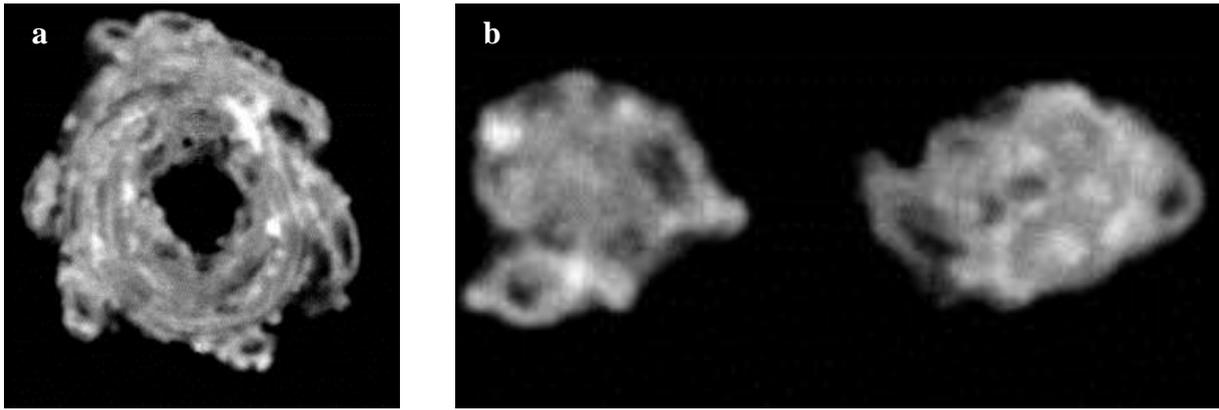
Figure 4.19. Neutron tomograms of SC1. a) A saggital slice revealing the presence of hollows among the wires, corrosion products as bright white areas and original winding path in dark gray. b) Frontal slice revealing the cross section of the ring and the presence of a core region inside the wire that remains intact only inside some strip wires.

SC2

This artefact is a copper ring which belongs to the poverty relief collection. It was found at MST in JS2(b) dump and its provenance is not clear (Appendix Appendix A. Table: SC2). Elementary microscopic study of the surface shows traces of treatment on the surface. The cuprite layer was removed from some parts as a result of over-cleaning and the bare metal is visible on these parts (Fig.4.20a). The treatment record shows that it had a distorted shape before any treatment and was covered by a continuous cuprite layer and dispersed light green corrosion on the surface (Fig.4.20b). The object was mechanically reformed to restore its circular shape by hammering it with a plastic hammer. No heat treatment was used during this process. The corrosion products were then removed by using air abrasion and glass bristle. In the final step the object was coated with Microcrystalline wax.
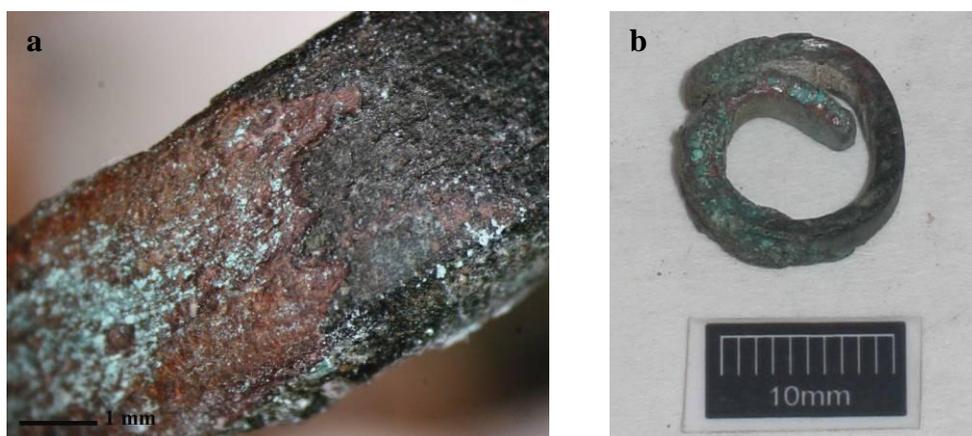
Figure 4.20. Small copper ring (SC2). a) Sever mechanical cleaning resulted in removing the cuprite layer from some parts of the surface. The jagged form of cuprite layer in edge shows it was produced as the result of surface abrasion by a hard material. b) Copper ring (SC2) before treatment.

77

The neutron tomograms show the ring has a robust and continuous metal core. Although it was coated by a layer of microcrystalline wax during its last treatment this layer is not observable in neutron tomogram slices. In some parts corrosion products penetrate inside the metal core (Fig.4.21). Based on the axial slices 6% of the object consists of corrosion products. A summary of the neutron tomography result of the object was given in Appendix D. Table: 4.1.
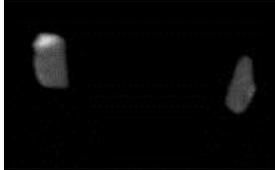
Figure 4.21. Neutron tomogram of SC2. Frontal slice. Corrosion has penetrated inside the metal core. Extra cleaning the object in its previous restoration caused unevenness on the surface.

EDS elemental analysis revealed the metal phase contains a low amount of nonmetallic elements namely silicon, sulphur, chlorine and oxygen as impurities (Appendix D. Table 4.2: analysis SC2a) which are probably present due to penetration of corrosion or even the presence of tiny inclusions. There were high numbers of globular inclusions mainly consisting of cuprite (Appendix D. Table 4.2: analysis SC2b) which have decorated the metallic phase in a banded structure. This evidence indicates the object was formed by hot working.

The etched transverse section shows inhomogeneous microstructure in its semicircular form. The copper grains were elongated toward straight sides of the sample with preferred orientation along the worked surface (Appendix B. Fig.78). In other parts the grains have a more angular form with both distorted grain boundaries and annealing twins (Appendix B. Fig.79). The average ASTM grain size in the areas with angular grains is 9. The microhardness is around 120 H_V which is similar to those reported for cold worked pure copper by Scott (1991). The evidence indicated that a cast piece of copper was forged to form the ring. This process led to the formation of a banding structure of the globular cuprite inclusions. This was followed by cold working which caused the formation of distorted annealing twins and elongation of grains towards one of the surfaces. The final cold working evidences could be the result of past conservation processes on the object. Reshaping of the object was one of the operations (Fig.4.20).

4.2.4. Nail

MC8

This nail was found in the northern dump and its form is quite different to that of the gold nails from Mapungubwe (Appendix A. Table: MC8). The gold nails are small with a square cross section in the shank and a flattened head. This nail (MC8) has a delicate structure with a long cylindrical shank which is tapered toward the point and a symmetric hemispheric head.

Neutron tomography shows this nail has a continuous metal core with a thick layer of corrosion crust (Fig.4.22). The corrosion crust has been cracked and given a wood-like surface to the nail. Texture of corrosion in this artefact is very different from the other copper objects in this study. A layer of aggressive corrosion products seems to have surrounded the metal core. A big void is visible within the round head of the nail. A summary of the neutron tomography result of the object was given in Appendix D. Table: 4.1.

Corrosion products with hydrogen content around metal core   Deep crack
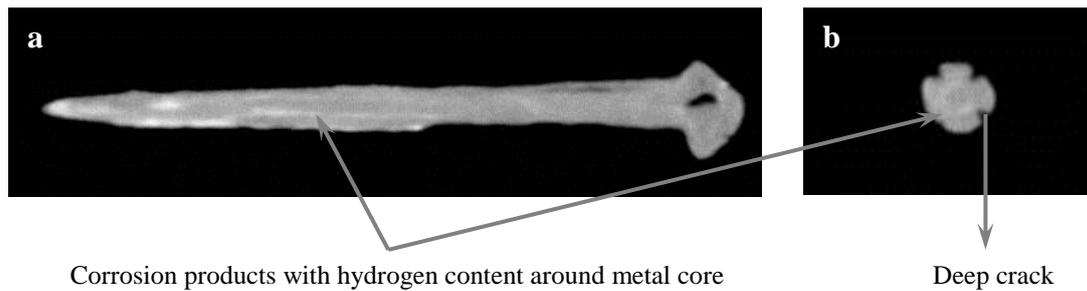
Figure 4.22. Neutron tomograms of MC8. a) Sagittal slice b) Axial slice.

The EDS analysis of the metal phase indicated the nail is a low tin bronze with about 6 wt% tin as alloying element and 0.7 wt% silicon as impurity (Appendix D. Table 4.2: analysis MC8a). Except for patches of corrosion products within the metallic phase and close to the central crack that was probably formed due to the manufacture method, with later expansion within the metallic phase in a burial environment, no traces of other inclusion is observable (Appendix B. Fig.80). The corrosion composition within the main open crack consisted of cuprite (Appendix D. Table 4.2: analysis MC8b) that has maintained pseudomorph structure of the solid solution α grains in this area. The corrosion product within the patches that were formed by act of inter- and intragranular corrosion in elemental proportion is almost close to a mixture of cuprite and tin oxide (SnO_2) in addition to small amount of impurities that originated from the environment (Appendix D. Table 4.2: analysis MC8c). The difference between the composition of the products within the main crack and patches around it can be due to the partial pressure of oxygen in these areas as suggested by Taylor and Macleod (1985). Within the open wide crevice where the condition was, well-oxidizing cuprite was formed in contrast to the areas with less oxygen in access where tin oxide was also detected in addition to cuprite. This phenomenon is known as the selective corrosion of bronze alloying elements (Scott 1990).

The metal phase consisted of homogeneous, very fine angular recrystallised grains of α, a solid solution of copper and tin, with both straight and distorted annealing twins. Most of the grains contain strain lines which can be seen in Appendix B. Fig.81. The average ASTM grain size number is 12 and microhardness is around 190 H_V. Lack of globular oxide inclusions which are usual products in remelted copper (Tylecote 1962, Scott 1991, Miller 2001), indicated that the nail was most probably manufactured from a piece of bronze that was produced in a direct process of smelting.

79

Microstructural evidence shows that the alloy, was worked and annealed to form fine recrystallised grains with annealing twins. The occurrence of strain lines in addition to both straight and distorted twins indicates the pin underwent cold working after final annealing. It is also possible that stress lines and distorted twins were partly formed later during utilization of the pin. It seems the nail was formed by hammering a piece of narrow rod, then the spherical head was formed by forging in a bowl shape header. The void within the head of the nail, which was revealed in neutron tomography (Fig.4.22), appears to have been formed during hammering of the rod. The nail shape and well-defined composition of the alloy indicate the skill of the metalworker in the production of alloy and the manufacture of the nail.

4.2.5. *Plano convex ingot*

MC9

This copper ingot was found in an unknown rock shelter in the area adjacent to Mapungubwe Hill. The small size of this copper, bun ingot (Plano convex) indicates that it could be the result of a secondary casting process, although a compositional analysis of the copper is needed to determine this for verification (Appendix A. Table: MC9). Its mould surface of the MC9 is irregular. Deep gas porosity holes can be seen in one part. In another zone there are a few shallow holes, combined with a small number of tiny blisters.

The texture of the mould surface is related to several factors, including the material used to make the mould, the presence of humidity in the mould structure, the amount of humidity present in the atmosphere during casting, irregularities in the mould manufacturing process and the amount of trapped gas in the molten metal (Mangou & Ioannou 2000). In this case the presence of large gas porosity holes on the mould surface indicates that it was casted in a non-porous material such as a stone or less porous clay mould (Pulak 2000) which did not allow the trapped gas to be easily displaced at the interface by the molten metal. Taking into account the upward movement of gases during casting, the origin of gases in the case of shallow and deep hollows could be the presence of humidity in the mould or high humidity in the atmosphere during casting. The inhomogeneous structure of the mould that may have been caused by its manufacture, with more porosity in one side, probably resulted in an irregular texture of the mould surface.

On the upper surface (rough surface) small blisters, along with two deep gas porosities, are observed in a small area just above the holes in the mould surface. In addition to the protrusion of molten copper in the middle of the rough surface, the presence of small blisters, are the results of casting in a one-piece open mould (Stech 1989). Here the use of radiography and tomography could assist in finding out more about the distribution of internal voids and, consequently, also about the conditions of casting without resorting to destructive sampling.

The neutron tomography slices indicated that only a small upper crust of the sample (where the protrusion is seen) appears relatively pore-free whereas numerous large pores are distributed throughout the interior elsewhere. This is clearly illustrated by the frontal and axial slices shown in (Fig.4.23a, b). The pores are characteristic of trapped gas accumulation and are known to occur under given conditions of casting. In fact, the frontal and axial slices show that the molten copper cooled rapidly on the surface, and formed a copper crust. The cooling was clearly rapid enough to prevent escape of gas bubbles to the top surface. The particularly large pore in the frontal slice (Fig.4.23a) has an interesting shape that may be explained as being consistent with quick cooling. The gas that formed this blister became trapped between the rapidly solidifying top which is in contact with air and side surfaces, and deviating towards the remaining hot molten part that remained towards the right and middle of the ingot. Rapid cooling of the ingot is further supported by the formation of the central protrusion. The tomography evidence thus indicates that poured molten metal could not properly mix due to rapid cooling in the peripheral region. The high rate of cooling of the molten copper may be a result of the flat shape of the object, especially near the circumference, and may also point to the use of high purity copper (100% wt copper).

Figure 4.23. Neutron tomography of MC9. a) Frontal slice of the bun ingot shows the velocity of cooling on the surface and sides of the ingot was so high that the gas bubbles mostly trapped in the bulk of ingot. Change in the direction of large void toward the centre for releasing exhibits this fact. b) Axial slice. Corrosion has only seen on the surface and inside some of open voids.

Based on an analysis of neutron tomography axial slices, approximately 4% of the ingot consists of corrosion products. This consists of products with hydrogen content that are only observable in few places on the surface and inside of few voids that are connected to the surface (Fig.4.23b). In this experiment the tomograms were not able to reveal the thin cuprite layer on the surface of ingot which

81

is clearly visible in the small cross section under binocular microscope (see section 5.2.2, MC9). A summary of the neutron tomography result of the object was given in Appendix D. Table: 4.1.

High purity of the metal constituent of the ingot (Appendix D. Table 4.2: analysis MC9a) is one of several factors that can indicate it is a secondary cast ingot which has been made from remelted copper (Tylecote 1982) and is not a direct result of a smelting process. The composition of inclusions within the metal (a part of eutectic phase) verified this. There were numerous small globular inclusions with a maximum dimension of 1.3 μm that contain copper oxide with a composition close to cuprite (Appendix D. Table 4.2: analysis MC9b). Some of these globules had a small amount of iron (0.2 wt%) which might have originated directly from the ore or added flux (iron oxide) that were used in the primary smelting process (Appendix D. Table 4.2: analysis MC9c). Globular cuprite inclusions are general consequences of a remelting process in an oxidation condition in crucible as mentioned before.

High porosity of the ingot with numerous voids within the metallic matrix (Fig. 4.23) can partly be the effect of the high purity of copper. Pure copper needs at least a temperature of 1150°C for melting and pouring in an effective casting (Tylecote 1962). Temperatures lower than 1150°C cause an increase in the viscosity of molten copper which decreases the rate of releasing the dissolved gases during casting. Dissolved gases were consequently entrapped in the solid metal. It is not possible to exactly determine the origin of the porosity within metal. In general, the voids form due to dissolved gases within molten metal, humidity in the mould or even in the atmosphere during casting (Mangou & Ioannou 2000; Hauptmann *et al.* 2002).

Etched transverse section of the ingot in its peripheral shows a dendritic microstructure of primary dendrite of α-pure copper and (α + cuprite) eutectic within interdendritic channels (Appendix B. Fig.82). The average microhardness is 62 H_V. This structure was formed due to the formation of cuprite during the remelting process which resulted in segregation of two different phases with a dissimilar melting point in a slow solidification. According to a Cu-O binary phase diagram, the eutectic phase of (α + cuprite) is formed at a temperature of 1066°C for an oxygen content higher than 0.03 at.% in an equilibrium condition (Neumann *et al.* 1984).The α-Cu dendrites have rounded outlines which predominantly consist of primary and secondary arms. The dendrite size decreased towards the mould surface (Appendix B. Fig.83), as a result of the fast cooling of molten metal in the vicinity of the mould surface, but in general the size is quite large which made it possible to observe them in low magnification of ×5. The evidence indicates that a piece of primary smelting copper was remelted in a crucible and cast in a mould, probably stone, that allowed slow solidification of the molten metal to form dendritic structures. The large size of both the dendrite cells and the voids within the metal indicate that the cooling rate was quite low although on the surface and in contact with the air in an open mould the molten copper was solidified at a higher rate and prevented the release of the gas from this area (Fig. 4.23).

© University of Pretoria

4.3. Summary and conclusion

4.3.1. Classification of the exposed physical signs of manufacture, usage and wear

The exposed signs of manufacture, use, and wear on the surface or within the internal structure of the copper objects, which were revealed by observation of the surface and neutron tomography, can be summarized as follows:

1. Scratch marks

These marks are seen on the surface of copper wires which were used to produce ornaments (KC3) and bangles (MC12), in the form of striation, and on plates (MC6) in an unparallel form. These scratches could have been formed during the manufacturing process or through the use of the objects. The scratches on the wires may be related to the method of manufacture. In the case of KC3 and MC12 the parallel abrasion could possibly have been made by some form of drawing technique because of the tidy structure of the lines. In MC6 the abrasion lines could have been directly produced by use. Here the lines are irregular and run in various directions.

2. Crease (burr)

Crease marks are seen on the edges of the copper strip which was used in production of a ring (MC3) and are a direct result of cutting the strip from a sheet of copper with a sharp tool such as a chisel.

3. Gas porosities

Gas porosities are present on the surface of the ingot (MC9). These were the result of trapped gasses at the interface between the mould and molten metal during casting.

4. Stress crack

This mark is seen in copper bangle (MC2). The stress crack on the bangle was formed by subjecting it to external stress during usage or burial.

5. Voids

These marks are seen within the ingot (MC9). Trapped gases in molten metal, the humidity content of the mould and dampness of the environment are responsible for the formation of voids in artefacts during casting.

6. Longitudinal hollow

This mark is seen among the copper wires (KC1, KC5, MC2, MC10 and MC12).These signs could be the result of strip drawing or hammering a copper strip to form a wire.

7. Fibre or metal Core

A metal core is seen within the funnels (MC5, MC6 and MC7). In all three funnels a corroded thin strip was observed which was folded gradually toward their tapered point. It is possible that these funnels were used for strip drawing. The core within the strip twisting wire (SC1) might be a fibrous core alone or a fibrous core with finer iron wire strands incorporated into the fibre bundle. It was not possible to determine which of these cores is exactly present within strip twisting wire (SC1).

4.3.2. Classification of the objects based on their physical stability

A study of the neutron tomograms cleared the objects on the basis of the form of remnant metal core, percentage of corrosion products and inner physical defects are in different levels of stability. The copper artefacts are in better condition compared to the iron artefacts because of copper nobility. On average 54% of the iron artefacts are severely corroded with more than 50% corrosion products per volume. Converasly 83% of the copper artefacts have less than 40% corrosion products per volume. On the other hand, the original surface of the objects has been preserved in different states, from good to poor condition. A summary of these results is given in (Appendix D. Table 3.1 and 4.1). With consideration of the results the objects can be categorized in two main and five subordinate groups as follows:

1. Rigid

   a. Homogeneous metal core and intact original surface:
   The metal core is robust and is seen continuously along the object. The original surface is intact and only a thin layer of corrosion products covered the surface.
   b. Homogeneous metal core with damaged original surface:
   The metal core is robust and is seen continuously along the object but in this case limited internal defects are seen. The corrosion crust is thick and in some areas the original surface has been damaged.

2. Weak

   a. Homogeneous metal core with high internal defects:
   These metal objects have a continuous but weak metal core. The weakness of the metal core is due to cracks, laminations or penetration of corrosion.

84

b. Inhomogeneous:

These metal objects are without a continuous sound metal core. Corrosion has completely destroyed the metal in some places. The remaining metal core often contains defects. The original surface in some cases has remained intact among corrosion products.

c. No metal core:

This consists of completely corroded objects with a damaged original surface.

The objects in each classification are listed in Appendix D. Table 4.3.

4.3.3. Composition, microstructure and manufacture methods

A summary of the microstructural description of the copper artefacts on the basis of the metallography results, was submitted in Appendix D. Table 4.4.

4.3.3.1 Metal composition

The majority of the copper artefacts in this assemblage are pure and mainly have copper as the only metallic element (Appendix D. Table 4.2). Only one artefact (MC8) revealed a considerable amount of other metallic element (>1 wt%) within the metallic phase. MC8 consists of copper with about 6.1% tin by weight which is similar to the composition of previous reported bronze objects from Mapungubwe by Miller (2001). The constant composition of the bronze objects that were found in Mapungubwe shows that the production of bronze was under the control of a skilful smelter. The existence of metallic impurity in the form of tiny dispersed inclusions is seen in the case of MC4. Here low amounts of iron (0.5 wt%) was detected along with oxygen within the metallic phase. Chlorine and silicon are the non-metallic impurities which were detected in the metallic phase of a few artefacts (KC1, KC4, MC8, and SC2). The origin of these elements in the metal is probably the tiny dispersed inclusions.

4.3.3.2. Inclusions

The detected inclusions in the metal phase of the objects mainly contain cuprite. Another constituent of inclusions in a few of the artefacts (KC1, KC4 and SC2) is silica (SiO_2). It is the major impurity in copper ores which cannot be completely eliminated during smelting and usually a small amount remains in smelted metal. Sulphur is another element which was detected in low amounts in some copper inclusion (0.1- 0.5 wt%). The source of sulphur could be sulphates present in oxidized copper ore (Tylecote 1962).

The chemical composition and physical form of the inclusions within the metallic matrix are quite informative when retracing the metallurgical steps that were used in the manufacture of the objects. On the basis of these criteria the cupreous objects in this assemblage can be classified as follows:

1. *Those objects that were manufactured of secondary casting copper by remelting smelted copper and subsequent casting.* The major inclusions of unalloyed copper objects (KC1, KC2, KC4, KC5, MC2, MC9, MC10, MC11, MC12 and SC2) consist of cuprite (Cu_2O) with consideration the proportion of weight percentage of oxygen and copper. Cuprite as an inclusion is formed through partial oxidation of copper during remelting of the primary ingot or prill in open crucible and in an oxidizing condition (Tylecote 1962, Miller 2001). This kind of inclusion can be also formed by reduction of water vapor by copper during melting in crucible (Tylecote 1962). According to the binary phase diagram of copper and oxygen, cuprite is formed in temperatures of 1066°C for an oxygen content lower than 33.3 at.% (Neumann *et al.* 1984). In subsequent solidification cuprite is seen in the eutectic phase (Cu+ Cu_2O) along with pure copper dendrite for oxygen content lower that 1.7 at.% (eutectic composition). This structure is clearly seen in the case of MC9 and MC11. Therefore, the presence of globular cuprite inclusions shows casting of remelted copper was the primary step in the manufacturing of these artefacts as was also reported by Stanley (1937) and Miller (2001). In these objects numerous cuprite inclusions decorated the metallic phase mostly in a banding structure (KC1, KC4, MC2, MC10, MC12 and Sc2) which indicate the object was hot worked during the next phase of their manufacture (Miller 2001). Only in two of the artefacts (KC2 and KC5) globular inclusions of cuprite were dispersed randomly.

2. *Those objects that were fabricated by direct hammering of a piece of smelted copper.* Only two artefacts of this assemblage were in this category. In these objects cuprite globular inclusions in the metallic phase were not detected at all, such as MC8 (bronze nail) or are in low numbers and in admixture with iron oxides as in the case of MC4. The inclusions within metallic phase of MC4 are quite low in numbers while having an angular form of admixture of cuprite and magnetite (Fe_3O_4). The origin of magnetite, which is a common slag in the smelting process, can be the gangue as one of its material constituent or the excess amount of ferric oxides that were added to the ore in the stack as a flux. Therefore magnetite could be formed by partial reduction of iron(III) oxides that were used as flux (Cooke and Aschenbrenner 1975) or it remained unreduced as a part of the material constituent of the ore. It was reported that iron oxide as a flux was used occasionally in the smelting of copper in the metalworking of sub-Saharan Africa (Van der Merwe 1980, Miller & Van der Merwe 1994). On the other hand, the presence of magnetite as one of the material constituents of copper deposits in southern Africa such as Phalaborwa mine (Dawson & Hinton 2003) indicates that the copper ore could be the source of magnetite in smelted copper. Since the source of copper that was used in manufacture of the artefact is not clear it is not possible to prove which of these categories was the case. The presence of magnetite shows that the atmosphere of the furnace was not reducing enough to transform it to wüstite or even metallic iron in a solid state (Cooke and Aschenbrenner 1975).

It seems that the bronze that was utilized in the fabrication of (MC8) was a direct product of smelting copper and tin ores together in a one-stage smelting process. It is also possible that the bronze was produced by some kind of refining process during remelting. The recent lead isotopic study of Molofsky (2009) on one of the bronze objects from Mapungubwe shows that the source of tin and even copper could be from the Rooiberg tin and copper mines. This means the smelted tin and copper in the Rooiberg mines might be alloyed to produce bronze *in situ*. It is also possible that the metals originated from other deposits with the same geological age as the Rooiberg deposits. This evidence shows the smelters were familiar with the one-stage production of bronze during smelting or refining of the bronze during remelting. Present archaeological evidence on bronze production in southern Africa is sparse and to understand bronze production contexts and to date them more scientific work is necessary.

4.3.3.3. Methods of manufacture

Except for two specimens (MC9 and MC11) which kept their dendritic casting structure, the other artefacts contain angular recrystallised copper grains with annealing twins. This structure shows that the artefacts were subjected of successive hammering, hot or even cold, with a final annealing operation in the latter case. Hot working of the copper produces the same microscopic structure as when the metal is subjected to cold working with further annealing (Scott 1991). It is therefore impossible to ascertain which method was used in the manufacture of the copper objects. Evidence of cold-working is seen in the form of flattened grains and distorted annealing twins in the case of (KC4, MC2, MC4, MC8 and SC2). Except for MC8, which has strain lines almost all over its fine grains (ASTM 12), the other objects display traces of cold working in only a limited segment close to the surface. This shows up in conventional copper manufacture, the objects were left in a fully annealed state and signs of cold working are related to probable final finishing in the manufacture or were formed by wear. This was also reported by Miller (2001).

Cross section of one of the funnels (MC7) in this assemblage shows that these simple geometric objects were utilized in the manufacture of wire by drawing a thin strip of iron or copper through its tapered central interior. Through this method several funnels with diminishing vertex diameters were probably used to produce the desire thickness of the wire. The funnels were fixed on a stable base, or even held in the hand, and the strip was then firmly drawn through it using other hand. The thickness of the wires thus produced should be somewhat less than 3mm, taking into account the wire diameter within the examined funnel. Superficial, deep microscopic scratch marks on the surface of MC6 (Fig.4.11) could be evidence of the friction between the funnel wall and the base. A funnel with exact excavation provenance from the Hill indicates that this technique was in use during phase three of the settlement (1220- 1250) onwards.

Microstructure study of the round wire bangles (KC5, MC2, MC10 and MC12) with discontinuous internal hollows (Fig.4.4, 37, 45, 47) shows that they were manufactured by the working and annealing of cast copper. On the other hand, the only bangle (MC11) with dendritic structure which contains numerous small voids in the metal phase, shows any sign of longitudinal void in its tomograms. This means that discontinuous void within the metal phase in KC5, MC2, MC10 and MC12 was most probably formed during working. Certainly, the cross sections of the bangle close to the end (MC2, MC10 and MC12) have a form between rectangular and elliptical, with expanded separate arms in one direction which, in the case of MC10, were bent around the peripheral of the sample. This may be produced either by hammering and folding of a thick ribbon of copper (2-3 mm on the basis of bangle thickness) or passing it through a rough hole as Stanley (1937) suggested for spiral rounded wire. Oddy (1984) noted that the striation on the surface of the wires is not similar to those seen in drawn prehistoric European wire, and believes the first technique together with some kind of burnishing was utilized in their manufacture. The fully annealed structure of the bangles precludes complete interpretation of the various stages and techniques of working that the objects were subjected to after casting, and clearly the presence of the longitudinal voids and parallel striation on one of the artefacts (KC3) in this class will remain in ambiguity.

Chapter 5

Chemical stability and deterioration process

5.1. Introduction

Evaluating chemical stability in archaeological artefacts refers to the recognition of the process of chemical deterioration in their material constituents which causes loss of their integrity. In general chemical deterioration is the main factor in the disintegration of metals. This process, which is known as corrosion, is accompanied by a loss of material and the physical deformation in objects. Corrosion begins immediately after metal extraction from ore and continues during manufacture and later usage. The formation of corrosion is directly related to the composition and microstructure of the metal base and also to the surrounding environment. Corrosion results in loss of significant historical evidence in archaeological artefacts. To reduce the damage of corrosion numerous scientific studies have been conducted in both the fields of industry and conservation of historic metals. These researches are partly attributed to the revelation of chemical reactions involved in the corrosion process of metals in different environments (Walker 1982; Selwyn *et al*. 1999; Selwyn 2004; May 1953; Organ 1963; North & Pryor 1970; Lucey 1972; Macleod 1981; McNeil & Little 1992; Pollard *et al.* 1992; Scott 2000). The corrosion products, their chemical and physical properties in addition to the range of their stability in the environment were also considered in some of these investigations (Potter 1956; Evans 1923; Misawa 1973; Turgoose 1982*a*; Refait *et al*. 1997; Selwyn *et al*. 1999; Selwyn 2004; Gettens 1961; McNeil & Little 1992). Most of these researches were performed in a laboratory and the results may not be precisely the same as the reactions that naturally occur in nature but the outcomes are valuable in the conservation of metals.

This chapter focuses on evaluation chemical stability of the artefacts and consists of two main parts. The first part focuses on identifying the composition of corrosion products on the surface of metal artefacts. These products are a combination of the products that were formed during burial and later in the storage while some of them could be produced by alteration of the primary corrosion products. The chemical and physical properties of the identified products are also discussed in this chapter. The condition of formation, the range of their stability and the destructive effects of products are also referred to. Corrosion products layout on artefacts which is an important factor in the process of cleaning is defined. The results of this part of the chapter will assist to find a correct response to routine questions in the field of metal preservation. These are:

a. What is the composition of corrosion products?

b. In which conditions are the identified corrosion products formed?

c. What is the chemical range of stability of the identified products?

d. What is the layout of corrosion products on the object?

e. Which one of the corrosion products presents problems for the stability of the objects?

f. Can the original surface be identified in corrosion products or not?

In the second part of this Chapter the condition of the burial environment at K2, which had the only available soil samples, is assessed. The purpose of this part is to provide information for a better

89

interpretation of the present corrosion products on the surface of the artefacts which were excavated a long time ago. The soil corrosiveness as an effective factor in the disintegration of metals during burial is also discussed. This study helps to find scientific clarification about the poor condition of most excavated metal objects.

5.2. Study of corrosion structure and composition on artefacts

5.2.1. Iron artefacts

KI1

A study of the transverse section of the rod revealed a bilayer corrosion on the surface which consists of the internal layer (L1) adjacent to the metal surface and the external layer (L2). The external layer overlays the internal layer and is in close contact with the surrounding environment. The main obvious differences between these layers are the presence of two phases bloomery ghost inclusions in the internal layer and grains of silica in the external layer (Appendix C. Fig.1, 2). Both layers are porous and full of cracks. The open crevices in these layers were partially formed during sampling and are quite new (Appendix C. Fig.1) contrary to cracks which were filled by corrosion products in the past (Appendix C. Fig.2) or fine ones at the internal layer.

EDS results revealed that the internal and external layers consisted of different phases of iron oxides or oxy-hydroxides with a different proportion of oxygen in their chemical structure. The phases have non-distinctive stratification and irregular dissemination at both layers. The internal layer consisted of two distinctive compounds with a different oxygen percentage which is observable in light and dark grey (Appendix C. Fig.1). The light grey phase has a lower amount of oxygen compared to the darker phase (Appendix D. Table 5.1: analysis KI1L1a, b). The high amount of oxygen in the rest of the analyses in the dark grey phases at the internal and external layers (Appendix D. Table 5.1: analysis KI1L1b, KI1L2a, b) could be a sign of hydroxyl $(OH)^-$ in the corrosion composition or may indicate the presence of a hydrated form of iron compounds such as polymorphs of iron(III)oxyhydroxide and rust $(Fe_2O_3.H_2O)$ respectively. These analyses indicated that iron and oxygen are the main elements constituent of corrosion products, and that other corrosive elements from the environment such as chlorine and sulphur had no effect on corrosion. Analysis at the internal layer in position 1 and 2 (Appendix D. Table 5.1: analysis KI1L1a, b) shows a low amount (0.2%) of Mo, Na and Si that might have originated from a remnant of fine inclusions which were detected in the metallic phase (Appendix D. Table 3.2: analysis KI1a) or simply transported inward from the burial environment. Since Na and Mo were not detected within the external corrosion layer (Appendix D. Table 5.1: KI1L2a, b) it is more likely that they were derived from the inclusions with Mo and Na content present in the metal matrix. The extraneous elements at the external layer have more diversity

90

(Si, Ca, Mg and P) while their amount increases towards the surface. No traces of chlorine was detected by EDS in the corrosion layers.

Complementary analysis of corrosion on KI1 as a representative sample from K2 was performed by XRD to identify the products more accurately. The result revealed the presence of magnetite, lepidocrocite (γ-FeOOH), goethite (α-FeOOH), hematite (Fe_2O_3) and calcite as the main compounds in the crystalline form in the corrosion layer (Fig.5.1). On the basis of EDS results the detected calcium carbonate is related to the surface contaminations concentrated at the external layer (Appendix D. Table 5.1: analysis KI1L2a and KI1L2b).
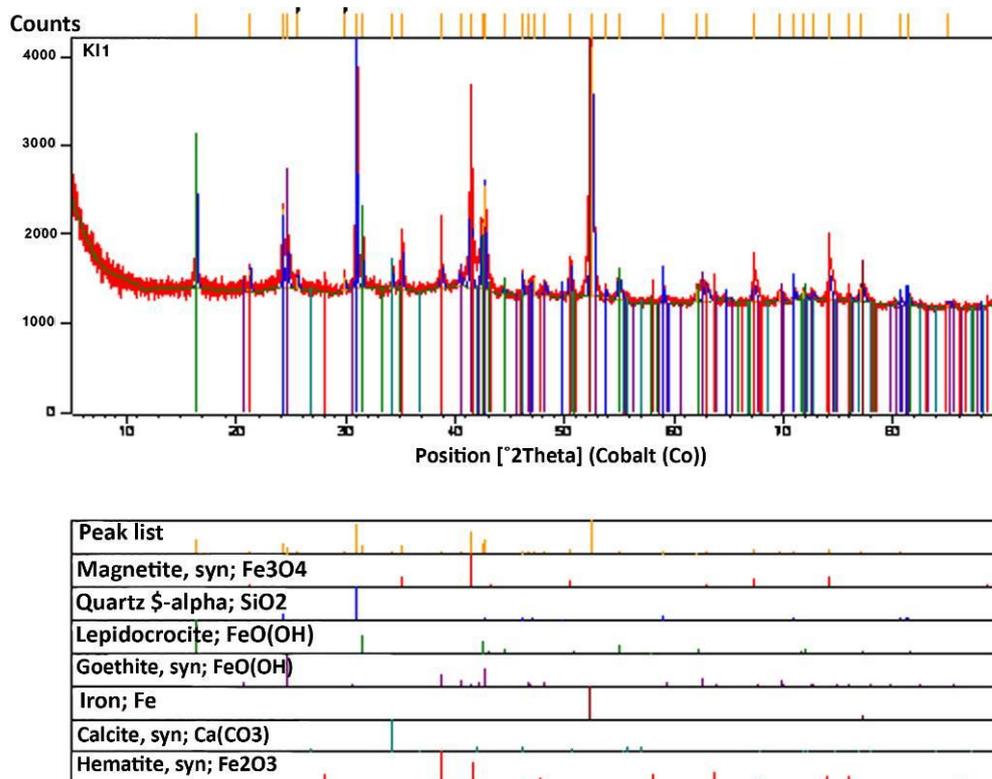
Figure 5.1. XRD scan of corrosion powder removed from KI1 surface.

Further analysis of the mounted sample by micro-Raman showed the position of the compounds by revealing their composition *in situ*. Identifying the exact composition of each phase was achieved by comparing the results with the Raman characterizations of pure iron oxides/hydroxides in Bell *et al*. (1997) and Froment *et al*. (2008). The Raman spectral signatures of iron oxides and hydroxide were given (Appendix D. Table 5.2).

The results indicate the light gray area at the internal layer consisted of two main phases (a) and (b) (Fig.5.2a, b). The phase (a) with a broad and strong peak at 679-706 cm^{-1}, weak peaks at 378 and 505 cm^{-1} is maghemite (γFe_2O_3). The weak peak at 547 cm^{-1} may relate to magnetite (Fe_3O_4) as a part of material constituent of this phase. The strong peak of magnetite at 670 cm^{-1} was covered by the broad

peak of maghemite in this region. The phase (b) consisted of hematite (αFe_2O_3) with strong double peaks at 220 and 288 cm^{-1}, weak peaks at 403 and 497 cm^{-1} as well as a medium peak at 658 cm^{-1}.
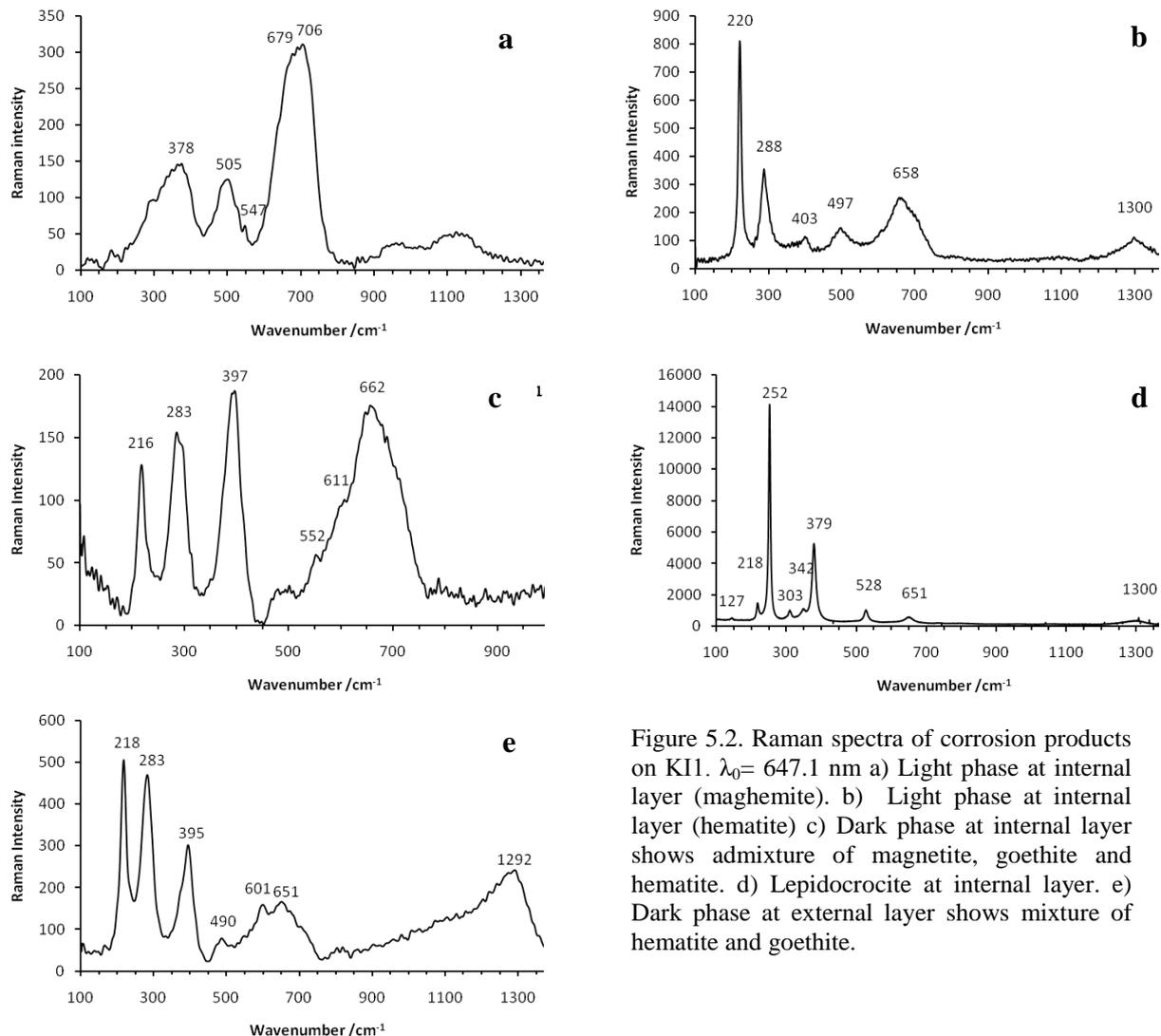
Figure 5.2. Raman spectra of corrosion products on KI1. λ_0= 647.1 nm a) Light phase at internal layer (maghemite). b) Light phase at internal layer (hematite) c) Dark phase at internal layer shows admixture of magnetite, goethite and hematite. d) Lepidocrocite at internal layer. e) Dark phase at external layer shows mixture of hematite and goethite.

The analysis of the dark grey phase at the internal layer (Fig.5.2c) revealed that it mostly consists of an admixture of magnetite, goethite and hematite. Signature doublet strong peaks of hematite with a downshift are observable at 216 and 283 cm^{-1} while the latter is quite broad as a result of overlapping with goethite medium peak at 300 cm^{-1}. This shift could be due to Si and Na in the structure of the dark phase at the internal layer (Appendix D. Table 5.1: analysis KI1L1b). The strong peak at 397cm^{-1} is the signature of goethite which overlapped the weak hematite peak at 403cm^{-1} and resulted in broadening of the peak. The shoulder in 482-519 cm^{-1} is due to the overlapping of the goethite and hematite weak peaks at 480 and 497 cm^{-1} respectively. The weak peak at 552 cm^{-1} is related to the goethite while the medium peak at 611 cm^{-1} belongs to hematite. The strong broad peak at 662 cm^{-1} can be the signature of magnetite which in pure sample is observable at 670 cm^{-1}. The

92

broadening is due to overlapping with goethite and hematite peaks in this region. Figure 5.2d shows an analysis of a well crystallized area at the interface of the internal/external layer. The strong peak at 252 cm^{-1}, medium peak at 379 cm^{-1} in addition to the weak peaks at 303, 528 and 651 cm^{-1} are the Raman characteristics of lepidocrocite (γFeOOH).

The analysis of the external layer showed that it mostly consists of hematite and goethite (Fig.5.2e). In Figure 5.2e the doublet strong peaks at 218 and 283 cm^{-1} are the signature of hematite while the strong peak at 395 cm^{-1} is characteristic of goethite. Analysis of light phases at the external layer rising to a spectrum similar to Figure 5.2b also revealed that this phase mostly consists of hematite.

KI3

A polished cross section of the sample cut off from the adze shaft revealed a bilayer corrosion on the surface as a result of generalized corrosion. On a large part of the section the external layer with grains of silica was not observable (Appendix C. Fig.3). It is due to the removal of this layer from a large area of the shaft, probably by mechanical stress at some point in time (See appendix A. Table: KI3). The internal layer predominantly consisted of two phases. The darker phase contained a high amount of oxygen which indicated the presence of hydrated compounds of iron as one of material constituents of the phase which cannot be identified exactly by the weight proportion of elements in the EDS result (Appendix D. Table 5.1: analysis KI3L1a). The light phase which is seen as patches among the darker phase had a composition approximating hematite (Appendix D. Table 5.1: analysis KI3L1b). The low amount of molybdenum (0.2 wt%) (Appendix D. Table 5.1: analysis KI3L1a) is related to the remnant of inclusion among corrosion products. Silicon was the prominent associated soil element at the internal layer. SEM BSE revealed the presence of two phases in the external layer. The light phase with a lower oxygen content probably contains iron oxides (Appendix D. Table 5.1: analysis KI3L2a).The dark phases had a high amount of oxygen content which presumably has hydroxide compounds of iron (III) as one of its material constituent (Appendix D. Table 5.1: analysis KI3L2b). Chlorine was not detected in corrosion.

KI5

A polished cross section of the drill showed generalized corrosion on the surface. The corrosion consisted of two distinctive layers (Appendix C. Fig.4 and 5). A dense inhomogeneous internal layer which contains mostly a composition approximating magnetite (Appendix D. Table 5.1: analysis KI5L1a) and patches of a darker phase with close elemental percentage with (KI5L1a), probably a mixture of different oxides (Appendix D. Table 5.1: analysis KI5L1b) in addition to a quite darker phase of iron oxyhydroxide (Appendix D. Table 5.1: analysis KI5L1c). A porous external layer with particles of silica in a matrix of iron oxyhydroxide (Appendix D. Table 5.1: analysis KI5L2a) and

93

hydrated compounds of iron oxide (Appendix D. Table 5.1: analysis KI5L2b) covered this layer. Chlorine was not detected in corrosion.

MI2

The transverse section of the hoe at the blade showed one porous corrosion layer on the surface as the result of both generalized and localized corrosion. In the area with localized attack the corrosion penetrated to the metal structure along the elongated inclusions (Appendix C. Fig.6). Linear EDS analysis of the corrosion layer revealed the presence of two compositions approximating iron(III) oxyhydroxide and hematite as the main products present in this layer (Appendix D. Table 5.1: analysis MI2L1a, c, d, e and analysis MI2L1b respectively).

MI4

The transverse section of the hook revealed both generalized and localized corrosion on the surface which consisted of two internal and external layers (Appendix C. Fig.7). SEM BSE revealed the presence of two phases at the internal layer. The dark phases had a high amount of oxygen content which presumably has hydroxide compounds of iron (III) as one of its material constituent (Appendix D. Table 5.1: analysis MI4L1a). The light phase with a lower oxygen content probably contains iron oxides (Appendix D. Table 5.1: analysis MI4L1b). The ghost remnants of inclusions were observable in this layer. At the external layer the quartz grains imbedded in an intermediate with the same elemental proportion as MI4L1a (Appendix D. Table 5.1: analysis MI4L2a). The intermediate between these two layers was defined as the original surface which is illustrated with a dash line in (Appendix C. Fig.7).

MI5

The transverse section of a small detached part of fused adzes revealed no metal remnant at the blade. An elongated void associated with its dense peripheral corrosion products has kept the previous form of the blade (Appendix C. Fig.8). SEM BEI revealed the presence of two phases in the corrosion. The light phase with a low amount of oxygen in comparison with the darker phase presumably contains iron oxides (Appendix D. Table 5.1: analysis of MI5L1a) while the darker phases have hydroxide compounds of iron (III) as a part of material constituent (Appendix D. Table 5.1: analysis MI5L1b and c). An external layer (L2) that contained particles of sand in a matrix of iron (III) compounds has covered this layer.

MI6

The transverse section of the rod revealed the presence of two corrosion layers on the surface (Appendix C. Fig.9). A thin inhomogeneous internal layer with numerous cracks was located adjacent

94

to the metal surface. The EDS analysis showed that the layer consisted of two phases. However, identifying the exact composition of compounds on the basis of these results was difficult. A high amount of oxygen in the dark phase (Appendix D. Table 5.1: analysis MI6L1a and L1c) could be an indication of an admixture of hydroxide compounds of iron (III). The light phase may contain different iron oxides such as magnetite, hematite and maghemite (Appendix D. Table 5.1: analysis MI6L1b). The internal layer was covered by a porous layer containing particles of quartz embedded in high oxygen content iron products (Appendix D. Table 5.1: analysis MI6L2).

Scraped corrosion products from a small section of MI6 as a representative sample from Mapungubwe was sent for complementary analysis by XRD. The result revealed a diversity of corrosion products on the surface (Fig.5.3). Goethite (α-FeOOH), lepidocrocite (γ-FeOOH), jarosite ($KFe_3(SO_4)_2(OH)_6$) with a low amount of magnetite (Fe_3O_4) were detected as iron products with a crystalline form on the surface. Hydrotalcite ($Mg\,Al)(OH)_2(CO_3)(H_2O)$, albite ($AlSiO_8$) and quartz ($SiO_2$) were the contaminants that adhered to the surface by diffusion of iron ions towards the environment . No trace of akaganite was detected on the surface.
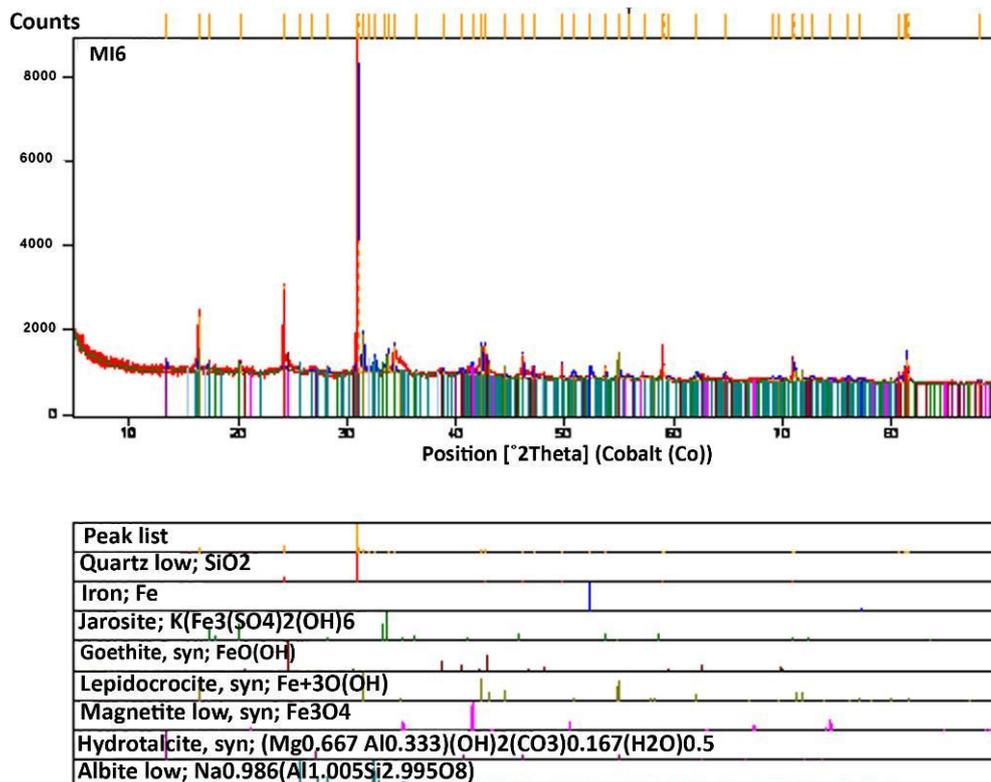
Figure 5.3. XRD scan of corrosion powder removed from MI6 surface.

MI7

A transverse section of the hoe blade showed a one-layer corrosion structure on the surface (Appendix C. Fig.10). This layer was dense with no trace of quartz grain. This indicated that the hoe

95

was not buried. The corrosion consisted of two phases. A light grey phase with probable iron oxides composition was located amongst the main dark phase (dark) with high oxygen content (Appendix D. Table 5.1: analysis MI7L1a). These compositions were associated with a low amount of soil elements.

MI8

A cross section of the block twisting wire revealed a bilayer corrosion structure on the surface that resulted from generalized corrosion (Appendix C. Fig.11). The internal layer with its inhomogeneous and dense structure contained numerous cracks. Two different compositions were detected in this layer by the EDS analysis. A light phase with probable iron oxides composition (Appendix D. Table 5.1: analysis MI8L1a) and a darker phase with a high amount of oxygen that presumably contains iron(III)oxyhydroxide as part of the material constituent (Appendix D. Table 5.1: analysis MI8L1b). The internal layer was covered by a layer that consisted of sand imbedded in a two-phase matrix. The main phase composition was quite similar to MI8L1b (Appendix D. Table 5.1: analysis MI8L1b) while a thin layer with a high amount of calcium (33.4%) covered the whole of surface (Appendix D. Table 5.1: analysis MI8L2b). This phase presumably contained calcium carbonate.

MI9

The polished transverse section of the hoe at blade showed a bilayer corrosion on the surface as the result of generalized and localized corrosion (Appendix C. Fig.12). The internal layer was dense, homogeneous, with numerous cracks. Some of these cracks, which are wide, were formed during sampling by inward stress. In some areas corrosion penetrated inside the metal structure along the inclusions. The ghost remnants of these inclusions were observable among internal corrosion products. EDS analysis of the layer revealed iron and oxygen as the main elements constituents while the oxygen weight percentage was quite high compared to the proportion of this element in routine corrosion products of iron (Appendix D. Table 5.1: analysis MI9L1). Consequently, in order to reveal the exact composition of the product needs further complementary analysis. The internal layer is covered with a thin external layer which contains small grains of sand. The external layer on MI9, compared to the layers on other iron artefacts with exact origins from Mapungubwe, was really thin.

MI10

The polished transverse section of the hoe at the blade showed one corrosion layer (internal layer) on the surface that resulted from generalized corrosion (Appendix C. Fig.13). Scanning electron back scatters (SEM, BEI) image revealed that the layer consisted of two phases. EDS analysis of the dark phase revealed iron and oxygen as the main elements constituent while the oxygen weight percentage was quite high compared to the light phase products (Appendix D. Table 5.1:analysis MI10L1a). On the basis of the complementary analysis by Raman on KI1 this phase probably contains iron (III)

oxyhydroxide as a part of its material constituent. Revealing the exact composition of this phase needs further complementary analysis. The light phase with a low amount of oxygen presumably contains iron oxides (Appendix D. Table 5.1: analysis MI10L1b). On the other hand the black appearance of corrosion on the surface of the hoe is an indication of magnetite as one of the corrosion constituent of the layer. A lack of an external layer with imbedded sand grains in addition to the presence of a black phase of probable magnetite on the surface, which is formed in regions with a low level of oxygen (reducing area) (Evans 1923; Potter 1956; Walker 1982), could indicate that the hoe was either cleaned in the past or an external layer flaked off the surface. In the probable process of cleaning, the usual red-brown rust which is formed in high levels of oxygen was removed, and the lower layer of magnetite was exposed on the surface.

SI1

Transverse polished cross section of the detached part of the spatula revealed a bilayer corrosion on the surface (Appendix C. Fig.14). An inhomogeneous internal layer in terms of composition was located adjacent to the metal surface. Five (5) different compositions were detected by EDS analysis in this layer. Dark grey corrosion near the metal surface consisted of iron, oxygen and a low amount of chlorine (4.2%wt) as the main elements while the amount of oxygen was quite high compared to the elements proportion in routine iron corrosion products (Appendix D. Table 5.1: analysis SI1L1a). In this area corrosion resulted in the formation of shell-like structure on the surface (Appendix C. Fig.14). The shells contained a high amount of chlorine in their composition (Appendix D. Table 5.1: analysis SI1L1b) which was probably the secondary corrosion products of iron akaganéite. A high amount of sulphur was detected at the peripheral of this area (Appendix D. Table 5.1: analysis SI1L1c) with composition approximating iron (II) sulphate. The two other phases had a composition approximating iron (III) oxyhydroxide (medium grey) and magnetite (light grey) (Appendix D. Table 5.1: analysis SI1L1d and SI1L1e respectively). The external layer consisted of grains of quartz embedded in a matrix of iron oxide with a high proportion of oxygen associated with a diversity of soil elements (Appendix D. Table 5.1: analysis SI1L2).

5.2.2. Copper artefacts

KC1

The transverse section of this bangle shows a generalized corrosion attack due to the high dissolution rate of copper. The corrosion crust thickness is about 900μm which is quite high. The corrosion crust on the surface consisted of three distinctive layers, an internal layer (L1), a cuprite layer (L2a) and an external layer which contains three sublayers of L2, L3 and L4 (Appendix C. Fig.15). The interface cuprite layer (internal/external) has been completely fragmented. Chlorine,

oxygen and silicon are the only elements which originated from the soil in the internal layer. This layer contained the highest chloride amounts compared to the rest of layers. The result of EDS in this layer shows the probable coexistence of cuprous oxide and chloride. The low hardness of the corrosion layer (L1) which was more abraded compared to both cuprite and external layers during standard sample preparation proves the presence of a composition with low hardness in corrosion such as cuprous chloride (nantokite) with the mohs hardness of 2.5.

The external layer has a lamellar structure from the vicinity of the internal layer towards the outermost of the corrosion crust. Copper trihydroxychloride and cuprite are the main phases of this structure with alternate layout (Appendix D. Table 5.3: analysis L2, L2a, L3, L3a and L4). L2a and L3 (light gray) was copper oxide with composition approaching to cuprite. L2, L3a and L4 in elements proportion were similar to copper trihydroxychlorides. Towards the surface in L3 (cuprite layer), grains of sand (dark gray) were observable which showed this layer was formed by the precipitation of dissolved copper ions on the surface. In the L4 the dark gray areas contained copper silicate (Appendix D. Table 5.3: analysis KC1 L4b). At the outer part of L4 copper trihydroxychloride (Appendix D. Table 5.3: analysis KC1 L4a) was seen in its crystalline form. Finding the exact crystal system to identify the kind of product was quite problematic since a complete form was not observable in this image. Nevertheless the crystals were approximately similar to the trigonal system and were probably paratacamite (Appendix C. Fig.16). The limit of the original surface is seen between L1 and L2.

KC2

As shown in (Appendix C. Fig.17) both types of patina, even and coarse, are seen on the surface of this rod. The thickness of the corroded layer is variable between 100- 500 μm in a different zone. Even and coarse patina consisted of two and three layers respectively. Cuprite layer, L1, which is seen in light gray at the even surface (internal layer) had almost been disintegrated at the coarse part by the accumulation of chloride ions but a thin part still has remained continuously on the whole metal surface (L1a). The obvious difference between the cuprite layers in these two zones is the presence of Al which originated from soil and the higher amount of Cl (3.2 wt%) in the uneven surface (Appendix D. Table 5.3: analysis KC2L1 and L1a). The source of sulphur in L1a is probably the remnant inclusions that were previously in the bulk of metal before corrosion (Appendix D. Table 5.3: analysis KC2 inclusion). Layer two in the uneven surface (internal layer) contained a high amount of chloride (23.6wt%) as a result of the migration of chlorides towards the anode (Scott 2000). This layer probably contains nantokite as one of its constituents (Appendix D. Table 5.3: analysis KC2 L2). The internal layer has been covered by a layer of cuprite and copper trihydroxychlorides alternately (external layer) (Appendix D. Table 5.3: analysis KC2 L3 and L4a). On an even surface the external layer has a composition which cannot be identified based on EDS results. This layer (L4) contains a

variety of soil elements with a maximum amount for silicon and oxygen, and particles of sands. The limit of the original surface remained intact in even surfaces and completely destroyed in coarse surfaces.

The XRD analysis of corrosion products which were scraped off from small parts of the object with a scalpel (Fig.5.4) revealed the presence of atacamite, paratacamite and nantokite as the main crystalline products in the corrosion layers. Quartz (SiO_2) and gypsum ($CaSO_4.2H_2O$) were the only products from the burial environment which were cemented together by cupric compounds on the surface and indubitably in L4.
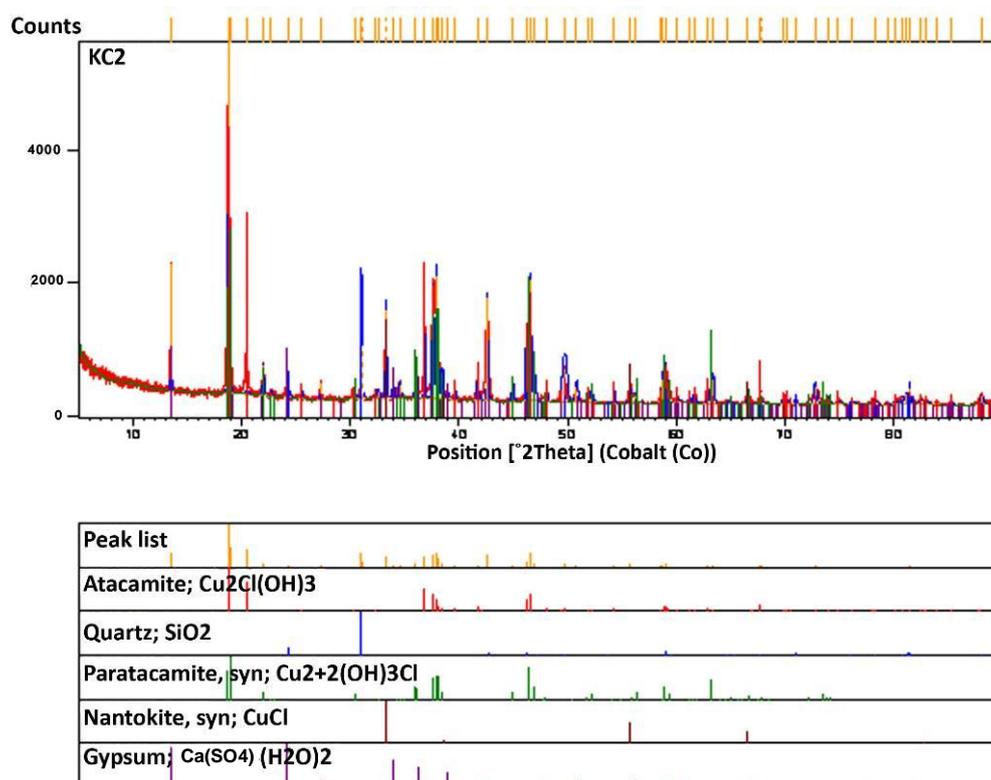
Figure 5.4. XRD scan of corrosion products removed from surface of KC2.

Complementary analysis on KC2 by micro-Raman was summarized in (Fig 5.5) while the focusing position of laser on the surface was submitted in Fig C.17. The position (1) corresponds to light areas in L1 and disperses light phases in L2 giving rise to spectra (Fig 5.5a) revealing that cuprite is present with its Raman signature at 146, 215, 638 cm^{-1} (Bouchard & Smith 2002). The efforts to obtain spectra in position (2) (the waxy texture phase) failed since high power laser (>4 mW) burnt the material and analysis with laser power less than this amount did not present any result. The position (3) attributes to an area in L2 within the waxy phase (b) leading to spectra (Fig.5.5b, c) revealing atacamite as a material constituent (Bouchard & Smith 2002; Frost 2003) with Raman signatures at 3435, 3349, 3328, 947, 913, 820, 513, 415, 149 and 120 cm^{-1}. The position (4) related to medium grey

99

phase in L4a directing to spectra (Fig.5.5d,e) exposing clinoatacamite as a material constituent of this zone (Frost 2003) with Raman signatures at 3437, 3388, 3351, 3305, 969, 929, 892, 512, 422, 367, 215, 139 and 116 cm^{-1}. Some of the bands of both atacamite and clinoatacamite do not fit perfectly with those submitted in literature by Bouchard and Smith (2002) and Frost (2003) but the differences are quite low. For instance, Frost (2003) attributes the following Raman bands to clinoatacamite: 3443, 3357, 3314, 969, 927, 892, 511, 420, 364, 206, 142 and 118 cm^{-1} which are close to bands achieved in position (d).These differences could be the results of impurities present in corrosion products.
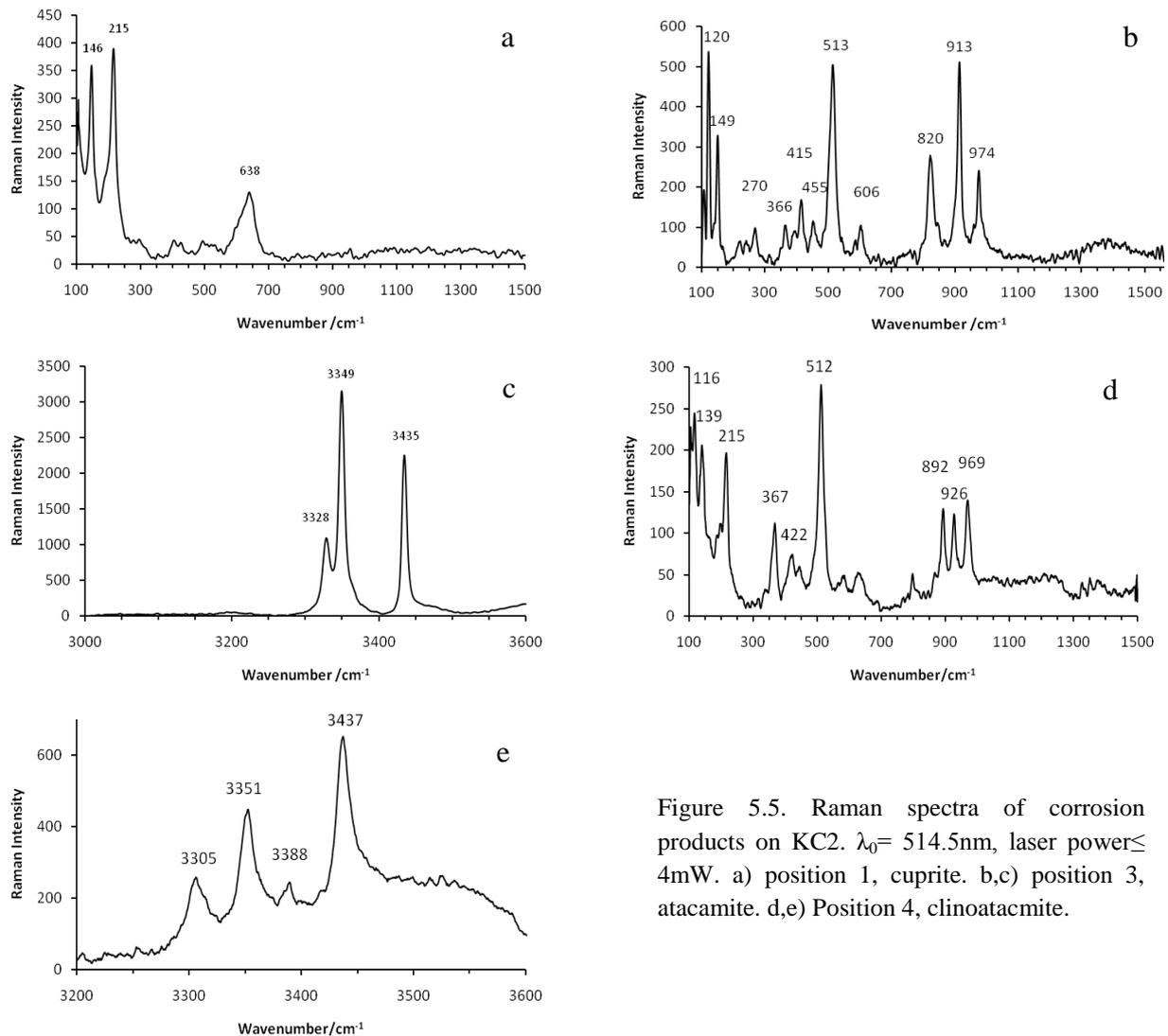
Figure 5.5. Raman spectra of corrosion products on KC2. λ_0= 514.5nm, laser power$\leq$ 4mW. a) position 1, cuprite. b,c) position 3, atacamite. d,e) Position 4, clinoatacmite.

The detected clinoatacamite (monoclinic) revealed that the identified paratacamite by XRD might be a fault due to the erroneous data with regard to crystal structure of paratacamite in the ICDD files, 25-1427 as was discussed in detail by Jambor *et al*. (1996). Paratacamite has a rhombohedral structure (Frondel 1950) while in ICDD files, it was attributed a monoclinic structure by Oswald and Guenter (1971). Scott (2000) suggested that it is a common error in recent conservation or archaeometric

100

literature which must be revised. With consideration that paratacamite has almost 2% zinc or other cations, such as nickel in its structure, lack of these cations in position 4 (Appendix D. Table 5.3: analysis KC2L4a) indicates the presence there of clinoatacamite which was not detected by XRD.

KC4

The transverse polished section of the plate showed the presence of both even and coarse surfaces on this object (Appendix C. Fig.18) as a result of generalized corrosion. The adjacent corrosion layer to the metal phase had a composition close to cuprite (Appendix D. Table 5.3: analysis KC4 L1). This layer (internal layer) is seen on the entire metal surface continuously with irregular thickness. The only element from the environment was oxygen in bilayer area (even surface). In areas with uneven surface a low amount of chloride (~0.3%) and Si was detected in cuprite layer (Appendix D. Table 5.3: analysis KC4 L1a). Internal layer in uneven surfaces consisted of chloride compounds of copper (L2).

Analysis in the area of L2 and close to the L1 revealed a composition approximating copper trihydroxychloride (Appendix D. Table 5.3: analysis KC4 L2b) meanwhile in the same area and closer to the above cuprite layer the amount of chloride was quite high (Appendix D. Table 5.3: analysis KC4 L2c). This indicated that the layer consisted of an admixture of different copper compounds with considerable amount of chloride such as nantokite as one of its constituents. A layer of cuprite is seen above this layer (L2c) which is covered by an external layer. The external layer on the even surface contained copper and soil elements from the environment and was quite porous (Appendix D. Table 5.3: analysis KC4 L2a).

KC5

The polished cross section of the bent rod showed three corrosion layers on the surface (Appendix C. Fig.19). The internal layer was copper oxide with bulk composition close to cuprite (Appendix D. Table 5.3: analysis KC5 L1). Except for oxygen no trace of other elements from the environment were detected in this layer and has an irregular shape with different thickness.

The middle layer contained a high amount of elements (Si, S, Ca) from the environment (Appendix D. Table 5.3: analysis KC5 L2). The external layer (crust) consisted of sand particles which were embedded in a matrix of copper compounds (Appendix D. Table 5.3: analysis KC5 L3). The amount of chlorine was quite low (0.3 wt%) with focus in the middle layer which revealed the bent rod to be in a stable condition as the result of the formation of a noble patina on the surface.

MC2

SEM image of the polished transverse section of this bangle showed that corrosion had a complex lamellar structure as a result of generalized corrosion (Appendix C. Fig.20). The thickness of corrosion was about 0.9 mm at least. The corrosion layers had a composition approaching cuprite,

101

copper trihydroxychloride and nantokite which placed above each other up to the metal surface. Based on the typology of corrosion, three distinctive layers were observable. A fragmented cuprite layer was placed adjacent to the metal surface which was filled with a composition approximating copper trihydroxychlorid (Appendix D. Table 5.3: analysis MC2 L1 and L1a respectively).

A disrupted cuprite layer covered the internal layer (Appendix D. Table 5.3: analysis MC2 L2). A compound with high chloride content was sandwiched in this layer and probably contained a considerable amount of nantokite as one of its constituents (Appendix D. Table 5.3: analysis MC2 L2a). This layer was covered by a crust with embedded sand particles in a matrix which consisted of three phases of cuprite and two complex compounds that needs further analysis to determine their exact composition (Appendix D. Table5.3: analysis MC2 L3 and L3a).

MC4

The polished cross section revealed a thick corrosion layer (about 1.4mm) which consisted of two layers on the surface as a result of generalized corrosion (Appendix C. Fig.21). The internal layer was completely fragmented and has a composition similar to cuprite (Appendix D. Table 5.3: analysis MC4 L1). The gaps in the fragmented cuprite layer were filled with a low hardness product which contained high amount of chlorine. This product has a composition approaching a mixture of nantokite and cuprite (Appendix D. Table 5.3: analysis MC4 L1a). A high amount of oxygen in this layer is the result of the porosity of the layer. In the upper part of L1 this matrix converted to a compound close to copper trihydroxychlorides (Appendix D. Table 5.3: analysis MC4 L1b). Particles of gypsum were entrapped among the internal layer (Appendix D. Table 5.3: analysis MC4 L1c).

A thick crust covered the internal layer which was formed by the precipitation of dissolved copper ions onto the surface (Robbiola *et al*. 1998). Sand particles which were embedded in this layer exposed the barrier between the original surface and the previous burial environment. Alkaline compounds of copper (Appendix D. Table 5.3: analysis MC4 L2a) and cuprite (Appendix D. Table 5.3: analysis MC4 L2) usually act as a matrix in the crust but finding the exact composition of some phases needs complementary analysis (Appendix D. Table 5.3: analysis MC4 L2b) which is not necessary here.

Analysis of corrosion products between two folded parts, in the centre of the rod, revealed the presence of a copper chloride compound with approximately the same elements in proportion to nantokite which due to its inaccessible place will cause problems in later conservation of the object (Appendix D. Table 5.3: analysis MC4L3). The presence of nantokite in association with copper trihydroxychlorides shows that the rod is subjected to active bronze disease.

MC7

The polished transverse section of the funnel revealed two main regions (a) and (b) on the surface (Appendix B. Fig.77). Region (a) consisted of iron corrosion products with a restricted zone which contains a higher amount of copper. Zone (b) predominantly contained copper products. These two corroded zones represented the folded iron strip within the funnel and the copper funnel respectively. The first layer of zone (a) at the conjunction between the iron strip and the copper plate contained a mixture of copper and iron corrosion products (Appendix D. Table 5.3: analysis MC7 L1a and L1b). The structure of the iron strip itself was converted to two main dark and light phases, similar to the other iron objects in this study. The darker phases contain more oxygen weight percentage (Appendix D. Table 5.3: analysis MC7 L1c) compared to the light phase (Appendix D. Table 5.3: analysis MC7 L1d) which indicates that these phases may have iron(III)oxyhydroxide as one of their material constituents.   In the middle of the iron wire a two- phase precipitation, with a high amount of calcium in one of them, were detected. This phase, in proportion, was close to calcium carbonate ($CaCO_3$) (Appendix D. Table 5.3: analysis MC7 L1e). The other phase contained iron corrosion products (Appendix D. Table 5.3: analysis MC7 L1f).

In zone (b) corrosion had a lamellar and foliated structure with two distinctive layers (Appendix C. Fig.22). The bulk of previous copper plate was in L2. This layer consisted of cuprite and copper chloride compounds with fluctuation in the chloride content alternately towards the fissure (Appendix D. Table 5.3: analysis MC7 L2a, L2b, L2c, L2d and e). From this point, compositions of corrosion approach to copper trihydroxychloride and chalcocite (Cu_2S). In this part, chalcocite was sandwiched between two layers of copper trihydroxychloride (Appendix D. Table 5.3: analysis MC7 L2f, L2g and L2h). Within copper trihydroxychloride (MC7 L2f and L2h), patches of a darker phase contained oxygen and copper in weight proportions close to malachite was detected (MC7 L2h1). A mixture with a composition approaching cuprite and chalcocite covered these layers and form the original surface (Appendix D. Table 5.3: analysis MC7 L2i). An external layer L3 of sand particles and fossilized plants was cemented to the funnel surface in a matrix of copper compounds (Appendix D. Table 5.3: analysis MC7 L3a, b and c) (Appendix C. Fig.23).

A discrete corrosion particle from the surface was analyzed by XRD for achieving to a complementary result about the exact composition of corrosion products (Fig.5.6). The results revealed cuprite, nantokite, paratacamite, malachite and chalcocite as the main compounds present in crystalline form among the corrosion crust. Chalcocite, one of the corrosion products in corrosion crust is a compound which is produced under reducing conditions and in the presence of sulphate-reducing bacteria (SRB) (McNeil *et al.* 1991). This evidence indicated the funnel was in a reducing environment during part of its burial history while in the rest sufficient oxygen presented in the environment to produce compounds such as malachite and paratacamite.
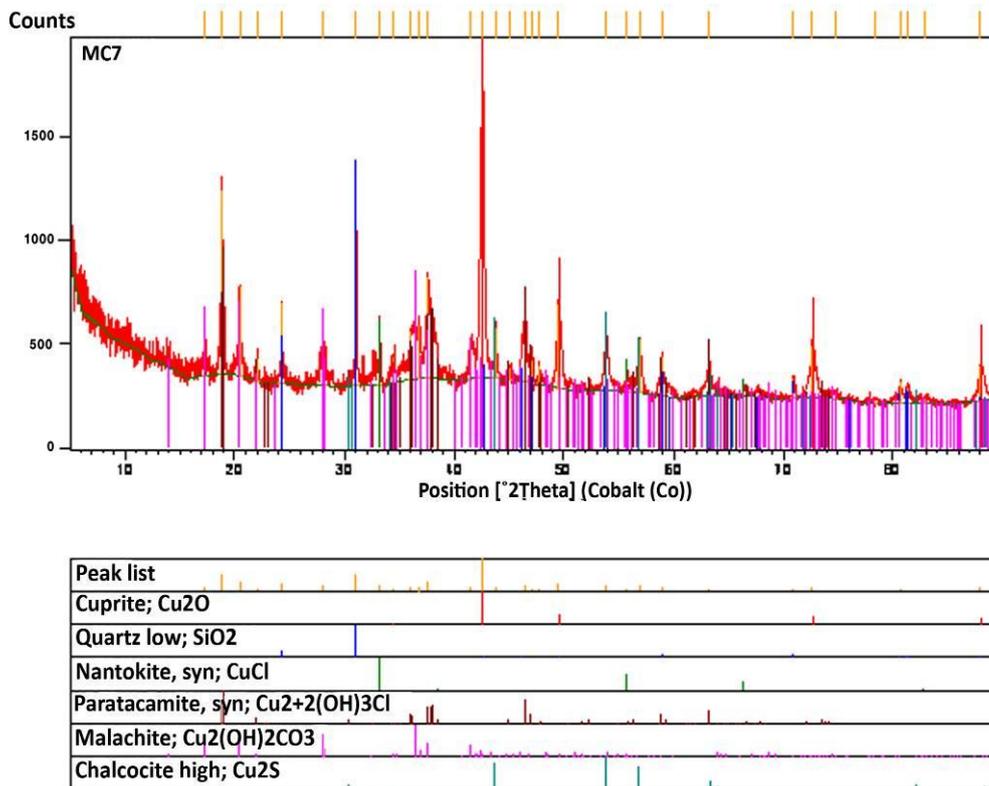
Figure 5.6. XRD scan of corrosion products removed from surface of MC7.

MC8

The polished transverse section of the pin showed generalized corrosion which results in complex stratification of corrosion layers on the surface (Appendix C. Fig.24-26). Corrosion structure on the surface of this low tin (6%) bronze was quite similar to the uneven surface (Type II) category that was suggested by Robbiola *et al.* (1998). It had a maximum thickness of 1.3 mm with perpendicular and longitudinal cracks across and along the layers respectively. The typology and analysis of the corrosion layers revealed that it consisted of two separate parts. It seems corrosion was halted at some time in the past and started again as a result of changing or fluctuating in the burial environment. Since the pin was found within the excavations deposit in the northern dump this hypothesis could be completely true.

EDS analysis revealed high amounts of chlorine and tin in association with soil elements at the internal layer and adjacent to the metal phase (Appendix D. Table 5.3: analysis MC8 L1 and L1a). In this layer the tin content is approximately three times higher than the alloy phase and consisted of lower copper due to decuprificaiton (Rubbiola *et al*. 1998). A layer with composition approaching copper trihydroxyclhoride covered the internal layer (Appendix D. Table 5.3: analysis MC8 L1b). A disrupted thick lamellar layer (banded structure) contained sublayers of cuprite or mixtures of cuprite and tin compounds covered the under layers (Appendix C. Fig.25.L1C and Fig.26.L2). The tin content

104

of the sublayers was not constant. In some layers the tin amount was quite high but lower than the internal layer. Copper had a higher weight percentage in this layer in contrast to chlorine with a significant lower amount compared to the internal layer (Appendix D. Table 5.3: analysis MC8 L1Cs). The amount of chlorine gradually increased towards the internal layer with the highest amount (0.9wt %) at the vicinity of this layer. This part of the corrosion layer (L1C) was separated from the above section by a layer (L1d) with a higher amount of silicon and a diversity of soil elements (Appendix D. Table 5.3: analysis MC8 L1d). It seems this layer was the external layer some time in the past and after starting the corrosion a   similar structure was rebuilt on the surface (Appendix D. Table 5.3: analysis MC8 L2a,b,c,d). Fissures along this layer were filled with a composition approaching copper trihydroyxchloride (Appendix D. Table 5.3: analysis MC8L2c). No traces of the original surface was detected as it was observable in the copper cases in both rough and even surfaces but Robbiola *et al*. (1998) suggested a hypothetical original surface could be within the disrupted cuprite layer (Appendix C. Fig.25).

MC9

The polished transverse section of the ingot showed three distinctive corrosion layers on the surface (Appendix C. Fig.27) with an approximate thickness of 225μm. The first layer (internal layer) contains high amounts of oxygen and chlorine as the only elements from the burial environment which indicates the probable presence of cuprous oxide and chloride (Appendix D. Table 5.3: analysis MC9 L1) but an identification of the exact composition of the compounds based on proportions of elements is not possible. A dense cuprite layer has covered the internal layer (Appendix D. Table 5.3: analysis MC9 L2) which contains a low amount of chlorine (1.2wt%).

The external layer is rich in oxygen and soil elements particularly silicon (Appendix D. Table 5.3: analysis MC9 L3). This layer is porous with sand trapped in it (Appendix D. Table 5.3: analysis MC9 L3a) as a result of the precipitation of copper ions onto the surface (Rubbiola *et al*. 1998).

MC10

The polished transverse section of small bangle showed three corrosion layers on the surface as a result of generalized corrosion (Appendix C. Fig.28). The thickness of corrosion is about 900 μm. The internal layer consisted of a fragmented copper oxide with a composition approaching cuprite with an associated low amount of chlorine as the only element from the burial environment (Appendix D. Table 5.3: analysis MC10 L1). A low thickness of this layer was still seen continuously on the surface. The space between the fragments was filled with a composition containing a high amount of chlorine (24.4 wt%) such as nantokite or a mixture of cuprite and nantokite (Appendix D. Table 5.3: analysis MC10 L1a). A low amount of sulphur in this layer was as the result of ghost cuprite inclusions with sulphur content (Appendix D. Table 5.3: analysis MC10 inclusion). The internal layer

105

was covered by a disrupted cuprite layer (Appendix D. Table 5.3: analysis MC10 L2) which contained a low amount of silicon besides the small particles of sand. A compound with a high amount of chlorine (31.7 wt%), which indicated the presence of nantokite as one of its constituents, was sandwiched between this layer and the external cuprite layer (Appendix D. Table 5.3: analysis MC10 L3). In the external layer (L3 and L4) large particles of sand were cemented to the surface with a mixture of cuprite and probably copper trihydroxychloride (Appendix D. Table 5.3: analysis MC10 L4 and L4a). Further analysis is needed to identify the exact composition of this layer. The original surface was destroyed in some parts and a trace of it has remained at the interface of L1 and L2.

MC11

The polished cross section revealed three main layers on the corroded surface of the bangle (Appendix C. Fig.29). It appears that the patina is the result of generalized corrosion that has grown gradually from the original surface towards the inside by the internal oxidation of copper. The thickness of the entire layer is about 160μm. The internal layer which is quite dense has a composition approximating cuprite (Appendix D. Table 5.3: analysis Mc11 L1). The structure above the internal layer consisted of two distinctive layers. The first one is a cuprite layer which contains sand particles towards the surface (L2). The limit of the original surface, which remained intact, is seen between these two cuprite layers. The latter was formed by the reduction of cupric ions in the cathodic zone (on the surface of the internal layer) and its subsequent reaction with water (reaction 5.12). The second layer contains a variety of elements from the environment which, silicon and oxygen among them, have a higher weight percentage (Appendix D. Table 5.3: analysis Mc11 L2a). The sand particles from the environment that were trapped in this part show that this layer was formed by precipitation of dissolved copper cations onto the surface and is a crust (Robbiola *et al.* 1998). It is impossible to identify the exact composition of this layer based on EDS results. Here the structure of the corrosion and low amount of chlorine (0.1 wt% at the internal layer) are characteristics of a noble patina.

The powder which was produced during sampling by a jeweller's saw was used for a complementary analysis of corrosion products by XRD. As the XRD result shows (Fig.5.7) the sample contained considerable amounts of contaminations which are seen as irrelevant compounds such as wüstite ($Fe_{1-x}O$), rutile (TiO_2) and Thoria (ThO_2). The source of these minerals was probably the material constituents of the saw blade. The other compounds consist of copper, cuprite, quartz, calcite ($CaCO_3$), eriochalcite ($CuCl_2.2H_2O$) and leisingite ($Cu_{1.78} Mg_{0.22} (Mg_{0.54}Fe_{0.46})TeO_6.6H_2O$) which are present in crystalline form in the corrosion layer. Except for cuprite, all other products are somehow related to the external layer with consideration of EDS results (Appendix D. Table 5.3: analysis Mc11 L2a). Nantokite and copper trihydroxychlorides are not seen among these products which indicate that the bangle is not subjected to bronze disease although the presence of eriochalcite

can make the sample susceptible to bronze disease. Eriochalcite is seen among the corrosion products on the objects that were found in soil with a high chloride ion content (Scott 1990).
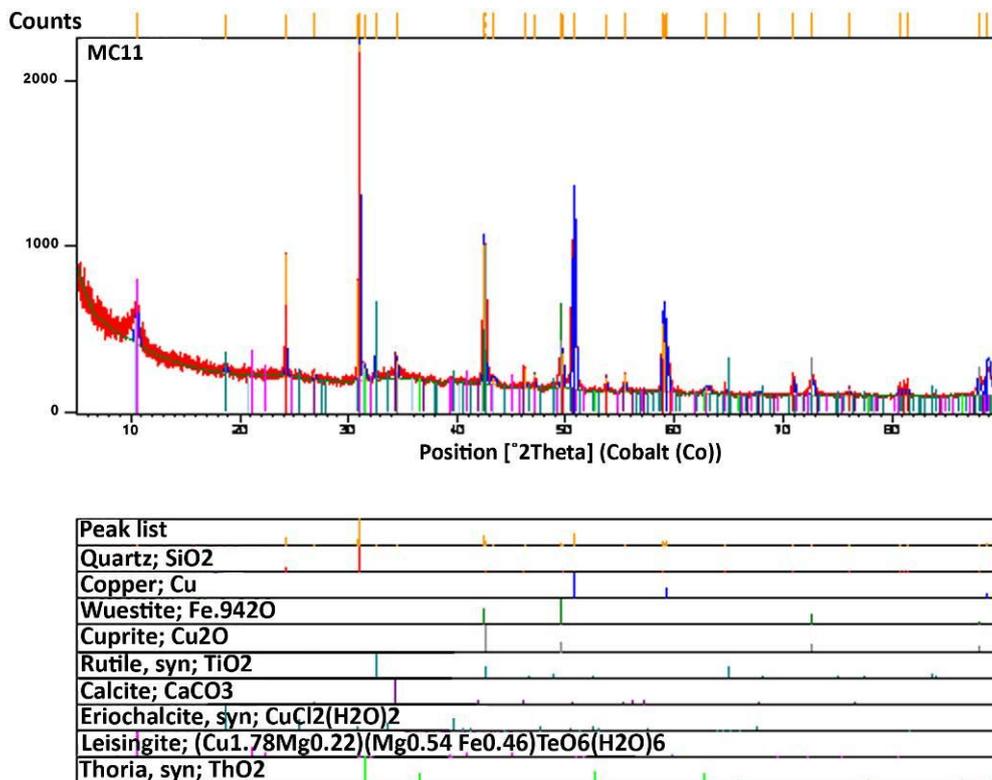
Figure 5.7. XRD scan of corrosion products removed from surface of MC11.

MC12

The polished transverse section showed the presence of both even and coarse patina on the surface of this bangle. In even surfaces the corrosion consists of three distinctive layers (Appendix C. Fig.30). The first layer (internal layer), adjacent to the metal, has a composition approaching cuprite (Appendix D. Table 5.3: analysis MC12 L1). Oxygen and a low amount of chlorine (0.2 wt%) are the only elements from the environment. The second layer (middle layer) also contains cuprite as its main constituents but with elements from the burial environment (Appendix D. Table 5.3: analysis MC12 L2). No traces of sand is seen in this layer. The external layer was identified by its low amount of copper and high amount of soil elements from the burial environment (Appendix D. Table 5.3: analysis MC12 L3). Sand particles were imbedded in this layer.

On coarse surfaces corrosion consisted of three layers (Appendix C. Fig.31). The internal layer with its high amount of chlorine (30.9 wt%) has a composition approximate to nantokite (Appendix D. Table 5.3: analysis MC12 L1a). A lamellar cuprite layer has covered this layer which is more consolidated in the vicinity of the internal layer (Appendix D. Table 5.3: analysis MC12 L2a). The

fissures between the cuprite lamellas were filled by a composition which is associated with a high proportion of soil elements and a low amount of copper compared to the underlayers (Appendix D. Table 5.3: analysis MC12 L3a). The external layer contained sand particles in a matrix with the composition approaching copper trihydroxychlorides (Appendix D. Table 5.3: analysis MC12 L4a). Although corrosion of the coarse parts destroyed the original surface, the limit of it has remained intact in the cuprite layer (Appendix C. Fig.30 and Fig.31).

There were several oblique cracks around the cross section which was filled with corrosion products. This indicated that these cracks were quite old and were related to the method of manufacture of the bangle (Appendix C. Fig.32 and Fig.33).

SC2

The polished transverse section of this ring showed a bilayer corrosion on the surface which is quite different to the other artefacts in this assemblage (Appendix C. Fig.34). Both layers had a composition approaching copper trihydroxychloride (Appendix D. Table 5.3: analysis SC2L1 and L2) with a different texture. The middle layer is much denser than the internal layer. No trace of a cuprite layer was detected in this sample. It shows that this layer was completely removed from some parts of the surface during the cleaning of the object in the past. It appears the present layers of corrosion were formed on the bare metal surface after the cleaning procedure. Copper Trihydroxychlorid shows the ring is still subjected to bronze disease.

5.2.3. Corrosion stratification and process of corrosion formation on artefacts

5.2.3.1. Corrosion structure on iron artefacts

Examination of corrosion in iron artefacts from K2 and Mapungubwe showed a bilayer stratification, internal and external layer, on all but MI2, MI7 and MI10 which only contained one corrosion layer (internal layer) on the surface. This structure was formed under ionic influence corrosion (IIC) with the following specific characteristics:

I. An internal layer adjacent to the metal phase with inhomogeneous composition, mostly of different oxide and oxyhydroxide compounds of iron such as magnetite, hematite, maghemite, goethite and lepidocrocite. In the case of MI6 and SI1 the detected sulphur in association with oxygen by EDS indicated sulphate to be a content in this layer. Only in one case, SI1, a high amount of chlorine (18.5% wt) was detected at the interface of corrosion/metal phase which could be an indication of a hydrated form of $FeCl_2$ and/or akaganéite (β-FeOOH). The amount of chlorine in other artefacts was between 0-0.7%wt.

II. An external layer of quartz grains in a matrix of corrosion products of iron, mostly oxides and oxyhydroxides (hematite and goethite). In two cases (KI1 and MI8) calcite was detected as material constituents of this layer. The external layer was not observed in a few of the iron objects in view of the fact that it was removed in the process of thorough cleaning or flaking such as in the case of MI10 or it was not formed at all such as with MI2 and MI7. The associated soil elements in the corrosion layer of these two items (MI2 and MI7) probably migrated inside the layer in a short contact between hoes and soil. This means the latter two were not buried deep inside the soil and were probably found on the surface.

EDS and XRD analysis of corrosion products on the iron objects in this assemblage revealed hydroxyl ions (OH^-) were the main oxidants that participated in corrosion reactions. These ions were generated in hydrolyzing or cathodic reaction in an aerobic condition. Chloride ions which were detected in a considerable amount on the surface of only one of the objects (SI1) were in the second level of importance in the process of corrosion. The amount of chlorine content at the internal layer of other objects was between a minimum of 0 wt% (KI1, KI3, MI10) and a maximum of 0.7 wt% in MI9 which is close to the value that has been reported for terrestrial sites (Wihr 1975). Complementary analysis of two representative samples from K2 and Mapungubwe (KI1 and MI6) by XRD revealed the more stable products such as magnetite, goethite, and hematite were associated with the less stable product (lepidocrocite). This indicates that the process of corrosion has not been halted. A high amount of sulphate was detected at the internal layer in SI1 with a composition approaching iron(II)sulphate, probably with ($FeSO_4.4H_2O$) formula and in MI6 in the form of jarosite. Knight (1982) suggested jarosite is formed by the slow oxidation of iron(II)sulphate in the air while the latter ($FeSO_4$) develops in a high concentration of sulphate and rapid drying after excavation. Therefore both these products were formed after excavation as the result of a high concentration of sulphate ions within the porosity of the corrosion layer. Jarosite is seen in the form of lemon yellow powdery patches on the surface of MI6. The formation of corrosion on iron artefacts of this assemblage followed the regular processes in aerobic condition that could be described as follows:

5.2.3.1.1. *Electrochemical corrosion of iron*

Iron is a thermodynamically unstable metal that easily corrodes in contact with moisture and oxygen via electrochemical corrosion. It is clear that the iron artefacts from K2 and Mapungubwe are inhomogeneous in terms of numerous dispersed inclusions (see Chapter 3). These inhomogeneities with the formation of numerous cathodic and anodic areas on the surface increase the rate of electrochemical corrosion.

In the regular process of corrosion when iron objects are placed in soil both anode and cathode are on the metal surface (Selwyn *et al*. 1999). In an alkaline soil and near neutrality such as K2 burial environment (see section 5.3.1) the involved cathodic reaction was reduction of oxygen in the

presence of water (reaction 1.4). Since the burial environment at both K2 and Mapungubwe was well-aerated because of the sandy texture of the soil (see Meyer (1998) and section 5.3.1), oxidation of the metal surface (anodic zone) was the first stage in electrochemical corrosion of the iron objects (Reaction 5.1). This process resulted in formation of Fe^{2+} ions at metal surface which is favoured at low levels of dissolved oxygen (Selwyn 2004).

$$Fe \rightarrow Fe^{+2}(aq) + 2e^{-} \hspace{4cm} (5.1)$$

Then the products of cathodic and anodic reactions were combined (Walker 1982) and solid iron(II) hydroxide, started to precipitate above pH 6 as was suggested in the general corrosion process of iron (reaction 5.2).

$$Fe^{+2} + OH^{-} \rightarrow Fe\,(OH)_2 \hspace{3.5cm} (5.2)$$
$$\text{White (solid)}$$

With consideration of a high amount of dissolved oxygen in the water content of the soil, as well as soil alkalinity (pH>6), the unstable iron(II) hydroxide was rapidly oxidized to iron(III)hydroxide which is amorphous (Nicholls 1973; Blesa *et al*. 1994). With time iron(III)hydroxide was converted to iron(III) oxyhydroxides (FeOOH), (Misawa 1973), which were detected at regions with high oxygen access at the internal and the external layers. At this time when the rate of corrosion as well as the dissolution of metal into the environment were high, the sand particles were entrapped among the corrosion products. Precipitation of porous insoluble products (iron(II)hydroxide, iron(III)hydroxide and iron (III)oxyhydroxides) along with soil particles on the surface resulted in passivation of the metal surface while the penetration of dissolved oxygen was only possible along the small cracks and pores which were formed during growing of the corrosion layer by volume expansion of corrosion products on the surface.

The passivation can separate the anodic and cathodic areas (Hjelm-Hansen *et al*. 1993; Tomashov 1966; Selwyn *et al*. 1999). Isolation of anodic zones from cathodic areas results in increasing the concentration of anions mostly chloride with its high mobility near the metal surface during burial (Turgoose 1982*a*) which was only seen in the case of SI1. In view of the fact that the burial environment at K2 had sufficient chloride content (see section 5.3.1) to participate in corrosion process, lack of chloride with its high mobility (Turgoose 1982*a*) at anodic zones at metal/corrosion interface of artefacts indicates the cathode remained on the metal surface during burial. This phenomenon might be due to the high porosity in internal and external layers that allowed sufficient dissolved oxygen access to the metal/corrosion interface for cathodic reaction. Shortage of soil samples from the Mapungubwe excavation site prevented   doing the relevant analysis to reveal the presence or lack of chloride in the soil. Consequently it is not possible to interpret scientifically the low amount of chlorine in the corrosion layers on the Mapungubwe iron artefacts.

With passivation of the metal surface the penetration of dissolved oxygen was only possible along the small cracks. In this stage Fe^{2+} ions on the basis of its domain stability (Fig.5.8) were diffused in pores and cracks that were saturated with water and precipitated as $Fe(OH)_2$ and converted to magnetite in areas with limited oxygen access (reaction 5.3, 4) (Evans 1923; Potter 1956; Walker 1982; Hamilton 2000; Selwyn 2004) in the form of inter-dispersed phases in iron(III)oxyhydroxide at the internal layer (dark phase) as was detected in the case of KI1.

$$6Fe\,(OH)_2 + O_2 \rightarrow 4H_2O + 2Fe_3O_4.H_2O \qquad\qquad (5.3)$$

White   Green hydrated magnetite (Green rust)

$$Fe_3O_4.H_2O \rightarrow H_2O + Fe_3O_4 \qquad\qquad (5.4)$$

                 Black magnetite

In places with higher oxygen access the Fe^{2+} ions were converted to iron(III)oxyhydroxides such as goethite and lepidocrocite at the internal and the external layers. In fact, the diffusion domain of Fe^{2+} ions across the corrosion crust towards the surface was completely controlled by EH and pH of the corrosion layers' microenvironment. This domain depends on the range of stability of the ferrous ions in specific quantity of Eh and pH that were considered in Pourbaix diagram and out of this range the Fe^{2+} ions precipitate as different products in an alkaline environment (Fig.5.8).

Figure 5.8. Eh-pH diagrams for system Fe -H_2O at 25°C. a) Range of stability of iron(III)oxyhydroxide. b) Range of stability of hematite (Adapted from Beverskog & Puigdomenech 1996.

111

With ageing of the corrosion crust, the unstable products gradually transformed to more thermodynamically stable ones. In this process lepidocrocite that usually forms first in transformation of Fe(III)hydroxide was converted to goethite (Stratmann 1990) in aqueous solution after a few years (Turgoose 1982*a*) while goethite (α-FeOOH) partly altered to hematite (light phase) (reaction 5.5).

$$2\alpha\text{-FeOOH} \rightarrow \alpha\text{-Fe}_2\text{O}_3 + \text{H}_2\text{O} \qquad\qquad (5.5)$$

The free energy of formation of this reaction is small and enables goethite to remain for a long time (Krauskopf 1979; Turgoose 1982*a*) along with more stable products such as hematite. Metastability of lepidocrocite in addition to its formation which is associated with a high quantity of Fe^{2+} ions in area of formation (Cornell & Schwertmann 2003) make this a possibility that the corrosion is still continuing in atmospheric conditions and in damp storage (see Fig.5.1, 3 and section 6.4.2.1.1). Maghemite which was detected in association with magnetite in the internal layer (Fig.5.2) could be formed by oxidation of magnetite (Cornell & Schwertmann 2003) in an area with higher oxygen access and probably after excavation. On the other hand lack of maghemite within the discovered corrosion compounds in XRD analysis (Figs.5.1, 3) can be due to its metastability and easy transformation to hematite by powdering that was reported in Romdohr (1969). The results also indicate that a low amount of Ni in KI5 metal phase as impurity has no effect on type of corrosion products detected on the surface. Takahashi *et al*. (2005) suggested that nickel content can have an effect on the fraction of goethite and magnetite within a major lepidocrocite constituent. In this study paucity of the samples prevented quantitative analysis of corrosion products. A Brief schematic process of the corrosion in this stage is given in (Fig.5.9).

Figure 5.9

Schematic process of electrochemical corrosion of iron during burial in aerobic environment

112

5.2.3.1.1.1. Corrosion of iron under influence of chlorine

1. *Before excavation*

High amounts of chlorine at the interface of metal/internal layer in SI1 can be explained by the separation of anodic and cathodic areas during burial as Turgoose (1982*a*) suggested. With the formation of a passive corrosion layer, anode remaining on the surface of metal and cathode shifted to an area with more oxygen access with electrical conductivity usually at the outermost of magnetite layer (Selwyn *et al*. 1999) which was detected in the light phase in the internal layer of SI1. The next stages on the basis of general corrosion of iron in the presence of chloride ions in environment are as follows:

In cathode which is located far from the metal surface at this time, oxygen is reduced to hydroxyl (reaction 1.4). This motivates production of ferrous ions at the anode and a flow of electrons (reaction 5.1). In anode the ferrous ions are hydrolyzed in reaction with water (Turgoose 1982*a*; Selwyn 2004):

$$Fe^{2+}(aq) + H_2O \rightarrow Fe(OH)^+(aq) + H^+(aq) \hspace{2cm} (5.6)$$
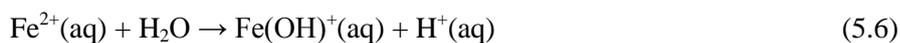
This reaction must also be accompanied by ions flow in solution. Cations move towards cathode and anions move in opposite direction (Turgoose 1982*a*). Chloride ions from surrounding electrolyte with its high mobility migrate towards the metal surface and maintain the charge balance (Turgoose 1982*a*). Formation of hydrogen and accumulation of chloride ions increase both the anodic dissolution of iron (reaction 5.8) and the concentration of these ions in the anodic area. Consequently pores of corrosion products near the anodic area are filled with acidic solution of ferrous chloride (Turgoose 1982*a*).

2. *After excavation*

Formation of the hollow shells at metal/corrosion interface of SI1 is directly related to the chemical changes after excavation (here after sampling) which can be described as follows. Concentration of acidic ferrous chloride in pores of corrosion products by drying of unearthed iron object causes cracks in corrosion layers (Cronyn 1990). This phenomenon is directly as the result of formation of hydrated salts of ferrous chloride. Turgoose's (1982*b*) research on properties of ferrous chloride shows that the drying of the object after excavation results in formation of hydrated salts of ferrous chloride in the forms of iron (II) chloride dihydrate and iron(II)chloride tetrahydrate that have more volume compare to its solution. Resembling the other hydrated salts, iron (II) chloride dihydrate is altered to tetrahydrate by absorbing water. The latter hydrated salt in turn is transformed to the liquid phase above the critical humidity. The formation of solution of ferrous chloride starts the corrosion again. Meanwhile readily diffusion of oxygen within the cracks causes a high rate oxidation condition in these areas. At this stage the ferrous ions in solution are oxidized to iron(III)

113

oxyhydroxide (akaganéite) (Refait and Génin 1997; Turgoose 1982*a*). The general reaction by consideration of the indirect role of chloride (Turgoose 1982*b*, 1993) may be the equation (5.7) which also results in formation of hydrochloric acid:

$$4Fe^{2+} + O_2 + 6H_2O \rightarrow 4FeOOH + 8H^+ \hspace{2cm} (5.7)$$
$$\text{Iron oxyhydroxide}$$
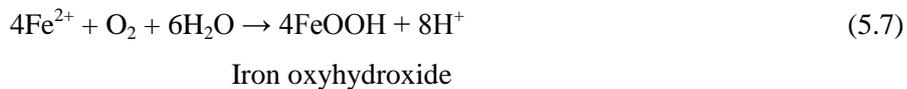
The amount of relative humidity in which the reaction proceeds depends on the presence or lack of metal core. Based on laboratory examinations of Turgoose (1982*b*) the critical RH 55% in 20˚C can convert ferrous chloride tetra hydrate to solution and formation of iron oxyhydroxide (akaganéite) and yellow liquid phase without the presence of a metal core. When this salt comes into contact with the metal core, RH 20% and above can produce akaganéite is much lesser than critical RH 55%. Consequently in the case of SI1 which has a metal core the RH 20% could promote the corrosion. This process results in the formation of globules of very acidic yellow liquid or tear on the surface of corroded iron which is known as weeping. In dry conditions the water content of this liquid evaporates and a hollow shell remains (Appendix C. Fig.14). Selwyn *et al*. (1999) suggested that the formation of the shell is the result of precipitation of FeOOH during oxidation and hydrolysis of the Fe^{2+} ions or hydrolysis of Fe^{3+} ions in the interface of liquid and air where concentration of dissolved oxygen is high. First the precipitant floats on the surface of liquid, forming a skin (North 1982) and finally coalesces into a solid shell.

On the other hand the acid that is produced by this reaction has a deleterious effect on structure of corrosion layer and corrosion rate of remaining iron (Turgoose 1982*a*). The acid can dissolve the corrosion products such as magnetite and chemically assisting in propagation of cracks and disintegration of object (Turgoose 1982*b*). The reduction of the pH in solution (reaction 5.7) increases the solubility of iron as well as the rate of corrosion. Corrosion can continue until all the metal phase is corroded (Turgoose 1993; Selwyn *et al*. 1999; Askey *et al*. 1993):

$$2Fe + O_2 + 4H^+ \rightarrow 2Fe^{2+} + 2H_2O \hspace{2cm} (5.8)$$

Among the various types of iron oxyhydroxides akaganéite is usually regarded as the prime cause for the breaking up of the objects after excavation (Turgoose 1993; Knight 1982; Hjelm-Hansen *et al*. 1993; Blesa *et al*. 1994; Selwyn *et al*. 1999). Solid akaganéite usually precipitates in the form of crystalline at the iron/corrosion interface (Turgoose 1993) since the concentration of $FeCl_2$ in this region is high (Selwyn *et al*. 1999). Akaganéite crystal structure is monoclinic with a framework of iron oxyhydroxide containing tunnels which has been partially filled with Cl⁻ or F⁻ (Post & Buchwald 1991; Schwertmann & Cornell 1991;   Selwyn *et al*. 1999). These tunnels are stabilized by the presence of chloride or fluoride ions (Cornell 1996; Selwyn *et al*. 1999). Akaganéite is a metastable product and after a few years is converted to other more stable products such as goethite. In this

process the entrapped chloride ions in its structure are released and again participate in the corrosion cycle (Keller 1969). Another destructive feature of akaganéite and the others FeOOH polymorphs is their high molar volume compared to iron itself. The volume that is occupied by 1 mole of each FeOOH are 21cm^3 (α-FeOOH), 22cm^3 (γ-FeOOH) and 25 cm^3 (β-FeOOH), calculated according to their densities (Cornell & Schwertmann 2003; Selwyn *et al.* 1999). These volumes are three times more than the volume occupied by one mole iron (Watkinson 1983). A Brief schematic process of corrosion of iron in the presence of dissolved chlorine is given in (Figure 5.10).

Figure 5.10

Schematic process of electrochemical corrosion of iron in presence of chloride

5.2.3.1.1.2. *Corrosion of iron under influence of sulphate*

Sulphate which was detected in the corrosion layers on SI1 and MI6 such as chloride can accelerate the rate of corrosion by participation in a cyclic corrosion (Graede 1990; Selwyn 1996). As noted by Graede (1990) and Selwyn (1996), this cyclic corrosion may not be as destructive as the one which was caused by the action of chlorine. In this process Fe^{2+} ions react with SO$_4^{2-}$ to form a readily soluble FeSO$_4$. Iron sulphate can be oxidized to form FeOOH and H$_2$SO$_4$. The released sulphuric acid similar to hydrochloric acid can attack the metal core and causes further corrosion. Unlike Cl$^-$, sulphate ions are gradually removed from the corrosion cycle by forming insoluble iron(III)hydroxysulphate salts such as Fe(OH)SO$_4$ or Fe$_2$(OH)$_4$SO$_4$. Jarosite presents in corrosion of MI6 is one of these insoluble salts.

© University of Pretoria

5.2.3.2. Process of corrosion formation on copper artefacts

A survey of the corrosion structure of copper artefacts in this assemblage revealed that two kinds of corrosion were responsible for their degradation:

    I. *Ionic influenced corrosion (IIC)*
    II. *Microbial influenced corrosion (MIC)*

These two process of corrosion resulted in the formation of even and uneven surfaces on the copper objects in this assemblage.

5.2.3.2.1. Ionic influenced corrosion (IIC)

All of the copper artefacts examined were corroded under ionic influence except one (MC7). The artefacts in this category can be divided into two sub-groups based on the type of ions which controlled corrosion events and characteristics of the corroded surface as was suggested by Robbiola (1990). These two subordinate groups are: corrosion under control of cations and corrosion under control of anions which result in formation of even and uneven surfaces respectively.

5.2.3.2.1.1. Characteristics of even surface in copper artefacts from K2 and Mapungubwe

Two artefacts (KC5 and MC11) in this assemblage had an even surface throughout while KC2, KC4 and MC12 had a combination of the two surfaces. The Structure of even surfaces on the copper artefacts from K2 and Mapungubwe consisted of two main layers and one external layer of which the latter is not considered part of the artefacts. Characteristic of these layers in order to their vicinity to the metal surface are:

I. An internal layer of cuprite adjacent to the copper surface with irregular shape and thickness. This layer is characterized by its high density and scattered large voids.

II. A middle layer with lower amount of copper compared to the internal layer and is characterized by soil elements from the environment (Si, Al, Ca, K, S and Cl). This layer may consist of different compositions but the main phase is cuprite. Complementary analysis of MC11 as a representative sample with an even surface by XRD revealed no traces of copper hydroxycarbonates such as malachite in this layer. The middle layer in KC5 is dark brown which indicated cupric carbonate with its green colour was not formed during burial. The Middle layer was not developed in some cases such as KC2 and KC4.

III. An external layer (crust) characterized by its high porosity and quartz grains which were embedded in a matrix of copper corrosion products. Indeed it was part of the burial environment

116

that adhered to the surface of the artefacts as the result of precipitation of dissolved copper. This layer had different colours from brown (KC5) to various shades of greens (MC11). Copper content of this layer is lower than both the internal and the middle layer and contained high amounts of soil elements specially silicon. Crust was observed on all even surfaces with a thickness between 20-100μm.

The limit of the original surface in even surfaces was preserved intact between the middle and the external layer. The process of formation of this structure is as follows:

5.2.3.2.1.1.1. *Mechanism of formation of even surface*

The first step in the formation of an even surface on pure copper is oxidation and dissolution of metal in a corrosive environment. Based on May's (1953) observation copper reacts directly with dissolved oxygen in corrosive water to produce soluble copper corrosion. Some of these products convert to insoluble salt which appears as a cloudy precipitation near the copper surface. Gradually a visible film of corrosion products forms on the surface of the metal. A layer of cuprite (Cu_2O) (internal layer) can appear under this layer or may replace it and reduce the rate of corrosion (Scott 2000) (reaction 5.9).

$$2Cu + H_2O \rightarrow Cu_2O + H_2 \tag{5.9}$$

However in a moist or wet environment the corrosion may progress further and result in the formation of the middle and the external layer. Under such conditions the properties of the cuprite layer beside the types of anions present in the environment have an important role in the mechanism of corrosion and diversity of corrosion products in the middle and external layers. Cuprite has a high electrical conductivity and permits copper ions to be transported easily in this layer (North & Pryor 1970; McNeil & Little 1992). Scott (2000) suggested that this layer acts as a bipolar electrode with an anodic reaction taking place at the inner surface and cathodic reaction occurring on the outer surface. Based on Lucey's (1972) investigation on mechanism of pitting corrosion, the anodic reactions are as follows:

Cuprous ions which are generated in anodic reaction oxidize again in anodic area to form cupric.

$$Cu^+ \rightarrow Cu^{2+} + e^- \tag{5.10}$$

This reaction increases the concentration of cupric ions in anode. To achieve an equilibrium between metal, cuprous and cupric ions, metallic copper will be dissolved.

$$Cu + Cu^{2+} \rightarrow 2Cu^+ \tag{5.11}$$

117

In the next stage cuprous ions react with water and form cuprite under the limit of the original surface or diffuse through this layer and are oxidized by the dissolved oxygen to cupric ions (reactions 5.12 and 5.13). The cupric ions thus produced can be lost into the soil groundwater or combine with the anions in the environment and precipitate on the metal surface. The cupric ions can also be reduced to cuprous ions at the outer surface of the cuprite layer (Scott 2000). This process results in formation of the middle and the external layer on copper. The middle layer of cuprite in MC11 and MC12 was the result of reduction of cupric ions in cathodic zone and its later reaction with water (reaction 5.12).

$$2Cu^+ + H_2O \rightarrow Cu_2O + 2H^+ \hspace{4cm} (5.12)$$
$$4Cu^+ + O_2 + 2H_2O \rightarrow 4Cu^{2+} + 4(OH)^- \hspace{3cm} (5.13)$$
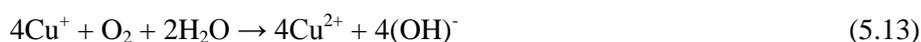
The composition of the products in the middle layer and crust depends on anions present in the environment. Complementary analysis of one of the artefacts with an even surface (MC11) by XRD revealed oxygen and chlorine were the only anions from the burial environment which had an influence in the second stage of corrosion (Fig.5.7). Chlorine appears to have had a lesser effect on the process of corrosion compared to oxygen. Although calcium carbonate was detected as contamination on the surface of this artefact (Fig.5.7) no traces of copper hydroxycarbonate was found. It seems carbonates only acted in passivation of corrosion by decreasing the amount of divalent copper as suggested by Kvashnina $et\ al.$ (2007). Adeloju and Duan (1994) noted pH buffering by HCO_3^- is responsible for this protection which stabilized the oxide layer rather than forming basic cupric carbonate. This passivation is only feasible in the environment with low concentration of chloride and carbonate or bicarbonate in concentration of 1.1 mM/L (61mg L^{-1}) (Kvashnina $et\ al.$ 2007).

5.2.3.2.1.2. Characteristics of uneven surface on copper artefacts from K2 and Mapungubwe

Except for KC5 and MC11 all copper artefacts have an uneven surface or at least in some areas on their surface. Since sampling is restricted to a small zone, on metal it cannot give a precise idea about distribution of uneven surfaces on the entire object. In this regard tomography gave more dependable results in this study. Uneven surface on copper artefacts in this assemblage consisted of three main layers.

I. An internal layer next to the metal surface. The structure of this layer is not completely similar in all uneven surfaces. In some cases (KC1, KC4 and MC9) it only consists of one phase with a high amount of chlorine and oxygen in the presence of a lower amount of copper compared to the bulk of metal with composition probably an admixture of cuprite and nantokite. Sometimes patches of copper trihydroxychloride were detected within this phase. In some instances (KC2, MC2, MC4,

118

MC10 and 12) fragmented cuprite layer was seen within the above mentioned compositions. Chlorine and oxygen are the main elements from the burial environment which were detected in high amounts in the internal layer. The two elements of silicon and aluminium are seen in lower amounts in this layer (Al< 0.2% and Si<1.3%).

II. A cuprite layer associated with low amounts of chlorine and silicon at the interface of the internal and external layers. This layer which is mostly fragmented or disrupted indeed was in the outer zone of cuprite patches within the internal layer (KC2, MC2, MC10 and MC12). Limit of original surface was seen around this layer.

III. The external layer mostly had a lamellar structure that consisted of Cu(I) and (II) compounds with embedded sand particles. Copper trihydroxychloride and cuprite were the main identified phases in this layer. This layer contains a high amount of Si and O together with a diversity of soil elements (Mg, K, Ca).

5.2.3.2.1.2.1. *Mechanism of formation of uneven surface*

I. *Effect of chloride before excavation*

Analysis of corrosion layers of copper artefacts revealed chloride was the main deleterious anion in the disintegration of the original surface and formation of uneven surfaces. The process of formation of uneven surface in the presence of chloride was explained by Lucey (1972) in regard to the formation of pitting corrosion. He suggested that the deleterious effect of chlorine is related to turbulence between production and consumption of cuprous ions. If the equilibrium between the rate of cupreous ions formation (reaction 5.11) and consumption of them via two latter reactions 5.12 and 5.13 is disturbed and tends to produce more cuprous ions, a layer of cuprous chloride (nantokite) will be formed:

$$Cu^+ + Cl^- \rightarrow CuCl \qquad\qquad\qquad (5.14)$$
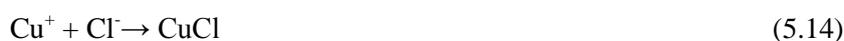
The presence of high amounts of chloride ions in environment (environment aggressiveness) with their high mobility is the main factors that affect this process (reaction 5.14). In fact chloride ions from groundwater migrate inward to maintain the neutrality (Scott 2000). The formation of an admixture of nantokite and cuprite within the internal layer of copper artefacts (KC1, KC2, KC4, MC4, MC8, MC9, MC10, and MC12) in this assemblage was the result of reactions 5.12 and 5.14. Here in the copper artefacts nantokite was formed:

    1. At the interface between the metal phase and cuprite layer (KC1, KC2, KC4, MC4, MC8, MC9, MC10, MC12).

2. Directly above the middle cuprite layer and covered by an external cuprite layer (MC2, MC10).

3. Between folded areas of plate in centre of object (MC4).

There is a lot of controversy about subsequent reaction of nantokite during burial which led to formation of the above mentioned structures. Organ (1963), Pollard *et al.* (1992) and Al Hajji and Reda (1996) contended nantokite can be hydrolyzed by direct reaction with moisture (reaction 5.15) to form cuprite and hydrochloric acid. The hydrochloric acid generated by this reaction leads to the dissolution of metal in a cyclic process (reaction 5.16) which resulted in pitting corrosion without giving rise to any external indication of bronze disease (Organ 1963):

$$2CuCl + H_2O \rightarrow Cu_2O + 2H^+ + Cl^- \qquad \Delta G= +56.5 \text{ kJmol}^{-1} \qquad (5.15)$$

$$2Cu + 2HCl \rightarrow 2CuCl + H_2 \qquad (5.16)$$

Nevertheless Macleod (1981) and Scott (1990) suggested normally the reaction 5.15 does not proceed because of its positive Gibbs free energy of formation. Pollard (1992) argued that despite the positive value it is the principal reaction which is important during burial and will proceed under most oxidizing conditions. El Warraky *et al.* (2004) in regard to the following steps in corrosion of copper in the presence of chlorine suggested that in low concentration of chloride ($C \leq 10^{-3}$ M) with presence of greater amounts of cuprous ions, the production of cuprous oxide by hydrolyzing of CuCl (nantokite) (reaction 5.15) leads to the formation of a cuprite layer above trapped nantokite. This process can be also conducted by reducing nanotkite in cathodic area by OH$^-$ (reaction 5.17) which is formed during cathodic reaction 1.4 (Bokris *et al.* 1981). This kind of cuprite layer which covered an under layer of nantokite was seen in (KC1, KC2, KC4, MC2, MC9, MC10 and MC12).

$$2CuCl + 2OH^- \rightarrow Cu_2O + H_2O + Cl^- \qquad (5.17)$$

In the case of MC4 the lack of a cuprite layer above the internal layer which consisted of nantokite could be related to a high chloride concentration in the corroded area. El Warraky *et al.* (2004) argued in high chloride concentration ($C \geq 10^{-2}$ M) cuprite is not formed and the produced film on the metal surface predominantly consists of CuCl which has no effective protection and this protection is rapidly lost under influence of chloride ions (Thomas & Tiller 1972) by dissolution of CuCl in the form of $CuCl_2^-$. In this condition Cu$^+$ easily passes through the layer and leads to the formation of soluble complex cuprous ions that can intensify the corrosive reaction (El Warraky *et al.* 2004).

II. *Deleterious effect of nantokite after excavation (bronze disease)*

Most of the copper, besides the only bronze artefact in this assemblage, are subjected to bronze disease. Porous light green corrosion products with the composition of copper trihydroxychloride on

the surface are the main symptom of this disease which was detected on (KC1, KC2, KC4, MC2, MC4, MC7, MC8, MC9, MC10, MC12 and SC2) both by the naked eye and analysis (Table: 5.3, Figs.5.4, 5, 6). Powdery light green corrosion is also observable on the surface of KC3, MC1 and MC3. Scott (1990) believed that the presence of nantokite accompanied by moisture and oxygen are the main factors in the production of bronze disease. He noted that cupreous chloride (CuCl) contrary to ferrous chloride that is present in the aqua phase during burial and intensifies the process of corrosion may remain dormant until confronted with oxygen and humidity. Based on laboratory examination he noted that the exact reaction which contributes to bronze disease is oxidation and hydrolysis of CuCl:

$$4CuCl + O_2 + 4H_2O \rightarrow 2Cu_2(OH)_3Cl + 2H^+ + 2Cl^- \qquad (5.18)$$
$$\Delta G = -1338 \text{ kJmol}^{-1}$$
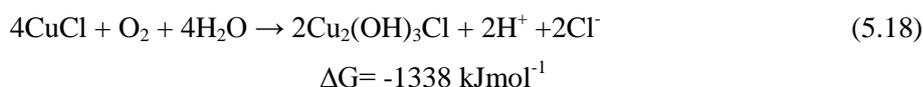
In this state the presence of cuprous chloride results in formation of copper trihydroxychloride and hydrochloric acid which endangers the stability of the object. In fact the combination of two reactions of 5.16 and 5.18 results in a cyclic corrosion until no metal remains. The resultant Copper trihydroxychloride also produces inhomogeneous layered structures on copper artefacts (McNeil & Little 1992). These products also have more volume compared to copper, nantokite and cuprite. In relation to copper, cuprous chloride (nantokite) has a relative molar volume (RMV) of about 3.36, while the copper trihydroxychlorides have RMVs of about 3.99. Cuprite has an RMV of 1.67. It shows formation of both nantokite and trihydroxychlorides producing considerable expansion force in the corrosion layers (Scott 1990). This kind of expansion resulted in the deformation of the limit of the original surface as it was seen in uneven surfaces on copper and bronze artefacts in this assemblage. Low solubility of nantokite especially when it is deep-seated in the metallic phase such as in the case of MC4 creates difficulties in the conservation of objects. In this case, it is very difficult to wash or stabilize such chloride content in depth (Scott 2000). Eriochalcite ($CuCl_2.H_2O$) which was detected on MC11 also has this potential to produce bronze disease (McNeil & Little 1992).

5.2.3.2.1.3. Characteristics of uneven surface on bronze artefact from Mapungubwe

The only bronze artefact in this assemblage has an uneven surface with a thick corrosion crust (1.3 mm) which consisted of three distinctive layers:

I. An internal layer adjacent to the metal surface with a low amount of copper and high tin content compared to the bulk of alloy. Chlorine and oxygen were the main elements in high quantity from environment which were detected at the internal layer. These elements are in association with a lower amount of silicon and aluminium.

121

II. A mirror disrupted lamellar (banded) layers consisting of sublayers of cuprite and a mixture of cuprite and tin compounds placed at the interface of the internal and external layers. The mirror surface between these two sections has a higher silicon content compared to other sublayers. This banded layer has higher copper content compared to the internal layer.

III. An external layer of green compounds of copper with high silicon and chlorine content. Tin is not detected in this layer.

5.2.3.2.1.3.1. *Mechanism of formation of uneven surface on bronze artefact*

Investigation by Robbiola *et al.* (1998) on the mechanism of formation of uneven patina in low content tin bronze (single phase) in an oxygenated corrosive medium, which is similar to the corrosive condition at Mapungubwe, clarified that the dissolution of copper (decuprification) is the main involved chemical reaction in corrosion process. In this type of patina the corrosion crust as is seen on MC8 is coarse and the original surface has been destroyed. High rate corrosion in form of generalized attack results in formation of a three-layer corrosion structure. Robbiola *et al.* (1998) suggested uneven surface forms during three distinctive phases whereas the outcome may occasionally have deviations from the regular structure. With consideration of these deviations the formation of uneven surface on MC8 can be explains as follows:

In the first phase alloy dissolves intensely as the result of either environment aggressiveness or presence of inhomogeneity in the alloy and environment. These conditions prevent the stabilization of tin compounds on the surface of the alloy and lead to the enrichment of the corrosive electrolyte with copper cations in. Copper ions react with anions in the environment and form a porous less protective layer on the surface. In MC8 this layer mostly consisted of copper trihydroxychlorides and silica. Formation of this layer and increasing its thickness gradually reduce the rate of alloy dissolution.

In the second phase with decreasing of dissolution of the alloy, tin compounds are stabilized between the middle layer and the alloy, forming an internal layer enriched in tin (compared to bulk of alloy) accompanied by cupreous oxides (reactions 5.19 and 5.20). The inward growth of the internal layer is controlled by migration of anions (O^{2-} and Cl^-) from the environment towards bulk of alloy and cations in the opposite direction.

$$Sn + 2H_2O \rightarrow SnO_2 + 4H^+ + 4e^- \hspace{4cm} (5.19)$$
$$3Cu + H_2O \rightarrow Cu_2O + Cu^+ + 2H^+ + 3e^- \hspace{3cm} (5.20)$$
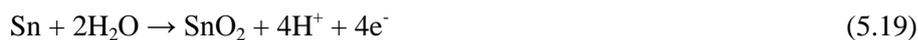
The middle layer on MC8 had a banded structure of cuprite and cuprite plus tin compounds which is known as Liesegang phenomena. Although it is clear that this layer was formed by dissolution and outward migration of copper and tin cations, formation of successive bands with fluctuation in tin content is not well understood yet. Scott (1985) suggested that the presence of tin as alloying element

122

acts as impurity which enhances formation of banding in this phenomenon. He noted that hydrated tin oxide forms gel-like compounds which can retain copper cations to react with anions present in the environment. The result of these reactions is the formation of insoluble products that deposit on the surface. In fact fluctuation in the rate of cations and anions transportation on the opposite side results in a banding structure. In this type of patina a great amount of chloride ions is present in the vicinity of the corrosion/alloy interface. The migration of chloride towards alloy and the mechanism of corrosion in presence of chloride are similar to what was referred to in the case of copper corrosion and can result in bronze disease which is also observable in MC8.

Phase three corresponds to the ageing of corrosion crust. Formation of fissures and cracks in the corrosion crust on MC8 is related to this phase. These mechanical cracks are the result of high thickness and porous structure of the corrosion layers. These cracks in the case of MC8 lead to the formation of a more complex stratified corrosion layer.

5.2.3.2.2. *Microbial influenced corrosion (MIC)*

MC7 was the only copper artefact in this assemblage with anaerobic corrosion characteristic along with bronze disease. This kind of corrosion forms in a reducing environment in presence of Sulphate-Reducing Bacteria (SRB). Scott (2002) suggested in such an environment SRBs reduce the sulphate:

$$2SO_4^{2-} \rightarrow S + S^{2-} + 4O_2 \tag{5.21}$$

The produced O_2 is utilized by the above mentioned organisms in their metabolism and the remained sulfide ions react with H^+ present in the environment to produce hydrogen sulfide:

$$S^{2-} + 2H^+ \rightarrow H_2S \tag{5.22}$$

Consumption of H^+ which was produced in the cathodic area results in depolarization of cathode and continuing of corrosion in the absence of oxygen. In next step hydrogen sulfide reacts with copper to produce cuprous sulfide with the general stoichiometry $Cu_{2-x}S$, $0<x<l$ (Little & Wagner 1993). In MC7, Cu_2S (chalcocite) was the only sulfide product which was detected on the surface.

Considering the burial environment at Mapungubwe which was covered by archaeological deposit, gravel, rubble and sandy soil (Meyer 1998) with high aeration capability the presence of chalcocite among corrosion products of copper was quite odd. Chalcocite was seen as a layer among other copper products which form either in a low reduction condition (Cu_2O) or high oxidation condition ($Cu_2(OH)_3Cl$ and $Cu_2(OH)_2CO_3$) (Appendix C. Fig.22, Figs.5.6, 5.11). For a better interpretation of the coexistence of these products looking at the history of the object was quite helpful. The object went through three stages after having been discarded in the past. These stages are the following:

123

I. Burial

II. Uncovering and remaining within the discarded archaeological deposit in the northern dump.

III. Re-excavation and remaining in storage.
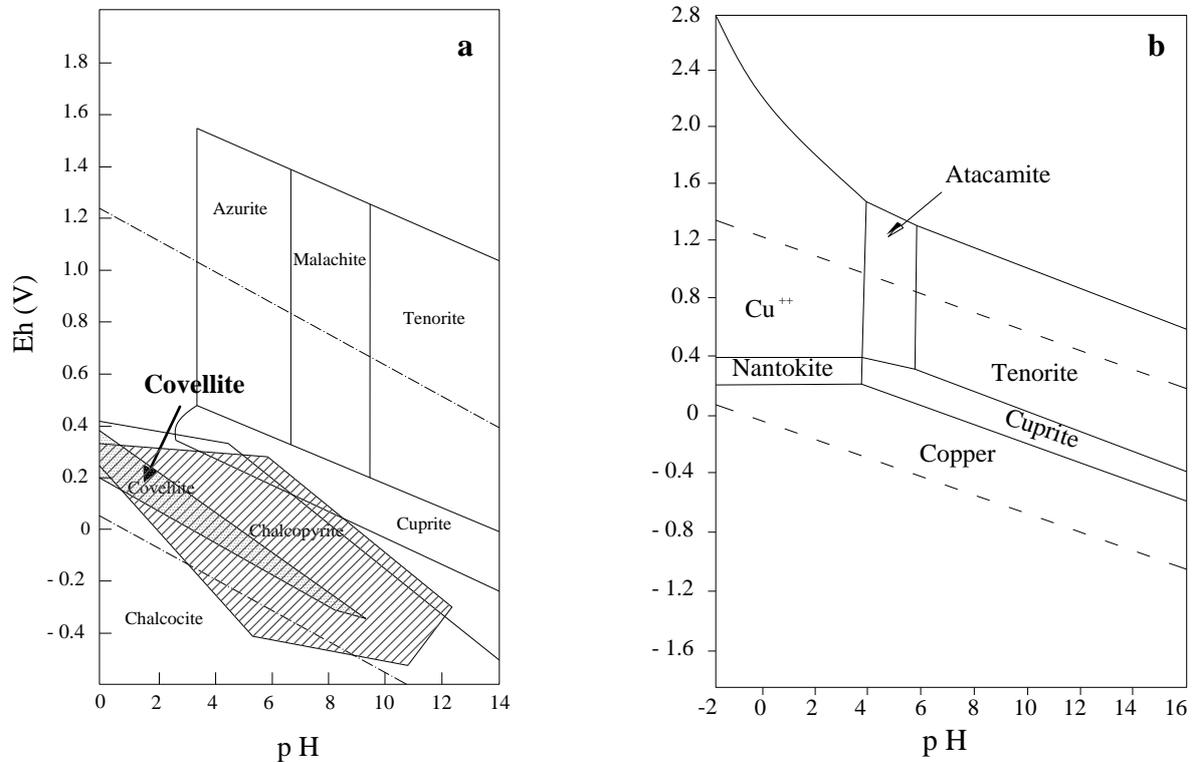
Figure 5.11. a) Pourbaix diagram for the Cu-S-H_2O system. (Adapted from Schweizer 1991). b) Pourbaix diagram for the system Cu-Cl-H_2O at chloride concentrations 350 ppm. (Adapted from Scott 2002)

The oxidizing environment of the latter two were not suitable for the formation of chalcocite and the survival of SRBs. SRBs are anaerobic bacteria which means they require an oxygen-free aqueous environment (Yuzwa & Eng 1991) such as a damp humus-rich soil (Schweizer 1991) for their survival. The northern dump was a man-made talus slope from Gardner's residual excavations and its soil content (silty sand) was quite dry (Calabrese 2000) which could not have a moist reducing environment for the growth of the SRBs. It seems the funnel, after it was discarded, was placed in an area with poor drainage like a shallow pit close to the sandstone bedrock of the hill together with other organic materials. Fossilized stems of plants amongst corrosion crust (Appendix C. Fig.23) are evidence in an organically rich burial environment. In this condition hydrogen sulphide which was produced as the result of SRB's metabolism (reaction 5.21, 22) reacted with dissolved copper and formed cuprous sulphide on the surface (McNeil & Odom 1992). Although cuprite can be formed by a direct reaction between copper and water (North & Pryor 1970) in moderately reducing environment (Fig.5.11) it could not be formed simultaneously with Cu_2S. Hydrogen sulphide in the environment

124

can react with cuprite and convert it to Cu_2S (reaction 5.23) with standard free energy of formation -110.2 kJ (McNeil & Odom 1992).

$$Cu_2O + HS^- \rightarrow Cu_2S + OH^- \qquad\qquad (5.23)$$

This reaction also reveals if any former cuprite layer was on the surface of the funnel; it might have been destabilized and acted as a source of metal-containing ions for reaction with sulphide in the environment (McNeil & Odom 1992; Little & Wagner 1993). It is obvious that the broad cuprite layer (Layer b1 in appendix B. Fig.77) was formed later by internal growth of corrosion in the copper plate in the absence of hydrogen sulphide and a change in the burial environment. The sulphide layer is porous, non-adherent and does not form a protective layer on the surface (McNeil *et al.* 1991). This property allows straightforward transportation of ions like chlorine or oxygen from the burial soil towards the metal surface, thereby accelerating the rate of corrosion in both reducing and oxidizing environments. Presence of copper trihydroxychloride among cuprite layer and on its surface (Appendix D. Table 5.3: analysis MC7L2b, c, e, f) indicated formation of nantokite during burial. Nantokite is a stable product in acidic and moderately reducing environment (Fig.5.11b) that indicates this product could form during SRB activity. The displacement of the funnel from Mapungubwe Hill to the northern dump with its oxidizing environment resulted in halting the microbial influenced corrosion (MIC). At this stage, corrosion has continued in an oxygenated environment with the formation of cuprite, copper trihydroxychloride and malachite, the formation of the latter two needing highly oxidizing conditions (Fig.5.11).

This indicates that the presence of a primary sulfide layer on the surface of MC7 with its poor protection could be a factor in the severe corrosion of the artefact in its further oxidizing environment at the northern dump or in storage. Hydrogen sulphide not only removed the probable primary cuprite layer which was produced on the surface during usage but also prevented the formation of cuprite layer in reducing conditions. Meanwhile chlorines easily migrated towards the metal surface through the porous sulphide layer to form nantokite in anaerobic environment (reaction 5.14). This nantokite later in oxidizing conditions was hydrolysed and oxidized to form hydrochloric acid and copper trihydroxychlorides at the metal/ corrosion interface. This reaction intensified the process of corrosion until no metal has remained.

5.3. *Survey on the condition of burial environment at K2*

Soil is a complex environment with different properties in various areas. Chemical composition and properties of soil such as pH are not precisely stable and can modify as the result of changing the climate and bioactivity at archaeological sites over time. Consequently the soil properties at archaeological sites at the time of discarding of the object and the initial corrosion activity could be quite different from the soil samples which were removed during excavation such as current soil

125

samples from K2. Nevertheless the properties of these types of samples are quite important as a part of the burial history of the artefacts.

In the presence of enough humidity soil acts as an electrolyte in establishing electrical current between anode and cathode in metals. Physical and chemical properties of soil which directly affect the corrosion of metals according to previous researches (Gerwin & Baumhauer 1999) are soil particles size, pH, *electrical conductivity* (EC) besides the amount and kind of soluble salts in this medium. Water content, Redox potential and amount of sulfide in the soil have also been referred to as affective factors (Palmer 1989). Recognition of these properties as well as demonstration of the aggressiveness of the soil makes it possible to retrace the correlation between corrosion compositions and soluble salts which is the important aim here. These factors are studied in this part with respect to the site of K2 since soil samples which related to each object burial place were unavailable.

5.3.1. Soil characteristics at K2

The archaeological and pedological characteristics of the soil layers are given in (Appendix D. Table 5.4). The result shows that the layers consisted of a homogeneous soil texture with average of 73% coarse sand, 19.7 % silt and a low percentage of clay. This type of soil is well-aerated and well-drained. The presence of a high percentage of coarse sand with its high porosity in the soil allows oxygen to penetrate easily through the voids in gaseous form or dissolved in water (rain). Although the drainage from the voids with greater size than 0.1 mm is sufficient in silty sand, the fine- grained particles such as silt and clay can retain the water in this type of soil (Cronyn 1990). The soil deposit at K2 is placed on an outcrop of weathered sand stone. The depth of the soil in Block 2 where the objects were found, is shallow. The depth is something between 0.61- 2.134 m in different sections based on Section on Datum Line A.3. Block 2 that was submitted in Gardner (1963). The sandstone bedrock reduces the amount of drainage consequently during the rainy season the silty sand in this region can have poor internal drainage. The high amount of salt content in the soil layers (Appendix D. Table 5.5) in part can be the result of this phenomenon since the dissolved salts cannot penetrate easily to the sandstone bedrock.

The pH value shows all the layers are weak alkaline (8-9) with the most alkalinity in layer 6. This range of pH is common in arid and semi-arid environments where the evaporation exceeds to precipitation. Evaporation results in an upward movement of bases (Ca^{2+}, Mg^{2+}, Na^+, K^+) along with water and retention of them in soil layers (Cronyn 1990).

The carbon content of the layers indicates the presence of low amount of organic matter. The highest amount of EC is seen in layer 6 and the lowest belongs to layer 2. The amount of electrical conductivity (EC) is directly related to the amount of soluble salts and moisture content of soil. In the presence of enough humidity increasing the amount of soluble salts will result in raising the EC and consequently the rate of corrosion.

Soluble salts in soil not only have an effect on EC and resistivity but also directly participate in the chemical composition of corrosion products. (Appendix D. Table 5.5) shows the amount of soluble salts in different layers in TS 1968.

The high concentration of anions is seen in layer 6 and 4 respectively and the lowest amount is observed in layer 2. The reason seems to relate to the well-drained soil which allows the soluble salts in the water to move towards the layers in the depth. The reduction of the amounts of salts in the layer 9 is the result of the action and interaction between precipitation and evaporation which exceeds in arid and semi-arid environments (Cronyn 1990). The evaporation of water results in upward movement of soluble salt in the layers. Chlorides and sulphates because, of high solubility (Cronyn 1990) are the most aggressive anions in the soil and have a deleterious effects on both iron and copper.

5.3.1.1. *Aggressiveness of the soil*

With consideration of the pedological data and based on AWWA rating- standard C105-72, the soil from K2 is severely corrosive. As Palmer (1989) suggested in this formula resistivity of the soil is the main controlling parameter in corrosion except in an environment with severe microbiological activity which is not seen in K2 soil. The other factors such as pH, Redox potential, sulphide content and moisture may be pertinent in identifying unusual soil conditions and distinguishing between otherwise similar soils (Palmer 1989). Table 5.6 shows the variables and their points in estimating corrosiveness of soil in AWWA formula.

The resistivity less than 700 ohm.cm is an indicator that the soil is severely corrosive. The K2 soil's electrical resistivity is between 400 ohm.cm in upper layer and 180.51 ohm.cm in layer 6. Since the amount of resistivity of K2 soil belongs to a water saturated soil sample, it can be much higher than the resistivity of the soil *in situ* and in a dry season. Pluviometry of the region shows the precipitation is 350 mm of mean per annum and seasonal (Smith 2005). This amount of precipitation can keep electrical resistivity low in a wet season. In the case of copper the resistivity less than 100-500 ohm.cm indicates a soil that could be aggressive (Myer & Cohen 1984).

The acidity of the soil will be considered if its amount is out of the range of 4-8.5. Here pH is between 8- 9.45 and based on AWWA formula it must add to corrosiveness of the soil. Looking at Pourbaix diagram (Fig.5.12a) indicates at this range of pH and positive Redox potential without presence of aggressive anions iron place in passive condition (corroding very slowly). Passivity at pH's above 8 is related to the formation of a protective film on the metal surface and its further stability. The reason for of increasing the rate of corrosion at about pH's above 8 appears to be related to the formation of a differential aeration cell which was described by Evans (1923). Pourbaix (1974:319) discussed the operation mode of Evans differential aeration cell in pH's about 7-10 as follows: '*Normal operation: passivation of the aerated zones, a large current and a large corrosion*

rate in the non-aerated zone'. In an oxidation conditions and in the absence of aggressive anions, pH's near neutral and weak alkaline result in the formation of insoluble salts in copper which decrease the rate of corrosion (Fig.5.12b). Nevertheless here also the formation of a differential aeration cell could increase the rate of corrosion at K2 soil.

Since the soil layer is not thick and contains mostly coarse sand it is well-aerated and the Redox potential must be quite positive (>100 mV). Therefore it cannot increase the rate of corrosion. This parameter also rebuffs the probable activity of sulphate reducing bacteria in the soil therefore sulphide content has no effect on corrosiveness of the soil at K2.

From what was referred to as the high corrosiveness of the soil from K2 directly is related to the pH and high amount of soluble salts, mostly chlorides and sulphates that can have an effect on affect on electrical conductivity and the rate of corrosion when enough humidity is present in the environment. Consequently the relevant archaeological metals had been buried in a well-aerated and high aggressive soil with low alkalinity for a lengthy period of time.
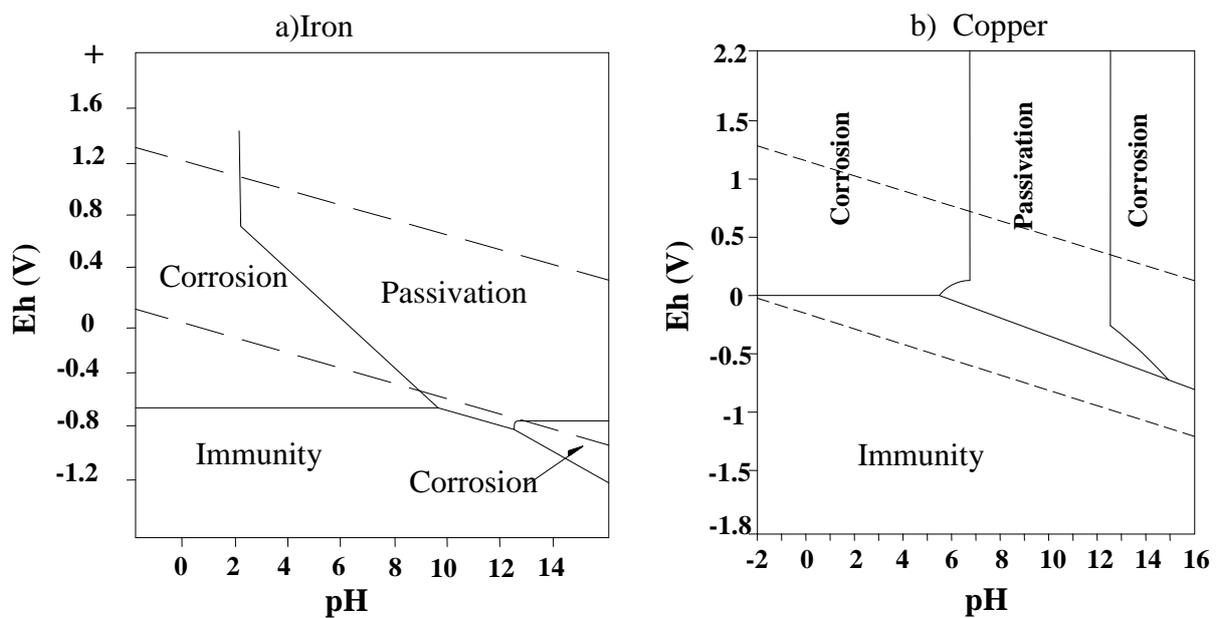
Figure 5.12. a) Simplified Pourbaix diagram for iron in water. Adopted from Palmer (1989). b) Sketch of Pourbaix diagram for copper in water in 25°C. Adopted from Pourbaix (1974)

5.3.1.2. Correlation between depth and corrosion percentage

The results of soil analysis show that the amount of deleterious anions has been increased by depth through layers at K2 (Appendix D. Table 5.5). This phenomenon could influence in state of preservation of excavated objects in different depths. The probable relationship between the degree of corrosion and depth is studied here, on the basis of percentage of corrosion in the objects which were found in different depths at K2. The number of objects is significant in achieving a reliable result in

128

this type of study. In this study the number of objects from K2 (Appendix D. Table 2.2) was very small which only produced indicative and not conclusive results.

The scatter graph below (Fig.5.13) shows the correlation between depth and percentage of corrosion in the metal artefacts from K2. The circles are the indicators of iron artefacts and triangles belonging to coppers. The trendlines indicate an obvious relationship between increasing the percentage of corrosion and raising the depth. For an estimation of the direction and strength of this relationship the Spearman's Rank Correlation Coefficient was used. Although the calculated coefficient (Spearman) suggested, that there is a strength link between these two parameters, the result has unclear statistical significance. Ranking coefficient values for iron and copper artefacts were + 0.95 and +0.65 respectively which are quite high. Nevertheless insufficient numbers of artefacts (n = 4, n = 5) were responsible for this unclear statistical significance.
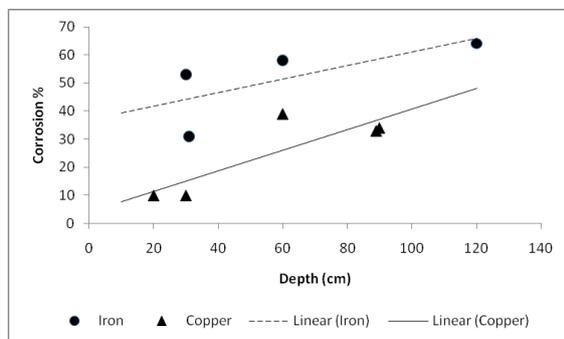
Figure 5.13: Correlation between corrosion percentage of archaeological metal artefacts and depth of excavation.

5.3.1.3. Survey on effects of burial environment on corrosion of metal at K2

Although the soil analysis of K2 showed high amounts of soluble salts such as chlorides, sulphates and carbonates (Appendix D. Table 5.5) a study of corrosion products on copper artefacts from K2 revealed that chlorine and oxygen were the main elements from the environment which directly participated in the corrosion process. In the case of the only copper artefact with an even surface from K2 (KC5) no trace of carbonate content product was detected on the surface. It seems, as discussed in the case of MC11 (see section 5.2.3.2.1.1.1), carbonates had only a buffering role in protecting the artefact from corrosion. In this process carbon dioxide and water produce the soluble calcium bicarbonate which prevents dissolution of copper (I) ions (Geilmann 1956; Scott 2002). In pH > 8 calcium bicarbonate can precipitate as carbonate (Scott 2002) on the surface as it was detected on KI1. Sulphates were only detected as contaminant precipitation on the surface of artefacts (KC2) from K2. In corrosion of iron artefacts hydroxyl (OH$^-$) was the predominant ions participating in electrochemical process of corrosion.

5.4. Summary and Conclusion

A comprehensive study was done on the chemical stability of some of the representative iron and copper objects in this assemblage. For this reason, the corrosion compositions and their stratification on the objects were scientifically studied by utilizing SEM-EDS, Raman, XRD and optical microscopes.

The results in the case of iron objects show that the main products consisted of magnetite, maghemite, hematite, goethite and lepidocrocite. Except for magnetite, which was formed in an alkaline solution under reducing conditions, the other products were formed under oxidizing conditions. Magnetite is generally observed at the interface of the metal surface and corrosion products where the amount of penetrating dissolved oxygen is quite low. On the basis of Pourbaix diagram (Fig. 5.8) all these products can be stable in a wide range of pH while the maghemite, hematite and all polymorphs of FeOOH almost have a same domain of stability.

These products formed a bilayer corrosion on the surface with an inhomogeneous composition. Among them lepidocrocite, maghemite and magnetite were only detected in the internal layer. Although goethite and hematite have the highest chemical stability among these products, the metastable phases such as lepidocrocite, maghemite and magnetite can also remain intact for a long time. This stability is due to the sluggish kinetics of transformations of iron oxides under ambient conditions (Cornell & Schwertmann 2003). Nevertheless the presence of metastable lepidocrocite in the internal layer, in addition to its formation which is associated with a high quantity of Fe2+ ions in area of formation (Cornell & Schwertmann 2003), creates the possibility that the corrosion might still continue in atmospheric conditions.

The most important destructive feature of FeOOH polymorphs is their high molar volume compared to the iron substrate. Consequently their formation results in the expansion of corrosion products on the surface which can cause cracks, deformation and physical instability in the iron objects. Only one of the iron artefacts (SI1) is instable due to the high amounts of chlorine and sulphate in the vicinity of the metal surface. Chlorine in this object with, formation of a cyclic corrosion, increases the rate of corrosion compared to those iron objects which have no chlorine content or a low amount of it (<0.7wt%).

The quartz grains which have adhered to the objects' surface by the outward growth of corrosion are the main observable signs that can indicate the limit of the original surface at the interface of the external and internal layers.

Contrary to the iron artefacts, most of the copper objects are subjected to bronze disease due to the penetration of chloride ions into the corrosion crust and their reaction with cuprous ions (Cu^+) in the vicinity of the metallic phase. This reaction resulted in the formation of metastable nantokite (CuCl) which easily reacts with oxygen and humidity in the atmosphere to start a cyclic corrosion with the formation of hydrochloric acid and polymorphs of copper trihydroxychlorides (atacamite,

130

clinoatacamite and paratacamite). These products were detected on the copper objects with the uneven surface and can be a sign of active corrosion in them. High molar volume of the copper trihydroychlorides compared to copper is one of their characteristic which can cause volume expansion in the corrosion layer. Cuprite is another product that was detected on both copper objects with even and uneven surfaces. Both even and uneven surfaces consist of three main corrosion layers with totally different compositions. In the artefacts with an uneven surface the original surface is seen as a fragmented cuprite layer above the internal layer which mostly consists of a composition with a high chlorine content probably in the form of an admixture of cuprite and nantokite. On the even surface the original surface has kept its pseudomorphic shape in a well-formed cuprite layer.

A survey of the K2 soil shows that the objects were buried in well-aerated silty sand with a low alkalinity. The soil has a high corrosiveness due to pH and a high amount of soluble salts. The amount of soluble salts such as chlorides, sulphates and carbonates in this soil is quite high which could effect on the corrosion rate of the objects. Although carbonates and sulphates can participate in corrosion reactions, corrosion analysis indicates chlorides and hydroxyls were the main anions that participated in the electrochemical corrosion of copper artefacts in this site. It appears that the carbonates had a buffering role in the corrosion of copper. Chlorine had a low or even no effect on the corrosion of iron in the K2 site which could be due to the position of cathode on the metal surface during corrosion. The amount of soluble salts rises with increasing depth of the soil until a certain depth of which the limit is defined by the range of precipitation and evaporation in the area. This phenomenon resulted in the increasing corrosion of metals relative to the increasing depth at K2. A study of the conditions of the soil during excavation is needed for more accurate data about the influence of a burial environment on corrosion. It is also necessary to identify the corrosion composition on archaeological metal immediately after excavation and before atmospheric conditions can change them.

Chapter 6

Cleaning and Preservation

6.1. Introduction

Cleaning and preservation in addition to the investigation are three fundamental gaols in conservation. All conservation experiences should be performed with due consideration of a proper balance between all these goals. Every object has historical and aesthetic values which together form a potential unity (Brandi & Basile 2005). Historical aspects refer to the evidence an object retains from the past. This evidence informs us about the materials from which the object was made, the technology of production and every incident that occurred in an object's life. Aesthetic value refers to every characteristic in an object which can provide aesthetic experience for every one who senses. These characteristics can be seen in the shape, colour and texture that gave a physical reality to the artist's intention during the process of creation. Aesthetic value can be seen in objects in different degrees. Functional objects such as tools usually have a lesser aesthetic value. (Caple 2000.)

These aspects can be obscured over time by the disintegration of an object's constituent materials and the formation of a layer of contamination on the surface due to environmental conditions. The degradation of constituent materials of an object is an irreversible process and if it is formed gradually and under the effect of natural conditions can be considered as 'age value'. The age value in artefacts was introduced by Riegl (1929) and refers to '*weathering, the patina, and the eventual changes caused to it since its first construction; 'Its incompleteness, its lack of wholeness, its tendency to dissolve form and colour set the contrast between age-value and the characteristics of new and modern artifacts'* (Jokilehto 1986:379). All the altered constituent materials, although they may obscure aesthetic and historic values, are inseparable parts of an artefact and form part of its history (Brandi & Basile 2005).

Cleaning and preservation are two useful actions in revealing and keeping intact the historical and aesthetic aspects in the objects as far as possible. There are two main reasons for cleaning of an object. The first one is related to the presence of any harmful layer above the original surface and the second one is associated with the enhancement of an object current appearance from aesthetic viewpoint. Cleaning, from a conservation point of view, however, does not aim to give an object a shiny, new appearance as it had when first made. Cleaning points to all practices followed to expose what remained of the original surface among the materials altered by corrosion. It must be done with a knowledge about the constituent materials of an object and chemical degradation in them over time. With this knowledge it is possible differentiate between degraded materials on the surface and contaminants that are not part of the object. During the cleaning process of metal objects only the contaminants which were sometimes entrapped within precipitated corrosion products, and harmful corrosion above the original surface, are removed.

Preservation theoretically means maintaining the object in its present condition and inhibiting further deterioration with preventive and/or interventive interferences. Although in modern preservation, it is advised to use preventive methods for halting the process of deterioration, sometimes using non-passive methods are preferable. The choice of these methods is completely

related to the condition of the objects regarding their physical stability and the presence or absence of detrimental compositions on their surface. Modern preservation consists of two main principles which must be considered to keep the potential unity in the objects. The first principle that was suggested by (Brandi 1963) refers that, '*a conservator only conserves the materials of the work of art*'(Jokilehto 1986:418). This means the conservator cannot remove the degraded material of an object and replace it with a new material, even if the new material has the same composition. The second principle states that '*restoration must aim at the reestablishment of the potential unity of the work of art, so far as this is possible without committing a fake, and without cancelling traces of its history*' (Brandi 1963, Jokilehto 1986:418). This means conservators can reintegrate an object under specific conditions to prevent artistic or historic fakes (Jokilehto 1986). One of the rules that Brandi (1963) suggested regarding reintegration states: '*Reintegration should always remain recognisable on close inspection, although from a distance they should not disturb the unity that it is the intention to re-establish*' (Jokilehto 1986:418). This rule allows a conservator to fill the gaps, which are mostly formed during the disintegration of an object or by sampling it, with a material that is different in composition and slightly different in texture and colour. This kind of reintegration would prevent artistic or historic fakes.

In this chapter, I have tried to introduce simple and cost effective methods for revealing and stabilizing the original form of artefacts which mostly exists within corrosion products. I also tried to adhere to the ethics and principles of modern conservation practice. In this chapter the treatment procedures were planned on the basis of physical stability of the objects in addition to the corrosion composition and stratification on their surface. These methods are recommended on the basis of available facilities and are chosen from those ones that have the least adverse effects on constituent materials of the objects. The recommended procedures consist of both passive and non-passive methods, the   selection of which to use would depend   on the decision of the curator and the allocated budget for conservation of metal artefacts.

6.2. Cleaning

Cleaning of the archaeological object is defined as removing all the extraneous materials which are not a part of it and the existence of which results in damage or obscuring the original material or shape of the object. The extraneous materials on the surface of archaeological metals are mostly soil particles and quartz grains that were entrapped within the corrosion layer. This layer was formed due to the outward growth of the corrosion in a burial environment and with precipitation of corrosion on the soil particles. The external corrosion layer on the surface of the artefacts is mostly rough and porous which promote water condensation in the pores (Selwyn 2004). The condensed water within the pores increases the rate of corrosion. The presence of this layer also forms a barrier for easy removal of the harmful anions from the internal layer during treatment of the objects. The K2 and Mapungubwe

133

metal assemblage which are kept at the University of Pretoria contains low numbers of objects that retain their physical integrity for display purposes. To prevent further disintegration of these objects it is recommended that those ones which have an external layer of embedded quartz grains in the corrosion products be cleaned. Removing such surface contaminants not only decreases the rate of corrosion but also facilitates the later removal of harmful anions such as chloride from deep inside the artefacts which suffers of active corrosion. The cleaning procedures, based on the physical stability of the object and chemical properties of contaminants, may differ. Here, on the basis of information gathered in Chapter 3, 4 and 5 the appropriate methods for cleaning of the objects are recommended. The summary of the chemical and physical stability of the objects was given in Appendix D: Table 4.3.

6.2.1. *Mechanical cleaning of the artefacts*

6.2.1.1.*Cupreous artefacts*

Except for KC5, MC6 and MC11, all the copper artefacts in this assemblage, as well as the only bronze object, have an uneven surface with a discontinuous original surface within the corrosion products (Appendix D: Table 4.3). Due to this characteristic mechanical cleaning is usually chosen for the removal of the external layer on the objects with bronze disease because chemical reactions associated with chemical and electrochemical cleaning cannot be easily controlled (Scott, 2002) and therefore may result in damage to the original form of the objects. Among these artefacts SC1 and MC7 have a porous, weak structure with no metal core and mechanical removal of the corrosion and contaminants from the surface might lead to complete disintegration of the object. It appears that MC5, having no metal core, is more stable and can undergo mechanical cleaning if undertaken with special care.

In the process of mechanical cleaning as suggested by Cronyn (1990) the external layer is removed by using simple tools such as a pin and scalpel with the occasional use of chemicals to soften overlying copper(II) minerals. Various different modern electrical tools such as a hand-held electric engraver with pin, electric stylus and air abrasion is another technique which can also be used in mechanical cleaning of these artefacts. Using air abrasion for weak objects group (c) (See Appendix D. Table: 4.3) is advisable since it produces less mechanical pressure on the surface. At first this process must be performed on a small area to reveal the original surface (investigative cleaning), then work on the whole object. To discover the limit between surface contamination and the original surface, all procedures must be done under binocular microscope with magnification of X 10 to X 40 (Scott 2002). The limit of the original surface in the copper artefacts is mostly defined by the presence of a cuprite layer and lack of quartz grains in the layer. The wart with cuprite overlying must be kept intact to prevent revealing the underlying pits while all eruption of powdery paratacamite must be removed from the surface.

Although the objects with bronze disease are vulnerable to humidity and aqua solution, the use of chemicals with an aqua base for softening the hard overlying minerals that cannot easily be removed is sometimes unavoidable. Contaminants on the surface of copper artefacts in this assemblage mostly consist of calcareous deposit (Appendix D.Table 5.2: analysis KC2L4, MC11L2a and Fig.5.4, 7). In such cases sodium tripolyphosphat, if used with caution, is a safe chelating agent compared to other sequestering agents for removing the calcareous accretions. Investigation by Sharma and Kharbade (1994) revealed that this sequestering agent has an alkaline pH during treatment which may result in the conversion of cuprite to tenorite in prolonged treatment (Pollard *et al*. 1990). Since cuprite is the main compound in the patina of copper artefacts in this assemblage to prevent this reaction, an optimum treatment duration of almost eight hours must be considered. To prevent the penetration of chemicals deep inside the object, the use of poultice or gel cleaning, instead of soaking in the solution, is recommended. Sharma and Kharbade (1994) suggested using carboxymethyl cellulose gel containing a 0.5%-2% aqua solution of sodium tripolyphosphate based on the thickness of the corrosion layer. The gel is applied in a thin layer onto the surface of the object using a soft brush and then left to dry. After removing the dried gel and loose contaminants, the object must be washed several times in hot distilled water in an ultrasonic bath until all chemical residues has been removed. After this the object must be completely dried and, in the case of objects with bronze disease, immediately sent for chlorine removal.

6.2.1.2. *Iron artefacts*

Revealing the original surface in weak iron objects, and rigid ones with structural defects such as cracking and flaking (Appendix D.Table 4.3. weak group: subgroup a, b; rigid group: subgroup b), require mechanical cleaning. The procedure is quite similar to that followed in the case of copper artefacts with the exception that corrosion products on iron objects have no obvious stratification and the only indication which shows the limit of the original surface is a lack of quartz grains among the corrosion products. Analytical results of corrosion products on iron artefacts (Appendix D. Table 5.1 and Figs.5.1, 6) indicated the presence of calcareous deposits on the surface of most iron artefacts in this assemblage. This accretion could be firmly stuck to the surface. To ease its removal the use of chemicals is sometimes necessary. For a safe mechanical cleaning the objects can be divided to two groups as follows:

a. In mechanical cleaning of the iron objects with a discontinuous metal core (Appendix D. Table 4.3. weak group: subgroup b) the dry technique without using any chemicals is recommended since rehydration may cause the objects to split apart (Blackshaw 1982). The objects which have voids in some parts as the result of the high dissolution of the metal core (MI5) need special care during this kind of cleaning to prevent their disintegration. Over-cleaning of this type of object can result in

135

revealing the hollow inside. When cleaning these objects it is important to consider the tomograms and should only be tried to reveal the main shape of the object within the bulk of corrosion.

b. In the case of the objects in rigid group (b) and weak group (a) (Appendix D. Table 4.3) it is recommended that calcareous accretion and rust stuck firmly   to the surface be removed with great care by softening them in chemicals. Detarex C, a solution of EDTA (ethylenediaminetetra-acetic acid) modified with sodium hydroxide to the tetra-sodium salt with pH of 13 is   suitable for softening the rust while this compound acts slowly and ensures careful control of the layers that are removed each time (Blackshaw 1982). In this regard Plenderleith and Werner (1971) suggested a mixture of 30ml Detarex C, 30g sodium hydroxide and 6gr sodium hyposulphite dissolve in one litre of water. The objects which have a uniform corrosion layer (KI1, MI4 and MI6) may be immersed in the solution (Blackshaw 1982) while the affected parts of those with a non-uniform layer (KI3, KI4 and SI2) must each be treated separately with a poultice soaked in the solution. During treatment the hardness of products is examined and loose contaminates are removed mechanically. After removal of all the extraneous products the object must be washed in several changes of de-ionized water. The object is then soaked in acetone and dehydrated by air.

6.2.2. *Electrolytic cleaning of the iron artefacts*

The iron objects with a thin oxide layer on the surface (Appendix D. Table 4.3. rigid group: subgroup a) may be cleaned chemically by dissolving the iron oxides because the original surface was mostly kept intact by the substrate metal. This method, in contrast to mechanical cleaning, is less time consuming and labour intensive while it is effective and achieves the desired result if applied accurately. Cronyn (1990) argued that electrolytic cleaning is a more suitable method for removing corrosion products in contrast to other chemical cleaning methods. This method has fewer drawbacks compared to some chemical compounds such as acids and commercial rust removers which could result in either etching or forming a deposit on the metal surface. In fact, with electrolytic cleaning iron is cathodically protected from etching by the electrical current (Cronyn 1990). To prevent over-cleaning which is associated with leaching the iron and revealing a pitted surface, utilizing a low density current is recommended during the first stage of treatment. This approach leads to the consolidation and/or reduction of some mineralized metal on the surface. In this process ferrous corrosion products are partly reduced to metal *in situ* and consolidate the corrosion layer (Hamilton 1999), and sometimes retaining the tool marks. This operation, particularly in the case of MI9, could reveal illegible notes on the handle.

The method was explained in detail by Hamilton (1999) but, in brief, the iron object is connected to a negative pole (cathode) of a low-voltage DC (6-12 volt) source while an inert metal such as mild steel or stainless steel is connected to the opposite pole (anode). Both are immersed to an electrolyte and the current turned on. Since the reduction of ferrous corrosion products is the objective, a 2-5%

136

(w/v) aqua solution of sodium hydroxide is recommended as electrolyte. In the case of a big object (KI5, MI2, MI7 and MI9) to achieve a coherent surface two anodes or an iron mesh (anode) must be placed around the object while the object itself must be connected to cathode steadily. Reduction of mineralized iron on the surface needs a low current density at the first stage while removing the low amount of chlorine and unreduced corrosion products in these artefacts needs a higher current density. Then treatment is started with low current density and after a short time the current is increased in two stages and finished with high density current. For this reason, during electrolysis, the current is adjusted based on the desired function of the treatment. Adjusting the current density is simply established by observing the amount of hydrogen evolution at anode while increasing the voltage or amperage results in intensifying the hydrogen effervescence. Continuous monitoring is necessary during the process. After treatment the objects must be thoroughly washed several times with distilled or de-ionized hot and cold water in an ultrasonic bath until all chemicals have been completely removed.

6.3. Initial examination of the copper artefacts with noble patina

The analytical study of corrosion on the copper objects (MC6 and MC11) with noble patina was restricted to only one of them (MC11) by removing a small section as well as surface corrosion products (Fig.3.39). This data may not be comprehensive to reveal all compositional aspects of the corrosion. Therefore it is necessary before taking any conservation decision, that these objects be examined more thoroughly for the probable presence of nantokite. For this reason the objects must be placed in a humidity chamber while the RH reaches above critical humidity for the transformation of nantokite to copper trihydroxychlorid, above 70% RH (Scott, 2002), at room temperature. If no trace of powdery green products is observed on the surface after 96 hours, it means that the objects are in a stable condition. In such a case the object is coated with a layer of appropriate corrosion inhibitor followed by a sealant which is referred to elsewhere in this thesis. On the other hand, observation of green powdery patches of corrosion indicates the object is not in a stable condition and needs further stabilization.

6.4. Stabilization

Stabilization means halting or reducing the rate of corrosion in artefacts that contain a metal core. Most of the copper artefacts in this assemblage, except for those without a metal core (SC1, MC5 and MC7), and those with noble patina (MC6 and MC11), suffer from active corrosion (bronze disease). In the case of iron artefacts, although the majority of them only have a low amount of chlorine content (0.1-0.6 wt%) that may be less hazardous to the stability of the objects, the nature of iron as a base metal makes them susceptible to further corrosion in the presence of oxygen and humidity. To stabilize the objects from further corrosion, two different active and passive methods are recommended whereas the choice of methods depends on the characteristics of the objects.

137

6.4.1. Interventive techniques

In these methods halting or reducing the rate of corrosion will be accomplished by chemical treatment. These chemicals are mostly utilized to eradicate the harmful ions such as chlorine from deep inside the objects thereby removing the corrosion products such as CuCl, or converting them to harmless ones. On the other hand, some of these chemicals are acting as corrosion inhibitors by forming a barrier between metal or unstable products and environmental variables such as humidity and pollutants. The choice of chemicals in stabilizing the antiquities depends on their efficacy and the chemical composition of the corrosion on the object while it should produce the lowest chemical alterations to the structure of the object, based on the ethics of conservation.

6.4.1.1. Copper artefacts with bronze disease

A study of small cross sections of copper artefacts with bronze disease revealed that the original surface generally consisted of a disrupted cuprite layer among the corrosion layers with a high chloride content in the form of products such as copper trihydroxychlorides and/or nantokite (see section 5.2.3.2.1.2). In these cases the total removal of harmful corrosion products by chemicals could damage or entirely eliminate the thin enveloping cuprite layer. In this condition stabilizing the artefact and keeping the original surface intact can be attained by the use of chemical compounds such as sodium sesquicarbonate or sodium carbonate that, instead of removing the harmful product (CuCl), convert it to a stable, harmless compound. Weisser (1987) suggested stabilization with a sodium carbonate solution in conjunction with benzotriazole (BTA) which has less drawbacks compared to sodium sesquicarbonate. Sodium carbonate, in contrast to sodium sesquicarbonate, does not dissolve the copper substratum by forming a complex compound with copper.

6.4.1.1.1. Sodium carbonate rinsing

The hydroxyl ions in alkaline solutions such as sodium sesquicarbonate and sodium carbonate react directly with insoluble nantokite to form cuprite. This reaction also neutralizes any hydrochloric acid by-product formed by hydrolysis of nantokite (reaction 5.17) to produce soluble sodium chlorides (Organ 1963; Oddy & Hughes 1970; Plenderleith & Werner 1971; Hamilton 1999). Hamilton (1999) explained the process of treatment as follows:

The object is immersed in 5% (w/v) aqua solution of sodium carbonate while the solution is changed successively until all extracted chlorines are removed. In the beginning the interval between each bath is one week while tap water is used in making the solution. In subsequent baths when the level of chloride ions in the solution decreases and reaches the level of tap water distilled water is used. The chlorine concentration in the solution is measured by a quantitative mercuric nitrate test or qualitative silver nitrate test. After finalizing the treatment the object is rinsed in successive de-ionized or distilled cold and hot water until the pH of the last bath is neutral. The use of ethanol instead of

138

distilled water in the final rinsing to prevent tarnishing is not necessary since the objects have a cuprite layer as patina. Then the object must be impregnate with a recommended corrosion inhibitor such as benzotriazole.

Treatment with sodium carbonate leads to the formation of chalconatronite caused by evaporation of the solution or residual treatment solution (Pollard *et al.*1990). Then, during treatment of the objects, it is essential to avoid formation of chalconatronite (green) on the surface by preventing evaporation of the solution. After treatment a thorough removal of the solution residual with de-ionized water will help to prevent formation of chalconatronite. At the appearance of any precipitation of green-blue products on the surface the solution must be changed (Scott 2002) and the surface cleaned with a soft brush. The process of washing in an alkaline solution, as discussed above, must be arrested following the reaction of $CuCl(s)$ to give $Cu_2O(s)$, and prior to subsequent conversion to $CuO(s)$ (Pollard *et al.*1990) which is seen as black spots on the surface.

6.4.1.1.2. Benzotriazole (BTA)

BTA is a corrosion inhibitor that not only keeps the corrosion products intact but also prevents further corrosion by forming a barrier between probable CuCl remnants in the object and moisture in the atmosphere. This barrier is developed by forming an insoluble complex compound between BTA and Cu(I) ions (Scott 2002). Impregnating the objects with BTA after rinsing in an alkaline solution increases the level of their stability by prohibiting the harmful effect of probable fluctuation in humidity on corrosion of the objects. Indeed, where small amounts of nantokite have remained from the preceding rinsing this coating can keep it dormant. The treatment procedure suggested by Hamilton (1999) and Scott (2002) is as follows:

The object is immersed in 1-3% (w/v) BTA in ethanol or water, based on the duration of the treatment. The best result will be achieved if the object is impregnated under vacuum for 24 hours. In this condition a 1% solution of BTA in water can also work well but in a shorter period, a 3% (w/v) BTA in ethanol gives a better result. Since ethanol can facilitate penetration of BTA in crevices and cracks it is recommended in the treatment of copper objects in this assemblage. After treatment the object is removed from the solution and wiped off with a rag saturated with ethanol to remove excess BTA and exposed to the air to dry. To facilitate the process of drying it is possible to immerse the object in a final bath of acetone or water/ethanol mixture to remove water thoroughly if a water base solution was used. After impregnating the object it is advisable to put the object in a humidity chamber at 90-95% RH and room temperature for 96 hours to reveal the presence of any unsealed nantokite on the object (Angelucci *et al.* 1978). If any powdery green corrosion appears it must be removed and the impregnation with BTA is repeated. Then the objects are coated with a layer of sealant. BTA is carcinogenic and working with it needs special care as has been referred to in Scott (2002).

In the case of copper objects with a noble patina (MC6 and MC11) impregnating with BTA followed by coating with a protective layer is also advisable. This protective layer prevents further corrosion of the objects when coming into contact with corrosion agents such as oxygen and humidity in display cases.

6.4.1.1.3. Sealant

After complete dehydration of the objects they are coated with a layer of clear acrylic lacquer or microcrystalline wax as sealant. Hamilton (1999) suggested the use of the commercially available KrylonClear Acrylic Spray No. 1301 for ease of application, durability, and availability. A 5% (w/v) solution of paraloid B72 in ethanol is also suggested by Scott (2002) as coating. Microcrystalline wax has no advantages over clear acrylic lacquer.

6.4.1.2.Iron artefacts

The elemental analysis of corrosion products on a few artefacts (KI1, KI3, MI4, MI5, MI6, SI1 and MI10) showed, except for SI1, that the rest have low amounts of chlorine content (0.1-0.7 wt%) in corrosion layers. Considering that no traces of active corrosion caused by chlorine in the form of weeping or globule shell is seen on the surface of these objects, chlorine removal seems unnecessary. In this case, after a preparatory cleaning (mechanical or electrolytic cleaning), the application of a layer of corrosion inhibitor (tannic acid) on the surface followed by a moisture sealant can prevent further corrosion. The only iron artefact that contains a high amount of chlorine (SI1) at the internal layer has a discontinuous metal core. In such cases passive preservation of the objects before stabilizing by a corrosion inhibitor and a final sealant is advocated.

The remainder of the iron artefacts (KI2, KI4, KI6, MI1, MI3, SI2 and SI3), as with the examined iron objects, are covered with a thick layer of red brown corrosion and have no traces of weeping or globule shells on the surface. These artefacts did not undergo sampling and elemental analysis in terms of chlorine content, and only the surface evidence can be considered as an indication for their stability. Another method that can show the chemical stability of these artefacts is immersion of the objects in an alkaline solution such as sodium sesquicarbonate or sodium hydroxide. Further quantitative or qualitative chlorine examination of the bath solution would show if chlorine is present within the corrosion layer (Plenderleith & Werner 1971).

In this method alkaline solution with passivating the iron surface assists in easy removal of Cl^- from the interface of the metal and corrosion layer. The alkaline solution, while increasing the concentration of OH^- on the metal surface, results in formation of $Fe(OH)_2$ which easily oxidizes to $Fe(OH)_3$ (See Section 5.2.3.1.1). The formation of insoluble products results in passivation of the metal surface which is only possible in the presence of enough dissolved O_2, for motivating the cathodic reaction, and a high concentration of OH^- in the solution (Selwyn 2004). Selwyn (2004)

suggested that the high concentration of OH$^-$ is necessary to react with Fe^{2+} ions as well as to maintain the alkalinity of the solution in a region where hydroxide ions formed insoluble salts. Among the different kinds of alkaline solutions such as sodium borate ($Na_2B_4O_7$, pH 9.2), sodium sesquicarbonate (equimolar solution of Na_2CO_3 and $NaHCO_3$, pH 10), sodium carbonate (Na_2CO_3, pH 11.2), and sodium hydroxide (NaOH, pH 12.6-13.5)   which can result in the passivation of bare iron (Mayne & Turgoose 1975; Hjelm-Hansen *et al.* 1993, Selwyn 2004), sodium hydroxide is preferred by conservators. NaOH is cheap, readily accessible and because of its high alkalinity is the most effective solution in the removal of soluble harmful chlorine in archaeological iron (Mathis 1994, North and Pearson 1978; North 1987; Selwyn 2004).

The immersion of archaeological irons in an alkaline solution is only applicable for those physical stable objects with continuous metal core. In this kind of treatment, some of iron oxyhydroxides such as lepidocrocite and akaganéite are converted to magnetite (Cornell & Schwertmann 2003) which has a lower molar volume (14.9 cm^3) than lepidocrocite (21.7 cm^3) and akaganéite (26.7 cm^3) (Selwyn 2004). Therefore, treatment in an alkaline solution decreases the mechanical integrity of the corrosion layer by increasing its porosity (Selwyn 2004) and where the corrosion has a non-adherent structure to the metal substrate; it can be easily eliminated from the surface. Among these objects, KI4 and SI2 are the only ones that have sufficient physical stability (Appendix D. Table 4.3. Rigid group: subgroup b) to be submerged in an alkaline solution. Chemical treatment of KI4 in an alkaline solution, with reduction of the corrosion products such as iron oxyhydroxides to magnetite, can prevent the spread of cracks and lamination into the metallic phase.

It is preferable that the remainder of the artefacts (KI2, KI6, MI1, MI3, SI1 and SI3), which have a weak structure (Appendix D. Table 4.3. weak group: subgroup b), be covered with a corrosion inhibitor and a sealant after mechanical cleaning. This process would prevent further corrosion in them.

6.4.1.2.1. *Rinsing in sodium hydroxide*

Rinsing in sodium hydroxide was recommended in many studies as an effective method for cleaning heavily corroded iron artefacts with chlorine contamination (Hjelm-Hansen *et al.* 1992, 1993; Mathias 1994; Al-Zahrani 1999; González *et al.* 2003; Selwyn *et al.* 2001; Selwyn & Argyropoulos 2005; Selwyn 2004). In this technique the objects, KI4 and SI2, are immersed in a 5% solution of sodium hydroxide (pH 12.6-13.5) in distilled water. The soluble salts are removed by the water while the sodium hydroxide solution prevents further corrosion of the metal. Halting the corrosion during desalination facilitates chlorine removal by decreasing the tendency for inward flow of chlorine as a result of potential gradient removal (Turgoose 1982*b*). The objects remain in the solution for one day in a covered container to prevent either evaporation of the solution or the possibility of exterior contamination. During this stage a sample of the solution is examined with the aid of a quantitative

141

chlorine test such as mercuric nitrate. If the amount of chlorine is lower than 20ppm and, with successive changing of the solution during the succeeding days it remains constant, the object has a low chlorine content and no further washing is needed (Watkinson 1983). The object will then be removed from the solution and undergo several rinses in distilled water. Hamilton (1999) suggested adding a corrosion inhibitor such as gluconic acid, sodium gluconate or sodium glucoheptanate to the distilled water to prevent rust during rinsing in the water and subsequent dehydration.

With a higher amount of chlorine in the solution (>20ppm) the successive rinses will continue with a daily change of the solution during the first week and then only weekly (Oddy & Hughes 1970) until the chlorine content remains constant and lower than 20 ppm after further washing (Watkinson 1983). The object is then rinsed in distilled water as explained above until all the chemicals have been removed and it is allowed to dry.

6.4.1.2.2. Drying

Since iron objects are sensitive to humidity and oxygen after treatment, leaving them in the atmosphere or applying heat to dry them could lead to the formation of rust on their surface. On the contrary, dehydration of the objects in water-miscible alcohol, acetone or isopropanol will prevent rusting by forming an oxygen-free environment during drying. Hamilton (1999) described the procedure as follows: after removal of the object from the distilled water bath, the object is wiped with clean rags and immersed in ethanol to remove most of the remaining surface water. In this way the object has less water and the remaining ethanol may be used for drying more objects. After a while the object is submerged in water-free isopropanol and remains there for a minimum of 24 hours for complete dehydration. If the water content of isopropanol becomes too high it can be used in the preliminary bath and fresh ethanol is used for the final bath.

6.4.1.2.3. Corrosion inhibitor (Tannic acid)

Different kinds of corrosion inhibitors were used in the preservation of iron artefacts to prevent rusting after treatment which was briefly discussed by Walker (1982). Among these tannic acid is widely used in the conservation of iron (Hamilton 1999). The use of tannic acid as a corrosion inhibitor was investigated by Knowles and White (1958) and later by Pelikan (1966) while unsuccessful treatment has also been reported (Stambolov 1970). Hamilton (1999) suggested that the success of treatment depends on the selection of the right tannic acid instead of non-effective ones. The recommended tannic acid solution should have a pH of 2.5-3.0 (such as Baker reagent tannic acid, $C_{76}H_{52}O_{46}$) that provides good, weather-resistant tannate films on the surface. He noted that tannin solutions react with iron or iron oxide to form ferrous tannate which then oxidises to a compact blue to black coloured ferric tannate.

142

The applicable concentration of solution depends directly on the penetration of the solution in corrosion products while optimal concentration, as revealed in previous studies (Logan 1989; Hamilton 1999), is between 2-10%. It is recommended that the less corroded iron artefacts (Appendix D. Table 4.3. Rigid group) be coated with several layers of a 5% (w/v) solution of acid tannic in a mixture of water and ethanol while the heavily corroded objects (Appendix D. Table 4.3. weak group) be coated with a 2-3% tannin solution. Lower concentration facilitates penetration of the solution in thick corrosion layers (Hamilton 1999). A dilution of the solution may lead to an increase of the pH. In this case phosphoric acid should be added to reduce the pH to a desired level (2.4) (Hamilton 1999). Although the small size of the objects allows impregnation in a vacuum, it is advisable that those with a weak structure (Appendix D. Table 4.3. weak group: subgroup a, b) be brushed on their surface with a low concentration of the solution (2-3%). At intervals between each coating the object should be dried completely.

6.4.1.2.4. Sealant (microcrystalline waxes)

Coating the iron objects with a layer of sealant after using a corrosion inhibitor will form a more protective barrier between the object itself and humidity and harmful gases in the environment. The characteristics of microcrystalline waxes, such as their high melting point beside their desirable hardness and their lesser permeability to water vapour compared to other sealants, make them a suitable choice in the conservation of iron artefacts (Rudniewski & Tworek 1963). Microcrystalline waxes also increase the structural strength   of artefacts with either a discontinuous or no metal core and can act as an excellent material in the consolidation of the objects (Hamilton 1999). For these reasons it is recommended, both for artefacts with rigid and weak structure, that they be impregnated with microcrystalline wax. Cosmoloid 80H, Gulf 75 Micro-wax and Witco180M are some of the types of microcrystalline waxes recommended in conservation literature. Choosing the type of wax depends on its availability and its applicability in the field of conservation. The process of coating as described by Hamilton (1999) is as follows:

The object is submerged in the molten wax and kept there until the effervescence of the gas bubbles has stopped. Then the wax is cooled to almost 90-107°C (which depends on the kind of wax used) and the object is taken out and excess wax is cleaned off with a rag. During submerging the temperature must be kept high, around the melting point of wax, to prevent the wax from solidifying on the surface. The temperature at which the object is removed is very important in determining the thickness of the final coating. A low temperature would result in a thick layer of wax forming on the surface, and in high temperature almost all liquid wax would run off. Achieving a desired thickness needs some experience when working with wax. Immersing the weak objects in molten wax must be done with great caution, and if the separation of any small part of the corrosion products from the surface is noticed, the process must be stopped and the object taken out of the molten wax.

6.4.1.3. Gap filling

The missing parts that were produced as a result of sampling or wearing and corrosion in the objects during their lifetime disrupted their integrity. It is possible to fill these lacunas with an appropriate amount of resin as prescribed by the ethics of collection conservation and restoration (See ICOM code of ethics for museums). Araldite XD725 was recommended by Scott (1991). The resin should be mixed with a sufficient amount of hardener and good quality artistic powder pigment to produce a colour close to the object's colour but not exactly the same. In this way the filled gap would be recognizable from the original parts on close inspection. Before filling the gap, the area must be coated with a reversible synthetic resin such as Paraloid B72 in toluene so that the filling material could be removed at a later stage. Two coats of 10% (w/v) solution were suggested by Scott (1991). Paraloid keeps its solubility in acetone and assists in the removal of the filled part by soaking it in acetone in further retreatment of the objects.

6.4.2. Passive method

The passive method basically means the preservation of archaeological objects from deterioration by controlling the environment without the use of any chemicals. As Cronyn suggested (1990), in the long term such techniques impose limitations on the study and display of objects and often do not prevent deterioration totally. Consequently, utilizing these techniques alone is mostly restricted to two cases. The first case consists of those objects with the limitation of undergoing chemical treatments such as SI1. The second case involves all the objects, before treatment, while they are kept in the storage area or in display cases. It should be noted that control of the environment in the storage area and in the display cases is crucial for both the objects that are only being preserved passively as well as those that have been treated chemically. The only difference between these two groups of objects is related to their different levels of sensitivity to corrosive factors in the environment.

Four main environmental factors in the deterioration of metal artefacts in museum and storage areas are:

1. Oxygen and relative humidity
2. Temperature
3. Air pollution
4. Particulates

Oxygen and relative humidity (RH) are the main factors that directly participate in corrosion reactions as discussed in chapter 5. Although reducing the RH and removing the oxygen in the ambient result in halting corrosion in metal artefacts, the latter is quite difficult to achieve with objects in storage and showcases. The only way to achieve an oxygen-free environment is to use sealed showcases or boxes with small outlets to replace the oxygen with an inert gas such as inert nitrogen (Cronyn 1990). In practice this technique is expensive and complex. On the contrary,

144

controlling the RH to form a dry ambient is quite simple and applicable even with simple and accessible methods.

In general high temperature accelerates chemical reactions such as the chemical reaction of sulphur dioxide (SO_2) on metal. Temperature also has an indirect role in the corrosion of metal artefacts by affecting the RH%. High temperature increases the capacity of air to retain more humidity while low temperature decreases this capacity. Therefore decreasing the temperature in an isolated space with a certain amount of humidity, by increasing the RH, may result in condensation of humidity on the metal surface. The appropriate temperature for maintaining metal artefacts is between minimum 15°C and maximum 25°C. (Cronyn 1990; Burke 2002; Purafil, Inc 2004.)

Air pollution in museums originates from harmful gaseous compounds formed by the combustion of fossil fuels in urban area and volatile gases that are emitted from materials that are used in a museum. Three main pollutant gases found everywhere in the atmosphere of the industrialized world are sulphur dioxide, nitrogen dioxide (NO_2) and ozone (O_3). These gases and their by-products such as sulphuric acid and nitric acid increase the rate of deterioration in metal objects. Sulphur dioxide by formation of sulphuric acid on the surface of metal objects acts as an electrolyte which increases the rate of corrosion. Ozone may increase the oxidation rate of iron or the sulphidation of copper. Nitrogen dioxide acts the same as sulphur dioxide in the deterioration of metals. NO_2 when reacting with moisture in the atmosphere forms nitric acid, a strong acid and oxidizing agent, which increases the rate of corrosion in metals by participating in electrochemical reactions. Among these gases, sulphur dioxide may also originate from wood, particularly oak, birch and beech. (Purafil, Inc 2004.)

Particulates consist of fine particles of soil (dust), soot, skin oil, perspiration, small organic fibres and other tiny materials that are absorbed from the environment by the surface of artefacts. These materials may contain harmful compounds for stability of metal artefacts such as chlorine, sulphur dioxide and nitrogen dioxide or simply may be hygroscopic and retain the moisture next to the metal surface. (Purafil, Inc 2004.)

Among these factors, RH and temperature as the main factors in the deterioration of metal artefacts were studied thoroughly in the storage area and one of the showcases in the Mapungubwe museum. Although the gaseous pollutants also have an important role in the deterioration of metals in museums and storage areas they could not be studied here; because the estimation of the level of gases in the museum atmosphere required scientific instruments that were not available. Recommended passive techniques in the preservation of the objects taking into account the stability level of the artefacts and the conditions of the Mapungubwe storage area as well as the only temporary showcase that was used in a short exhibition of iron and copper artefacts during this study. To have an idea about the environmental conditions of the storage area and showcase, which are used to keep the metal objects, their microclimate regarding RH and temperature was examined.

6.4.2.1.Conditions of Mapungubwe storage facility

The storage facility has an almost 3*7 m^2 area. This area is used to keep a mixed collection which mostly consists of bone, metal and ceramic objects. The metals mostly with dimension between 10 and 40cm have been placed in thick polyethylene foam in cardboard boxes. Some of the metal artefacts are kept in plastic bags inside the cardboard boxes. The boxes were put on wooden shelves (Fig.6.1). The storage area also has a wooden floor.

Figure 6.1. Mapungubwe museum storage area. The K2 and Mapungubwe metal assemblage are kept in this place.

Wood and wood-pulp products are not suitable materials for shelving and packaging metal artefacts because they release sulphur compounds and organic acid vapours such as acetic and formic acid (Logan 2007). These compounds can cause further corrosion in the metal artefacts especially in a small room with no ventilation such as the Mapungubwe museum storeroom. The best materials for shelving are the inert materials such as metal (Logan 2007). For preventing further corrosion, it is recommended that the present shelving system be replaced with metal (steel) which was not coated with oil-based or alkyd paints because they release volatile material for long periods (Logan 2007).

The storage area is quite tidy and clean and no dust is seen on the surfaces of shelving but is present inside the cardboard boxes. Dust presents a serious problem for the stability of the metal objects. Dust may contain harmful elements such as chlorine or hygroscopic materials that retain moisture close to the surface of artefacts. Therefore, in the case of using open shelving, it is better if metals are kept in well-sealed clear polyethylene boxes to prevent the penetration of dust. Metal drawers and cabinets with well-sealed doors are also appropriate storing systems which by producing a close system will protect metals from dust and pollutants in the storage area (Logan 2007). These

146

storage facilities are more expensive than the open shelving and the choice between them depends on the curator's decision and the museum budget.

The metal artefacts in the storeroom are not well-organized. This means objects with different levels of stability have been stored together by the same method and in the same environmental conditions. No silica gel for controlling the RH was used in the boxes although the material of the boxes (cardboard) and physical characteristics of them such as untight seams prevents the use of silica gel as a desiccant.   The atmosphere of storage is quite damp which makes it hard to stay there even for a short time. There was no ventilator or dehumidifier and except for the entrance door that connects this area to other storage spaces there is no other outside connection. No attempt was made to estimate the fluctuation of RH and temperature in the storage area before this study.

6.4.2.1.1. *Monitoring the (RH) and temperature in the storage facility*

A digital hygrometer was placed in the storage facility from May to December while the maximum and minimum amounts of RH and temperature registered weekly. The result is given in (Fig. 6.2) with the average amounts for each month. As the diagram shows, the highest RH percentage was registered in May and December with amounts of 75% and 73% respectively while the lowest amounts were between 54 and 56% in August. It shows a considerable RH fluctuation between dry months (July to September with the RH under 60%) and the damp months (December to May with the RH above 70%). On average the RH and its seasonal fluctuation in the storage area is in the range of 65%±10%. The monthly fluctuation in RH is 5% maximum which is negligible.
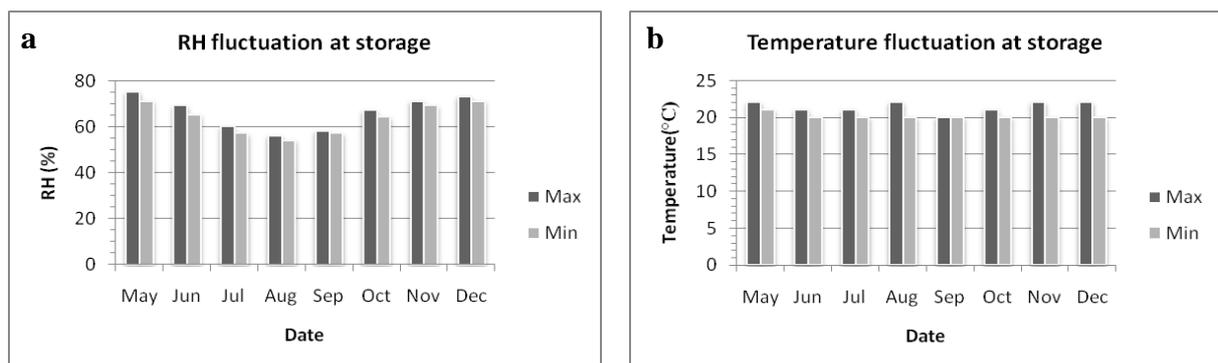
Figure 6.2. The plots show RH (a) and temperature (b) fluctuation at storage with consideration of maximum and minimum amount in each month during May to December.

Monitoring the temperature during this period indicated an inconsiderable fluctuation, in the range of 21°C ±1°C. This temperature is actually in the range of the maximum acceptable temperatures (19-25°C) in museum and storage areas for preventing deterioration in artefacts. In general monthly change of ±5°C in temperature is permissible. The temperature in storage can be kept lower than the

147

public area in the museum but the temperature difference between these two areas should not be too high to cause condensation on the metal surface during relocation of the objects. (Purafil, Inc 2004).

6.4.2.2.Characteristics of the metals' showcase in museum

The archaeological metals are not always on show. During an exhibition, the selected objects may be relocated to different display cases. The position of the portable showcases also may be changed from one gallery to another gallery in the museum during one exhibition of the metal objects. For the sake of this study the objects were kept in one showcase and in one place for 9 months. The showcase had a wooden frame with glass panels. The base of the case had been covered with a fabric. The showcase has no false base to make a space for using silica gel for controlling the RH. At present no silica gel is used to control the RH inside the showcase. Till now no examination was done to make it clear, that the materials inside the showcase are inert and safe for copper and iron objects or not.

As mentioned before wood may result in corrosion in metal artefacts and is not a suitable material to be close to the metal objects unless it has been tested for off-gassing (Burke 2004). It is recommended before the exhibition of metals in such showcases, that the materials inside are examined for off-gassing. One of the ordinary methods to show the presence of sulphur dioxide, nitrogen dioxide and hydrogen sulphide, and chlorine compounds is the Oddy-test. In this method, standard coupons of sensitive metals, usually copper, silver and lead, are placed with the material sample and specific volume of distilled water in a well sealed glass container (test tube). The container is kept in 60°C for 28 days to see the result of probable reactions between the metal coupons and volatile gases emitted from the sample (Oddy 1973, 1975; Green & Thickett 1995; Bamberger, Howe & Wheeler 1999).

Activated charcoal paper or cloth is one of the beneficial materials for controlling of the air pollution in showcases (Burke 2004). Charcoal absorbs organic vapors and pollutants that penetrate inside the showcase from the atmosphere of the museum. Because the charcoal can act as a cathode in a direct contact with the metal surface, it is recommended that the activated charcoal cloth be placed under the false baseboard or used to cover the back panel of the showcase without any contact with the metals. The activated charcoal cloth is black with a woven texture. To hide its color or to prevent its contact with metals, it may be covered with a linen or cotton fabric with the desired color.

A well-sealed showcase with a false baseboard with enough connection between two produced spaces is appropriate for exhibition of the metal artefacts. The showcases that are made of humidity impermeable materials such as glass and metal are preferable.   The false baseboard allows the use of silica gel or other RH and air pollution controlling devices such as activated charcoal in the showcase without being visible from outside.

148

6.4.2.2.1. *Monitoring of the (RH) and temperature in the display case*

A hair hygrometer, in addition to a thermometer, was placed in the display case where copper and iron artefacts are on display. The RH and temperature were monitored during May to January while the amount was registered daily, and twice a day in the morning and in the afternoon when temperature was almost at its maximum degree during the day. The result was recorded in (Fig. 6.3) with the average amount for each month.
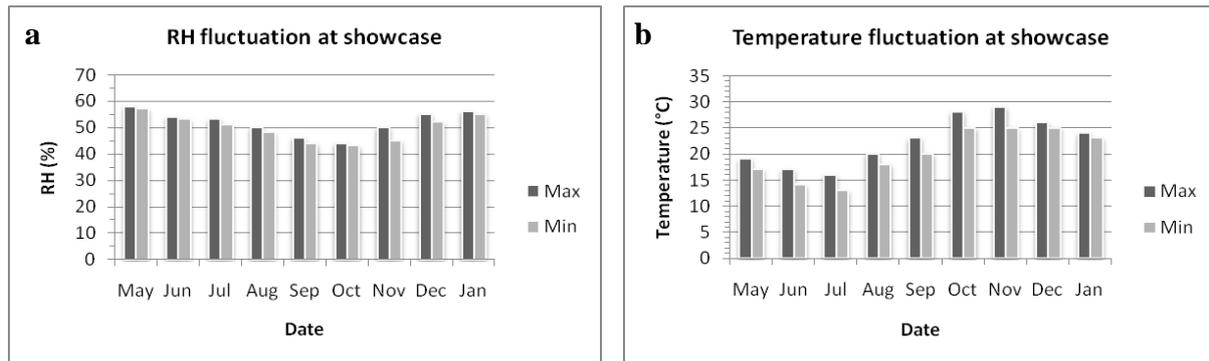
Figure 6.3 The plots show RH (a) and temperature (b) fluctuation at showcase with consideration of maximum and minimum amount in each month during May to January.

As the diagram shows, the highest (RH) was registered in May and January with amounts of 58% and 56% respectively while the lowest amount was 43% in October. The results show that the period between August and November, with RH lower than 50%, can be considered to be the driest months in the display case in its present position compared to the other months with the RH above 50%. On average the RH and its seasonal fluctuation in the museum showcase is in the range of 50%±8%. The daily RH fluctuation in the showcase is about 1% which is quite low to cause problems for the stability of the objects. Usually a daily fluctuation of more than 3% may cause problems for the stability of sensitive materials such as metal (Murdock & Johnson 2001). The RH has a gradual change between dry and wet months while the seasonal fluctuation is about 8%, which is in the range of 10% acceptable RH fluctuations (Murdock & Johnson 2001). At present the only buffering agents that keep the RH consistent in the display case are the coverage material on the baseboard of the showcase.

Contrary to the storage area the temperature in the display case is not constant. The minimum and maximum temperatures were registered in July with 12°C and in November with 29°C respectively. The average temperature and its seasonal fluctuation is 20°C ±9°C. The maximum registered temperature is around 5°C higher than the suggested maximum temperature for comfort of people and the minimum registered temperature is 7°C lower than the suggested minimum temperature. It is recommended that this temperature is kept as level as possible with the general standard temperature. Stabilizing the temperature within the acceptable range can also assist in controlling the RH in the

149

showcases. Comparing the two diagrams of the RH and temperature in the display case (Fig.6.3) indicates that with the rising of the temperature in August the RH fell. Falling the RH continued till October. This phenomenon is due to an increase in the capacity of the air in holding water vapour (SH) with a rise in the temperature (Cronyn 1990). From November onward, although the temperature compared to the cold months was quite high, the RH rose as a result of precipitation during the wet months (October to March) in Pretoria. Whereas, during the period May to July the precipitation was quite low in Pretoria, the RH in the display case was above 50% which was due to the low temperature during these months.

6.4.2.3. *Appropriate RH in preservation of the iron objects*

6.4.2.3.1. *Before treatment*

The study of chemical stability of the iron artefacts revealed that most of them, except for SI1, do not suffer of active corrosion under the effect of chlorine (Appendix D: Table 4.3). For these objects the RH below 40% was recommended to prevent raising the rate of corrosion in the remnant metal core in storage (Cronyn 1990). Meanwhile the RH below 40% may result in crumbling of the objects with a weak structure (Cronyn 1990) in subgroup b (Appendix D. Table 4.3). Considering the RH in the storage area (65%±10%) and usage of this area for keeping different materials together (bone, ceramic, sea shell, metal …) it is recommended that a separate microclimate be provided for the iron artefacts kept there. This can be achieved by utilizing polyethylene boxes and controlling their internal RH, passively with silica gel.

To achieve this, the objects should be taken out of the cardboard boxes. Cardboard boxes in which the objects are kept because of the high acid content of the paper they are made of (Sease 1994) and their property for easy humidity exchange with the environment does not make them suitable packaging material for the storage of metals. Afterwards the objects must be divided into two main groups, one with continuous and one with discontinuous metal core, as set out in Appendix D. Table: 4.3. Each group should be packaged separately since the latter needs more periodic inspection.

The small objects must be placed in a well-sealed clear polyethylene or polyolefin box while each one is put in a separate polyethylene bag. The polyethylene bags must be perforated to allow air-exchange between the interior atmosphere of the bag and the box. These small objects should be placed parallel to each other in such a way that they do not press to the adjacent objects. The larger artefacts such as MI2, MI7 and MI9 should have an individual support such as thick polyethylene foam to prevent any movement in the box during the relocation of the boxes. Their shape must be carved in the foam and the object then placed inside the mould. It is preferable that these large objects are put in a separate box to prevent damage to the small artefacts. At present the big objects have polyethylene supports. The hoes that are placed in polyethylene foam must be reversed from time to

time to prevent the formation of differential aeration cell and further corrosion of any of their surfaces which is in contact with the foam.

Sufficient amounts of conditioned silica gel in perforated plastic bags are then placed in a polyethylene box next to the iron objects without them touching. The rigid objects (Appendix D. Table 4.3) can bear a desiccated environment (RH<40%) while the weak artefacts should be kept at/or slightly above 40% RH. It is recommended to use Rhapid Gel which has a very large buffering capacity in the mid RH range between 40-55% while at least 4 kg/m^3 of gel is needed for an efficient effect in a permanent (1year) maintenance-free case (Weintraub 2002). This silica gel contains no lithium chloride and does not create any problems for the stability of the artefacts. It must be noted that Rhapid Gel is only available in sheet form, containing 750 grams of Rhapid Gel per m² (Weintraub 2002). The sheet can be easily cut with scissors to any shape and size. A humidity strip in each box will indicate the exact amount of RH in the box during storage.

Since there is no obvious temperature fluctuation in storage (Fig. 6.2b) it appears that the temperature may not have an effect on RH fluctuation in the polyethylene boxes. The rate at which the RH rises or falls after utilizing conditioned silica gel should be carefully monitoring in the boxes. To prevent a decrease of the RH below 40% or an increase above this level, especially in regard to weak objects in subgroup b (Appendix D. Table 4.3), silica gel should be conditioned. To prevent a lowering of the RH level it is recommended that sufficient water vapour be added to the silica gel, for example by putting a wet pad inside the box close to the silica gel and not in contact with the metals. To decrease the RH level a sufficient amount of dry gel should be added. The amount of required water or silica gel may be calculated on the basis of the kind of silica gel that is used (Weintraub 2002). After a while when the humidity strip indicates the silica gel is unable to lower the humidity inside the box it must be removed and replaced by dry gel while the used gel can be desiccated by heating in an oven at the recommended temperature by the manufacturer of the Gel. Among weak objects, SI1 should be kept in a desiccated condition in RH almost 20% as was recommended by Turgoose (1982*a*) to halt the corrosion in the artefacts which indicate active corrosion under the effect of chlorine. Corrosion in untreated archaeological iron artefacts, however, may even continue in RH less than 15% (Keene 1994*b*, Selwyn 2004). Therefore it is recommended to treat the objects with exhibition value before they disintegrate completely.

It is also recommended to utilize a domestic dehumidifier to reduce the amount of RH to around 40-50% in the storeroom which has a small area to form a more appropriate ambient to prevent further corrosion in the metals and disintegration of the other archaeological materials stored there specially under the effect of micro-organisms. Among different types of dehumidifiers, the compressor (refrigerant) type appears to be more suitable for the warm climate of the storage area which also does not have any vent (Purafil Inc, 2004).

151

6.4.2.3.2. After treatment

After treatment, the iron objects will have more chemical and physical stability. In the museum (Mapungubwe museum) the objects are exhibited in temporary display cases with considerable seasonal RH fluctuation. The average RH in the display case is about 50% which is higher than the required range of RH (40-45%) for keeping the stable iron objects safe after treatment. The RH in the display case has a fluctuation of almost 8% which occurs under the effect of seasonal temperatures and precipitation (Fig. 6.3). This could be prevented by putting a thin layer of conditioned silica gel under a perforated false bottom in an airtight display case. Rhapid Gel is recommended since it has a very large buffering capacity in the RH range 40-55% (Weintraub 2002). At least 2 kg/m^3 quantity of Rhapid Gel to buffer or control the RH within the temporary display case for 90 days was recommended by Weintraub (2002). The exact amount of gel which each display case needs varies and depends on different factors such as, dimensions of the showcase, the number of air exchange per day and the difference between the external RH and RH within the exhibit case (Weintraub 2002).

It would be advisable before switching the objects around in the new case to fill it with the appropriate amount of reconditioned gel. Only when the appropriate RH is achieved, the objects should be relocated to the new case. It is also advisable to retain the position of the metal artefacts' showcase constant during an exhibition. The RH in display cases must be carefully monitored with the use of a humidity strip while fluctuation must be prevented in the same way as described elsewhere in this thesis with regard to the preservation of the objects in storage before treatment (See section 6.4.2.2.1).

6.4.2.4. Appropriate RH in preservation of the cupreous objects

6.4.2.4.1. Unstable objects

All the copper artefacts with distinguished active bronze disease are included in this category (Appendix D. Table 4.3). Scott (1990) noted that RH less than 39% stifles the reaction of cuprous chloride and prevents further corrosion of the remaining metal core. It is therefore recommended that the copper artefacts with active bronze disease be removed from cardboard boxes and placed in airtight polyethylene boxes with sufficient silica gel to establish a microclimate with a lower RH than the surrounding environment (39%), following exactly the same procedure as prescribed with regard to the storage of iron objects. The objects with bronze disease should not be in close contact with the stable metal artefacts or even in one polyethylene box because their chlorine content may be transferred to the stable ones by the dust of corrosion.

6.4.2.4.2. Stable objects

The copper artefacts with noble patina and all the copper objects after treatment are included in this category. RH lower than 75% has been recommended by Cronyn (1990) to prevent further corrosion in stable copper artefacts whereas Scott (1990) maintained that RH between 42% and 46% provides adequate conditions in storage or exhibition areas. He further states that the humidity should not be allowed to rise to 55%. Consequently, it is advisable to keep the RH in display cases with copper artefacts between 42% and 46%. Since the RH in display cases has an almost 8% seasonal fluctuation, utilizing silica gel can keep it constant. The process of using the gel is similar to that suggested for iron.

6.4.2.5. General suggestions for an effective passive preservation

For an effective passive preservation of archaeological metal objects in the museum and the store room some general instructions are available which can enhance the passive preservation of the metal artefacts. These are as follows:

1. RH and temperature fluctuations should be monitored and the results registered every day. The results should be regularly estimated accurately. The appropriate hygrometer and thermometer are those that can register the maximum and minimum RH and temperature during a day and can be calibrated.

2. Because the museum is in an urban area, it is advisable not to leave doors and windows open for ventilation to avoid entry of the air pollutants and particulates (Burke 2002). Use of fans in storage area and in the museum can prevent a built-up of corrosive gases in one place and allow the formation of an even RH and temperature by maintaining airflow (Logan 2007).

3. The weak metal objects should be transport in a tray. It is also advisable that the metal artefacts not be handled with bare hands to prevent further damage through oil and sweat from the skin (Burke 2002).

4. The gloves that are used for handling of the metals should not have any chlorine or sulphur in their composition since these elements can cause oxidation in the metal objects. Before using cotton gloves, be sure that no PVC (polyvinyl chloride) was used in the form of nub in them. Some brands of synthetic rubber gloves also contain high proportions of sulphur and chlorine. (Burke 2002.)

5. The untreated metal objects should not be put directly in contact with the baseboard in the showcase. This condition may result in the formation of differential aeration cell and further corrosion on any of their surfaces which is in contact with the baseboard as can be seen in the case of MI9. These objects should be placed in exhibit mounts which have been padded to prevent scratching.

153

6.5. Conclusion

Iron artefacts in this study assemblage are mostly stable and do not show active corrosion under the effect of chlorine. The passive condition of the iron artefacts scientifically means that they are corroding with a constant low rate which does not result in their immediate disintegration. In this condition iron is slowly corroded especially in RH above 50%. Presence of a thick external corrosion layer which contains various salts in addition to the soil particles may increase the rate of corrosion by adsorbing water molecules within its highly porous structure. This phenomenon intensifies if hydrated salts exist in the corrosion layer. The copper artefacts in this assemblage mostly have been subjected to active corrosion under effect of chlorine and are not chemically stable. Same as the iron artefacts, high RH (>37%) and its fluctuation can increase the rate of deterioration in these cupreous artefacts. Preservation of these objects passively is difficult because a slight increase in RH in the environment may result in adsorption of water within the pores which can act as an electrolyte with the presence of soluble salts.

Most of the excavated metal artefacts in K2 and Mapungubwe lost their integrity due to their burial and storage environmental conditions. The small size and delicate structure of implements and jewellery which are mostly in the form of helical wounded strips of iron and copper is another reason that intensified the process of degradation in them. Because the numbers of objects that kept their complete shapes in the K2 and Mapungubwe assemblage are quite low, it appears interventive preservation is a more secure method in reducing the risk of their complete deterioration in the future.

Preservation of the objects non-passively by removal of the soluble harmful salts or stabilizing them by changes in their chemical composition increases the stability of the artefacts in front of probable RH fluctuation. Most of the objects with a well-kept shape have a weak physical structure which prevents using wet methods in their treatment. The cleaning, stabilizing and consolidating of these artefacts needs real caution and accuracy in following the relevant procedures of preservation to prevent physical disintegration. Wet methods of treatment with different chemicals should also be approached with utmost caution. The concentration of the chemicals and their duration, condition and procedure of the treatments should be considered carefully to prevent undesirable alterations in the objects. The identified corrosion stratification and position of the original surface on the iron and copper artefacts should be considered during cleaning of the objects to prevent over-cleaning. Precautions should be taken when working with chemicals such as strong alkaline solutions, BTA and molten waxes. Preferably all the chemical procedures should be done under a chemical fume hood to prevent inhalation of chemical gasses. During all procedures the wearing gloves or even goggles for safety by the conservator is recommended.

Current environmental conditions in the storage area and showcase in the museum are not suitable for passive preservation of the artefacts both before and after treatment. The artefacts also do not have an appropriate packaging and shelving in the storage area. Wood is seen almost everywhere in the

storage area. Because wood and wood-pulp material may emit volatile corrosive gases their use for shelving, covering of the floor, packaging of the artefacts or in the structure of showcase is not appropriate. Inert and moisture impermeable materials such as metal, polyethylene and glass should be utilized for shelving, packaging and display cases respectively. All the materials such as fabric that are going to be used in a showcase of metals should be tested for off-gassing. Till now no testing has been done for estimating the amount of air pollutants in the atmosphere of the museum and no facility has been used for adsorbing the probable corrosive gasses in showcases. Activated charcoal cloth or paper is an appropriate choice to reduce these gases that might originate from urban air pollution or by emitted gasses from material inside the showcase or museum environment.

At present except for a few humidity strips that are used in fixed showcases in one of the galleries no other hygrometers and thermometer are used for monitoring the RH and temperature fluctuation in the museum and in the storage area. Passive preservation of the metal artefacts in their present conditions and before treatment needs accurate inspection of the collection by monitoring the RH fluctuation in the storage area, the museum, the polyethylene boxes and the showcases that are used in the exhibition of metal artefacts. The RH fluctuation should be controlled passively in the polyethylene boxes and showcase by silica gel while it should be controlled actively by utilizing a dehumidifier in the storage area. The RH% and its fluctuation are not high to need active dehumidification of the environment in the museum. It appears the use of silica gel is enough to control the RH inside the showcase to be appropriate for exhibition of the stable metal artefacts.

It is advisable that the position of the showcase of the metal objects during an exhibition be kept constant and away from windows and stairways to prevent RH fluctuation and air pollution as far as possible.

Chapter 7

Conclusion

A study of several metal artefacts which belong to the K2 and Mapungubwe metal assemblage at the University of Pretoria was undertaken for the purpose of conservation. A technical study of the iron artefacts showed that some of them belong to a much later date after the heyday of K2 and Mapungubwe. These objects consist of iron hoes with ambiguous provenance (MI2 and MI7) and the one that was found in an anonymous rock shelter in the area (MI9). The evidence indicates that they were formed in a blasting furnace in a process such as puddling which was practiced in Europe during the late 18th to 19th centuries. MI7 and MI9 were fabricated in Britain while the incomplete manufacture of the MI2 shows it was fabricated in the area. Ni content (0.3-0.7 wt%) of two iron artefacts, in addition to their low corroded structure and their typology (KI5 and MI4), also revealed these were fabricated elsewhere by means of a different ore composition and to be recent items that were left at the sites. Except for two hoes (MI7 and MI9), the other objects were inhomogeneous in terms of carbon content and generally fabricated of hypoeutectoid steel with an exception in the case of block twisting wire (MI8) with 1.2 wt% carbon. The diversity in the carbon content of the objects was related to unintentionally decarburizing or carburizing during forging. The high lime content of the inclusions within the metallic phase of the three indigenous artefacts (KI1, MI6 and MI10) could have originated from ore, fuel ash, refractory ceramics and/or even flux. To find out the exact origin of the lime, the CaO content of the iron ores, refractory ceramics and fuel that were utilized in smelting in the region needs to be examined. It must be also examined how each one of these categories could have an effect on mass percentage of Ca in inclusions in a bloomery smelting process. The iron objects generally have a normalized structure and were rarely annealed. The sign of slight cold working was only seen in one of the indigenous artefacts.

Indigenous copper artefacts in this assemblage were pure and only in one case (MC4) was metallic impurity detected which originated from dispersed tiny inclusions containing Fe. The artefacts were mostly fabricated of secondary casting copper with hammering, hot or cold, followed by annealing. Only two of the artefacts were directly manufactured of smelted metal, a copper rod (MC4) and the unique bronze nail (MC8). In the copper rod the inclusions contain an admixture of iron oxide (magnetite) and cuprite. The iron oxide could have originated from the added flux (Miller & van der Merwe 1994) or the utilized copper deposit in the process of smelting (self-fluxing ore).

The only bronze artefact in this assemblage was a low tin bronze with 6 wt% tin in copper which is similar to those reported by Miller (2001). The source of tin in the production of the alloy could be the Rooiberg tin mines (Molofsky 2009) but considering that no study was done on the lead isotopic analysis of the copper deposits in Rooiberg valley it is impossible to conclude that the bronze was produced *in situ*. The metallurgical evidence indicated that the alloy was produced in a direct process of smelting or by remelting, along with some kind of refining process. Because little archaeological evidence is present about bronze production methods in southern Africa, it is hard to say which one of these techniques was used.

Although both the rods as raw material in the production of the bangles and the bangles themselves, with or without internal discontinuous voids, were sampled and studied to arrive at a precise idea about their exact method of fabrication, this was not achieved. In general, all the bangles were made of secondary cast copper. In cases where the cast round wire had the desired shape, the artisan formed a circular bangle by slight hammering. In this case (MC11) the dendritic structure was well-preserved. In the other cases the severely worked rods were annealed to a degree which has eliminated the deformation of the grains. In these bangles discontinuous central voids were detected which can hardly be produced by hammering alone. It appears some kind of drawing technique such as drawing a ribbon of copper through a hole was utilized in their production.

Estimating the physical stability of the iron artefacts by neutron tomography showed the indigenous artefacts are mostly weak in structure with more than 50% corrosion. Few artefacts are in a better condition with defects in the continuous metal core and thick corrosion layer on the surface. The corrosion percentage in these artefacts is not less than 30%. Only the modern artefacts had a robust metal core with a thin layer of corrosion on the surface. Copper artefacts are in a better condition and 83% of them have less than approximately 40% corrosion in their structure. On the basis of these results the artefacts were classified in two basic groups of rigid and weak as well as five subgroups. This classification assisted in submitting systematic procedures in the conservation of the artefacts.

The radiography results clearly revealed the complementary nature of X-ray and neutron radiography techniques. Whereas the metal core in the small spatula (SI1) could be seen best with X-rays, the larger objects required neutron imaging for proper evaluation as a result of the opacity of the heavy metal components to soft energy X-rays (100 kV and lower). Neutrons also allowed corrosion products to be seen more clearly. Both techniques therefore have a place in artefact studies but for large metal artefacts and details of highly corroded structures, neutrons hold a distinct advantage. For instance, neutron tomography of heavily corroded funnels with unclear function revealed the existence of folded strips inside them which indicate that these simple ordinary conical tubes were used to fabricate delicate wires by drawing a thin strip of iron or copper through them. This indicates that the Mapungubwe inhabitants during the Phase 4 settlement were familiar with the strip-drawing technique and its usage in the fabrication of wire. On the basis of existing metalwork evidence this was an innovation in wire making that could be the earliest practice of its kind in southern Africa.

The fundamentally different transmission properties of neutrons allow neutron radiography and tomography to be an excellent qualitative and quantitative diagnostic tool for artefact investigation. The results also conclusively showed the advantage of full 3-D neutron tomography above 2D radiography for more complicated geometry clarification by producing accurate three-dimensional images of objects, from which virtual cuts through any required plane can be visualized. The advantages of neutron tomography as gleaned from this study can be summarized as follows:

157

1. It is a reliable non-destructive analytical method that allows quantitative evaluation of material fractions due to the accurate area and volume assessment capabilities once the 3D virtual object has been compiled. Defects such as cracks and pores as well as traces of manufacture are easily recognized via neutron 3D tomograms whereas they are often missed in 2D radiographs.

2. A survey on a 3D reconstructed image or tomogram of the object clearly elucidates the exact position of the defect in 3D space.

3. In both low and high thickness metal artefacts, accurate neutron radiographs and tomograms can be achieved.

4. Different composition of corrosion products with their various attenuation coefficients is recognizable on the surface of the objects. In the case of copper where the corrosion layer usually has a lamellar structure this phenomenon is observable.

5. Quantitative estimation of the approximate amount of corrosion products, based on adjusting the contrast of the individual slices of the tomogram to separate the metal zone from corrosion products, is possible provided that the corrosion products contain hydrogen or that other high neutron attenuating elements are present.

The advantages listed above made it possible to retrace the fabrication methods used in heavily corroded and encrusted artefacts and to also generate vital information needed for proper conservation and maintenance planning.

The study of the corrosion structure on the surface of the representative samples from K2 and Mapungubwe by means of SEM-EDS, XRD and micro-Raman revealed the same corrosion stratification on their surface which was formed under ionic influence corrosion. The corrosion crust that was formed in a well-aerated burial environment and later by continuing corrosion in atmospheric conditions during storage, consists of an internal and external layer with an inhomogeneous composition. Iron(III)oxyhydroxides (goethite and lepidocrocite), along with iron oxides such as magnetite, maghemite and hematite, were detected on the surface while magnetite, maghemite and lepidocrocite were restricted to the internal layer. Composition of products on the surface of these artefacts which consists of iron(III) oxyhydroxides and iron oxides, revealed corrosion formation was mostly under the effect of diffusion of dissolved oxygen in water through pores and cracks towards the metal surface. The amount of chlorine at the corrosion/metal interface was mostly between 0-0.7 wt% which is quite low. Lack of anions such as chloride originates from the surrounding soil at the metal/corrosion interface of some of artefacts, indicated the cathodic zones were placed on the metal surface during burial. Sulphates were rarely detected on the objects and their compositions (Jarosite and $FeSO_4.4H_2O$) indicated that they formed after excavation due to a high concentration of sulphate

158

ions within the porous material of the corrosion layer. Metastability of lepidocrocite, in addition to its formation which is associated with a high quantity of Fe2+ ions in the area of formation (Cornell & Schwertmann, 2003), creates the possibility that the corrosion is still continuing in atmospheric conditions. It also revealed the apparent differences between the internal and the external layer in the bilayers corrosion on the surface of iron artefacts that are the presence of fossilized inclusions and quartz grains. Among these the quartz grains which can be easily recognized with low magnification are the best indicator for revealing the interface between the internal layer and the surface contaminants during cleaning of the objects. The study also revealed the capabilities of micro-Raman in identifying a combination of different iron corrosion products together.

The study of corrosion structure and composition on the surface of representative copper artefacts shows that the corrosion was mostly formed under the effect of ionic influence and only one of the samples had signs of microbial corrosion. However, this result in combination with the soil analyses point at probable climatic variations at a site. The objects mainly have uneven surface and suffer of bronze disease which indicate chlorine had an important role in accelerating the corrosion. In these objects corrosion consisted of three layers. The layer adjacent to the metal surface mostly consisted of of Cu and oxygen with a high amount of Cl, probably an admixture of nantokite and cuprite. A fragmentary layer of cuprite separated this layer from a lamellar external layer that consisted of Cu (I) and (II) compounds. The limit of the original surface was seen around this layer. The only bronze artefact in this assemblage falls in this category which also shows Liesegang phenomena. The objects with an even surface also consisted of three main layers, the internal layer, the middle layer and the external layer of which the latter is not a part of the object. The two interior layers mostly consisted of cuprite with this discrepancy that the middle layer had a considerable amount of soil elements. Quartz grains, in addition to variant compounds of copper and soil elements, are the main constituents of the external layer that also gave different colours to the surface of the artefact. Copper hydroxy carbonate in the form of malachite was only detected on one of the objects which also showed signs of microbial corrosion from some stage of its corrosion history. In this object chalcocite is seen among the compounds that are formed in a low reducing or high oxidizing condition. This variety of compounds on the surface refers to the different environments that the objects located to during its life from a damp humus-rich soil on the hill to a well-aerated sandy soil in the northern dump.

The study of chemical and physical properties of the soil samples from K2 showed the interment soil to be severely aggressive. The high corrosiveness of the soil is directly related to the pH and high amount of soluble salts, mostly chloride and sulphate, that can affect electrical conductivity (EC) and the rate of corrosion when enough humidity is present in the ambient. In general, the results revealed that the relevant archaeological metals had been buried in a well-aerated and high aggressive soil with low alkalinity for a lengthy period of time. Although a high amount of soluble salts such as chlorides sulphates, carbonates and phosphates were detected in the soil it was revealed that chlorides and hydroxyls were the main anions that participated in the electrochemical corrosion of metals. The

159

chemical properties of soil and corrosion products can modify under effect of atmospheric conditions after excavation. To find accurate results on effects of burial environment on corrosion, it is necessary, soil and corrosion on artefacts be studied during excavation. This naturally leads to close collaboration between the field archaeologist and archaeologists working with laboratory archaeology and conservation.

Monitoring the environment of the objects from May to January 2011 in the storage area showed that the RH is quite high while a considerable RH fluctuation ($\pm 10\%$) is present during the dry months (July to September) with the RH below 65%, and the damp months (December to May) with the RH above 65%, while inconsiderable fluctuation in temperature was registered during these months. In the display case, in its present position at the main entrance, the period between August and November, with RH lower than 50%, are considered to be the driest months, compared to the other months, with RH above 50%. The RH fluctuation in the showcase is around $\pm 8\%$. Here the fluctuation in temperature ($20°C \pm 9°C$) and amount of precipitation had a direct influence on the variation of RH%.

In view of the above information, appropriate methods in the preservation of the objects were submitted to keep the objects safe both before and after treatment. These methods consist of passive and non-passive techniques which were suggested on the bases of chemical and physical stability of the objects and the environmental conditions of the storage area and the museum showcase.

Passive preservation of the objects by controlling the environmental conditions has an important role in decreasing the rate of deterioration of the metal objects both before and after treatment. Undesirable ambient conditions may start the corrosion even after interventive treatment. The storage area and the only showcase that was used for the exhibition of copper and iron artefacts during this study do not have the appropriate conditions for passive preservation of the objects. The RH in the storage area is quite high ($65\% \pm 10\%$). Wood that was used for shelving and covering of the floor in this area can be the source of volatile corrosive gases. The cardboard boxes that were used for packaging the objects easily exchange humidity with the environment and their perforated structure also allows the easy penetration of particulates inside them. All these factors increase the rate of corrosion in the metals. The only showcase that was used for the metals exhibition in the museum also had a RH higher than the appropriate amount for the safe preservation of the copper and iron artefacts before and after treatment. The case has a wooden frame which, as mentioned before, is not an appropriate material for storing metal artefacts. Before this study no attempt was made to monitor and control the RH and temperature fluctuations in the storage area and in the museum, and except for a few humidity strips in some of the fixed showcases no other devices are present for monitoring the RH. The metal artefacts are kept in an ordinary showcase and are in direct contact with the baseboard. To passively preserve the objects from further corrosion before and after treatment in the storage area and in the display, the following suggestions should be considered:

160

1. *Daily monitoring of the RH and temperature fluctuations:* Monitoring of the RH% and temperature will give sufficient information about the environmental conditions of the storage area and the showcases. In this way the curator will be able to establish whether the environment is or is not suitable for the safekeeping of metal objects.

2. *Passive controlling the RH:* For passive controlling of the RH in the showcase and packaging box silica gel is the most appropriate material. Silica gel is an inert and non-toxic material which can easily adsorb and release the moisture to stabilize the RH in the microenvironment of the well-sealed showcases or polyethylene boxes.

3. *Using active RH controlling in storage area*: Because of the warm environment in the storeroom and the lack of a vent, the use of a refrigerant dehumidifier is recommended to lower the RH%.

4. *Use of inert materials for storage and exhibition of the metal artefacts*: It is recommended that inert materials such as polyethylene boxes, metal and ceramic tiles are used for packaging, shelving and covering of the floor respectively in the storage area. Glass and metal are suitable materials to be used in the construction of showcases for metal artefacts. All the materials intended for use in the showcase should be examined for off-gassing.

5. *Controlling the air pollution in interior environments as far as possible*: This goal can be hardly achieved without the presence of HVAC equipment in the Mapumgubwe museum but with some simple strategies the amount and harmful effects of air pollutants can be reduced. For example by keeping the doors and windows closed and by utilizing fans to create airflow, it will be possible to reduce the intrusion of exterior air pollutions and to prevent their high local concentration. Utilizing charcoal cloth for the absorption of corrosive gasses is also a helpful strategy to lower the risk of corrosion in showcases.

6. *Well-sealed showcases and boxes*: For an effective passive control of RH in showcases and packaging boxes, they should have a well-sealed structure to prevent easy air exchange between interior and exterior environments.

7. *Adjusting the temperature in the museum:* The temperature in the museum should be kept as level as possible with the suggested standard temperature at 19°C -25°C. This range of temperature not only is suitable for the comfort of the visitors but also is the best range that keeps deterioration of the artefacts as low as possible. Adjusting the temperature within this rang also prevents increasing the RH during the cold months.

8. *Safe handling of the artefacts*: Avoid handling metal artefacts with bare hands to prevent contaminating their surface with skin oil and sweat. The gloves with sulphur and chlorine content also should not be used for handling artefacts. All the objects, particularly those that have a weak structure, should be carried in a tray.

Three main reasons make an interventive preservation necessary for those copper and iron artefacts that have kept their physical shape. These reasons are the following:

161

1. The excavated iron artefacts from K2 and Mapungubwe disintegrated almost completely due to their delicate structure in addition to their burial and storage environmental conditions. Only a few iron tools have kept their physical forms. Most of these iron artefacts have a weak structure with a discontinuous metal core. Further corrosion in these artefacts can result in their complete disintegration.

2. The iron and copper objects mostly covered with a thick external corrosion layer. This layer not only disfigures the objects may also increase the rate of corrosion by adsorbing moisture within its porous structure.

3. Most of the copper artefacts subjected to bronze disease which makes them sensitive to high RH and its fluctuation.

In these artefacts, a non-passive preservation would support their durability in the presence of corrosive factors in the environment more than passive methods alone. It was recommended that the process of treatment of the objects be started by removing the external layer from the surface and to continue with the stabilization of the artefacts that have high chloride ions in their corrosion crust by immersing them in an alkaline solution. Wet treatment with chemicals is only applicable for those objects that have enough physical stability. It was recommended that the objects with a metal core be impregnated with an appropriate corrosion inhibitor after stabilization or surface cleaning followed by a coating with a protective layer (sealant).

Glossary

A$_1$ temperature: The eutectoid temperature of a steel (Samuels 1980).

A$_3$ temperature: The temperature at which proeutectoid ferrite begins to separate from austenite under conditions of slow cooling (Samuels 1980).

A$_{cm}$ temperature: The temperature at which proeutectoid cementite begins to separate from austenite under conditions of slow cooling (Samuels 1980).

Allotrimorph: A particle of a phase that has no regular external shape (Samuels 1980).

Annealing: The process of softening a metal hardened by cold working (e.g.hammering). The lowest temperature at which a metal will soften varies with the degree of cold working, greater the amounts of work tending to reduce it (Tylecote 1962).

Annealing twin: In FCC metals such as copper, a process of recrystallization (often of worked and annealed metals) in which a mirror plane in the crystal growth results in two parallel straight lines appearing across the grain when the metal is etched (Scott 1991).

Anode: Component of a system that is usually corroded. In an electrochemical reaction, the electrode at which oxidation occurs.

Austenite: A non-magnetic form of iron normally existing only at high temperature (above 720°C) (Tylecote 1962).

Bloomery iron: Iron that has been produced in a solid condition directly as a result of the reduction of iron ore. Pure iron melts at 1535°C, but bloomer iron usually has never been heated above about 1250°C (Tylecote 1962).

Bronze disease: It refers to the process of interaction of chloride-containing species within the bronze patina with moisture and air, often accompanied by corrosion of the copper alloy itself (Scott 1990).

Carburization: The process of increasing the carbon content of the surface layers of a metal (often wrought iron) by heating the metal below its melting point with carbonaceous matter such as wood charcoal (Scott 1991).

Casting: The operation of pouring metal into sand, plaster, or other molds and allowing it to solidify.

Cathode: In an electrochemical cell, the component on which reduction takes place. In many corrosion processes, the cathodic regions are protected during corrosion, while attack takes place at anodic regions (Scott 1991).

Cementite: A compound of iron with the formula Fe_3C. Very hard and brittle, forming one of the constituents of pearlite. It also appears as a separate constituent in the grain boundaries of wrought iron containing about 0.02% carbon, and in irons containing more than 0.89% carbon (Tylecote 1962).

Cold working: The plastic deformation of a metal at a temperature low enough to cause permanent strain hardening (Scott 1991). If the temperature of working is increased, a point is reached at which hardening no longer occurs, i.e. the **hot working** temperature is reached (Tylecote 1962). The dividing line between hot and cold working is different in various metals.

Decuprification: Selective dissolution of copper in the process of corrosion in bronze (Robbiola *et all.* 1998).

Differential aeration cell: A special type of concentration cell in which potential differences are established due to local differences in dissolved oxygen content (Hanifan 2010).

Dendrites: A fern- or leaf – like growth formed by a solid metal or constituent growing from the liquid (Tylecote 1962).

Electrical conductivity: The ability of a material to transmit an electrical current and is commonly expressed in units of milliSiemens per meter (mS/m) (Grisso *et al.*2009). **Electrical resistivity** is the reciprocal quantity and its SI unit is the ohm.metre (Ω.m).

Ellingham-Richardson Diagram: It is a plot of ΔG versus to temperature. Richardson added a nomographic scale for P_{O2} along the right-hand edge of the diagram (Mitchell 2004).

Eutectic: In binary alloys the composition with the lowest melting point. The eutectic is a fixed composition in binary alloys and is often a fine intermixture of two phases, typically α and β (Scott 1991).

Eutectoid: Decomposition from a solid phase into two finely dispersed solid phases creates a structure called a eutectoid. The eutectoid point is fixed in binary alloys and in morphology may resemble the eutectic (Scott 1991).

Fayalite: The most common component of ancient slags, often occurring as slag stringers in wrought iron. Fayalite is an iron silicate, $2FeO.SiO_2$ which melts at about 989 °C, crystallizes in the orthorhombic system, and usually takes the form of broken, elongated grey laths in silicate based slags (Scott 1991).

Ferrite: A magnetic form of iron, almost devoid of carbon but capable of containing various amounts of other elements such as phosphorus (Tylecote 1962).

Grain: In crystalline metals, the grain is an area or zone of crystal growth in a uniform and homogeneous form. Most metals consist of grains and the grain boundaries are the interface between a succession of grains in the solid mass of crystals (Scott 1991).

General corrosion: A form of attack that produced overall uniform wastage of the metal often associated with atmospheric corrosion and some high temperature oxidation or sulfidation attack (Craig 1989).

Hypereutectoid: Containing a greater amount (often of carbon steels) than that required to form a completely eutectoid structure. In steels this would require more than 0.8% carbon, the amount needed to create a completely pearlitic structure (Scott 1991).

Hypoeutectoid: Containing a lesser amount (often of carbon steels) than that required to form the eutectoid structure of 0.8% carbon (Scott 1991).

Liesegang phenomenon: A chemical reaction between a suspended compound in a gel and a reactant which is allowed to permeate through the gel. Under these conditions it is then possible for the reaction products to form a number of banded structures as a result of a rhythmic deposition of insoluble precipitate (Scott 1985)

Normalizing: The term is often used for ferrous alloys that have been heated above the upper critical temperature and then cooled in open air (Dosset & Boyer 2006).

Pearlite: It consists of a mixture of ferrite and cementite which is usually laminated (Tylecote 1962).

Phase: A homogeneous chemical composition and uniform material, describing one component in a metallic system (Scott 1991).

Pitting corrosion: a high localized attack of the metal creating pits of varying depth, width and number. Pitting may often lead to complete perforation of the metal with little or no general corrosion of the surface (Craig 1989).

Pseudomorphic: The replacement in the corrosion process of a material with another that mimics the form of the replaced product. Pseudomorphic replacement of organic materials is common on iron artefacts and can occur on copper alloys and silver-copper alloys as well (Scott 1991).

Slag: A glassy phase or mixture of phases usually to be found in ancient or historic wrought iron or steel. The slag is an important by-product of the smelting of metals. It may be incorporated in copper or iron alloys as a result of incomplete separation or incomplete melting during extraction, as in the bloomery process (Scott 1991).

Standard free energy of formation (ΔG): The free-energy change that occur when one mole of substance is formed from its elements in their stable state at 1 atm and at a specified temperature (usually 25°C) (Ebbing & Gammon 2007).

Widmanstätten structure: The structure occurring in steel which have been fairly rapidly cooled from high temperature (1000°C). Ejection of ferrite or cementite takes place along certain crystal planes forming a mesh-like arrangement (Tylecote 1962).

Bibliography

Adeloju, SB & Duan, YY. 1994. Influence of bicarbonate ions on stability of copper oxides and copper pitting corrosion. *British Corrosion Journal 29* (44): 315-320.

AIC. 1994. *Code of ethics and guidelines for practice*. http://aic.stanford.edu/pubs/ethic.html (Accessed 20March 2009).

Al Hajji, JN & Reda, MR. 1996. Role of solution chemistry on corrosion of copper in synthetic solutions: effect of bicarbonate on uniform or localised attack. *British Corrosion Journal* 31:125- 131.

Al-Zahrani, AA. 1999. *Chloride ion removal from archaeological iron and Ǝ-FeOOH.* PhD Thesis. University of Wales, Cardiff.

Angelucci, S, Fiorentino, P, Kosinkova, J & Marabelli, M. 1978. Pitting corrosion in copper and copper alloys: Comparative treatment tests. *Studies in Conservation* 23: 147-155.

Askey, A, Lyon, SB, Thompson, GE, Johnson, JB, Wood, GC, Cooke, M & Sage, P. 1993. The corrosion of iron and zinc by atmospheric hydrogen chloride. *Corrosion Science* 34: 233-247.

Axelson, E.1973. *Portuguese in South-East Africa 1488-1600.* Johannesburg: C. Struik LTD.

Babcock, CL. 1977. *Silicate glass technology methods.* New York: Wiley.

Bamberger, JA, Howe, EG & Wheeler, G. 1999. A variant Oddy test procedure for evaluating materials used in storage and display cases. *Studies in Conservation* 44 (2): 86 - 90.

Beach, DN. 1977. The Shona economy: branches of production, in *Roots of Rural Poverty*, editors R Palmer & N Parsons. London: Heinemann: 37–65.

Becker, J. 1979. Metallurgiese waarnemings, in *Die kulture van Greefswald* (Vol. II), editor JF Eloff. Pretoria: University van Pretoria.

Bell, IM, Clark, RJ & Gibbs, PJ. 1997. Raman spectroscopy library of natural and synthetic pigments (pre- 1850 AD). *Spectrochimica Acta Part A* 53: 2159-2179.

Beverskog, B., & Puigdomenech, I. 1996. Revised Pourbaix diagrams for iron at 25-300 ˚C. *Corrosion Science*, 38 (12): 2121-2135.

Blesa, MA, Morando, PJ& Regazzoni, AE. 1994. *'Iron oxides'* in *Chemical dissolution of Metal Oxides*. London: CRC Press: 269-308.

Blakelock, E, Martinón-Torres, M, Veldhuijzen, H, Young, T. 2009. Slag inclusions in iron objects and the quest for provenance: an experiment and a case study. *Journal of Archaeological Science* 36: 1745-1757.

Blackshaw, SM. 1982. An appraisal of cleaning methods for use on corroded iron antiquities, in *Conservation of iron*, editors RW Clarke & SM Blackshaw. London: Trustees of the National Maritime Museum: 16-20.

Bokris, JO, Conway, BE, Yeager, E & White, RE. 1981. *Comprehensive Treatise of Electrochemistry* (Vol. 4). New York: Plenum Press.

Bouchard, M & Smith, DC. 2002. Catalogue of 45 reference Raman spectra of minerals concerning research in art history or archaeology, especially on corroded metals and coloured glass. *Spectrochimica Acta Part A* 59: 2247-226.

Brandy, C. 1963. *Teoria del restauro*. Roma: s.n.

Brandy, C. & Basile, G. 2005. *Theory of restoration.* Roma: Istituto centrale per il restauro.

Brasunas, A, Berry, WE, Compton, K, Fontana, M G, Godard, HP, Greene, ND, Hackerman, N, Hamner, NE, Hochman, RF, LaQue, FL, Lifka, B, Logan, HL, McGeary, F, Moran, Jr, Parker, ME, Peabody, AW, Peacock, JH, Snavely, ES& Vernik, E. 1984. *Corrosion Basics, An introduction,* Houston,Texas: National association of corrosion engineers.

Burke, M. 2002. Curatorial care of metal objects, in *NPS Museum Handbook, part I, Museum collection.* [e-Book]. http://www.nps.gov/museum/publications/MHI/AppendI.pdf (accessed 19 September 2012).

Calabrese, JA. 2000. Metals, ideology and power: the manufacture and control of materialized ideology in the area of the Limpopo-Shashe confluence, c.AD 900 to 1300, in *African naissance: The Limpopo valley 1000 years ago*, editors M Leslie & T Magg. *Goodwin series* 8: 100-111.

Caple, C. 2000. *Conservation skills Judgement, Method and Decision Making*, London: Routledge.

Chakrabarti, DK. & Lahiri, N. 1996. *Copper and its alloys in ancient India*. New Delhi: Munshiram Manoharilal Publishers.

Chase, WT.1994. Chinese bronzes: casting, finishing, patination, and corrosion, in *Ancient and historic metals, Conservation and Scientific Research,* editors DA Scott, J Podany & BB Considine. Marina del Rey, Calif: Getty Conservation Institute: 85-118.

Chirikure, S, Hall, SL & Miller, D. 2007. One hundred years on: What do we know about tin and bronze production in southern Africa?, in Metals and mines: Studies in archaeometallurgy, editors S La Niece, D Hook & PT Craddock. London: Archetype Press: 112–118.

Chirikure, S, Heimann, RB, Killick, D. 2010. The technology of tin smelting in the Rooiberg Valley, Limpopo Province, South Africa, ca. 1650–1850 CE. *Journal of Archaeological Science* 37: 1656–1669.

Childs, ST& Killick, D. 1993. Indigenous African metallurgy: nature and culture. *Annual Review of Anthropology* 22: 317-37.

Cline, WW. 1937. *Mining and Metallurgy in Negro Africa*. Menasha: Banta

Cooke, SRB& Aschenbrenner, S. 1975. The Occurrence of Metallic Iron in Ancient Copper. *Journal of Field Archaeology* 2: 251-266.

Cornell, RM & Schwertmann, U. 2003. *The iron oxides: structure, properties, reactions, occurrences and uses*. Weinheim: John Wiley-VCH.

Craddock, PT, Freestone, IC, Willies, L, Paliwal, HV, Gurjar, LK & Hegde, KTM. 1998. Ancient industry of lead, silver & zinc in Rajasthan, in *Archaeometallurgy in India*, editor V Tripathi. Delhi: Sharada Publishing House: 108-133.

Craig, BD. 1989. *Handbook of corrosion DATA*. Ohio: ASM International.

Cronyn, JM. 1990. *The elements of archaeological conservation.* Great Britain: TJ Press.

David, N, Heimann, R, Killick, D& Wayman, M. 1989. Between bloomery and blast furnace: Mafa iron-smelting technology in North Cameroon. *African Archaeological Review* 7: 183–208.

Dawson, JB & Hinton, RW. 2003. Trace-element content and partitioning in calcite, dolomite and apatite in carbonatite , Phalaborwa, South Africa. *Mineralogical Magazine 67 (5): 921-930.*

de Beer, FC. 2005. Characteristics of the neutron/X-ray tomography system at the SANRAD facility in South Africa. *Nuclear Instruments and Methods in Physics Research A 542*: 1-8.

de Maret, P. 1980. Ceux qui jouent avec le feu: la place du forgeron en Afrique Centrale. *Africa* 50:263-79.

de Maret P. 1985. The smith's myth and the origin of leadership in Central Africa, in *African iron Working,* editor R Haaland& P Shinnie. Oslo: Norwegian Univ.Press: 73-87.

Deschler-Erb, E, Lehmann, EH, Pernet, L, Vontobel, P & Hartmann, S. 2004. The complementary use of neutrons and x-rays for the non-destructive investigation of archaeological objects from Swiss collections. *Archaeometry* 46 (4): 647-661.

De Vaal, JB. 1942. An ancient mine in the Transvaal. *African Studies* 1(2): 151-152.

Dossett, JL & Boyer, HE.2006. *Practical heat treating.* Ohio: ASM International.

Ebbing, D & Gammon, SD. 2007. *General Chemistry.* United States of America: Charles Hartford.

Edson, G (ed). 1997. *Museum Ethics.* London and New York: Routledge.

Eloff, JF. 1979. *Die kulture Van Greefswald* (Vol. Deel II). Pretoria: Universiteit VanPretoria.

El Warraky, A, El Shayeb, HA & Sherif, EM. 2004. Pitting corrosion of copper in chloride solution. *Anti-Corrosion Methods and Materials* 51 (1): 52-61.

Evans, UR. 1923. The electrochemical character of corrosion. *Journal Institute of metals* 30: 263-267.

Evers, TM & Van den Berg, RP. 1974. Ancient Mining in Southern Africa, with reference to a copper mine in the Harmony Block, north-eastern Transvaal. *Journal of the South African Institute of Mining and Metallurgy* 74: 217-226.

Fouché, L. 1933. *Unpublished inventory of Mapungubwe finds*. UP/AGLID/800. Mapungubwe Museum Archives. University of Pretoria.

Fouché, L. 1937. *Mapungubwe Ancient Bantu Civilization on the Limpopo, Reports on excavations at Mapungubwe (Northern Transvaal) from February 1933 to June 1935*. London: Cambridge University Press.

Freeman-Grenville, GSP. 1975. *The East African Coast: Selected documents from the first to the earlier nineteenth centuries.* London: Collings.

Friede, HM. 1980. Iron Age mining in the Transvaal. *Journal of the South African Institute of Mining and Metallurgy* 80: 156-165.

Froment, F, Tounie, A & Colomban, P. 2008. Raman identification of natural red to yellow pigments: ochre and iron-containing ores. *Journal of Raman Spectroscopy* 39: 560-568.

Frondel, C. 1950. Paratacamite and some related copper chlorides. *Mineralogical Magazine* 29: 34-45.

Frost, RL. 2003. Raman spectroscopy of selected copper minerals of significance in corrosion. *Spectrochimica Acta Part A* 59: 1195- 1204.

Gardner, GA. 1963. *Mapungubwe* (Vol. 2). Pretoria: J.L.van Schaik.

Geilmann, W. 1956. Verwitterung von Bronzen im Sandboden. *Angewandte Chemie* 68: 201- 12.

Gettens, RJ. 1961. Mineral alteration products of ancient metal objects. *Studies in Conservation* 6 (4): 125-126.

González, NG, de Viviés, P, Drews, MJ & Mardikian, P. 2003. Characterizing the chloride in the wrought iron rivets from the Hunley. In: NACE Northern Area Eastern Conference. Ottawa, Sept 15-17, Proceedings on CD. Ottawa: NACE.

Gordon, RB & Killick, DJ. 1993. Adaptation of technology to culture and environment: bloomery iron smelting in America and Africa. *Technology and Culture* 34: 243–270.

Gerwin, W & Baumhaver, R. 1999. Effect of soil parameters on the corrosion of archaeological metal finds. *Geoderma* 96: 63-80.

Graedel, TE, & Frankenthal, RP. 1990. Corrosion mechanisms for iron and low alloy steels exposed to the atmosphere. *Journal of the Electrochemical Society* 137: 2385-2394.

Grant, MR. 1990. A radiocarbon date on a tin artefact from Rooiberg. *South African Journal of science* 86: 83.

Green, LR & Thickett D. 1995. Testing materials for use in the storage and display of antiquites - a revised methodology. *Studies in Conservation* 40 (3): 145-152.

Grisso, RB, Alley, M, Wysor, WG, Holshouser, D & Wade, T. 2009. *Precision Farming Tools: Soil Electrical Conductivity*. http://pubs.ext.vt.edue/442/442-508/442-508.html (Accesses 25 April 2010).

Hall, SL. 1981. *Iron Age sequence and settlement in the Rooiberg, Thabazimbi area.* Unpublished MA dissertation. University of the Witwatersrand.

Hamilton, DL. 1999. *Methods of Conserving Archaeological Material.* http://nautarch.tamu.edu/class/ANTH605 (Accessed 4 May 2011).

Hamilton, DL. 2000. *Metal conservation: Preliminary steps*. http://nautarch.tamu. edu /fileo.htm (Accessed 11 July 2008).

Hanifan, R. 2010. *The engineering language: A consolidation of the words and their definitions.* New Jersey: Momentum Press.

Hanisch, EOM. 1974. Copper working in the Messina district. *Journal of the South African Institute of Mining and Metallurgy* 74: 250-253.

Hauptmann, A, Maddin, R & Prange, M. 2002. On the Structure and Composition of Copper and Tin Ingots Excavated from the Shipwreck of Uluburun. *Bulletin of the American Schools of Oriental Research* 328: 1-30.

Herbert, EW. 1984. *Red gold of Africa, copper in precolonial history and culture.* Madison: University of Wisconsin Press.

Herbert, EW. 1993. *Iron, Gender and Power: Rituals of Transformation in African Societies.* Bloomington: Indiana University Press.

Herbert, EW. 1996. Metals and power at Great Zimbabwe, in *Aspects of African Archaeology*, editors G Pwiti & R Soper. Harare:University of Zimbabwe Publications: 642–647.

Hjelm-Hansen, N , van Lanschot, J, Szalkay, CD, & Turgoose, S.1992. Electrochemical monitoring of archaeological iron artifacts during treatment. *3rd International Conference on Non-Destructive Testing, Microanalytical Methods and Environmental Evaluation for Study and Conservation of Works of Art.* Viterbo, Italy, October 4–9, Brescia, Italy: Italian Society for Nondestructive Testing: 361–373.

Hjelm-Hansen, N, Van lanschot, J, Szalkay, CD & Turgoose, S. 1993. Electrochemical assessment and monitoring of stabilisation of heavily corroded archaeological iron artifacts. *Corrosion Science* 35: 767-774.

Huffman, TN. 1972. *Iron Age Archaeological report. 22nd Expedition.* Tshibidzini. Bulawayo: Rhodesian School Exploration society.

Huffman, TN. 1986. Iron Age settlements patterns and the origins of class distinction in southern Africa, in *Advances in world archaeology*, editors F Wendorf & E Close. New York: Academic Press: 291-338.

Huffman, TN. 1996. Archaeological evidence for climatic change during the last 2000 years in southern Africa. *Quaternary International 33:* 55-60.

Huffman, TN. 2000. Mapungubwe and the Origins of the Zimbabwe Culture, in *African Naissance: The Limpopo Valley 1000 Years Ago*, editors M Leslie & T Magg. *Goodwin Series* 8:14-29.

Huffman, TN. 2007. *Handbook to the Iron Age: the archaeology of pre-colonial farming societies in southern Africa.* Pietermaritzburg: University of KwaZulu-Natal Press.

ICOM. 2006. *ICOM code of ethics for museums.* http://icom.museum/ethics.html (Accessed 20 March 2009).

Jambor, J, Dutrizac, J, Roberts, A, Grice, J & Szymanski, J. 1996. Clinoatacamite, a new polymorph of $Cu_2(OH)_3C1$, and its relation to paratacamite and "anarkite". *The Canadian Mineralogist* 34: 61-65.

Jokilehto, J. 1986. *A history of architectural conservation.* [e-Book]PhD thesis. The University of York. Available at: http://www.iccrom.org/pdf/ICCROM_05_HistoryofConservation00_en.pdf since February 2005 (Accessed 9 September 2011).

Kardjilov, N, Fiori, F, Giunta, G, Hilger, A, Rustichelli, F & Strobl, M. 2006. Neutron tomography for archaeological investigations. *Journal of Neutron Research 14* (1): 29-36.

Keene, S. 1994a. Objects as system: A new challenge for conservators, in *Restoration: Is it acceptable?*, editor A Oddy. British Museum occasional paper No.99. London: British Museum Press.

Keene, S. 1994b. Real-time survival rates for treatments of archaeological iron, in *Ancient & Historic Metals: Conservation and Scientific Research*, editors DA Scott, J Podany & B Considine. Marina del Rey: Getty Conservation Institute: 249–264.

Keller, P. 1969. Vorkommen, Entstehung und Phasenumwandlung von β-FeOOH in Rost. *Werkstoffe und Korrosion* 20: 102-108.

Killick, DJ. 1990. *Technology in its social setting: bloomery iron-working at Kasungu, Malawi, 1860-1940.* PhD thesis.Yale University.

Killick, D. 2009. Cairo to Cape: The Spread of Metallurgy Through Eastern and Southern Africa. *Journal of World Prehistory* 22: 399–414.

Knight, B. 1982. Why do some iron objects break up in store?, in *Conservation of iron,* editors RW Clarke & SM Blackshaw. London: Trustees of the National Maritime Museum: 50-51.

Knowles, E & White T. 1958. The Protection of Metals with Tannins. *Journal of Oil and Colour* 41: 10-23.

Krauskopf, KB. 1979. *Introduction to geochemistry.* London: McGraw-Hill.

Kvashnina, KO, Butorin, SM, Modin, A, Soroka, I, Marcellini, M & Nordgren, J. 2007. In situ X-ray absorption study of copper films in ground water solutions. *Chemical Physics Letters* 447: 54–57.

Little, B & Wagner, P. 1993. Microbiologically influenced corrosion in offshore oil and gass system.The New Orleans Section of the National Association of corrosion Engineers, *New Orleans offshore corrosion conference.* New Orlean, 1993. http://www.dtic.mil/cgi-bin/GetTRDoc?AD=ADA275195 (Accessed 10 May 2009).

Logan, J. 1989. Tannic Acid Treatment. *CCI Notes* 9.5. Ottowa: Canadian Conservation Institute. http://www.cci-icc.gc.ca/publications/notes/9-5_e.pdf (Accessed 8 May 2011).

Logan, J. 2007. Storage of metal. CCI Notes 9/2. Ottowa: Canadian Conservation Institute. http://www.cci-icc.gc.ca/publications/notes/9-2_e.pdf (Accessed 20 September 2012).

Lucey, VF. 1972. Developments leading to the present understanding of the mechanism of pitting corrosion of copper. *British Corrosion Journal* 7: 36-41.

MacLeod, ID. 1981. Bronze dissease: an electrochemical explanation. *ICCM Bulletin* 7 (1): 16-26.

Maggs, T. 1982. Mabhija: pre-colonial industrial development in the Tugela Basin. *Annals of the Natal Museum* 25(1): 123–41.

Mangou, H & Ioannou, PV. 2000. Studies of the Late Bronze Age Copper-based Ingots Found in Greece. *ABSA* 95: 207-17.

Mason, R. 1974. Background to the Transvaal Iron Age-new discoveries at Olifantspoort and Broederstroom. *Journal of the South African Institute of Mining and Metallurgy* 74: 211-216.

Mason, R. 1982. Prehistoric mining in South Africa and Iron Age copper mines in the Dwarsberg, Transvaal. *Journal of the South African Institute of Mining and Metallurgy* 82: 134-144.

Mathias, C. 1994. A conservation strategy for a seventeenth century archaeological site at Ferryland, Newfoundland. *Journal of the International Institute for Conservation- Canadian Group* 19: 14–23.

May, R. 1953. Some observations on the mechanism of pitting corrosion. *Journal of the Institute of Metals* 82: 65-74.

Mayne, JEO, & Turgoose, S.1975. Significance of the redox potential in the inhibition of the corrosion of iron by non-oxidising inhibitors in the pH range 5–13. *British Corrosion Journal* 10:44–46

McNeil, MB, Jones, JM & Little, BJ. 1991. Production of sulfide minerals by sulfate-reducing bacteria during microbiologically influenced corrosion of copper. *Corrosion* 47(9): 674-677.

McNeil, MB & Little, BJ. 1992. Corrosion mechanisms for copper and silver objects in near-surface environments. *Journal of the American Institute for Conservation* 31(3): 355-366.

McNeil, MB & Odom, AL. 1992. Prediction of sulfiding corrosion of alloys induced by consortia containing Sulfate Reducing Bacteria (SRB). *International Symposium on Microbiologically Influenced Corrosion (MIC) Testing.* Miami, FL: ASTM.

Meyer, A. 1998. *The archaeological sites of Greefswald*. Pretoria: University of Pretoria.

Miller, D. 1995. 2000 years of indigenous mining and metallurgy in southern Africa A review. *South African Journal of Geology* 98: 232- 238.

Miller, D. 1996. *The Tsodilo jewellery Metal work from northern Botswana*. Cape Town: University of Cape Town.

Miller, D. 2001. Metal assemblages from Greefswald areas K2, Mapungubwe Hill and Mapungubwe southern terrace. *South African Archaeological Bulletin* 56: 83-103.

Miller, D. 2002. Smelter and smith: metal fabrication technology in the southern African Early and Late Iron Age. *Journal of Archaeological Science* 29: 1083-1131.

Miller, D, Desai, N & Lee-Throp, J. 2000. Indigenous gold mining in southern Africa: a review, Southern African Archaeological Society, in *African naissance: The Limpopo valley 1000 years ago*, editors M Leslie & T Magg. *Goodwin Series* 8: 91-99.

Miller, D & van der Merwe, NJ. 1994. Early metal working in sub-Saharan Africa: A review of recent research. *Journal of African History* 35: 1-36.

Miller, H. 1851. *First impressions of England and its people.* Boston:Gould and Lincoln.

Mitchell, P. 2002. *The archaeology of southern Africa,* England: Cambridge University press.

Mitchell, BS. 2004. *An introduction to materials engineering and science for chemical and materials engineers.* Canada: Jhon wiley & sons.

Misawa, T. 1973. The thermodynamic consideration for Fe-$H_2$0 system at 25˚C. *Corrosion Science,* 13: 659-676.

Molofsky, LJ. 2009. *A novel approach to lead isotope provenance studies of tin and bronze.*Master of science thesis. The University of Arizona.

More, CE. 1974. Some observation on ancient mining at Phalaborwa. *Journal of the South African Institute of Mining and Metallurgy* 74: 227-232.

Murdock, C, Johnson, JS. 2001. Curatorial care of archaeological objects, in *NPS Museum Handbook, part I, Museum collection.* [e-Book]. http://www.nps.gov/museum/publications/MHI/AppendI.pdf (accessed 19 September 2012).

Myers, JR & Cohen, A. 1984. Conditions Contributing to Underground Copper Corrosion. *Journal American Water Works Associaition ?* :68-71.

Neumann, JR, Zhong, T & Chang, YA. 1984. The Cu-O (Copper-Oxygen) System. *Bulletin of Alloy Phase Diagrams* 5: 136-140.

Newbury, BD & Notis, MR. 2004. The history and evolution of wire drawing techniques. *JOM Journal of the Minerals, Metals and Materials Society* 56 (2):33-37

North, NA.1982. Corrosion products on marine iron. *Studies in Conservation* 27:75-83.

North, NA. 1987. Conservation of Metals, in Conservation of Marine Archaeological Objects, editor C Pearson. London: Butterworths: 207–252.

North, NA & Pearson, C. 1978. Washing methods for chloride removal from marine iron artifacts. *Studies in Conservation* 23:174–186

North, RF & Pryor, MJ. 1970. The influence of corrosion product structure on the corrosion rate of Cu-Ni alloys. *Corrosion Science* 10: 297-311.

Oddy, WA. 1973. An unsuspected danger in display. *Museums Journal* 73: 27-28.

Oddy, WA. 1975. The Corrosion of Metals on Display. In:*Conservation in Archaeology and the Applied Arts. Preprints of the Contributions to the Stockholm Congress*. 2-6 June 1975, London: The International Institute for Conservation of Historic and Artistic Works (IIC): 235-237.

Oddy, WA.1977. The production of gold wire in antiquity, hand-making methods before the introduction of the draw-plate. *Gold Bulletin* 10(3):79-87

Oddy, WA. 1984. Gold in the southern African Iron Age. *Gold Bulletin* 17: 70-78.

Oddy, WA. 2007. Gold foil, strip, and wire in the Iron Age of southern Africa, in *Ancient and historic metals*, *Conservation and Scientific Research,* editors DA Scott, J Podany & BB Considine. Marina del Rey, Calif: Getty Conservation Institute: 183-196.

Oddy, WA & Hughes, MJ. 1970. The Stabilization of Active Bronze and Iron Antiquities by the Use of Sodium Sesquicarbonate. *Studies in Conservation* 15: 183-189.

Organ, RM. 1963. Aspects of Bronze Patina and Its Treatment. *Studies in Conservation* 8 (1): 1-9.

Oswald, HR & Guenter, JR. 1971. Crystal data on paratacamite, $Cu_2(OH)_3C1$. *Journal of Applied Crystallography* 4: 530-531.

Palmer, JD. 1989. Environmental Characteristics Controlling the Soil Corrosion of Ferrous Piping, in *Effects of Soil Characteristics on Corrosion, ASTM STP 1013*, editors V Chaker & JD Palmer. Philadelphia: American Society for Testing and Materials: 5-17.

Pelikan, JB. 1966. Conservation of Iron with Tannin. *Studies in Conservation* 11(3): 109-115.

Pienaar, G. 1979. Metallurgiese waarnemings, in *Die kulture van Greefswald (Vol. II)*, editor JF Eloff. Pretoria: University van Pretoria.

Pikirayi, I. 1993. *The archaeological identity of the Mutapa State: Towards an historical archaeology of northern Zimbabwe*. Uppsala:Societas Archaeologica Upsaliensis.

Pikirayi, I. 2001. *The Zimbabwe culture: origins and decline of southern Zambezian*. Walnut Creek/ CA: Alta Mira Press.

Plenderleith, HJ & Werner, AE. 1971. *The Conservation of Antiquities and Works of Art*. Oxford: Oxford University Press. (Revised Edition ed.)

Pollard, AM, Thomas, RG & Williams, PA. 1990. Mineralogical Changes Arising from the Use of Aqueous Sodium Carbonate Solutions for the Treatment of Archaeological Copper Objects. *Studies in conservation* 35 (3): 148-152.

Pollard, AM, Thomas, RG & William, PA. 1992. The copper chloride system and corrosion: a complex interplay of kinetic and thermodynamic factors, in *Dialogue/89: The Conservation of Bronze Sculpture in the Outdoor Environment*, editor T Drayman-Weisser. Texas: National Association of Corrosion Engineers: 123-133.

Post, JE & Buchwald, VF. 1991. Crystal structure refinement of akaganeite. *American Mineralogist* 76: 272-277.

Potter, EC. 1956. *Electrochemistry: Principles and Applications*. London: Cleaver-Hume.

Pourbaix, M. 1974. *Atlas of electrochemical equilibria in aqueous solution*. Houston: National Association of Corrosion Engineers.

Pulak, C. 2000. The copper and tin ingots from the Late Bronze Age Shipwreck at Uluburun. *Der Anschhnitt: Zeitschrift für kunst und kulture im Bergbau* 13: 137-158.

Purfail, Inc. 2004. Environmental control for museums, libraries, and archival storage areas. *Technical Bulletin 600 A*.United states of America: s.n. http://www.airqualitycontrols.com/pdf/Environmental%20Control%20for%20Museums%20and%20Archives,%20TB-600.pdf (Accessed 20 September 2012).

Recknagel, R. 1908. On some mineral deposits in the Rooiberg district. *Transactions of the Geological Society of South Africa* 11: 83–106.

Refait, Ph, Drissi, SH, Pytkiewicz, J & Génin, JMR. 1997. The anionic species competition in iron aqueous corrosion: role of various green rust compounds. *Corrosion Science* 39 (9):1699-1710.

Refait, PH & Génin, JMR. 1997. The mechanisms of oxidation of ferrous hydroxychloride β-$Fe_2(OH)_3Cl$ in aqueous solution: the formation of akaganeite vs goethite. *Corrosion Science* 39 (3): 539–553.

Riegl, A. 1929. *Gesammelte Aufsätze*. Augsburg-Wien: s.n.

Robbiola, L. 1990. *Caractérisation de l'altération de bronzes archéologiques enfouis à partir d'un corpus d'objets de l'Age du Bronze: Mécanismes de corrosion*. Ph.D. dissertation, Université de Paris-6 Pierre et Marie Curie.

Robbiola, L, Blengino, JM & Fiaud, C. 1998. Morphology and mechanisms of formation of natural patinas on archaeological Cu-Sn alloys. *Corrosion Science* 40 (12): 2083-2111.

Romdohr, P. 1969. *The ore minerals and their intergrowths*. Toronto: Pergamon Press.

Rostoker, W & Dovorak, JR. 1977. *Interpretation of metallographic structures*. New York: Academic Press.

Rudniewski, P & Tworek, D. 1963. A Review of Present Methods of Conserving Metal Antiquities, in *Conservation of Metal Antiquities*, translator J Dlutek. Warsaw, Poland: The Scientific Publications Foreign Cooperation Center of the Central Institute for Scientific, Technical, and Economic Information: 197-213.

Samuels, LE. 1980. *Optical microscopy of carbon steels*. Metals Park, Ohio: American Society of Metals.

Schmidt, PR. 1997. *Iron Technology in East Africa, Symbolism, Science, and Archaeology*. Bloomington: Indiana University Press.

Schweizer, F. 1991. Bronze objects from lake sites: From Patina to Biography, in *Ancient and Historic Metals, Conservation and Scientific Research*, editors DA Scott, J Podany & BB Considine. Marina del Rey, Calif: Getty Conservation Institute: 33-50.

Schwellnus, CM. 1937. Short notes on the Phalaborwa smelting ovens. *South African Journal of Science* 33: 904-912.

Schwertmann, U & Cornell, RM. 1991. *Iron Oxides in the Laboratory*. New York: VCH Publishers.

Scott, DA. 1985. Periodic corrosion phenomena in bronze antiquities. *Studies in Conservation* 30 (2): 49-57.

Scott, DA. 1990. Bronze Disease: A review of some chemical problems and the role of Relative Humidity. *Journal of the American Institute for Conservation 29* (2): 193-206.

Scott, DA. 1991. *metallography and microstructure of ancient and historic metals*. Singapor: The Getty Conservation Institute.

Scott, DA. 2000. A review of copper chlorides and related salts in bronze corrosion and as painting pigments. *Studies in Conservation* 45 (1): 39-53.

Scott, DA. 2002. *Copper and bronze in art, corrosion, colorants, conservation*, Los Angeles: The Getty conservation institute.

Sease, C. 1994. *A conservation manual for the field archaeologist*. Los Angeles: Institute of Archaeology, University of California.

Selwyn, LS. 2004. Overview of archaeological iron: the corrosion problem, key factors affecting treatment, and gaps in current knowledge. *Proceedings of Metal 2004*. National Museum of Australia Canberra ACT, 2004.

Selwyn, LS & Argyropoulos, V. 2005. Removal of chloride and iron ions from archaeological wrought iron with sodium hydroxide and ethylenediamine solution. *Studies in Conservation* 50 (2):81-100.

Selwyn, LS, McKinnon, WR & Argyropoulos, V. 2001. Models for chloride ion diffusion in archaeological iron. *Studies in Conservation* 46: 109–120.

Selwyn, LS, Sirois, PJ & Argyropoulos, V. 1999. The corrosion of excavated archaeological iron with details on weeping and akaganeite, *Studies in conservation* 44 (4): 217-232.

Sharma, VC & Kharbade, BV. 1994. Sodium tripolyphosphate: A safe sequestering agent for the treatment of excavated copper objects. *Studies in conservation* 39 (1): 39-44.

Smith, JM. 2005. *Climatic change and agropastoral sustainability in the Shashe/Limpopo river basin from AD 900*. Ph.D. thesis. University of the Witwatersrand.

Stambolov, T. 1970. *The corrosion and conservation of metallic antiquities and works of art. A preliminary survey*. Amesterdam: Central Research Laboratory for Objects of Art and Science.

Stanley, GH. 1937. Mapungubwe metallurgical material, in *Mapungubwe Ancient Bantu Civilization on the Limpopo, Reports on excavations at Mapungubwe (Northern Transvaal) from February 1933 to June 1935,* editor L Fouché. London: Cambridge University Press.

Stech, T. 1989. Nuragic Metallurgy in Sardinia. Third Preliminary Report, in *Old world Archaemetallurgy*, editors A Hauptmann, E Pernicka & GA Wagner. Bochum, Germany: Selbstverlag des Deutschen Bergbau Museums: 39-44.

Steel, RH. 1974. Iron Age copper mine 47/73. *Journal of the South African Institute of Mining and Metallurgy* 74: 244-245.

Steel, RH. 1980. Iron Age mining and metallurgy in South Africa, in Settlement *in Botswana*, editors RK Hitchcock & MR Smith. Marshaltown: Heinemann: 94-97.

Swan, LM. 2007. *Mineral and manager.* Sweden: Uppsala University.

Schmidt, P. 1997. *Iron technology in east Africa.* United states: Indiana university press.

Takahashi, Y, Matsubara, E, Suzuki, S, Okamoto, Y, Komatsu, T, Konishi, H, Mizuki, J & Waseda, Y. 2005. In-situ X-ray Diffraction of Corrosion Products Formed on Iron Surfaces. *Materials Transactions*, 46: 637 to 642.

Taylor, R & Macleod, I. 1985. corrosion of bronze on shipwrecks: A comparison of corrosion rates deduced from shipwreck material and from electrochemical methods. *Corrosion (National Association of Corrosion Engineers)* 41: 100-104.

Tessman, G. 1913. *Die Pangwe. Vols. 1,2*. Berlin: Wasmuth.

Thomas, JGN & Tiller, AK. 1972. Formation and Breakdown of Surface Films on Copper in Sodium Hydrogen Carbonate and Sodium Chloride Solutions: I. Effects of anion concentrations. *British Corrosion Journal* 7: 256.

Thompson, M. 1942. *The total and free energies of formation of the oxides of tirty-two metal.* ?:The electrochwmical society.

Tiley, S. 2004. *Mapungubwe South Africa's Crown Jewels.* Cape Town: Sun Bird publishing in association with the University of Pretoria.

Timmins, S. (ed). 1866. *The resources products, and industrial history of Birmingham and the Midland Hardware District: A series of reports, collected by the local industries committee of the Biritish association at Birmingham in 1865*. London: Robert Hardwicke.

Tomashov, ND. 1966. *Theory of Corrosion and Protection of Metals.* New York: Macmillan.

Turgoose, S. 1982a. The nature of surviving iron objects, in *Conservation of iron: Maritime monographs and report 53*, editors RW Clarke & SM Blackshaw. London: National Maritime Museum: 1-7.

Turgoose, S. 1982b. Post-Excavation changes in iron Antiquities. *Studies in Conservation* 27(3): 97-101.

Turgoose, S. 1993. Structure, composition and deterioration of unearthed iron objects, in *Current Problems in the Conservation of Metal Antiquities*, editor A Shigeo. Tokyo: National Research Institute of Cultural Properties: 35-52.

Tylecote, RF. 1962. *Metallurgy in Archaeology, A prehistory of metallurgy in the British isles*. London: Edward Arnold LTD.

Tylecote, RF. 1976. *A History of Metallurgy*. London: Metals Society: 1-182.

Tylecote, RF. 1982. The late Bronze Age: copper and bronze metallurgy at Enkomi and Kition, in *Early metallurgy in Cyprus, 4000-5000 B.C.*, editors JD Muhly, R Maddin & V Karageorghis. Nicosia, Cyprus: Department of Antiquities: 81-104.

Upton, C. 1993. *A History of Birmingham.* ?: Phillimore & Co Ltd.

Van der Merwe, NJ. 1980. The advent of iron in Africa, in *The Coming of the Age of Iron*, editors TA Wertime & JD Muhly. New Haven: Yale University Press: 463-506

Van der Merwe NJ & Avery DH. 1987. Science and magic in African technology: traditional iron smelting in Malawi. *Africa* 57(2): 143-72

Van der Merwe, NJ & Killick, D. 1979. Square: An Iron Age smelting site near Phalaborwa, in *Iron Age Studies in Southern Africa*, editors N.J. van der Merwe & T.N. Huffman. South African Archaeological Society *Goodwin series* 3:86-93.

van der Merwe, NJ & Scully, RTK. 1971. The Phalaborwa story: archaeological and ethnographic investigation of a South African Iron Age group. *World Archaeology* 3: 179-202.

Verwoerd, WJ. 1956. Sekere produkte van primitiewe koper-, yster-, en bronssmeltery in Oos Transvaal met besonder verwysing na Phalaborwa. *Tegnilkon* 9: 91-104.

Vining. WJ. 2011. *General Chemistry II, Chem 112.* http://employees.oneonta.edu/viningwj/chem112/Chapter_19_Thermo_Full.pdf (Accessed 6 Agust 2012).

Vogel, JC. 1998. Radiocarbon dating of the Iron Age sites on Greefswald, in *The Archaeological sites of Greefswald stratigraphy and chronology of the sites and history of investigations*, editor A Meyer. Pretoria: University of Pretoria Press: *296-301*.

Voigt, EA. 1983. *Mapungubwe: an archaeozoological interpretation of an Iron Age community.* Pretoria: Transvaal Museum.

Walker, R. 1982. The Role of corrosion inhibitors in the conservation of iron, in *Conservation of iron*, editors RW Clarke & SM Blackshaw. London: Trustees of the National Maritime Museum: 58-65.

Watkinson, D. 1983. Degree of mineralization: its significance for the stability and treatment of excavated ironwork . *Studies in Conservation* 28: 85–90.

Weintraub, S. 2002. Demystifying Silica Gel, in *AIC Objects Speciality Group Postprints* 9. Washington, D.C.: American Institute for Conservation.

Weisser, TD. 1987. The Use of Sodium Carbonate as a Pre-Treatment for Difficult-to-Stabilize Bronzes, in *Recent Advances in the Conservation and Analysis of Artifacts*, editor J Black. London: Summers Schools Press:105-108.

Wihr, R. 1975. Electrolytic desalination of archaeological iron. *Conservation in archaelogy and the applied Arts*. Stockholm: IIC Congress:189-193.

Williams, CR. 1924. *Catalogue of Egyptian Antiquities : Gold and Silver jewelry and related objects*. New York: New York Historical Society.

Wilson, M. 1989. Historical aspects of mining in and around Venda. *Newsletter of the South African Development trust Corporation* 4(4): 6-7.

Wood, M. 2000. Making Connections: Relationships Between International Trade and Glass Beads from the Shashe-Limpopo Area. South African Archaeological Society Goodwin Series 8:78-90.

Wood, M. 2005. *Glass Beads and Pre-European Trade in the Shashe-Limpopo Region*. MA thesis. University of the Witwatersrand, Faculty of Humanities.

Yuzwa, GF & Eng, B. 1991. Corrosion by sulphate reducing bacteria . *Alberta public works, supply &services property management operations division water treatment co-ordinators' meeting # 14*. Edmonton, Alberta.

Appendix A

K2 and Mapungubwe metal artefacts records

May 2010

Table: KI1

Accession No. -		Acquisition source: Excavated (23/6/36)	
Site: K2	Square: B.2 S.1	Layer: 14'. 11'. 1'	Box No. Miller stuff
Metal type: Iron	Estimate value: exhibition, cultural		Current object use: storage

Physical description: An iron bar with square cross section. It tapers toward one end.

Measurement and dimensions

Weight: 11.5g	Width:	Inside diameter:
Length: 87.39mm	Height:	Thickness: 7.15- 4.47 mm

Condition and damage: Heavily corroded with soil and calcareous deposits. In its narrow point corrosion was exfoliated and has a deep crack which is observable with naked eye.

Facilities, report of location

Type of support, frame and package: It has been placed in a plastic bag in a carton box in the storage area.
Environment control: -

Photographic documentation

Details of the damaged parts

Table: KI2

Accession No. -			Acquisition source: Excavated (21/7/36)	
Site: K2	Square: B2.S15		Layer: 11'. 12'. 2'	Box No. Miller stuff
Metal type: Iron	Estimate value: exhibition, cultural			Current object use: storage

Physical description: An iron spatula. It is really delicate with an almost triangle blade and a narrow handle.

Measurement and dimensions

Weight: 4g	Width:	Inside diameter:
Length: 77.44 mm	Height:	Thickness: Blade 0.92- 2.45mm
		Handle: 3.29- 3.74 mm

Condition and damage: Heavily corroded with soil and calcareous deposits on the surface. It has a missing diagonal edge in the blade.

Facilities, report of location

Type of support, frame and package: It has been placed in a plastic bag in a carton box in the museum storage area.
Environment control: -

Photographic documentation

Details of the damaged parts

175

Table: KI3

Accession No. C/3938		Acquisition source: Excavated (1971)	
Site: K2	**Square:** -	**Layer:** -	**Box No.** C172a
Metal type: Iron	**Estimate value:** exhibition, cultural		**Current object use:** storage

Physical description: An iron instrument. It contains a shaft and a blade. Its blade has a rectangular shape that has a lower thickness in its edge. The shaft is tapered in its end with an almost square cross section.

Measurement and dimensions

Weight: 104.1 g	Width:	Inside diameter:
Length: 137.25 mm	Height:	Thickness: blade: ~1.87– 11.46 mm handle: 13.57- 4.09 mm

Condition and damage: Heavily corroded with soil and calcareous contamination. Corrosion layer exfoliated in some palaces especially in handle. This object is deteriorating with calcareous deposits and chip.

Facilities, report of location

Type of support, frame and package: It has been mounted in a dense polyethylene foam. The foam is in a cardboard box in the museum storage facility.
Environment control: -

**Photographic documentation**

Details of the damaged parts

176

Table: KI4

Accession No. –			Acquisition source Excavated (24/6/36)	
Site: K2	**Square:** B.2S.12	**Layer:** 6'. 7'. 1'		**Box No.** Miller stuff
Metal type: Iron	**Estimate value:** exhibition , cultural			**Current object use:** in storage

Physical description: Iron Adze with an almost triangle form. It has a broad blade which is tapered toward the edge. The shaft has a square cross section.

Measurement and dimensions

Weight: 80.1g	Width:	Diameter:
Length: 83.42 mm	Height:	Thickness: blade ~1.62- 7.54 mm

Condition and damage: Heavily corroded. In the shaft it has a lamellar structure with a missing part. On the surface the signs of accretion, calcareous deposits, flaking and material loss are observable.

Facilities, report of location

Type of support, frame and package: it was placed in plastic bag in carton at museum storage.
Environment control: -

Photographic documentation

Details of the damaged parts

177

Table: KI5

Accession No. C/3932		Acquisition source: Excavated	
Site: K2	Square: -	Layer: -	Box No. C171a
Metal type: Iron	Estimate value: exhibition , cultural		Current object use: in storage

Physical description: Iron chisel (drill). It has a long rectangular shaft and a cylindrical point which is tapered toward the end.

Measurement and dimensions

Weight: 43.4g	Width:	Diameter:
Length: 162 mm	Height:	Thickness: Rectangle part ~8.01* ~5.90mm Circular part: 7.15- 1.96 mm

Condition and damage: Moderately corroded. Corrosion layer in some parts were exfoliated.

Facilities, report of location

Type of support, frame and package: It has been mounted in a dense polyethylene foam. The foam is in a cardboard box in the museum storage facility.
Environment control: -

Photographic documentation

Details of the damaged parts

178

Table: KI6

Accession No. –		Acquisition source Excavation 5/9/1936	
Site: K2	Square: B.2 S.11	Layer: 10'.12'.4'	Box No. Miler stuff
Metal type: Iron	Estimate value: exhibition, cultural		Current object use: in storage

Physical description: Iron rod with a round cross section. It is tapered toward its curved end.

Measurement and dimensions		
Weight: 6.6 g	Width:	Diameter:
Length: 99.87 mm	Height:	Thickness: 4.84- 4.15mm

Condition and damage: Heavily corroded with a lamellar structure in its narrow point. It has soil and calcareous deposits on the surface.

Facilities, report of location

Type of support, frame and package: It has been placed in a small plastic bag in a large carton box in the museum storage area.
Environment control: -

Photographic documentation

Details of damaged parts

179

Table: KC1

Accession No. –		Acquisition source Excavated by Gardner	
Site: K2	**Square:** (S 26.27); Block 1, section 12 or Block 1, section 13	**Layer:** (1', 26', 3') or (6', 0', 3')	**Box No.** MRF
Metal type: Copper	**Estimate value:** exhibition, cultural		**Current object use:** in storage

Physical description: Copper bangle. It was manufactured by bending of a round rod.

Measurement and dimensions

Weight: 23.9g	Width:	Diameter: 69.84mm
Length:	Height:	Thickness: 4.02- 5.91mm

Condition and damage: Moderately corroded with light and dark green as well as brown corrosion on the surface. Soil and calcareous deposits are observable on the surface. It has a little distortion in the middle.

Facilities, report of location

Type of support, frame and package: It is kept in a small mail pocket in a plastic bag in the Mapungubwe research facility storage area within a cardboard box.
Environment control: -

Photographic documentation

Details of the damaged parts

180

Table: KC2

Accession No. –		Acquisition source: Excavated by Gardner	
Site: K2	Square: (S 26.27); Block 1, section 12 or Block 1, section 13	Layer: (1', 26', 3') or (6', 0', 3')	Box No. MRF
Metal type: Copper	Estimate value: Exhibition, cultural		Current object use: storage

Physical description: Copper rod.

Measurement and dimensions		
Weight: 14.5g	Width:	Inside diameter:
Length: 119.31mm	Height:	Thickness: 5.32- 4.06mm

Condition and damage: Heavily corroded with an uneven surface. Light powdery and dark green corrosions along with soil particles are observable on the surface. The rod was bent in the middle.

Facilities, report of location
Type of support, frame and package: it was kept in a mail pocket in plastic bag in MRF storage. Environment control: -

Photographic documentation

Details of the damaged parts

Table: KC3

Accession No. –		Acquisition source: Excavated (1976)	
Site: K2	Square: TS 4	Layer: 2	Box No. MRF
Metal type: Copper	Estimate value: Aesthetic, exhibition		Current object use: in storage

Physical description: Coiled wire in two symmetric round shapes.

Measurement and dimensions		
Weight: 7.8g	Width:	Diameter:
Length:	Height:	Thickness: 2.32mm

Condition and damage: Moderately corroded with brown and light powdery green corrosion. Soil deposits is observable in corrosion.

Facilities, report of location

Type of support, frame and package: It is kept in cotton wool in a small cardboard box in the MRF storage facility.
Environment control: -

Photographic documentation

Details of the damaged parts

Table: KC4

Accession No. –		Acquisition source Excavation 15/7/1936	
Site: K2	Square: B.2 S.8 -2nd strip	Layer: 7'.18'.2'	Box No. Miller stuff
Metal type: Copper	Estimate value: Research		Current object use: in storage

Physical description: A copper plate with a non-geometric shape and an uneven surface.

Measurement and dimensions		
Weight: 1.9 g	Width:	Diameter:
Length: 36.93 mm	Height:	Thickness: 1.47 mm

Condition and damage: Moderately corroded with light and dark green corrosion products. Soil contamination is observable on its surface.

Facilities, report of location

Type of support, frame and package: It is in a small plastic bag in a large cardboard box in the museum storage facility.
Environment control: -

Photographic documentation

183

Table: KC5

Accession No. –		Acquisition source: Excavation 23/6/1936	
Site: K2	**Square:** B.2 S.9	**Layer:** 11'.26'.1'	**Box No.** Miller stuff
Metal type: Copper	**Estimate value:** Research		**Current object use:** in storage

Physical description: It is a bent round wire. One of its ends was tapered and the another end was cut straight probably by sampling.

Measurement and dimensions

Weight: 12.2 g	**Width:**	**Inside diameter:** 65.31 mm
Length: 36.93 mm	**Height:**	**Thickness:** 4.49 mm

Condition and damage: Moderately corroded with a dark brown corrosion and soil contamination on its surface.

Facilities, report of location

Type of support, frame and package: It is placed in small plastic bag in large box in museum storage.

Environment control: -

Photographic documentation

Details of the damaged parts

Table: MI1

Accession No. C/711		Acquisition source: excavated	
Site: Map Hill	Square: -	Layer: -	Box No. C80
Metal type: Iron	Estimate value: exhibition, cultural		Current object use: in storage

Physical description: An iron arrowhead with a barbed triangular shape and a long shaft with a circular cross section.

Measurement and dimensions		
Weight: 8.6g	Width:	Diameter:
Length: 107.90mm	Height:	Thickness: Shaft: ~4.80 mm Blade: 2.77mm

Condition and damage: Heavily corroded with soil and calcareous deposits on the surface.

Facilities, report of location

Type of support, frame and package: It has been mounted in a dense polyethylene foam and kept in a cardboard box in the museum storage area.
Environment control: -

Photographic documentation

Details of damaged parts

185

Table: MI2

Accession No. C/2326		Acquisition source: 1939	
Site: Map Hill	**Square:** -	**Layer:** -	**Box No.** C109
Metal type: Iron	**Estimate value:** exhibition		**Current object use:** in storage

Physical description: An iron hoe with a square blade and a long shaft. The shaft is tapered toward its end and has a rectangular cross section. The blade does not have a narrow edge. The edges of the blade have broad flat surfaces. It seems it has an incomplete manufacture.

Measurement and dimensions		
Weight: 1435.5g	**Width:**	**diameter:**
Length: 380 mm	**Height:**	**Thickness:** Handle: 10.99-14.68 mm Blade: 16.93- 3.81mm

Condition and damage: Low corroded.

Facilities, report of location

Type of support, frame and package: It has been mounted in a dense polyethylene foam. The foam is in a cardboard box. It is kept in the museum storage facility.
Environment control: -

Photographic documentation

Details of the damaged parts

186

Table: MI3

Accession No. MAP/03/244		Acquisition source: Excavated	
Site: Map Hill (northern dump)	Square: -	Layer: -	Box No. MNP/044
Metal type: Iron	Estimate value: exhibition, cultural		Current object use: in storage

Physical description: A spoon like iron object. It has a circular cross section shaft.

Measurement and dimensions		
Weight: 8.3 g	Width:	Diameter:
Length: 81.58 mm	Height:	Thickness: handle: 4.76mm blade: 2.94 mm

Condition and damage: Heavily corroded. Its shaft was bent in the conjunction with the blade and the corrosion was exfoliated in this part. Soil and calcareous deposits are observable on the surface.

Facilities, report of location

Type of support, frame and package: It is kept in a sealed plastic bag in a cardboard box in the storage area.
Environment control: -

Photographic documentation

Details of the damaged parts

Accession No. MAP/03/424			**Acquisition source:** Excavated in northern Dump	
Site: MAP Hill	**Square:** -		**Layer:** -	**Box No.** MNP/044
Metal type: Iron	**Estimate value:** exhibition, cultural			**Current object use:** in storage
Physical description: An iron Hook. It made of a round wire which was bent to form a hook with a sharp point at one end. The other end of wire was bent to form a loop.				
Measurement and dimensions				
Weight: 4.6g	**Width:**		**Diameter:**	
Length: 58.91 mm	**Height:**		**Thickness:** 3.54 mm	
Condition and damage: Moderately corroded with flaking. Entrapped soil particles are observable in corrosion on the surface.				
Facilities, report of location **Type of support, frame and package:** It has been placed in a plastic bag in a cardboard box in the storage facility. **Environment control: -**				
Photographic documentation				
Details of the damaged parts				

Table: MI5

Accession No. –		Acquisition source: Excavated (1973)	
Site: MAP Hill	Square: MK1/ B3	Layer: L11	Box No. Miller stuff
Metal type: Iron	Estimate value: research, cultural		Current object use: in storage

Physical description: Two iron spatulas that were fused together and completely covered with soil deposits.

Measurement and dimensions		
Weight: 33.7 g	Width:	Inside diameter:
Length: 91.50 mm	Height:	Thickness:

Condition and damage: One of the adzes has a shaft missing and the other one has a missing part in the blade.

Facilities, report of location

Type of support, frame and package: It is kept in a plastic bag in a cardboard box in the museum storage area.
Environment control: -

Photographic documentation

Details of the damaged parts

189

Table: MI6

Accession No. –		Acquisition source Excavated by Gardner (1940)	
Site: Map Hill	**Square:** B.5 S.5	**Layer:** 9'.3'.11'	**Box No.** Miller Stuff
Metal type: Iron	**Estimate value:** exhibition, cultural		**Current object use:** storage

Physical description: An iron point (rod). It is gradually become narrower from one end to another.

Measurement and dimensions		
Weight: 9.6 g	**Width:**	**Diameter:**
Length: 130.28 mm	**Height:**	**Thickness:** 8.26- 4.12mm

Condition and damage: Heavily corroded with soil and calcareous deposits on the surface. Corrosion flaked in some parts.

Facilities, report of location

Type of support, frame and package: It is kept in a plastic bag in a cardboard box in the museum storage area.
Environment control:-

Photographic documentation

Details of the damaged parts

Table: MI7

Accession No. C/965		Acquisition source: 1935	
Site: Shashe-Limpopo (rock shelter)	Square: -	Layer: -	Box No. C80
Metal type: Iron	Estimate value: -		Current object use: in storage

Physical description: An iron hoe. Its handle becomes thicker in the conjunction with the blade. Its blade gradually becomes thinner towards the edge.

Measurement and dimensions		
Weight: 406.5 g	**Width:**	**Diameter:**
Length: 198.08 mm	**Height:**	**Thickness:** Handle:8.93-17.40 mm Blade: 10.55- 4.95 mm

Condition and damage: Low corroded. On the shaft it has a gap which was filled with plaster. The plaster has contaminated the surface.

Facilities, report of location

Type of support, frame and package: It has been mounted in a dense polyethylene foam. The foam has been placed in a cardboard box in the museum storage area.
Environment control: -

Photographic documentation

Details of the damaged parts

191

Table: MI8

Accession No. MAP/03/425		Acquisition source Excavated	
Site: MAP Hill	**Square:** -	**Layer:** -	**Box No.** MNP/044
Metal type: Iron	**Estimate value:** Cultural , research		**Current object use:** in storage

Physical description: A piece of block-twisted strip.

Measurement and dimensions		
Weight: 2 g	**Width:** 6.25 mm	**Diameter:**
Length: 36.15 mm	**Height:**	**Thickness:** 1.76 mm

Condition and damage: It has a corroded surface. Soil particles and calcareous deposits are observable on the surface. In one end it was broken.

Facilities, report of location

Type of support, frame and package: It is kept in a plastic bag in a cardboard box in the museum storage area.
Environment control: -

Photographic documentation

Details of the damaged parts

Accession No. C/960		Acquisition source: Excavated (1933)	
Site: Shashe-Limpopo Rock Shelter	**Square:** -	**Layer:** -	**Box No.** C81
Metal type: Iron	**Estimate value:** exhibition, cultural		**Current object use:** in exhibition

Physical description: An iron hoe with a scapula shape blade and a long shaft. The blade has a narrow edge. The shaft has a rectangular cross section which tapers toward the end.

Measurement and dimensions		
Weight: 850g	**Width:** Blade 11.73-2.26 mm Handle 14.80- 7.87 mm	**Diameter:**
Length: 310 mm	**Height:**	**Thickness:**

Condition and damage: Moderately corroded. One of the surfaces of the blade has dark brown corrosion products and on the other surface loose light orange corrosion products are observable. The latter surface was in a direct contact with the base board of the showcase.

Facilities, report of location

Type of support, frame and package: It is kept in a display box at Mapungubwe museum.
Environment control: -

Photographic documentation

Details of the damaged parts

Table: MI10

Accession No. C/490			Acquisition source: excavated (1933)	
Site: Map Hill	Square: JS4	Layer: -		Box No. C89
Metal type: Iron	Estimate value: exhibition cultural			Current object use: in storage

Physical description: An iron hoe with a short handle which is tapered towards the end. The blade thickness gradually decreases towards the edge.

Measurement and dimensions		
Weight: 192 g	Width:	Diameter:
Length: 154.42 mm	Height:	Thickness: Handle: 6.76 – 9.78 Blade: 7.03 - ~1.47 mm

Condition and damage: Heavily corroded. The iron hoe has two missing parts in the blade. Corrosion layers were exfoliated in some places.

Facilities, report of location

Type of support, frame and package: It has been mounted in a dense polyethylene foam. The foam has been placed in a cardboard box in the museum storage area.

Environment control: -

Photographic documentation

Details of the damaged parts

194

Table: SI1

Old Field /analysis ref No. 6) 02.01		Acquisition source: Excavated (1971)	
Site: MST	Excavation: K8	Layer: l(iii)	Box No. 214 (MRF)
Metal type: Iron	Estimate value: exhibition, cultural		Current object use: in storage

Physical description: A sweat scraper with a screw feature on the shaft. The shaft has a loop. The blade has a triangular shape.

Measurement and dimensions			
Weight: 7.1g	Width:	Inside diameter:	
Length: 69.48 mm	Height:	Thickness: Blade: 1.33mm Shaft: 5.29mm	

Condition and damage: Heavily corroded with calcareous and soil deposits in corrosion on the surface. Corrosion products in some places flaked and the loop of the shaft was cut off.

Facilities, report of location

Type of support, frame and package: It is in a small glass container with a plastic lid in the MRF storage facility.
Environment control: -

Photographic documentation

Details of the damaged parts

195

Table: SI2

Accession No. –		Acquisition source: Excavated (1971)	
Site: MST	Square: H5	Layer: 4 (i)	Box No. Miller stuff
Metal type: Iron	Estimate value: exhibition, cultural		Current object use: storage

Physical description: An iron adze with a rectangular shape blade which is tapered towards the shaft. The blade thickness decreases gradually towards the tip. The shaft has a rectangular cross-section. Two big areas were removed by previous researcher from the blade and the shaft.

Measurement and dimensions		
Weight: 127.1 g	Width:	Inside diameter:
Length: 115.92 mm	Height:	Thickness: Handle: 11.74 mm Blade: 5.17 mm

Condition and damage: Heavily corroded. The corrosion was exfoliated from the blade surface. A calcareous deposit is observable on the shaft. It has a $150*150$ mm^2 gap in the blade. A sample was also removed from the shaft but no evidence is present to show its dimensions.

Facilities, report of location

Type of support, frame and package: It is kept in a small plastic bag in a cardboard box in the museum storage area.

Environment control: -

Photographic documentation

Details of the damaged parts

196

Accession No. –		Acquisition source: Excavated (1971)	
Site: MST	Excavation: K8	Layer: L13 (B24)	Box No. Miller stuff
Metal type: Iron	Estimate value: exhibition, cultural	Current object use: in storage	

Physical description: A spatula. It has a triangle shape blade with a shaft with a round cross section. The shaft has a sphere.

Measurement and dimensions

Weight: 8.3g		Width:	Diameter: Sphere 8.98 mm
Length: 80.07 mm	Height:		Thickness: Blade 14.19-3.60 mm Handle: 5.18 mm

Condition and damage: Heavily corroded with soil and calcareous contaminants on the surface.

Facilities, report of location

Type of support, frame and package: It has been placed in a small plastic bag and in a cardboard box in the museum storage area.
Environment control: -

Photographic documentation

Details of the damaged parts

197

Table: MC1

Accession No. –		Acquisition source: Excavated by Gardner (1940)		
Site: MAP Hill	Square: B.5 S.5	Layer: 8'. 4'. 11'		Box No. Miller Stuff
Metal type: Copper	Estimate value: exhibition, cultural			Current object use: in storage

Physical description: A ring. It was made of a coiled wire with a circular cross section.

Measurement and dimensions		
Weight: 10.2 g	Width:	Inside diameter:
Length:	Height:	Thickness: 3.79 mm

Condition and damage: Heavily corroded with light powdery and dark green corrosion products on the surface.

Facilities, report of location

Type of support, frame and package: It is kept in a plastic bag in a cardboard box in the museum storage area.
Environment control: -

Photographic documentation

198

Table: MC2

Accession No. C/649			Acquisition source: Excavated by Gardner	
Site: Map Hill	Square: B.5 S.4		Layer: 45'. 15'. 5'	Box No. C89
Metal type: Copper	Estimate value: exhibition, cultural			Current object use: in storage

Physical description: A cooper bangle. It was made of a round wire with an open end.

Measurement and dimensions

Weight: 53.8 g	Width:	Inside diameter: 59.38 - 67.08 mm
Length:	Height:	Thickness: 5.94- 7.60 mm

Condition and damage: Heavily corroded with dark and light green corrosion products and white calcareous deposit on the surface. The bangle was deformed.

Facilities, report of location

Type of support, frame and package: It has been mounted in a dense polyethylene foam. The foam is in a cardboard box in the museum storage area.
Environment control: -

Photographic documentation

Details of the damaged parts

199

Table: MC3

Accession No. C/699		Acquisition source Excavated by Gardner (1940)	
Site: Map Hill	**Square:** B.5 S.4	**Layer:** 68'. 9'. 6'	**Box No.** C79
Metal type: Copper	**Estimate value:** exhibition, cultural		**Current object use:** in storage

Physical description: A copper ring. It was made of a strip of copper which bent to form a ring. The edges of the strip are not straight and have a light wavy feature. It has an open end.

Measurement and dimensions

Weight: 5.4 g	**Width:** 10.97 mm	**Inside diameter:** 10.39-12.32 mm
Length:	**Height:**	**Thickness:** 1.64 mm

Condition and damage: Moderately corroded with dark and light green corrosion products and calcareous contaminants on the surface.

Facilities, report of location

Type of support, frame and package: it has been mounted in a high dense polyethylene foam and covered with a polyethylene sheet in a cardboard box.
Environment control: -

Photographic documentation

Details of the damaged parts

200

Table: MC4

Accession No. C/3942		Acquisition source: excavated	
Site: Map Hill	Square: -	Layer: -	Box No. 172a
Metal type: Copper	Estimate value: exhibition, cultural		Current object use: storage

Physical description: A copper rod with a bent end. It has rectangular cross section and become narrower in the gouge end.

Measurement and dimensions			
Weight: 15.6 g	Width:		Diameter:
Length: 165mm	Height:		Thickness: 2.75- 5.6mm

Condition and damage: Heavily corroded with a light powdery green corrosion and soil contaminants on the surface. It has uneven surface.

Facilities, report of location

Type of support, frame and package: It has been mounted in a high dense polyethylene foam and covered with a sheet of polyethylene foam in a cardboard box.
Environment control: -

Photographic documentation

Details of the damaged parts

Table: MC5

Accession No. MAP/03/082		Acquisition source excavated	
Site: Map Hill	**Square:** Gardner west	**Layer:** -	**Box No.** MNP/019
Metal type: Copper	**Estimate value:** exhibition, cultural		**Current object use:** in storage

Physical description: A funnel shape copper object that was made by rolling a copper sheet. The seam was joined together without any welding or any other mechanical or heating method.

Measurement and dimensions			
Weight: 2.6g	**Width:**	**Diameter:** 7.94- 4.42 mm	
Length:	**Height:**	**Thickness:** 1.93mm	

Condition and damage: Heavily corroded. It has light and dark green corrosion products on the surface. The surface is uneven. A calcareous deposit is seen on some parts of the surface.

Facilities, report of location

Type of support, frame and package: It is in a sealed plastic bag in a cardboard box in the storage facility.
Environment control: -

Photographic documentation

Details of damaged parts

202

Table: MC6

Accession No. MAP/03/082		Acquisition source: excavated	
Site: Map Hill	Square: Gardner west	Layer: -	Box No. MNP/019
Metal type: Copper	Estimate value: exhibition Cultural		Current object use: storage

Physical description: A funnel shape copper object that was made by rolling of a copper sheet. The seam was joined together without any welding or any other mechanical or heating method.

Measurement and dimensions

Weight: 1.9g	Width:	Diameter: 6.49– 2.84mm
Length: 28.56mm	Height:	Wall thickness: 0.64mm

Condition and damage: Low corroded. It has a small bend close to the funnel's open seam and in peripheral of the wide part of the funnel.

Facilities, report of location

Type of support, frame, and package: It is in a sealed plastic bag in a cardboard box in the storage facility.
Environment control: -

Photographic documentation

Details of the damaged parts

Table: MC7

Accession No. MAP/03/248		Acquisition source: Excavated	
Site: MAP Hill	Square: Northern Dump	Layer: -	Box No. MNP/044
Metal type: Copper	Estimate value: exhibition, cultural		Current object use: in storage

Physical description: A funnel shape copper object. A copper sheet was rolled to form it.

Measurement and dimensions			
Weight: 3g	Width:	Diameter: 9.20- 5.15mm	
Length: 32.46mm	Height:	Wall thickness: 1.59 mm	

Condition and damage: Heavily corroded with fossilized fibers in light corrosion products on the surface. Corrosion layer in some places was cracked and flaked.

Facilities, report of location

Type of support, frame and package: It is kept in a small sealed plastic bag in a cardboard box in the storage facility.
Environment control: -

Photographic documentation

Details of the damaged parts

204

Accession No. MAP/03/226			Acquisition source Excavated (Northern Dump)	
Site: MAP Hill	Square: -	Layer: -		Box No. MNP/044
Metal type: Bronze	Estimate value: exhibition, cultural			Current object use: in storage

Physical description: A nail with a hemisphere head and a long shank with a round cross section. The nail shank is moderately become narrower towards the end.

Measurement and dimensions			
Weight: 3.9g	Width:	Diameter: 2.88mm- 5.04 mm head: 8.34	
Length: 52.52mm	Height:	Thickness: 1.59 mm	

Condition and damage: Heavily corroded with a small amount of light green corrosion products on the surface. Soil contaminants and longitudinal cracks are observable on the surface.

Facilities, report of location

Type of support, frame and package: It is kept in a small sealed plastic bag in the storage facility.
Environment control: -

Photographic documentation

Details of the damaged parts

Table:MC9

Accession No. -		Acquisition source: Excavated by Gardner (July 1935)	
Site: Map Hill (rock shelter)	**Square:** -	**Layer:** -	**Box No.** 223 (research facility)
Metal type: Copper	**Estimate value:** exhibition, cultural		**Current object use:** storage

Physical description: A copper ingot with a lentiform shape. On the mold surface, it has several voids. On the rough surface, it has a protrusion in the middle.

Measurement and dimensions

Weight: 132.2 g	**Width:**	**Diameter:** 54.50mm
Length:	**Height:**	**Thickness:** Centre 15.62 Edge: ~6.90

Condition and damage: Low corroded. Brown and light green corrosion products with soil contaminants are observable on its surfaces. It has several voids on the mold surface.

Facilities, report of location

Type of support, frame, and package: It is kept in a mail paper pocket in a cardboard box in Mapungubwe research facility (MRF) storage area.

Environment control:-

Photographic documentation

Details of the damaged parts

206

Table: MC10

Accession No. C/1040			Acquisition source: Excavated by Gardner (Oct.1937)		
Site: Map Hill	Square: B.1 S.4		Layer: 5'. 47'. 4'		Box No. C79
Metal type: copper	Estimate value: exhibition, cultural			Current object use: storage	

Physical description: A copper ring. It was made by bending of a round wire.

Measurement and dimensions

Weight: 7.7 g	Width:	Inside diameter: 19.17-24.72 mm
Length:	Height:	Thickness: 3.34-4.40mm

Condition and damage: Heavily corroded with dark and light green corrosion products on the surface. The surface is uneven. Calcareous deposits are also observable on the surface. The ring was deformed by pressure during its usage or burial.

Facilities, report of location

Type of support, frame, and package: It has been mounted in a dense polyethylene foam. The foam is in a cardboard box in the museum storage facility.
Environment control: -

Photographic documentation

Details of the damaged parts

Table: MC11

Accession No. C/680			Acquisition source Excavated by Gardner (1940)	
Site: Map Hill	Square: B.5 S.4		Layer: 25'. 7'. 4'	Box No. C79
Metal type: Copper	Estimate value: exhibition , Cultural			Current object use: in storage

Physical description: A copper bangle. It was made by bending of a round wire and has an open end.

Measurement and dimensions			
Weight: 24.4 g	Width:	Inside diameter: 55.37-56.37 mm	
Length:	Height:	Thickness: 3.90-4.68mm	

Condition and damage: Moderately corroded with a dark green patina. In some parts, light green corrosion is observable on the surface. Corrosion products in some places were exfoliated. The object has a little distortion.

Facilities, report of location
Type of support, frame, and package: It has been mounted in a dense polyethylene foam. The foam is in a cardboard box in the museum storage area.
Environment control:

Photographic documentation

Details of the damaged parts

Table: MC12

Accession No. C/641		Acquisition source Excavation by Gardner	
Site: Map Hill	**Square:** B.5 S.4	**Layer:** 64'. 14'. 8'	**Box No.** C89
Metal type: Copper	**Estimate value:** exhibition, cultural		**Current object use:** storage

Physical description: A copper bangle. It was made by bending of a round wire and has an open end.

Measurement and dimensions			
Weight: 55 g	**Width:**	**Inside diameter:** 62.53-62.65mm	
Length:	**Height:**	**Thickness:** 6.98 mm	

Condition and damage: Moderately corroded with dark and light green corrosion products on the surface. Soil and calcareous contaminants are also observable. Corrosion was abraded from the surface in one place and along the bangle length. It has a distortion almost in the middle.

Facilities, report of location

Type of support, frame, and package: It has been mounted in a dense polyethylene foam in a cardboard box in the museum storage area.
Environment control: -

Photographic documentation

Details of the damaged parts

209

Table: SC1

Accession No. –		Acquisition source Excavated (1971)	
Site: MST	**Square:** K8	**Layer:** L14	**Box No.** Miller stuff
Metal type: Copper	**Estimate value:** Research	**Current object use:** in storage	

Physical description: A copper ring. A copper helix of several strip twisting wires was coiled to form this ring.

Measurement and dimensions

Weight: 4.5g	Width:	Diameter: 20.12- 21.87 mm
Length:	Height:	Thickness:

Condition and damage: Heavily corroded. It has dark and light green corrosion products with soil particles on the surface. This object is brittle.

Facilities, report of location

Type of support, frame, and package: It is kept in a small plastic bag in a cardboard box in the museum storage area.
Environment control: -

Photographic documentation

Details of the damaged parts

Table: SC2

Accession No. MAP/03/026			Acquisition source Excavated	
Site: MST	Square: JS2(b)		Layer: -	Box No. MNP/001
Metal type: copper	Estimate value: Exhibition, cultural			Current object use: in storage

Physical description: A copper ring with an open end. It was made of a piece of strip which has a rectangular cross section.

Measurement and dimensions		
Weight: 24.4 g	Width: 3.65-3.82 mm	Inside diameter: 13.79 mm
Length:	Height:	Thickness: 1.82 mm

Condition and damage: Moderately corroded with light green and brown corrosion products. In some places the cuprite layer was mechanically removed from the surface as the result of over cleaning.

Facilities report of location

Type of support, frame, and package: It is kept in a small plastic bag in a cardboard box in the storage facility.
Environment control: -

Photographic documentation

Details of the damaged parts

211

Appendix B

Metallographic images of iron and copper samples
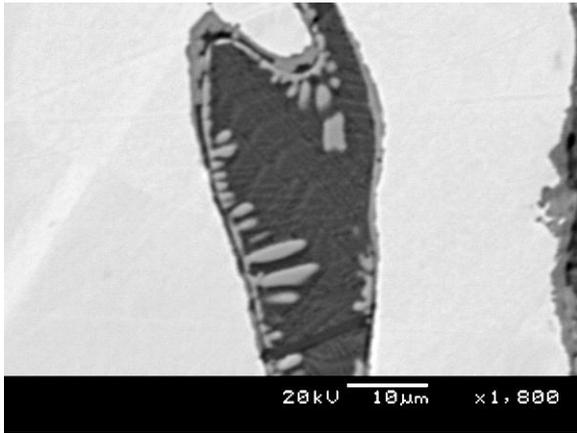
Figure 1. Polished section of iron rod (KI1) showing bloomery two-phase inclusion (KI1a) of wüstite dendrites in dark slag. (SEM-BSE)
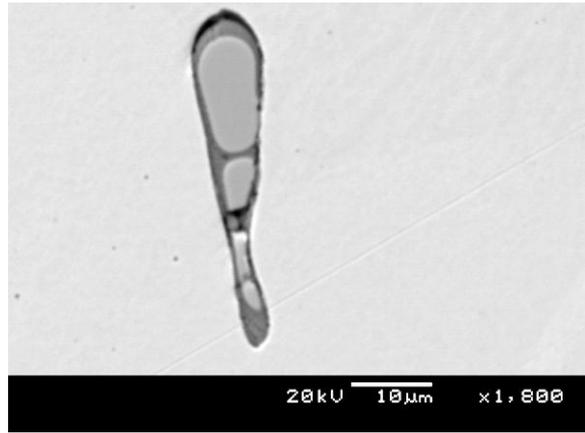
Figure 2. Polished section of iron rod (KI1) showing bloomery two-phase inclusion (KI1b) with dark-grey slag surrounding light gray wüstite globules. (SEM-BSE)
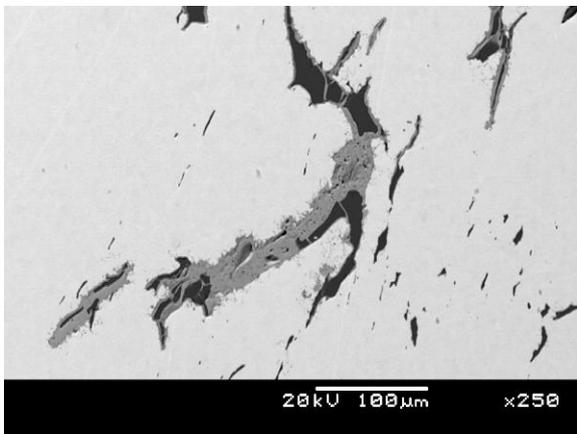
Figure 3. Polished section of iron rod (KI1) showing slag inclusion (KI1c) of light iron oxide in accompany with dark glassy phase. (SEM-BSE)
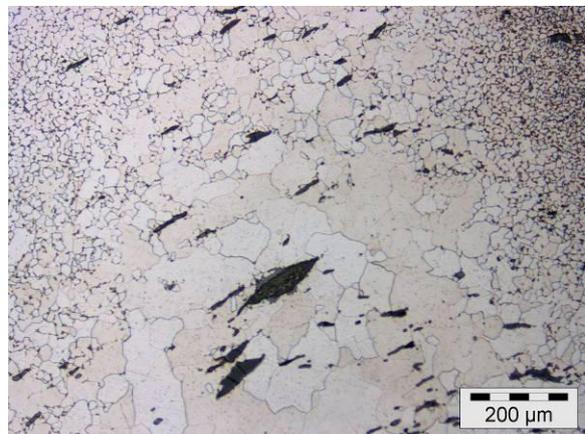
Figure 4. Etched section of iron rod (KI1) showing critical growth of ferrite grains within the metal core and close to the metal surface.
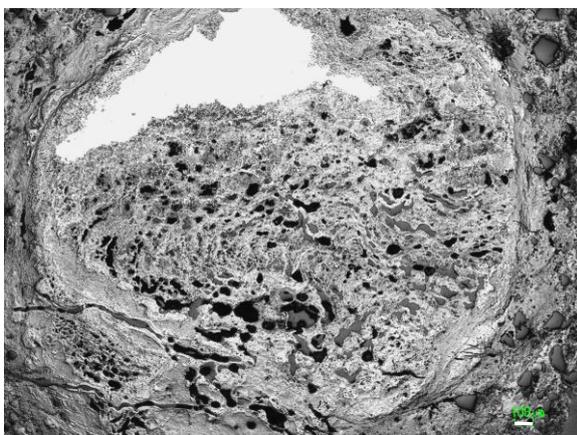
Figure 5. Overall micrograph of the rod (MI6) showing small metal remainder within corrosion products which have kept the physical shape of the metal. (Scale: 100μm)
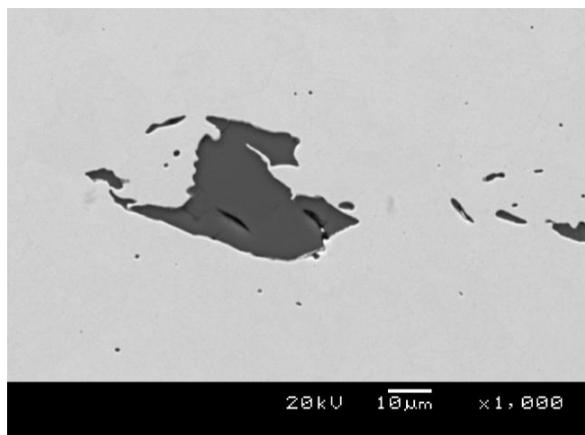
Figure 6. Glassy inclusions within reminder of metal phase in MI6. (SEM-BSE)

212
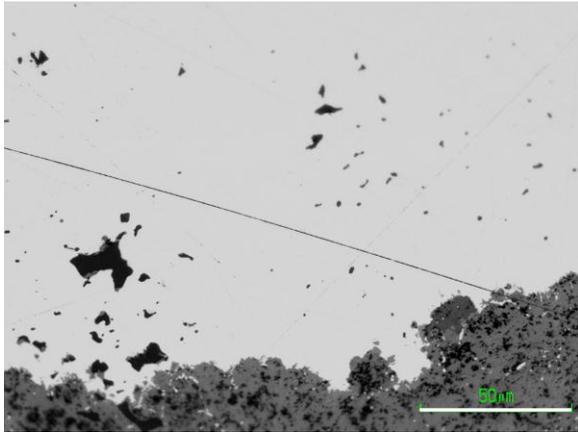
Figure 7. Micrograph of a small inclusion with lime content in peripheral of void within metallic phase in MI6. (Scale: 50μm)
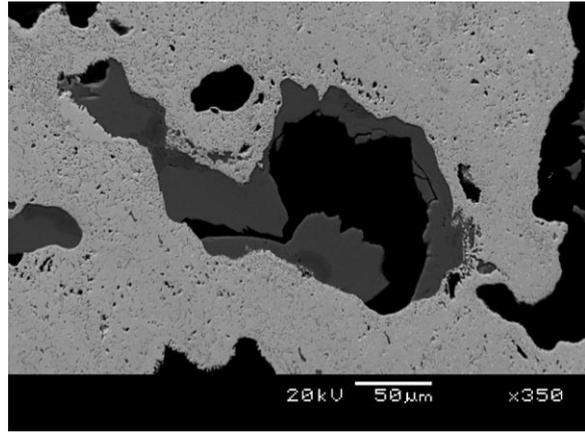
Figure 8. The inclusion with lime content in peripheral of a void within corrosion products in (MI6). (SEM-BSE)
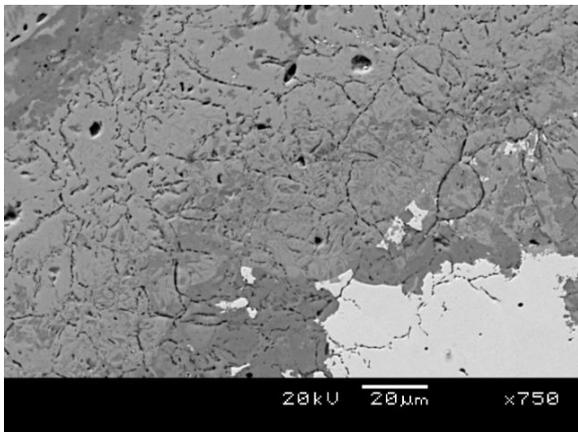
Figure 9. Polished transverse section of (MI6) shows fine cracks within the metal matrix and its fossilized structure within corrosion products. (SEM-BSE)
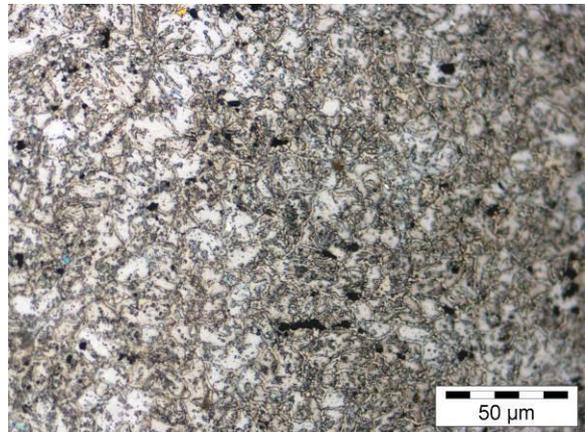
Figure 10. The etched micrograph of MI6 showing former austenite grains with grain boundaries of cementite.
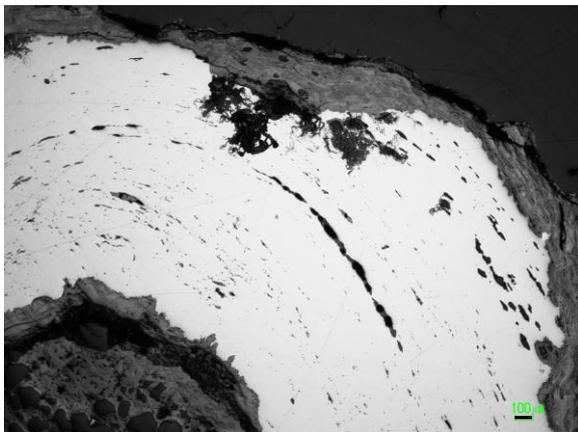
Figure 11. Polished cross section of SI1 showing elongated stringers of slag passing along the length of the heavily worked surfaces. (Scale: 100μm)
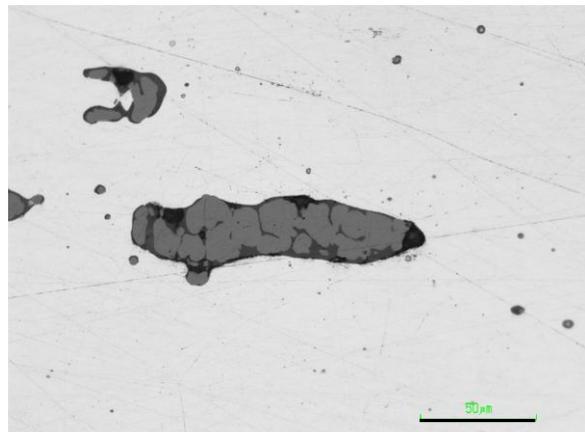
Figure 12. Micrograph of transversely section of (SI1) showing dendrite of wüstite in a matrix of slag. (Scale: 50μm)

213
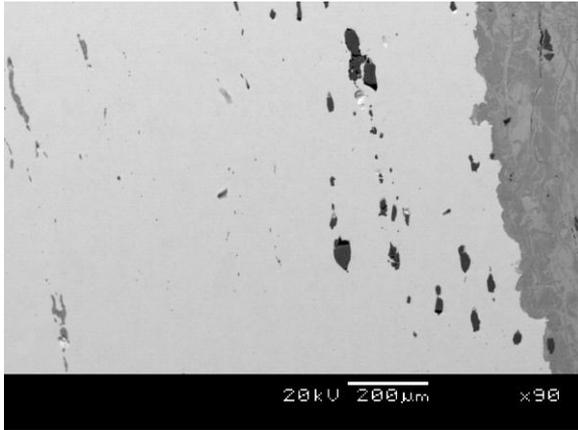
Figure 13. Polished transverse section of SI1 showing elongated dark glassy slag in the right close to the corroded surface. (SEM- BSE)

Figure 14. Etched transverse section of SI1 in the shaft shows a carburized structure with a lamellar form with a gradient from peripheral high carbon content to a lower carbon content zone in the middle.
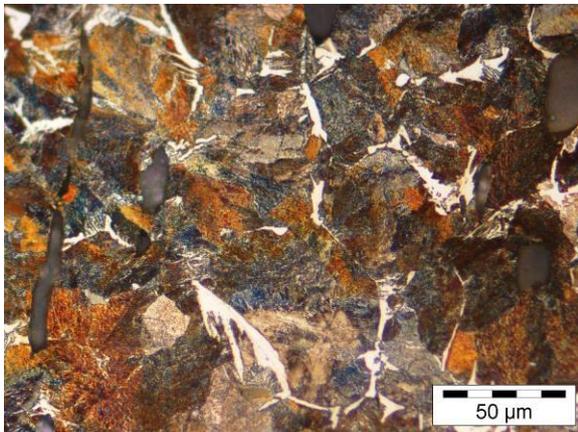
Figure 15. Etched transverse section of SI1 in the shaft in the carburized zone shows laths of ferrite on former austenite grain boundaries with Widmanstätten structure.
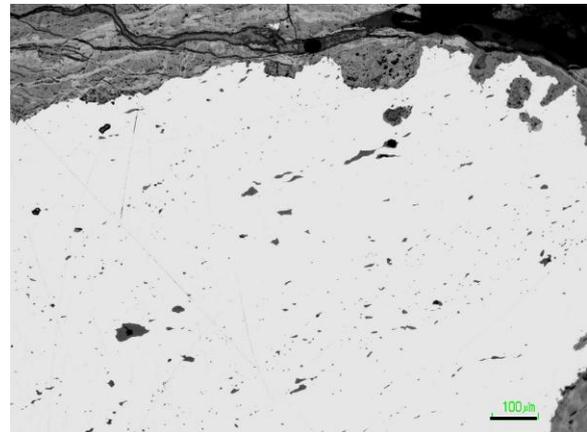
Figure 16. Micrograph of polished cross section of iron adze (KI3) shows numerous irregular inclusions along with few elongated slag that placed parallel to the surface. (Scale: 100μm)
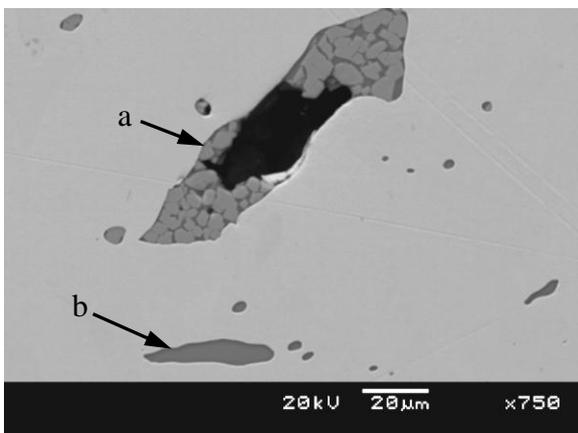
Figure 17. Polished section of iron adze (KI3) showing a complex multiphase inclusion (a) and numerous round and elongated glassy slag around it (b). (SEM-BSE)
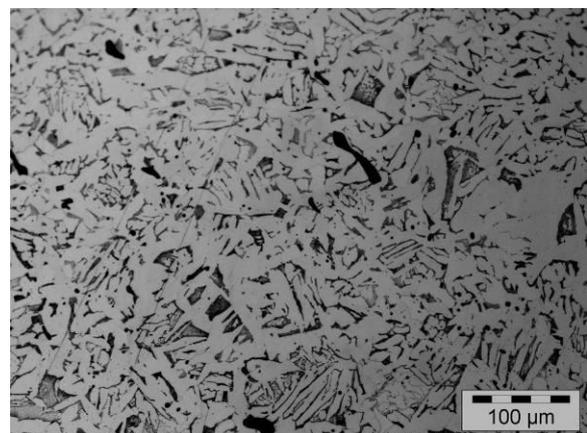
Figure 18. Etched section of KI3 shows proeutectoid Widmanstätten ferrite with regular pearlite colonies.

214
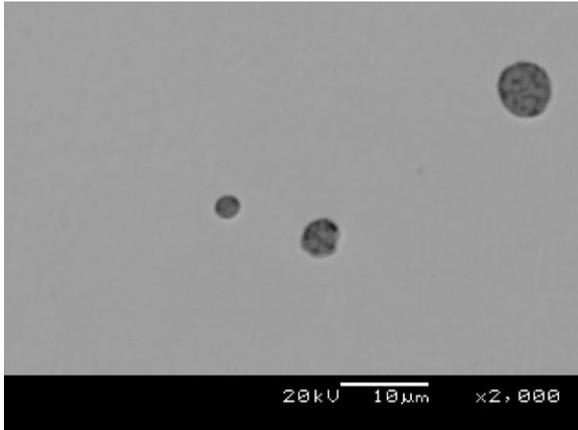
Figure 19. Polished section of iron drill (KI5) showing small globules of fayalite inclusions (SEM-BSE).
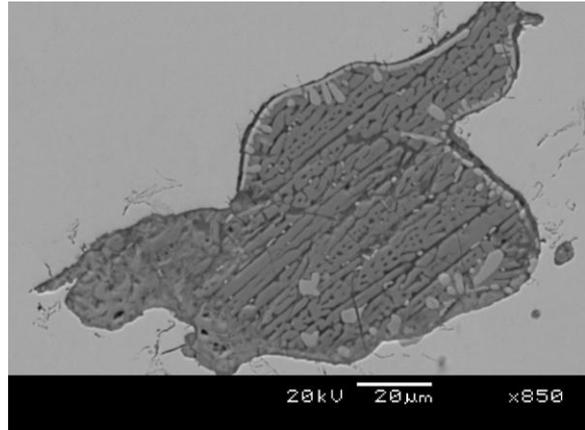
Figure 20. Polished section of iron drill (KI5) showing light dendrite and globule of wüstite in dark fayalite. (SEM-BSE)
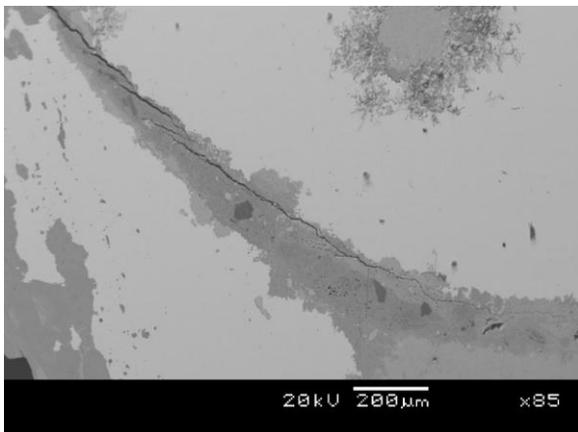
Figure 21. Polished section of iron drill (KI5) showing big rounded oxide inclusions as well as entrapped iron oxide and quartz grain within metal matrix. (SEM-BSE)
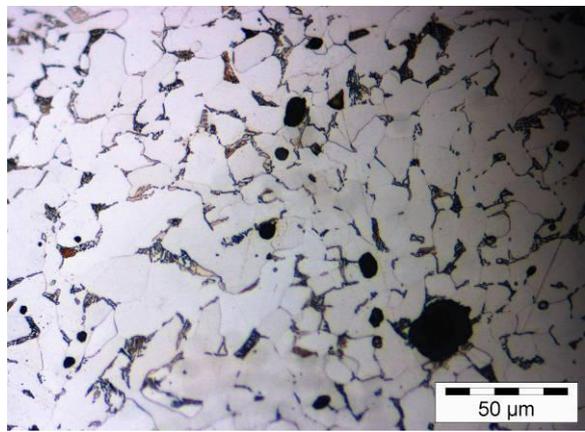
Figure 22. Etched transverse section of iron drill (KI5) at outermost surface shows irregular ferrite grains with pearlite islands and cementite film at grain boundaries.
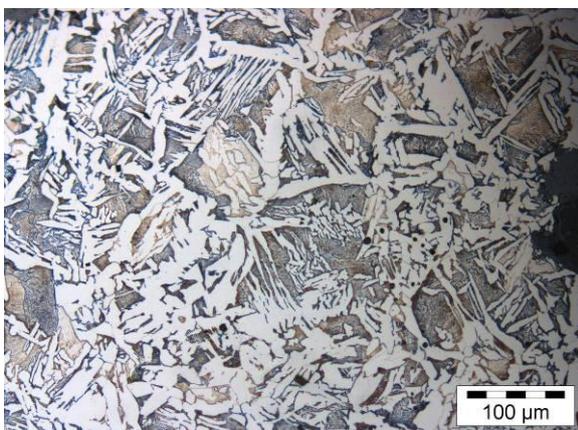
Figure 23. Etched transverse section of iron drill (KI5) at core shows ferrite grain boundaries with Widmanstätten side and intragranular plates.
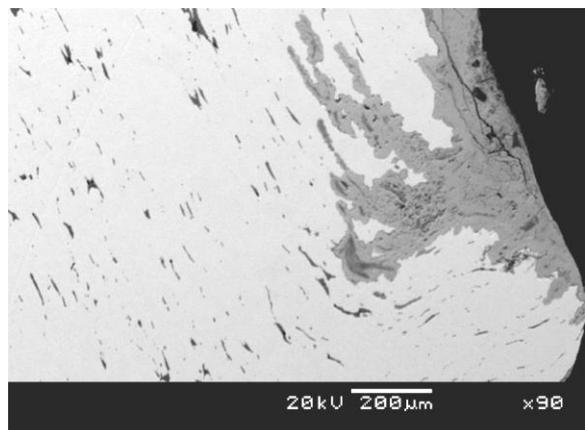
Figure 24. Polished longitudinal section of iron hoe (MI2) in the blade showing elongated glassy inclusions parallel to the surface. (SEM-BSE)

215
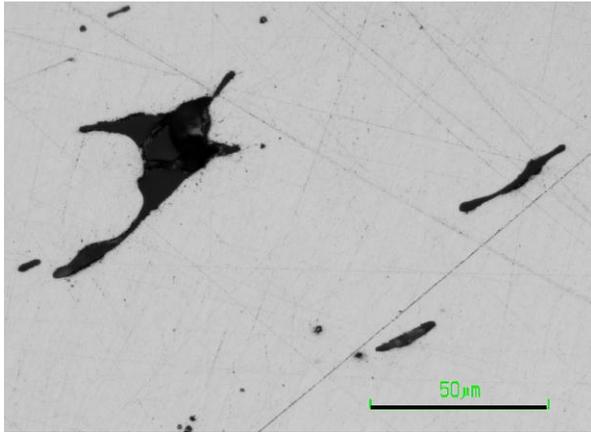
Figure 25. Granulate glassy phase among void within the blade of (MI2). (Scale: 50μm)
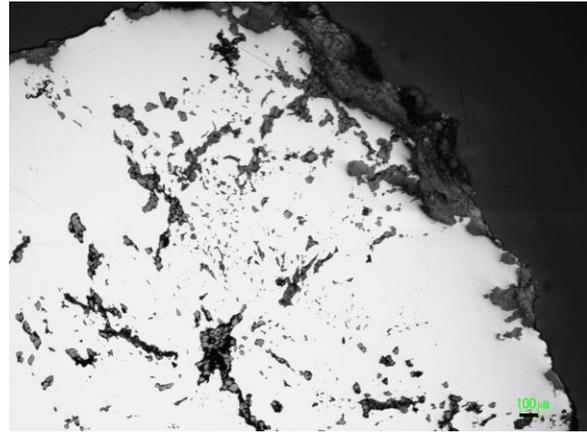
Figure 26. Polished transverse section of iron hoe (MI2) in the shaft showing irregular shape inclusions. (Scale: 100μm)
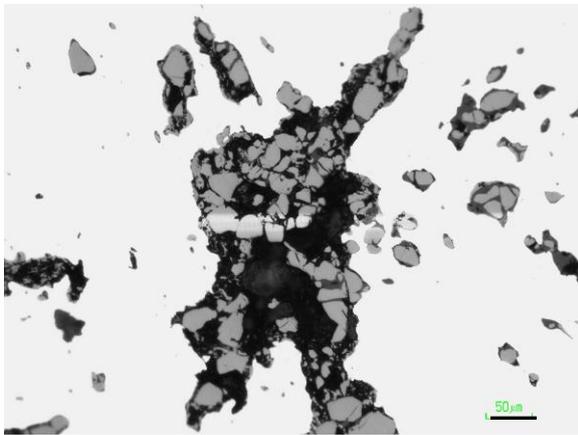
Figure 27. Micrograph of polished section of iron hoe (MI2) in the shaft showing irregular voids containing of two phase inclusions of light grey globules in dark grey matrix. (Scale: 50μm)
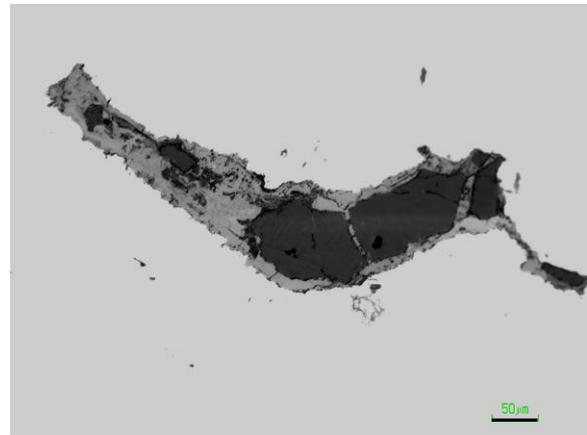
Figure 28. Micrograph of slag and oxide inclusion within metal phase in (MI2 shaft) with transverse fracture in glassy phase. (Scale: 50μm)
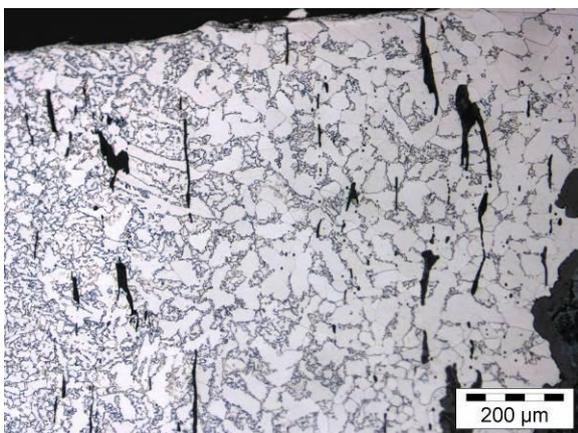
Figure 29. Non uniform ferrite grain size in MI2 blade.
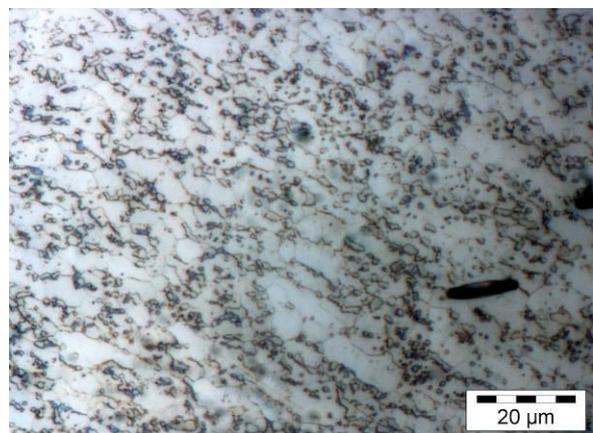
Figure 30. Full spheroidized particles of cementite along grain boundaries and intragranular areas in front edge of the blade.

216
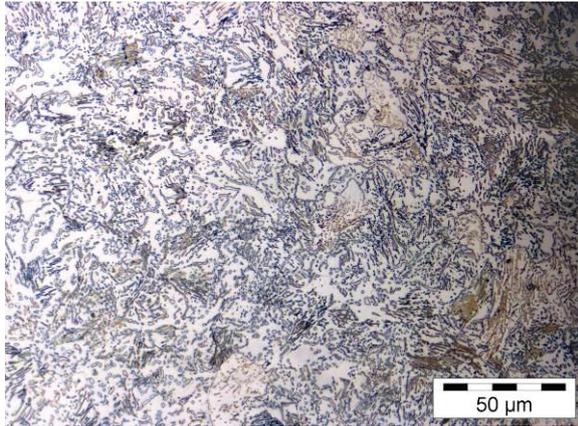
Figure 31. Etched section of MI2 showing partial spheroidizing of eutectoid pearlite at one of the lateral surface of the shaft.
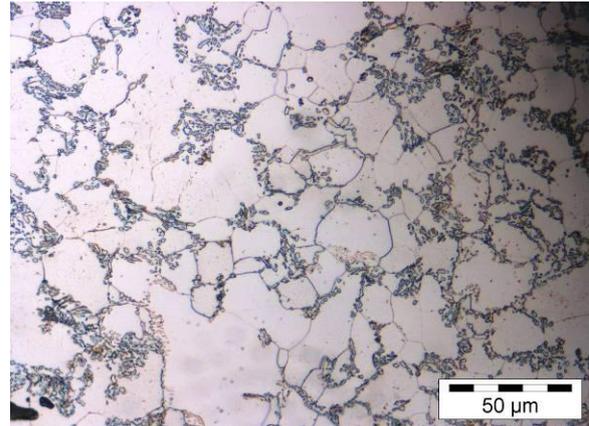
Figure 32. Etched section of MI2 shaft showing degenerate pearlite and intragranular spheroidized cementite.
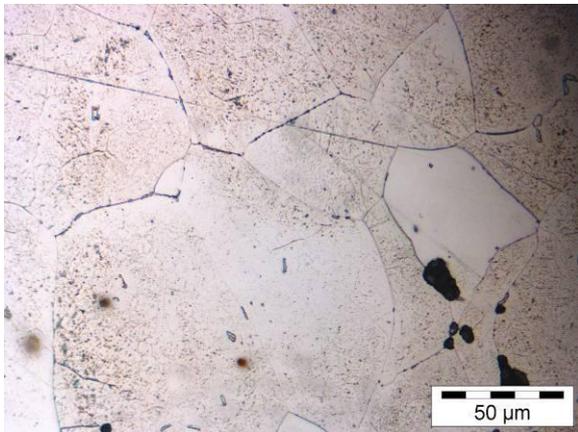
Figure 33. Etched section of MI2 in shaft (point) shows equiaxed grains of ferrite with thin grain boundary film of cementite and etch-pitting effect.
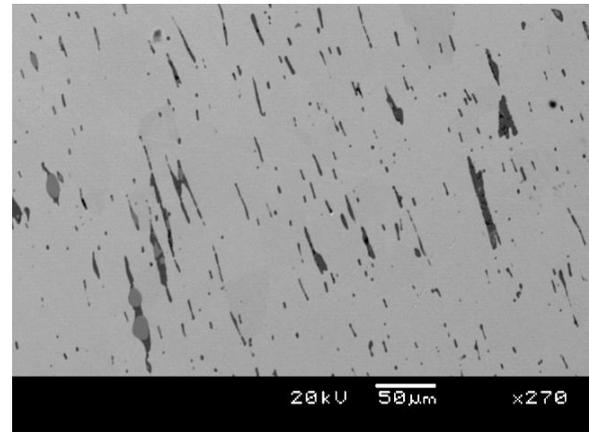
Figure 34. Longitudinal section of hoe blade (MI7) showing numerous elongated dark grey slag with light dendrite or globule of wüstite. (SEM-BSE)
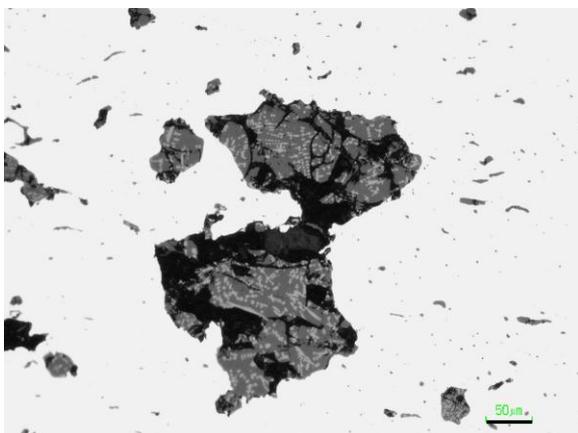
Figure 35. Cross section of hoe shaft (MI7) showing numerous angular inclusions of dark glassy phase containing dendrite of wüstite. (Scale:50μm)
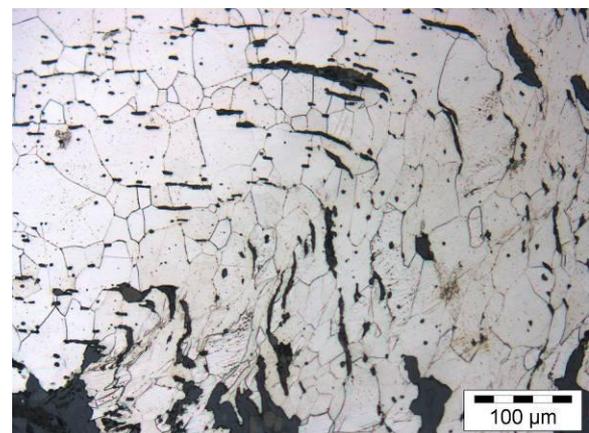
Figure 36. Etched transverse section of MI7 in blade shows massed ferrite with equiaxed grains which were deformed toward the tip.

217
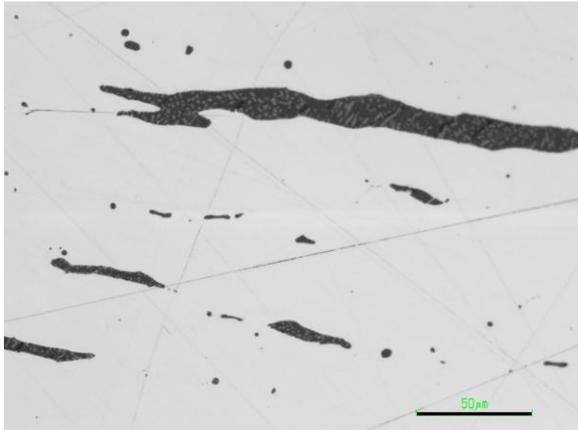
Figure 37. Longitudinal section of MI9 in blade showing elongated stringers of dark-grey slag containing dendrite of wüstite. (Scale: 50μm)
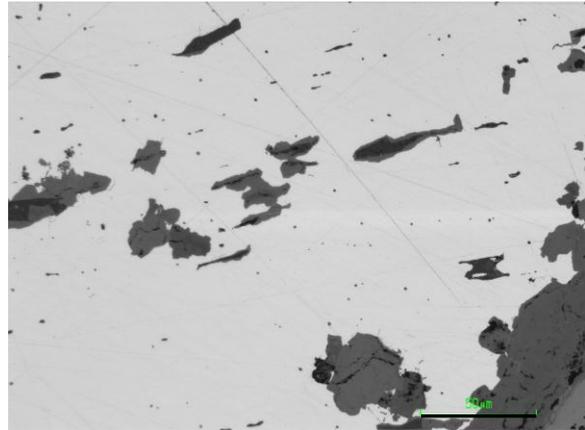
Figure 38. Polished section of (MI9) in blade showing slag and oxide inclusions. (Scale 50μm)
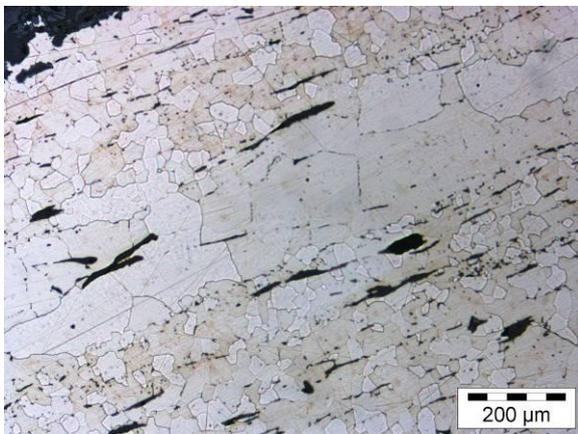
Figure 39. Longitudinal etched section of MI9 blade shows critical growth of ferrite grains within the sample.
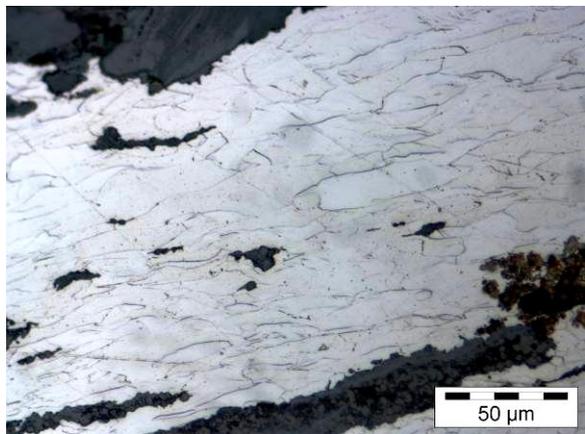
Figure 40. Etched transverse section of MI9 in the shaft shows massed ferrite with film of cementite grain boundaries and cold working deformation toward the surface.
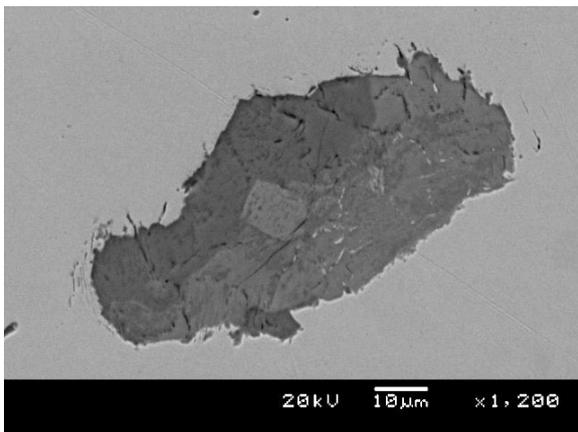
Figure 41. Polished cross section of iron hoe (MI10) in blade showing oxide inclusion within the metal phase. (SEM-BSE)
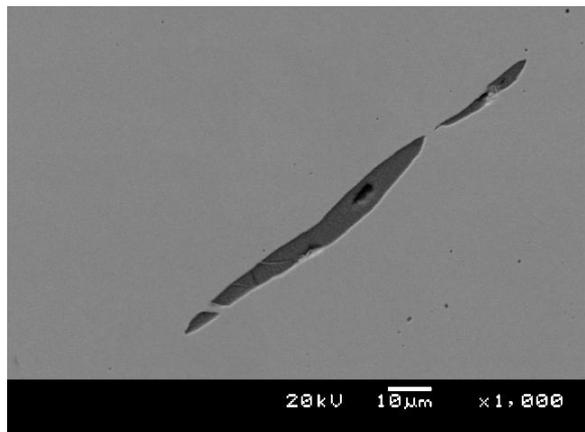
Figure 42. Micrograph of transversely section of (MI10) in blade showing elongated fine slag passing along the heavily worked surface. (SEM-BSE)

218
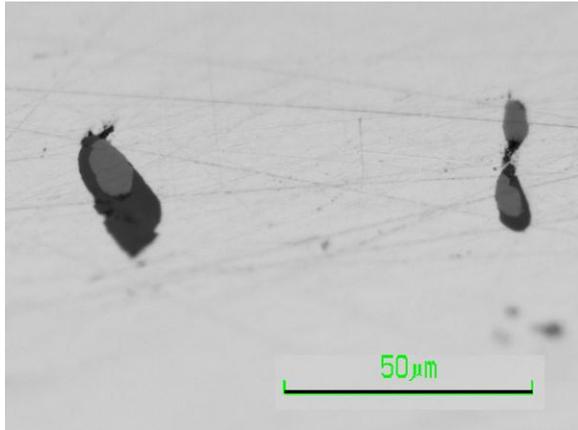
Figure 43. Micrograph of inclusions with globule of light phase in dark-grey slag within MI10 shaft. (Scale: 50μm)
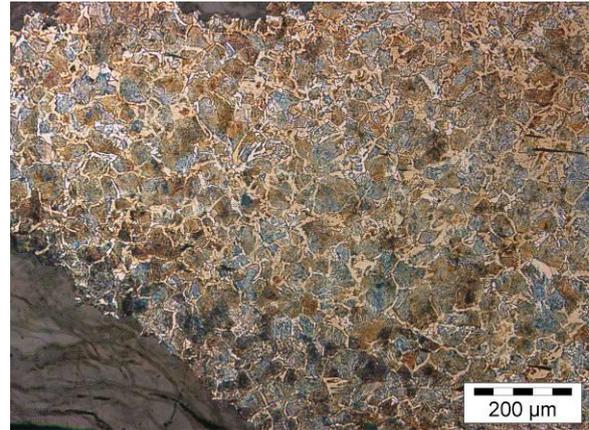
Figure 44. Etched transverse section of MI10 in blade shows slightly inhomogeneity in carbon content with higher amount toward the surfaces which is seen darker toward the bottom of image.
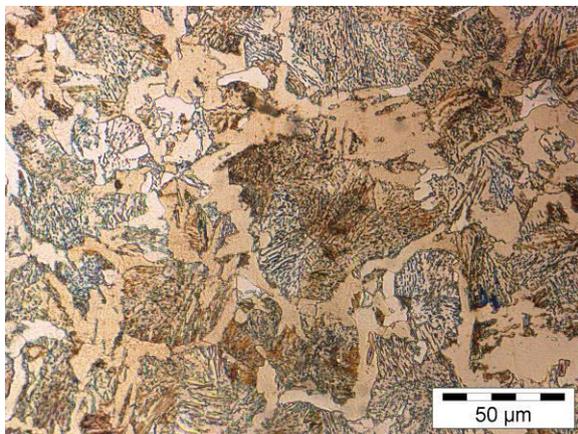
Figure 45. Etched transverse section of MI10 in the blade (middle) shows allotriomorphs ferrite grain boundaries with Widmanstätten intragranular and side plates morphologies.
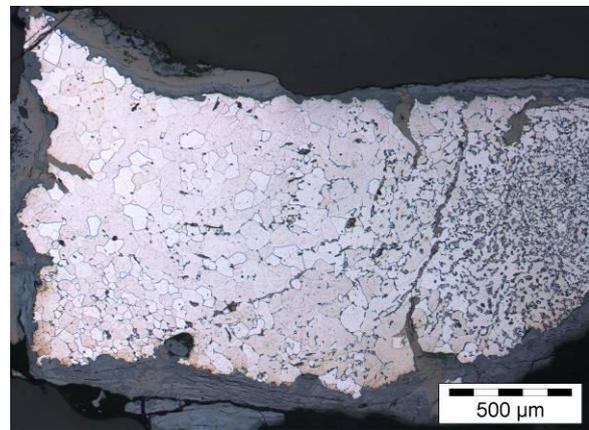

Figure 46. Etched transverse section of MI10 in the shaft shows a gradient in carbon content between two lateral surfaces.
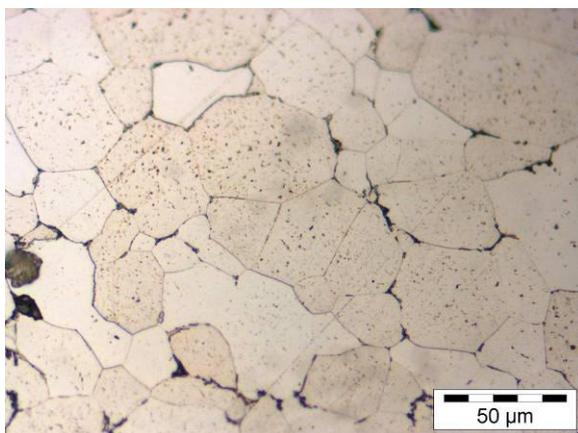
Figure 47. Etched transverse section of MI10 in the shaft shows equiaxed ferrite grains with thin film of cementite at grain boundaries.
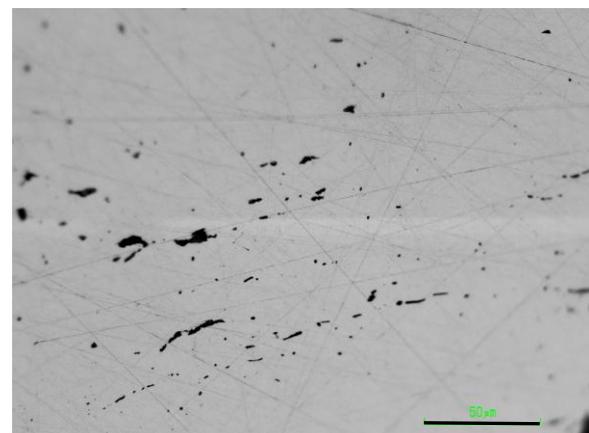

Figure 48. Micrograph of polished cross section of iron hook (MI4) showing fine stringers of slag elongated parallel to the surface. (Scale: 50μm)

219
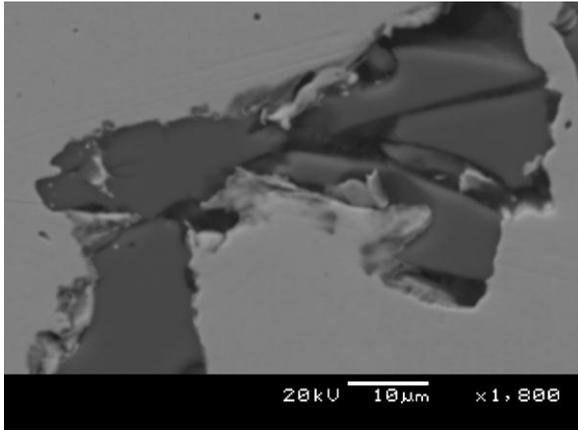
Figure 49. Glassy inclusion with high amount of silicon within metal phase in (MI4). (SEM- BSE)
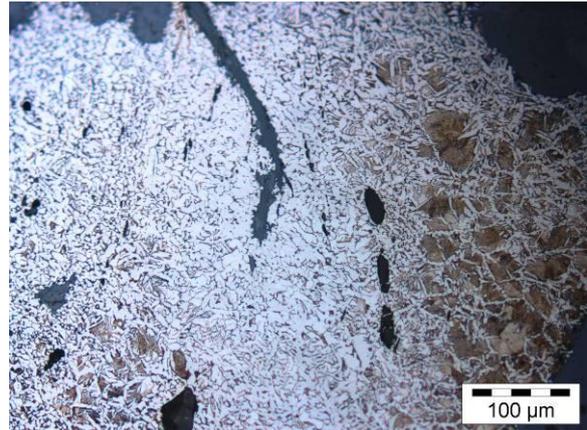
Figure 50. Etched transverse section of MI4 shows composition diversion with lighter lower carbon content and darker higher carbon content zones.
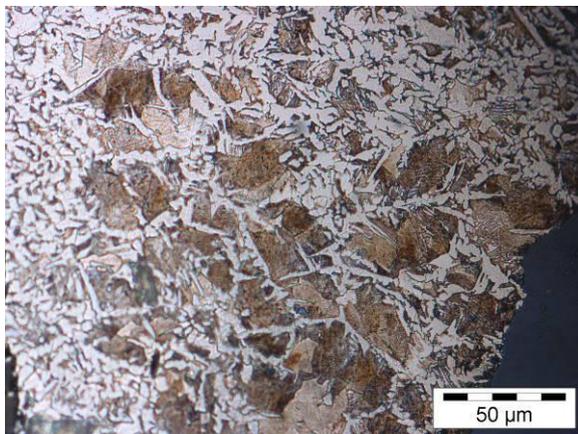

Figure 51. Etched transverse section of MI4 shows ferrite grain-boundary allotriomorphs with Widmanstätten structure.
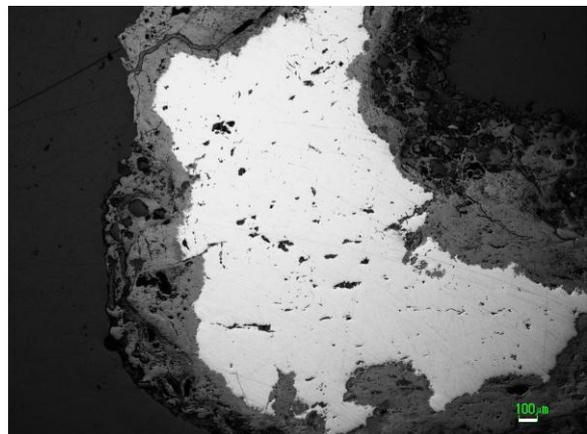

Figure 52. Micrograph of transversally section of (MI8) showing inhomogenously scattered inclusions. (Scale: 100μm)
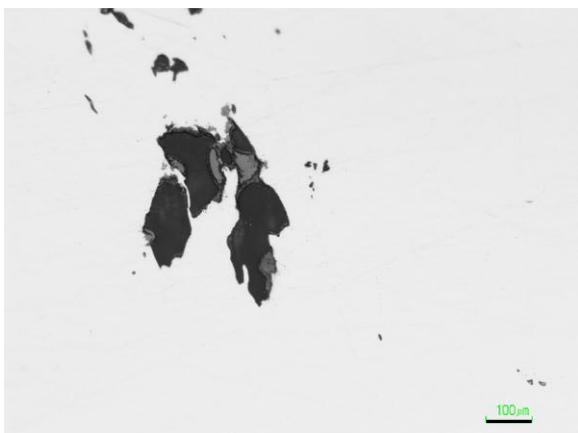

Figure 53. Micrograph of two phases inclusion in (MI8) with light-grey globule of wüstite within dark-grey glass. (Scale: 100μm)
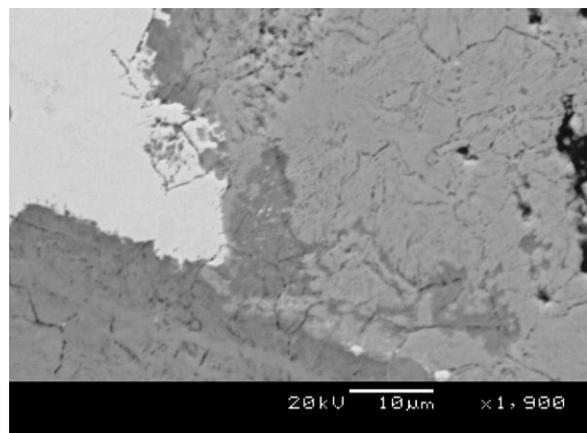

Figure 54. Stress corrosion resulted in formation of fine cracks in metal phase in block twisting wire (MI8). (SEM-BSE)

220
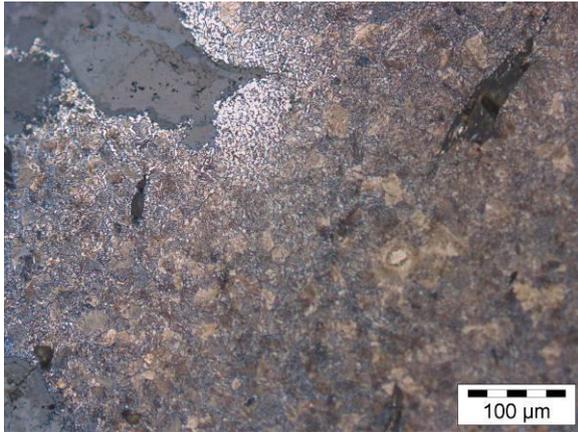
Figure 55. Etched transverse section of MI8. Entrapped oxide phased formed during forging.
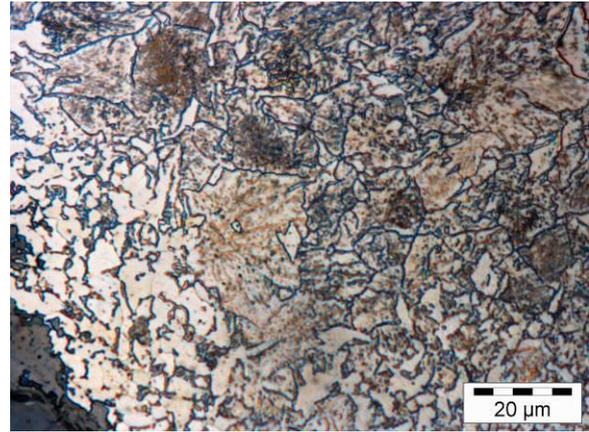

Figure 56. Etched transverse section of MI8 shows high carbon interior and decarburized fringe.
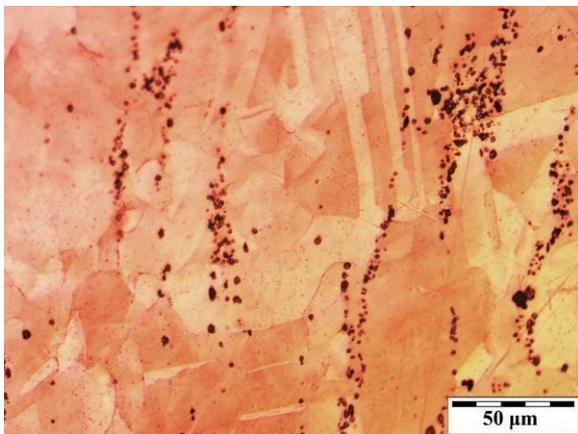
Figure 57. Etched transverse section of KC1 shows banded nodular inclusions of copper oxide along with fine precipitates within angular recrystallised grains of copper with annealing twins.
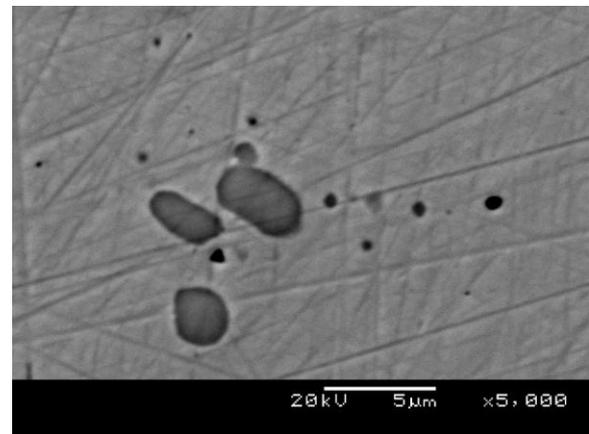
Figure 58. Nodules of cuprite inclusion in central part of the KC1 sample. (SEM-BSE)
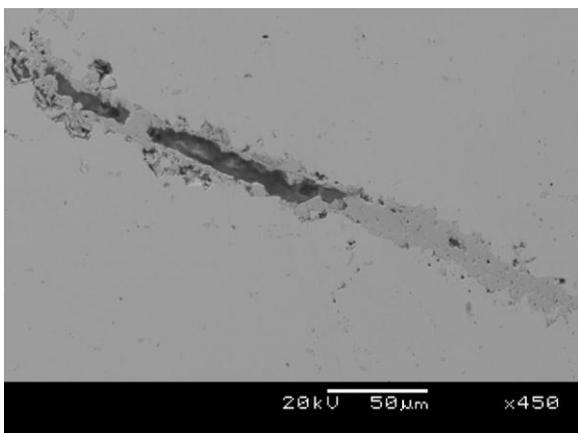
Figure 59. Polished transverse section of KC5 shows longitudinal central void within metallic matrix that was partially filled of cuprite. (SEM-BSE)
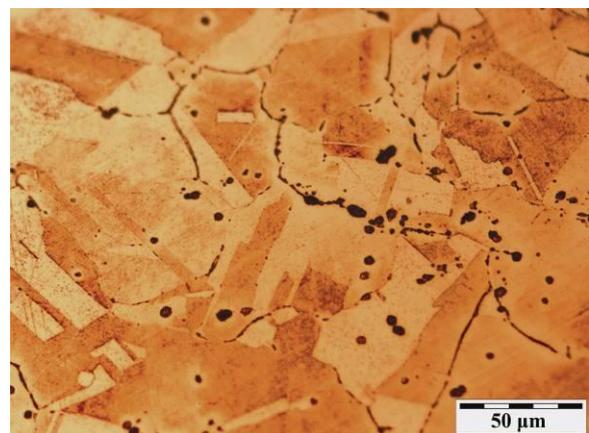
Figure 60. Etched cross section of KC5 showing uneven dispersion of cuprite inclusions within metallic phase with twinned angular recrystallised grains.

221
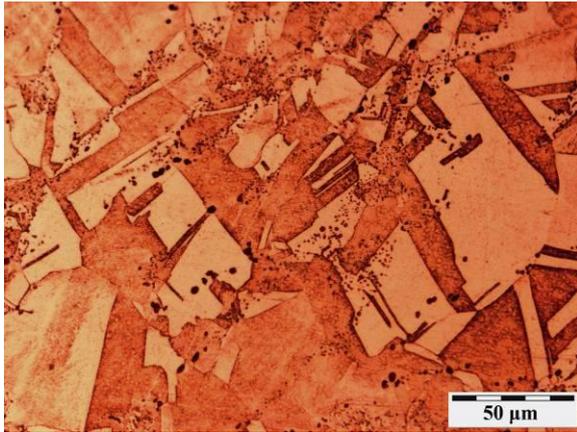
Figure 61. Etched cross section of MC2 showing broad annealing twins with banded cuprite inclusions.
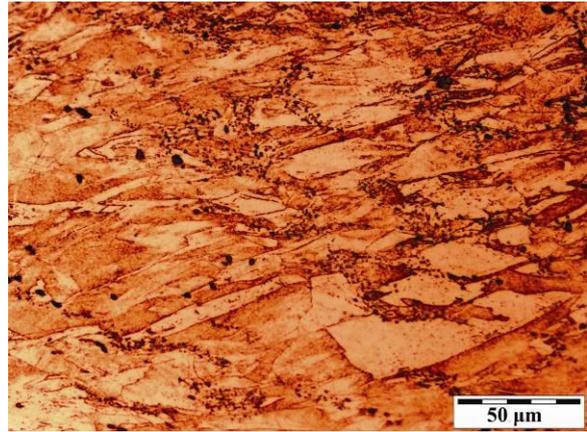
Figure 62. Etched transverse section of MC2 showing flattened copper grains with distorted twin lines.
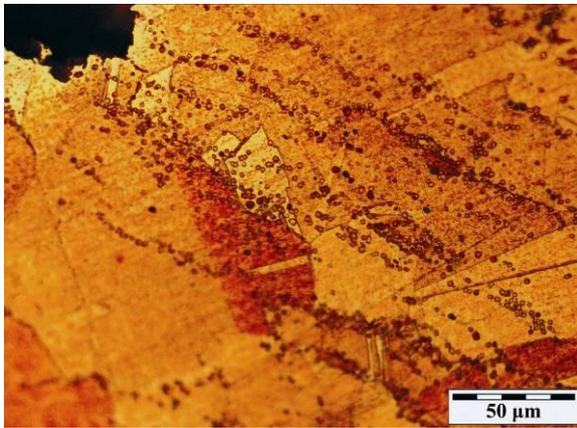
Figure 63. Etched cross section of MC10 shows cuprite inclusions in a banding structure.

Figure 64. Etched cross section of MC10 shows angular grains of copper with annealing twins.

Figure 65. Micrograph of MC11 shows numerous voids within the metal phase with higher concentration toward rough surface (right). The dendrites were deformed on top of the image.
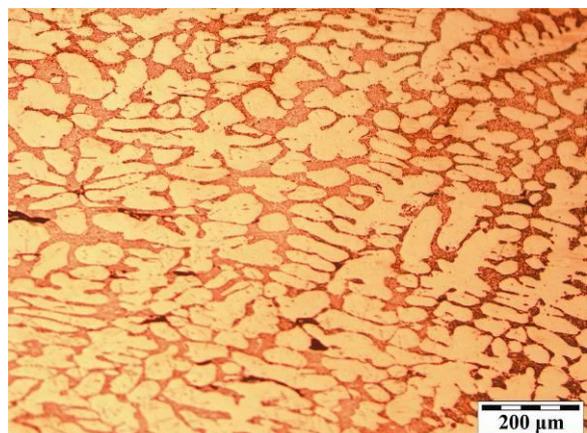
Figure 66. Transverse section of the bangle (MC11) shows dendritic structure of α-Cu within $(\alpha + Cu_2O)$ eutectic.

222
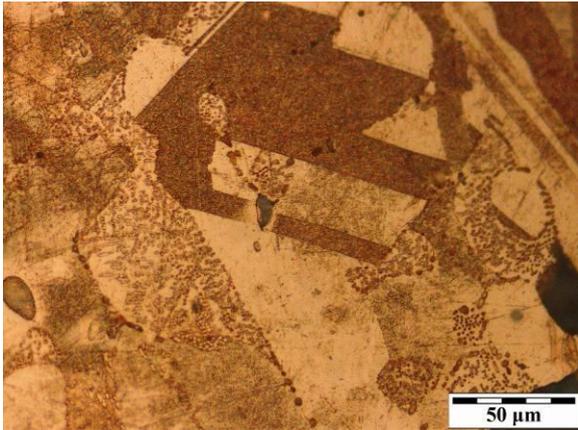
Figure 67. Etched transverse section of MC11 shows straight annealing twins within dendrite.
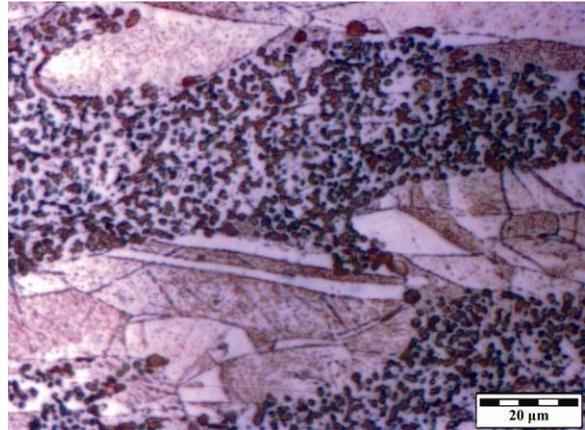
Figure 68. Etched transverse section of MC11 shows straight annealing twins within dendrite of α-Cu resulting from insufficient annealing operation.
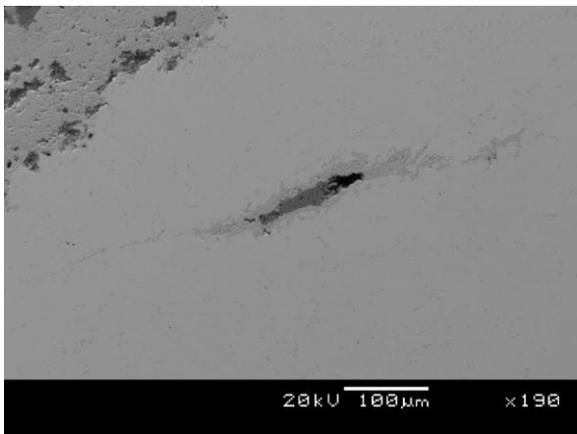
Figure 69. penetration of corrosion within fissure present in metal phase in MC12. (SEM- BSE).
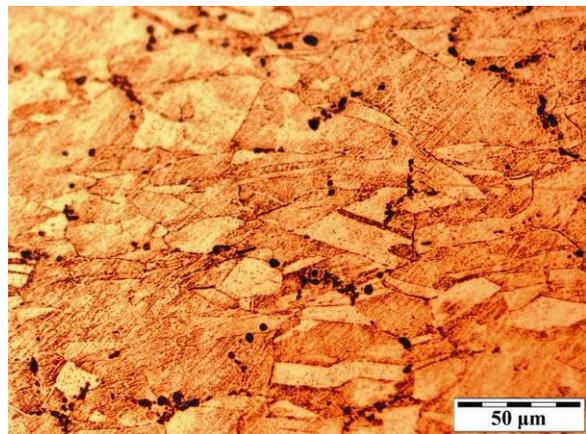
Figure 70. Etched transverse section of MC12 shows angular grains of copper with distorted annealing twins.
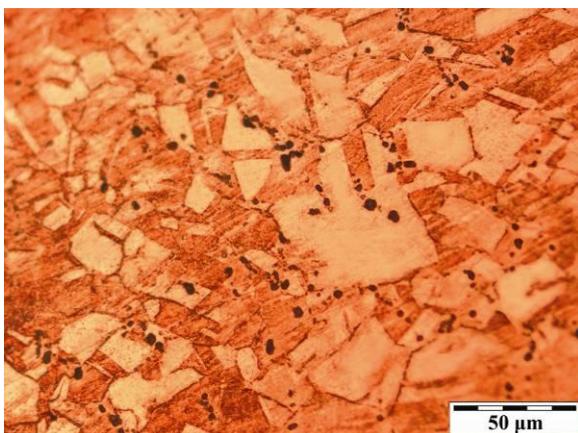
Figure 71. Etched transverse section of KC2 shows angular grains of copper with annealing twins.
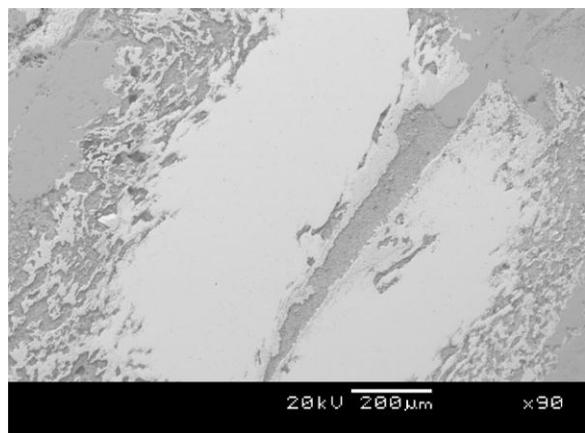
Figure 72. Polished cross section of MC4 shows a bulky plate was folded over to form a thicker section. (SEM-BSE)

223
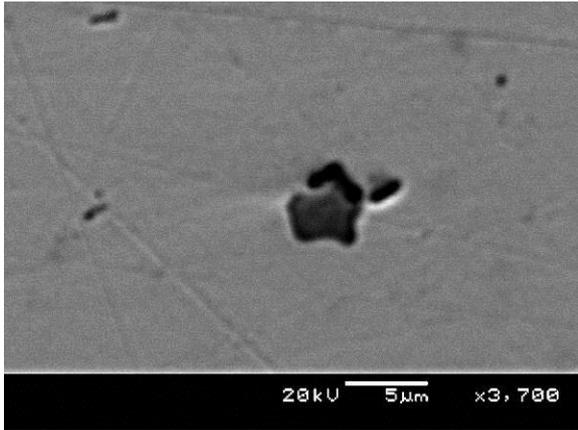
Figure 73. MC4 cross section. Angular dark grey inclusion of iron and copper oxides in vicinity of voids which is seen in black. (SEM-BSE)
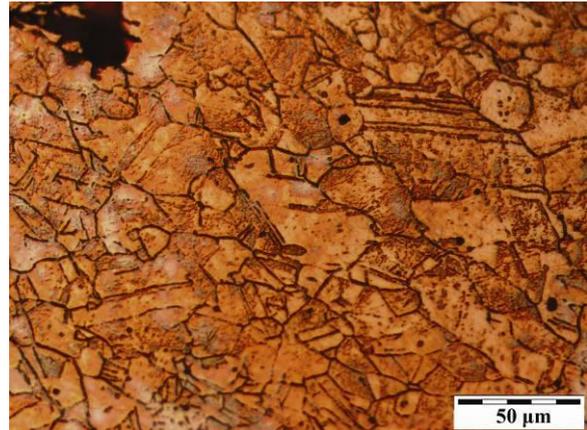
Figure 74. Polished and etched cross section of MC4 shows annealing twins in angular grains of copper.
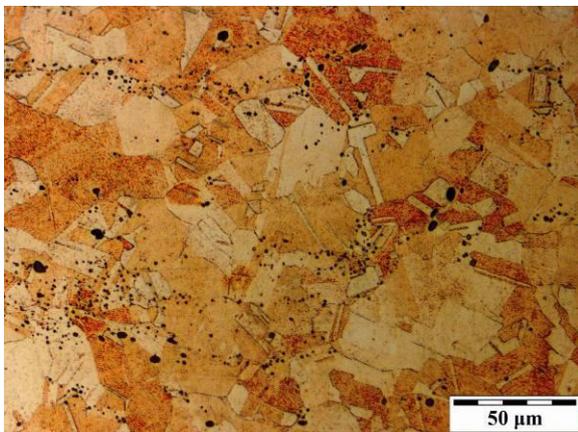
Figure 75. Etched transverse section of KC4 shows globular oxide inclusions and annealing twins.

Figure 76. Flattened copper grains toward thicker side of the plate (KC4) with preferred orientation along cold-worked surface.
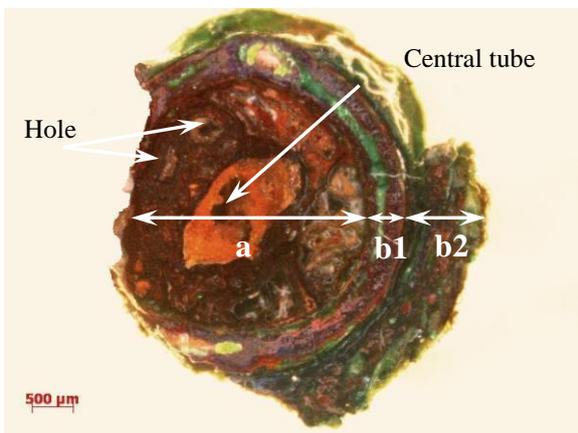
Figure 77. Microstructure of transverse section in narrow point of MC7. Zone *a*: folded strip among funnel. Zone *b1*: funnel wall. Zone *b2*: corrosion products on exterior surface of funnel.
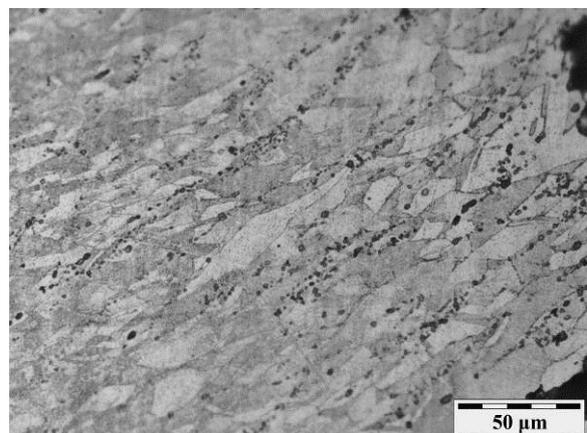
Figure 78. Etched transverse section of SC2 shows elongated grains of copper with cuprite inclusions in a banding structure sub-parallel to the straight surface of the sample.

224
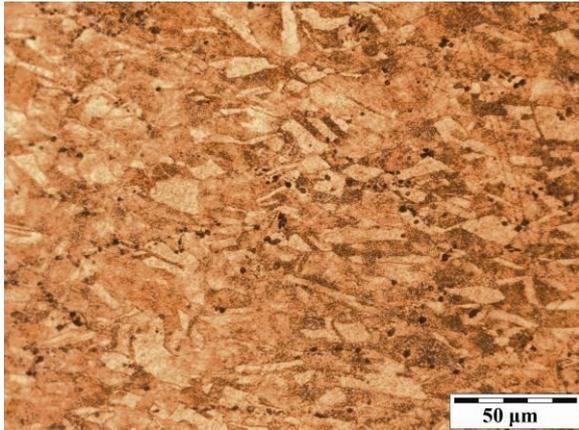
Figure 79. Etched transverse section of SC2 shows distorted annealing twins.
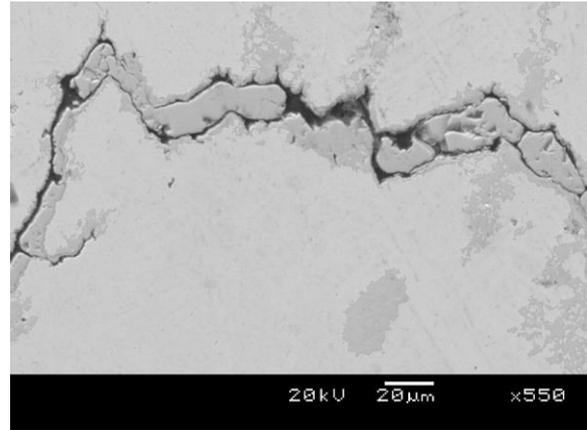
Figure 80. Transverse section of MC8 in shank shows central open wide crack within metal phase along with of patches of corrosion in its vicinity. (SEM-BSE)
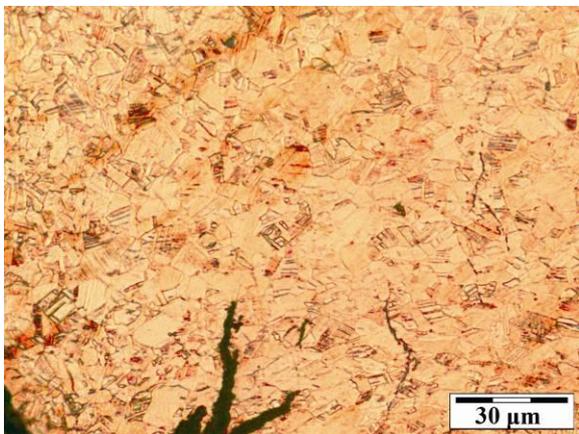
Figure 81. Etched cross section of MC8 shows recrystallised fine α grains (solid solution of tin in copper) with slip lines.
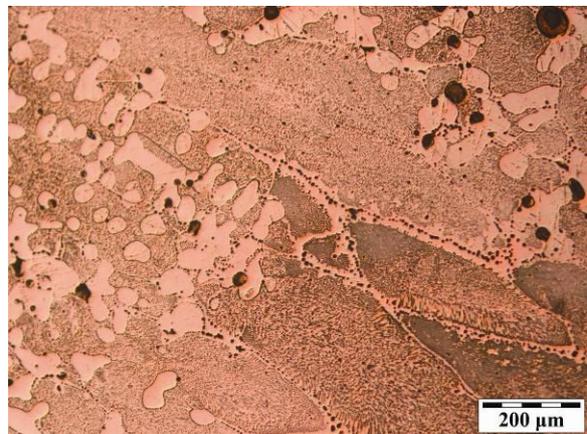
Figure 82. Etched cross section of MC9 shows dendrite of α-Cu within (α + Cu$_2$O) eutectic. Columnar grains of eutectic phase is seen in the right of the image.
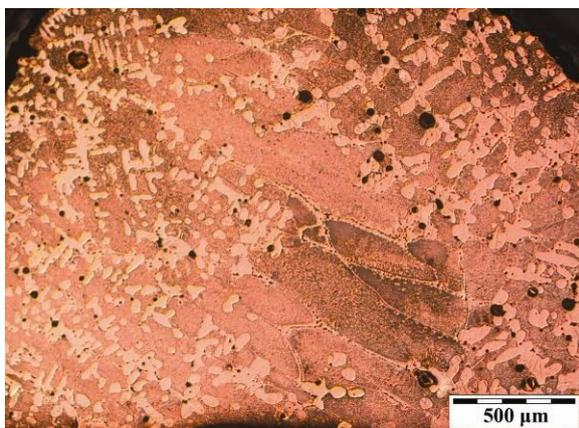
Figure 83. Etched cross section of MC9 shows smaller dendrites of cuprite at the mold surface in the left part of the image.

225

Appendix C

SEM-BSE micrographs of corrosion layers on iron and copper samples
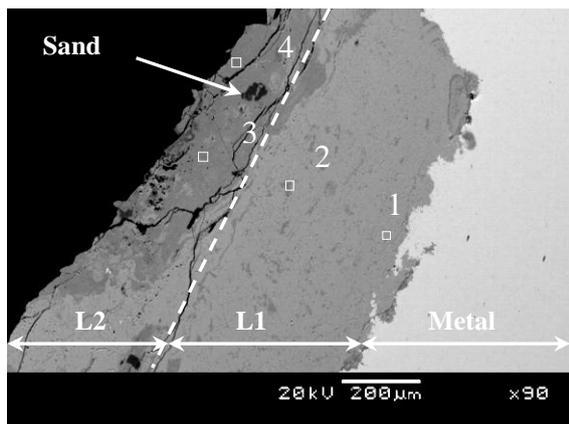
Figure 1. Microstructure of corrosion layers on KI1. a) In light grey: metal surface; in medium grey: magnetite; in dark grey: sand. Dash line shows the limit of original surface.
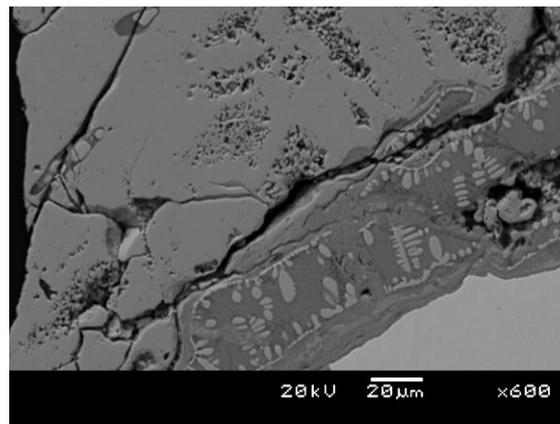
Figure 2. Microstructure of corrosion layers on KI1. Ghost bloomery inclusion at internal layer; in light grey: wüstite; in medium grey: fayalite.
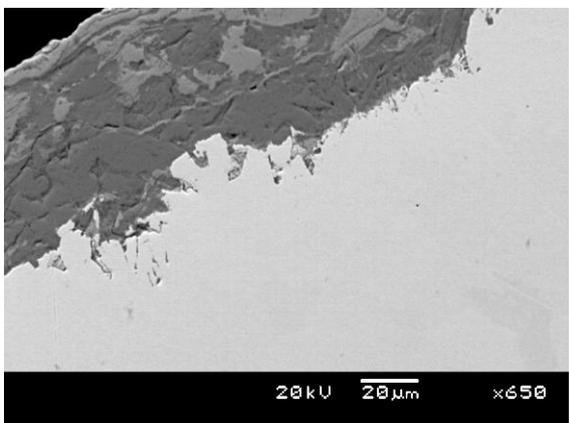
Figure 3. Microstructure of the internal layer on KI3.
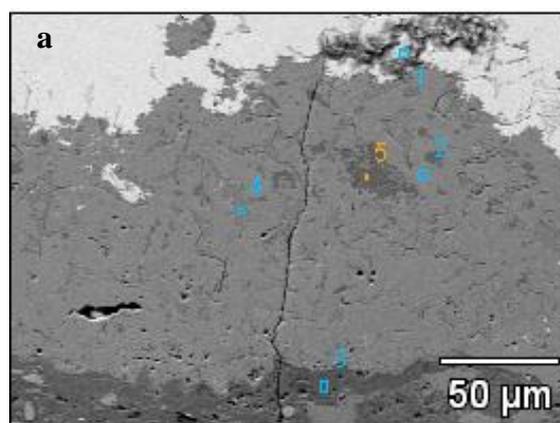
Figure 4. Microstructure of corrosion layers on KI5. Internal layer; 2) Magnetite; 3 and 5) Goethite; 4) Hematite.
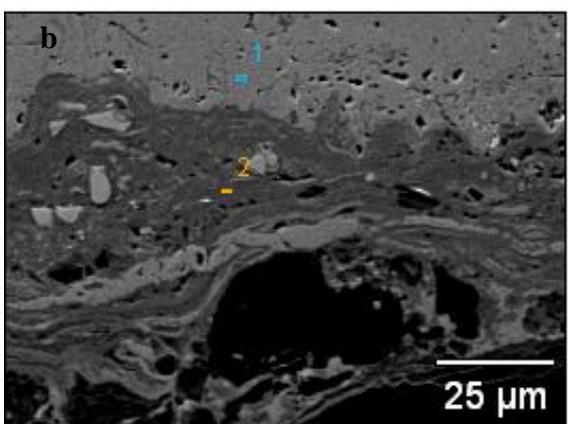
Figure 5. Microstructure of corrosion layers on KI5. Porous external layer. 2) Goethite.
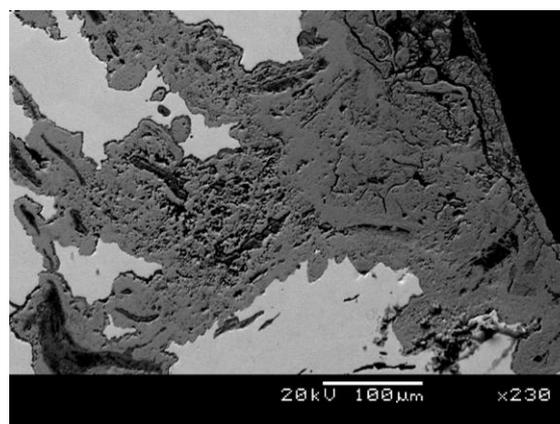
Figure 6. Microstructure of corrosion layers on MI2. Localized attack is seen in the form of penetration of corrosion along elongated inclusions.

226
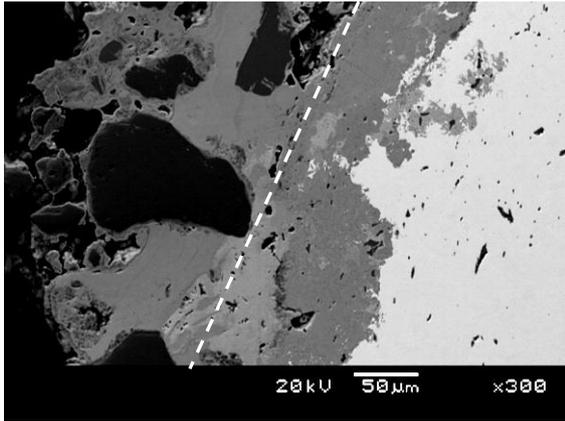
Figure 7. Microstructure of corrosion layers on MI4. In white: metal; in black: quartz; dash line limit of original surface.
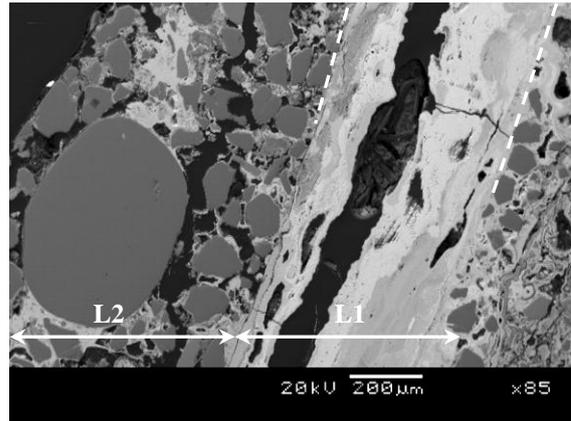
Figure 8. Microstructure of corrosion layers on MI5. L1: central void and peripheral dense corrosion products; L2: external layer with quartz grains; dash line shows limit of original surface.
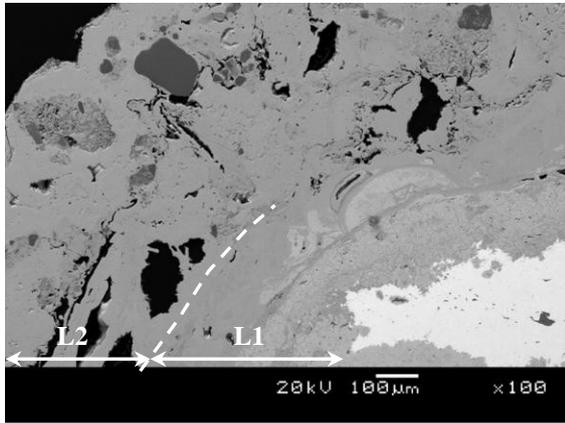
Figure 9. Microstructure of corrosion layers on MI6. L1: internal layer; L2: external layer; in white: metal; in black: sand; dash line indicates limit of original surface.
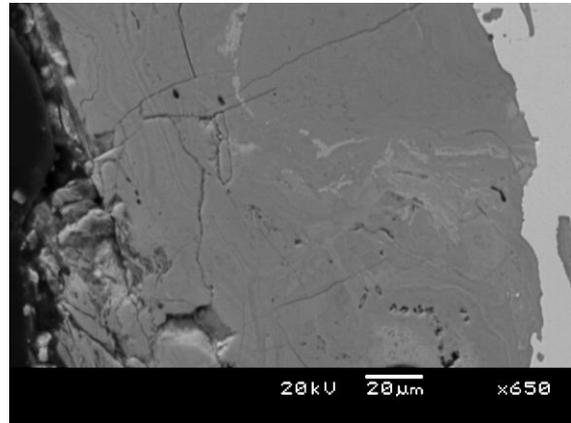
Figure 10. Microstructure of corrosion layers on MI7. One dense layer of corrosion is seen on the surface. In white: metal; in light grey presumably iron oxyhydroxide.
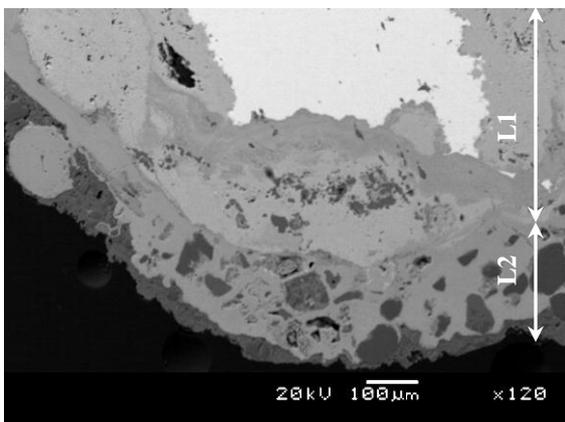
Figure 11. Microstructure of corrosion layers on MI8. L1: internal layer; L2: external layer with grains of sand and a thin layer calcium carbonate.
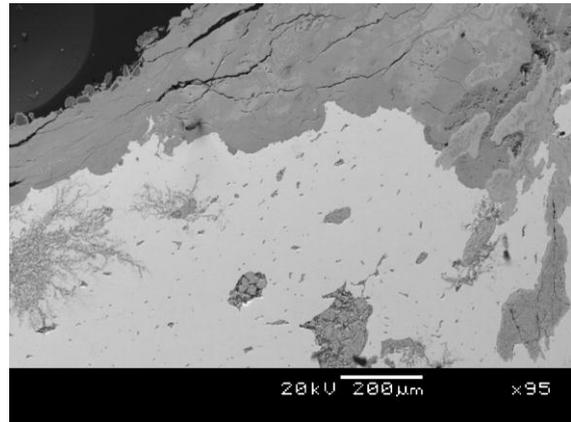
Figure 12. Microstructure of corrosion layers on MI9. In white metal; localized corrosion is seen in right along inclusions.

227
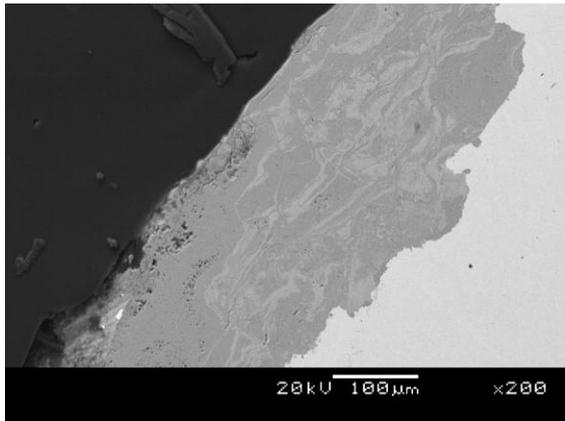
Figure 13. Microstructure of corrosion layers on MI10. One-layer of dense corrosion is seen on the surface. In white: metal.
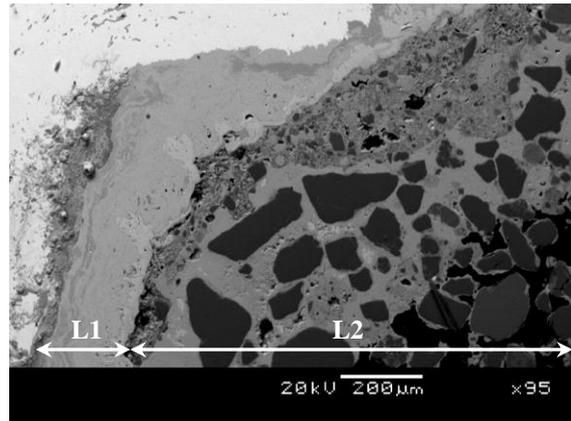
Figure 14. Microstructure of corrosion layers on SI1. In white: metal; L1: internal layer with spherical shells; L2: external layer with angular quartz grains.
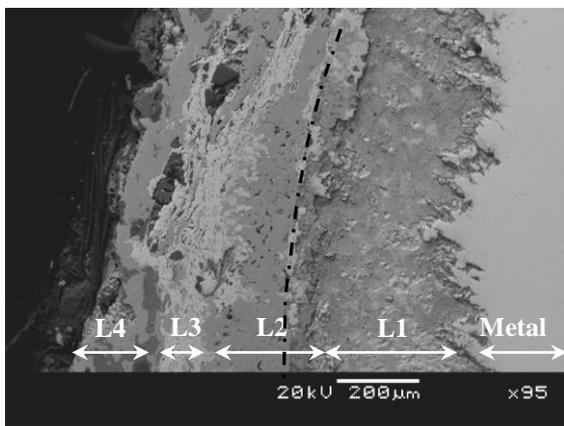
Figure 15. Microstructure of corrosion layers on KC1. Lamellar corrosion; in light grey: cuprous oxide; in dark grey: cupric compounds. Dash line: the limit of original surface.
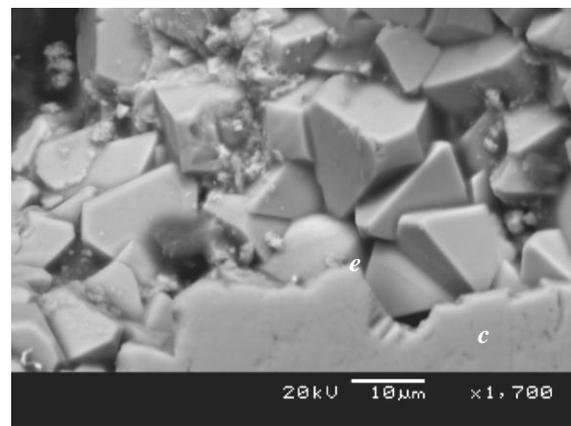
Figure 16. Microstructure of corrosion layers on KC1. b) Copper trihydroxychloride in its crystalline form.
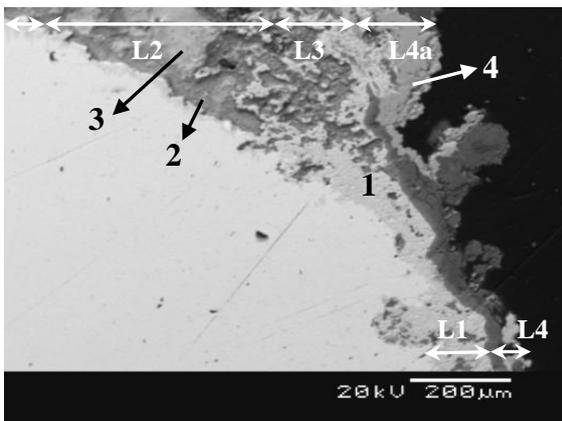
Figure 17. Microstructure of corrosion layers on KC2. Lamellar corrosion; in light grey: cuprous oxide; in medium gray: cupric compounds; in dark gray: products with high amount of silicon and oxygen.
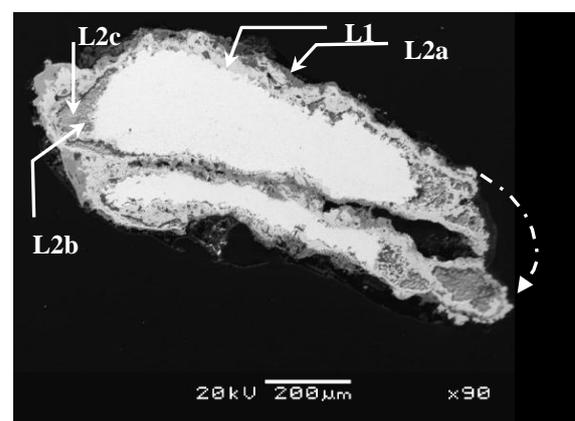
Figure 18. Microstructure of corrosion layers on KC4. Lamellar corrosion ; in light grey: cuprous oxide; in dark grey: cupric compounds; dash line shows the point and direction of folding.

228
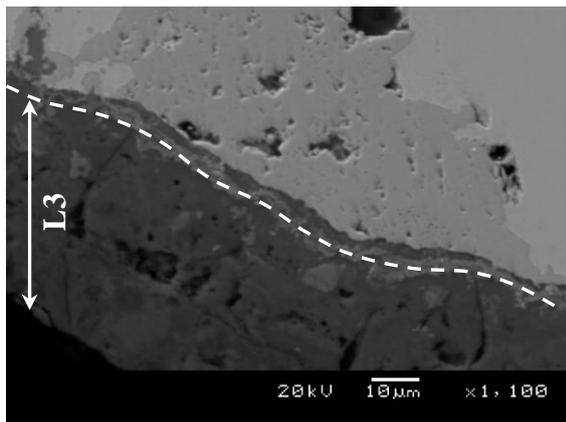
Figure 19. Microstructure of corrosion layers on KC5. Noble patina; in light grey: cuprous oxide, in dark grey: outer and external layer; dash line shows the limit of original surface.
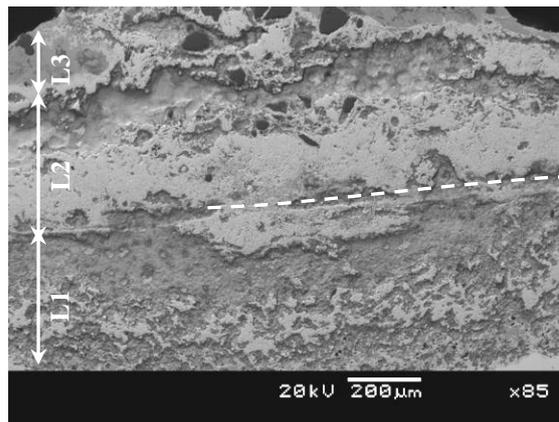
Figure 20. Microstructure of corrosion layers on MC2. In light grey: cuprous oxide; in medium grey: Cu(II) alkaline chloride compounds and nantokite; in dark grey: sand; dash line shows the limit of original surface.
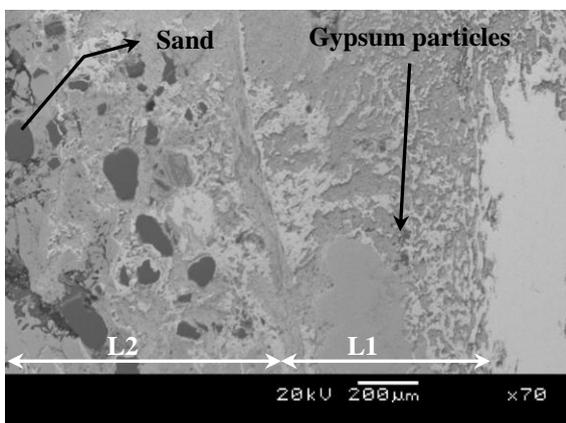
Figure 21. Microstructure of corrosion layers on MC4. In light grey: cuprous oxide; in medium grey: alkaline compounds of Cu(II); in dark grey: sand; dash line shows the limit of original surface.
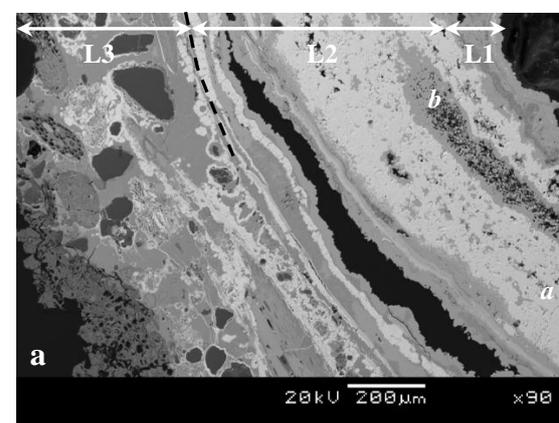
Figure 22. Microstructure of corrosion layers on MC7. Region A; broad light gray: cuprite; thin light gray close to the fissure: chalcocite; in dark gray: chloride compounds of copper.
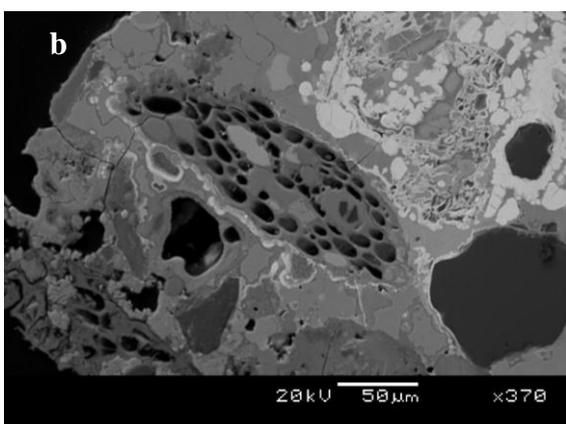
Figure 23. Microstructure of corrosion layers on MC7. Embedded sands and plant in a matrix of cupric compounds.
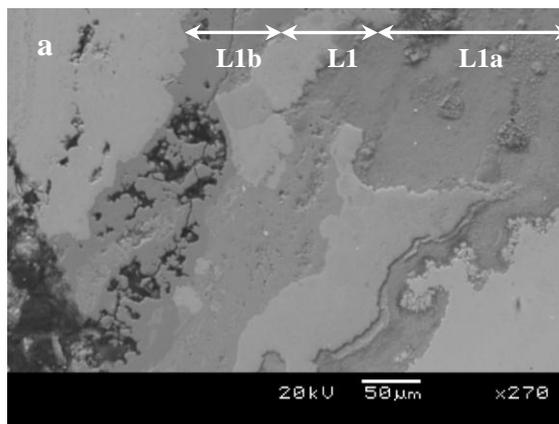
Figure 24. Microstructure of corrosion layers on MC8. L1,a and b: adjacent layer to the alloy phase.

229
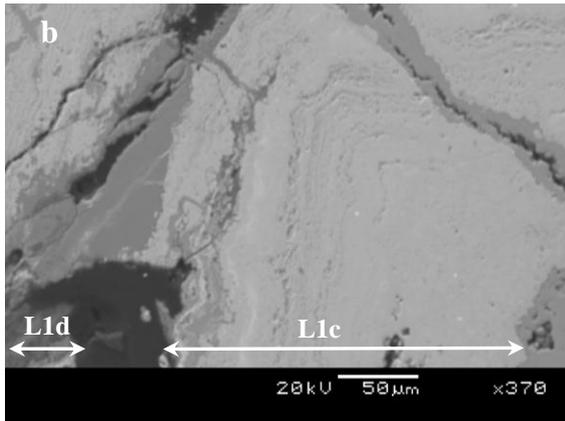
Figure 25. Microstructure of corrosion layers on MC8 with Liesegang phenomena. L1c, d: Disrupted lamellar layer at intermediate of internal outer layer. The hypothetical original surface is among this layer.
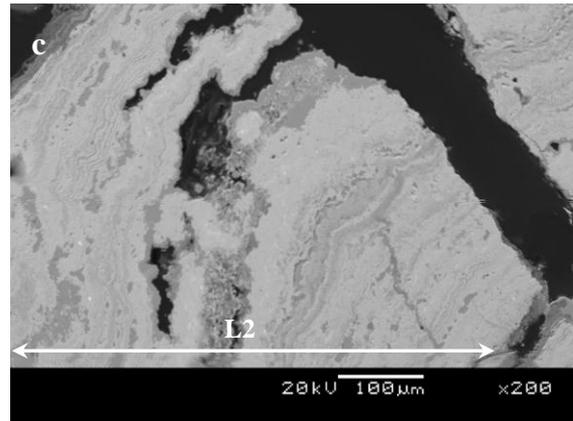
Figure 26. Microstructure of corrosion layers on MC8 with Liesegang phenomena. L2: The outer corrosion layer which formed after restarting the corrosion.
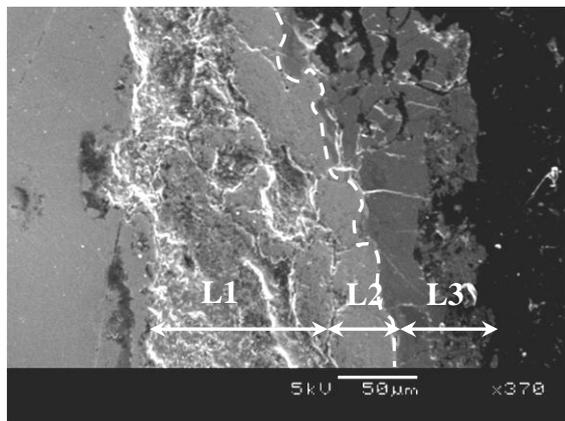
Figure 27. Microstructure of corrosion layers on MC9. A generalized corrosion; L1: internal layer; L2: intermediate layer; L3: external layer; dash line: limit of original surface.
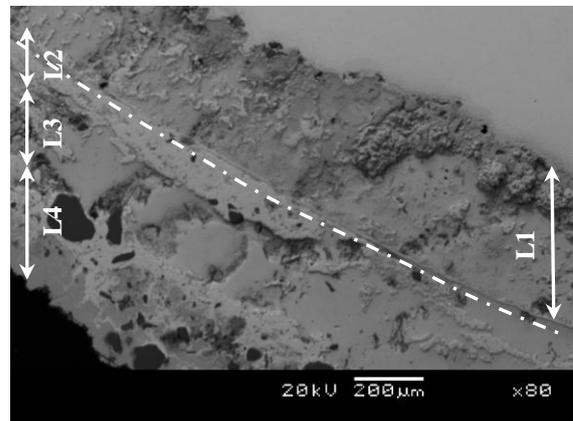
Figure 28. Microstructure of corrosion layer on MC10. A generalized corrosion; L1: internal layer; L2: disrupted cuprite layer; L3 and L4: external layer; dash line: the limit of original surface.
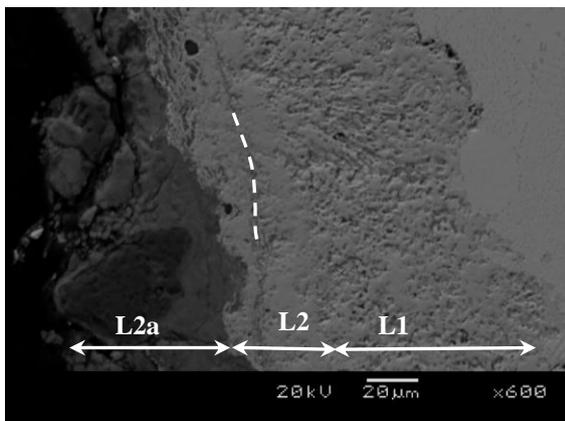
Figure 29. Microstructure of corrosion layers on MC11. A bilayer corrosion; in light grey: cuprite; in dark grey: cupric compounds in accompany with sands; dash line: the limit of original surface.
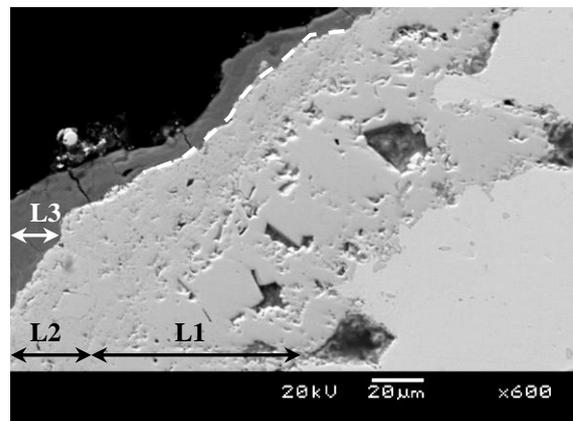
Figure 30. Microstructure of corrosion layer on MC12. Even surface; L1: internal layer; L2: outer layer; L3: external layer; dash line: the limit of original surface.

230
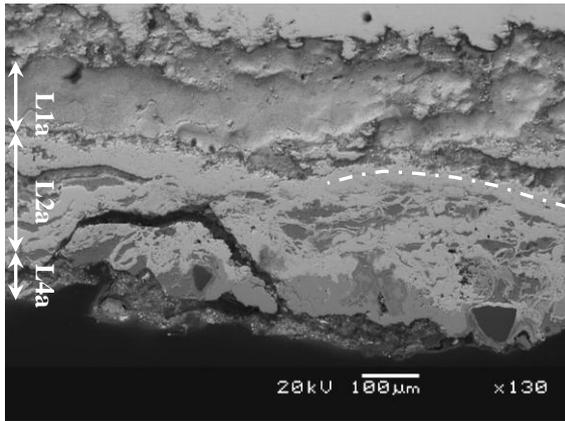
Figure 31. Microstructure of corrosion layer on MC12. Coarse surface; in light grey: cuprite; in medium grey and with a waxy texture nantokite; in dark grey copper trihyrdoxychloride with sand; dash line: the limit of original surface.
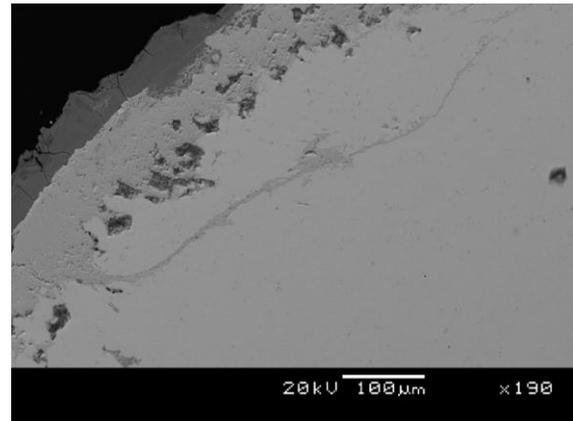
Figure 32. Microstructure of corrosion layer on MC12. Penetration of corrosion along structural defect at peripheral of the sample.
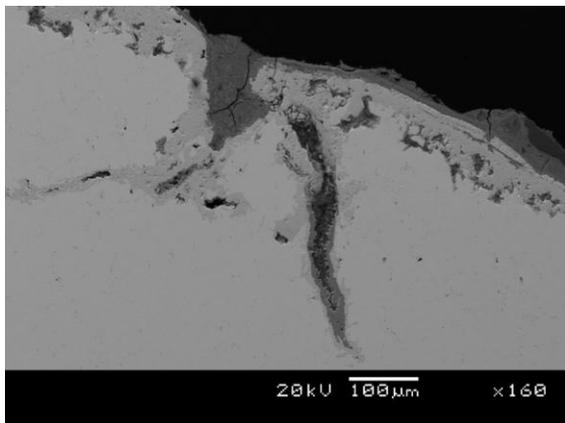
Figure 33. Microstructure of corrosion layer on MC12. Penetration of corrosion along structural defect at peripheral of the sample.
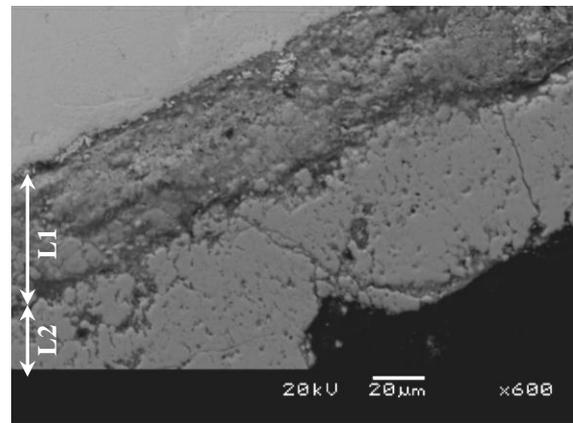
Figure 34. Microstructure of corrosion layers on SC2.

231

Appendix D

Tables

Table 2.1

Mass attenuation coefficients of some metals and element constituent of corrosion products for thermal neutrons and 125kV X-rays

Element	H	O	Cl	Fe	Cu	Zn	Ag	Sn	Au	Pb
Atomic mass	1.0	15.9	35.4	55.8	63.5	65.3	107.8	118.7	196.9	207.2
Density ($g.cm^{-3}$)	0.09	1.4	3.2	7.8	8.9	7.1	10.5	7.3	19.3	11.3
X-rays $\mu`$ (cm^2/g)	0.22	0.11	0.07	0.20	0.22	0.23	0.54	0.55	1.86	2.02
Thermal neutrons $\mu`$ (cm^2/g)	38.2	0.12	0.42	0.15	0.12	0.05	0.38	0.03	0.32	0.03

Sources: http://physics.nist.gov/physRefData/XrayMassCoef/tab3.html and

http://www.ncnr.nist.gov/resource/n-lenghts/list.html

Table 2.2

Archaeological characteristics of the objects with relevant soil samples from K2

Object	KI1	KI4	KI2	KI6	KC3	KC5	KC4	KC1	KC2
Layer	2	2	4	9	2	2	4	6	6
Depth (cm)	30.48	30.48	60.96	121.92	20-40	30.48	60.96	91.44	91.44
Corrosion %	53	31	58	64	10	10	39	34	33

Table 3.1
Summary of neutron tomography results of iron artefacts from K2 and Mapungubwe

Object[a]	Metal core	Physical stability	Internal structure[b]	Original surface[c]	Trace of fabrication	Corrosion %
KI1 Bar 30-40 cm	+	Weak	Homogeneous cracks	damaged	-	53
KI2 Spatula 60-70cm	+	weak	Inhomogeneous cracks	intact	-	58
KI3 Adze -	+	rigid	homogeneous flakes	damaged	-	37
KI4 Adze 30-40cm	+	rigid	homogenous lamination, flakes, cracks	damaged	Stress cracks	31
KI5 Drill -	+	rigid	homogenous small crack in the point	Intact	-	15
KI6 Rod 120-130cm	+	weak	inhomogeneous lamination , cracks	damaged	-	64
MI1 Arrowhead -	+	weak	inhomogeneous	Intact	-	51
MI2 Hoe -	+	rigid	homogenous	intact	voids	-
MI3 Spatula -	+	weak	Inhomogeneous cracks	damaged	-	66
MI4 Hook -	+	rigid	homogeneous	intact	flake	35
MI5 spatula 190-220cm	+	weak	inhomogeneous	intact	Loop, screw feature	-
MI6 Rod 330-340cm	+	weak	homogeneous	intact	-	62
MI7 Hoe -	+	rigid	homogeneous	intact	arrow shape impression	-

233

Table 3.1. Summary of neutron tomography results of iron artefacts from K2 and Mapungubwe (continue)

Object[a]	Metal core	Physical stability	Internal structure[b]	Original surface[c]	Trace of fabrication	Corrosion %
MI8 Wire -	+	rigid	homogeneous	intact	-	22
MI9 Hoe -	+	rigid	homogeneous	intact	voids	-
MI10 Hoe -	+	weak	inhomogeneous	damaged	-	-
SI1 Spatula 40-50 cm	+	weak	inhomogeneous flakes, lamination	damaged	Screw feature	59
SI2 Adze 150-170 cm	+	rigid	homogeneous	damaged	-	43
SI3 Spatula 250-300 cm	+	weak	inhomogeneous	damaged	loop	-

Notes: **a;** catalogue number; classification; depth
b; *Homogenous*: Metal core is seen continuously among artifact
Inhomogeneous: Metal core in some parts has been completely vanished
c; *Intact*: Original surface has kept its form among corrosion products

234

Table 3.2
Elemental composition of iron artefacts from K2 and Mapungubwe (EDS results / wt%)

Object	Target	O	Na	Mg	Al	Si	P	S	K	Cl	Ca	Ti	Mn	V	Fe	Ni	Mo
KI1	metal					0.1									99.9		
KI1a	glass	38.5	0.3	0.6	3.5	12.8	0.4		0.6		2.7	0.1	0.6		39.4		0.2
KI1a1	wüstite	30.7				0.1									69.2		
KI1b	glass	36.8		0.3	2.6	9.1	2.2		0.5		2.9		0.5		44		0.9
KI1b1	wüstite	27.9		0.1	0.2	0.1							0.2		71.4		
KI1c	oxide	37.6			0.2	0.7			0.1		0.3		0.2		60.8		
KI1c1	oxide	44.7	0.2	0.2	0.2	0.5		0.1			0.5				53.4		
KI1c2	glass	49.8		1.9	7	23.4			2.6		7.3	0.3	2.6		4.8		0.2
KI3	metal					0.2									99.8		
KI3a	glass	44.3			4.1	18	0.5		0.9		4.4	0.7			26.9		0.2
KI3a1	glass	39.8		0.3	0.1	12.3					0.3			2	47.2		
KI3b	glass	45.8	0.6	0.5	2.1	18.8	0.2		1		3.4	0.2			27.4		
KI3c	glass	53.5	0.9	0.5	3.4	27.8			1.5		3.2	0.4			8.6		0.2
KI5	metal					0.1									99.2	0.7	
KI5a	fayalite	30.4	0.3	0.6	1	14	0.5		1.8		2.3		1.2		47.8		
KI5b	fayalite	31.4	0.2	1.3	0.3	13.6	0.1				1.4		1.9		49.7		
KI5b1	wüstite	21.9		0.1	0.2	0.3							0.8		76.5		
KI5c	glass	40.8	0.5	1	1	13.4	0.3		1		2.3		2.3		37.4		
MI2	metal														100		
MI2a	glass	52.5	0.6	3.5	4.6	17	0.6		1.5		13.5	0.3	0.9		5		
MI4	metal					0.1	0.1								99.5	0.3	
MI4a	glass	34.9	0.2		0.8	8.3	1.4		0.6		0.2		0.3		53.1		
MI4b	glass	52.6	0.3	1.4	6.5	25.4			3.8		3.6	0.3	2.7		3.3		

235

Table 3.2: Elemental composition of iron artefacts from K2 and Mapungubwe (continue)

Object	Target	O	Na	Mg	Al	Si	P	S	K	Cl	Ca	Ti	Mn	V	Fe	Ni	Mo
MI6	metal					0.1									99.9		
MI6a	glass	55	0.5	1	4.9	26.3			2		4	3	0.5		2.8		
MI6b	lime	58		1.2				0.8			39.3				0.7		
MI7	metal					0.1	0.1								99.8		
MI7a	glass	39.4		0.1	0.3	6.5	4.8	0.1	0.1	0.3	0.5		1.7		46.1	0.1	
MI7a1	wüstite	29.1			0.2	0.3						0.2	0.6	0.4	69.1		
MI8	Metal														100		
MI8a	glass	55.3	0.3	2.2	5.7	25.2			3.8		4.5	0.2	1.1		1.7		
MI8a1	wüstite	37.6				0.5				0.2	0.2				61.5		
MI8b	glass	57	0.2	2.5	5.3	26.5			3.8		2.6	0.2	0.3		1.6		
MI9	metal						0.3								99.7		
MI9a	glass	44.4		0.6	0.2	8.7	3	0.3			1		3.1		38.5		
MI9a1	wüstite	32.2			0.2	0.3							1		66.2		
MI10	metal														100		
MI10a	oxide	40.2				0.2				0.1	0.4				59.9		
MI10a1	oxide	47				0.4		0.4			0.2				52		
MI10b	glass	39.2	0.7	1.1	3.4	17.7		2.2			10.9	0.2			24.6		
MI10c	glass	39.2		0.3	2	11.6	0.5		0.8		0.4		2		43.2		
SI1	metal					0.1									99.9		
SI1a	glass	37.5		0.4		11.5	0.1				0.5				50		
SI1a1	wüstite	28.2			0.3	0.8			0.1		0.3			0.1	70.2		
SI1b	glass	36.5		0.1	1.6	10.5	0.4		1		1.3				48.6		
SI1c	glass	58.3	0.2	0.3	1.1	36			0.5		0.9	0.1			2.6		
SI1d	glass	58		0.4	2.7	33.7			1.3		1.8	0.3			1.8		

Table 3.3
Summary of metallography results of iron artefacts from K2 and Mapungubwe

Object	Carbon content wt%	Microstructure	Grain size ASTM	Hardness H_V	Deformation	Fabrication
KI1 Bar 30-40 cm	0.08-0.2 inhomogeneous	Polygonal ferrite with etch pitting; Ferrite laths with degenerated pearlite island.	4; 10	170; 243	-	Forging below the A3 temperature followed by annealing in temperature below the A1.
KI3 Adze -	0.2 homogeneous	Ferrite laths with Widmanstätten morphology.	8	135	-	Normalized from above the A3 temperature.
KI5 Drill -	0.1-0.2 inhomogeneous	Ferrite laths with pearlite island and film of cementite; Ferrite grain boundaries with Widmanstätten structure at former austenite grains.	9; 4 Aust	254; 243	-	Decarburized, Normalized from above the A3 temperature.
MI2 Hoe -	0.2-0.6 (blade) 0.08-0.8 (shaft) inhomogeneous	Fully spheroidized cementite with elongated banding in areas with high reduction; ferrite grains with eutectoid degenerated pearlite island gradually were converted to equiaxed ferrite grains with etch pitting.	6-10; 5 Fer	108-163; 250-230	-	Decarburized, forged below the A3 with subsequent annealing below the A1 temperature.
MI4 Hook N/D	0.1-0.2 inhomogeneous	Laths of ferrite with pearlite island; Ferrite grain boundaries with Widmanstätten structure.	11; 7 Aust	266; 279	-	Decarburized, normalized from above the A3 temperature.
MI6 Rod 330-340cm	homogeneous	Allotriomorphs cementite grain boundaries at former austenite with cementite plates infill.	10	230	Fine cracks at grain boundaries	Slowly cooled from slightly above the A_1 temperature (annealing).
MI7 Hoe -	0.08 homogeneous pure iron	Equiaxed ferrite with thin film of cementite. Etch pitting	6-8	133-247; -	Shear band	Hot forged, annealed in slightly above the A1 temperature.
MI8 Wire -	1.1-1.2; 0.1-0.4 inhomogeneous	Eutectoid pearlite with grain boundaries allotriomorph cementite; Laths of ferrite with pearlite islands	-; 11	292; 287	Fine cracks at grain boundaries.	Decarburized, austenitized above the A_1 temperature following by slow cooling (annealing).

237

Table 3.3. Summary of metallography results of iron artefacts from K2 and Mapungubwe (continue)

Object	Carbon content wt%	Microstructure	Grain size ASTM	Hardness H$_V$	Deformation	Fabrication
MI9 Hoe -	0.08 homogeneous Pure iron	Massed equiaxed ferrite in blade and shaft in addition to elongated grains toward one lateral surface in the shaft.	3-6.5; 8-11	260-165; 297	-; shear bands	Forged bellow the A3 temperature, annealed above the A1 temperature. Cold worked.
MI10 Hoe -	0.4-0.6 (blade); 0.08-0.2 (shaft) inhomogeneous	Have a gradient in carbon content. Grain boundaries allotriomorph ferrite with Widmanstätten morphology; Equiaxed ferrite grains with thin film of cementite and etch pitting; Irregular ferrite grains with pearlite island.	6; 6; 5	168-189; 95; 145		Carburized, austenitized in reducing condition above the A3 temperature. Air cooled.
SI1 Spatula 40-50 cm	0.8- 0.2 inhomogeneous	Ferrite grain boundaries with Widmanstätten structure and eutectoid pearlite.	6; 4	230- 125		Carburized, austenitized in reducing condition above the A3 temperature. Air cooled.

238

Table 4.1

Summary of neutron tomography results of copper artefacts from K2 and Mapungubwe

Object[a]	Metal core	Physical stability	Internal structure[b]	Original surface[c]	Trace of fabrication	Corrosion %
KC1 Wire (bangle) 90-100 cm	+	rigid	homogeneous pitted	Intact to damaged in few parts	-	34
KC2 Rod 90-100 cm	+	rigid	homogeneous	Intact to damaged in few parts	diverse cross section	33
KC3 Wire 20-40 cm	+	rigid	homogeneous	intact	hollow various diameter	Very low
KC4 Plate 60-70 cm	+	rigid	homogeneous	Intact	-	39
KC5 Wire 30-40 cm	+	rigid	homogeneous	intact	hollow	Very low
MC1 Wire (ring) 330-340 cm	+	rigid	homogeneous pitted	damaged in few parts	hollow	34
MC2 Wire (bangle) 150-160 cm	+	rigid	homogeneous crack	Intact to damaged	hollow	31
MC3 Ring 170-180 cm	+	rigid	Homogeneous pitted	Intact to damaged	-	16
MC4 Rod -	+	weak	homogeneous pitted	Intact to damaged	diverse cross section	34
MC5 Plate (funnel) -	-	weak	inhomogeneous	damaged	internal tube	high
MC6 Plate (funnel) -	+	rigid	homogeneous	intact	internal core	Very low
MC7 Plate (funnel) -	-	weak	completely corroded	deformed	internal core	high
MC8 Nail -	+	weak	Homogeneous cracks	damaged	hollow	-

239

Table 4.1. Summary of neuton tomography results of copper artefacts from K2 and Mapungubwe (continue)

Object[a]	Metal core	Physical stability	Internal structure[b]	Original surface[c]	Trace of fabrication	Corrosion %
MC9 Ingot -	+	rigid	homogeneous	intact	voids	4
MC10 Wire (ring) 120-130 cm	+	rigid	homogeneous pitted	Intact to destroyed	various diameter hollow	36
MC11 Wire (bangle) 120-130 cm	+	rigid	homogeneous	intact	-	Very low
MC12 Wire (bangle) 240-250 cm	+	rigid	homogeneous	Intact among corrosion	hollow	9
SC1 Wire (ring) 290-320 cm	-	weak	completely corroded	damaged	hollow	75
SC2 Ring -	+	rigid	homogeneous	damaged	-	6

Notes: **a;** catalogue number; classification; depth
b; *Homogenous*: Metal core is seen continuously among artifact.
Inhomogeneous: Metal core in some parts is completely vanished.
c; *Intact*: Original surface has kept its form among corrosion products.

240

Table 4.2
Elemental composition of copper artefcts from K2 and Mapungubwe (EDS Results/wt%)

Object	Target	O	Al	Si	P	S	Cl	Ca	Fe	Cu	Sn
KC1a	Metal	1.7		0.4						97.9	
KC1b	Inclusion	13.6		0.6		0.1	0.6			85	
KC1c	Inclusion	17.2		0.3						82.5	
KC2a	Metal									100	
KC2b	Inclusion	11.1				0.3				88.5	
KC4a	Metal	0.8		0.2						98.8	
KC4b	Inclusion	10.8		0.2						89	
KC4c	Inclusion	11.3		0.1						88.6	
KC5a	Metal									100	
KC5b	Corrosion	15.9					0.4			83.8	
KC5c	Inclusion	14.1				0.1				85.6	
MC2a	Metal									100	
MC2b	Inclusion	13.4				0.1				86.5	
MC4a	Metal	0.3							0.5	99.2	
MC4b	Inclusion	26.9							69.1	3.9	
MC4c	Inclusion	24.2							55.4	20.4	
MC8a	Metal	4.4		0.7						88.6	6.1
MC8b	Corrosion	14.4		0.4			0.1			85.1	
MC8c	Corrosion	17.6		0.5			0.5			69.4	12
MC9a	Metal									100	
MC9b	Inclusion	14								86	
MC9c	Inclusion	12.3							0.2	87.5	
MC10a	Metal									100	
MC10b	Inclusion	12.9				0.1	0.1			86.8	
MC11a	Metal									100	
MC11b	inclusion	12								88	
MC12a	Metal						0.1			99.9	
MC12b	Inclusion	13.2				0.5	0.2			86	
MC12c	Corrosion	14.9					0.8	0.1		84.2	
MC12d	Corrosion	41.6	0.1	0.2	0.1	0.1	0.1	0.8		56.9	
SC2a	Metal	3.5		0.7		0.1	2			93.7	
SC2b	Inclusion1	11.4								88.6	

Notes: c, centre of the sample; s, surface of the sample.

241

Table 4.3.
Classification of the objects based on physical and chemical stability

			Stable								
Rigid objects	**Iron**	**a**	KI5	MI8	MI9	MI2	MI7				
		b	KI3	KI4	SI2	MI4					
			Bronze disease						Even surface		
	Copper	**a**	KC3	KC4	MC2	MC9	MC12		MC6	KC5	MC11
		b	KC1	KC2	MC1	MC3	MC10	SC2			
			Stable							Instable	
Weak objects	**Iron**	**a**	KI1	MI6							
		b	**KI2**	**KI6**	**MI1**	**MI3**	**MI5**	**SI3**	**MI10**	**SI1**	
			Bronze disease		Stable						
	Copper	**a**	MC4	MC8							
		b									
		c			SC1	MC5	MC7				

Notes: The items in bold have discontinues metal core

242

Table 4.4
Summary of metallography results of copper artefacts from K2 and Mapungubwe

Object	Microstructure	Inclusion	Grain size ASTM	Hardness H_V	Deformation/Defect	Fabrication
KC1 Bangle	Recrystallized angular grains of copper with annealing twins.	Copper oxides, Cu+Nb oxides in a banding structure.	7	107	-	Hot-working of a casted piece of copper.
KC2 Rod	Recrystallized angular grains of copper with annealing twins.	Globular cuprite in a dispersed structure.	8	109	-	A casted piece of copper was hammered with final annealing operation.
KC4 Plate	Recrystallized angular grains of copper with annealing twins.	Globular cuprite in a banding structure.	8	88; 117	An oblique cut with flatten grains and distorted annealing twins.	Hot-working of a casted piece of copper followed by a final cold working resulting from cutting off.
KC5 Bangle	Recrystallized angular grains of copper with annealing twins.	Globular cuprite in a dispersed structure.	5.5	97	-	A casted piece of copper was hammered followed by final annealing operation.
MC2 Bangle	Recrystallized angular grains of copper with annealing twins.	Globular cuprite in a banding structure with minor amount of sulphur.	7	117; 139	In a part, flatten grains with distorted annealing twins.	Hot-working of a casted piece of copper followed by slight cold working.
MC4 Rod	Recrystallized angular grains of copper with annealing twins.	Low number of angular inclusions of mixed copper and iron oxides (cuprite + magnethite).	8	105; 117	Distorted annealing twins on the surfaces.	Forging or even cold-working of a smelted piece of pure copper followed by annealing and finall slight cold working.
MC8 Bronze nail	Recrystallized grains of copper-rich solid solution of tin in copper with annealing twins.	-	12	190	Strain lines, both straight and distorted annealing twins.	A piece of low tin bronze was forged or even cold worked followed by annealing operation and final cold-working. The bronze was produced in smelting.
MC9 Ingot	Cast structure. Dendrite of pure copper with (Cu+Cu$_2$O) eutectic infill.	Globular cuprite in eutectic phase with low amount of iron as impurity in some of them.	-	62	Voids	Melted and casted in a probable stone mould. Slow solidification with higher rate toward the mould surface.

Table 4.4. Summary of metallography results of iron artefacts from K2 and Mapungubwe (continue)

Object	Microstructure	Inclusion	Grain size ASTM	Hardness H_V	Deformation/Defect	Fabrication
MC10 Ring	Recrystallized angular grains of copper with annealing twins.	Globular cuprite in a banding structure.	5.5	75	-	A cast piece of copper was forged followed by final annealing.
MC11 Bangle	Cast structure. Dendrite of pure copper with (Cu+Cu$_2$O) eutectic infill. Straight annealing twins.	Globular cuprite in eutectic phase.	voids	84-120	-	A cast rod slightly forged. The temperature or final annealing operation was not sufficient to reconstruct angular grains.
MC12 Bangle	Recrystallised angular grains with distorted annealing twins.	Globular cuprite in a banding structure.	7	117	Elongated void	As cast rod was forged with probable final annealing followed by slightly cold-working.
SC2 Ring	Recrystallised angular grains with both distorted grain boundaries and annealing twins.	Globular cuprite in a banding structure.	9	120	Elongated grain toward the surface.	As cast rod was forged with probable final annealing followed by cold-working.

244

Table 5.1
EDS analysis of corrosion layers on iron artefacts from K2 and Mapungubwe (wt%)

Objects/layer	O	Na	Mg	Al	Si	P	S	Cl	K	Ca	Fe	Mo
KI1L1a	32.9										66.9	0.2
KI1L1b	41.5	0.2			0.2						58.1	
KI1L2a	43.3		0.1		0.7	0.1				0.2	55.6	
KI1L2b	46.2		0.2		3.3	0.7				1.1	48.5	
KI3L1a	47.7				0.1	0.1					52	
KI3L1b	37.6				0.1						62.2	
KI3L2a	38.2		0.1		1.2					0.2	60.2	
KI3L2b	47.5		0.1		0.4	0.1				0.2	51.7	
KI5L1a	27.8				0.1	0.1					71.9	
KI5L1b	28.9					0.1					71	
KI5L1c	35.5				0.1						64.4	
KI5L2a	37.1		0.1	0.1	1.4	0.1		0.1		0.1	61	
KI5L2b	46.8		0.1	0.1	1	0.1					51.9	
MI2L1a	35.2		0.5	0.6	2.3	0.4		0.6		1.4	59	
MI2L1b	30.9			0.1	0.2						68.8	
MI2L1c	35.1		0.2		0.2			0.1		0.2	64.1	
MI2L1d	36.2		0.2		0.4			0.2		0.8	62.1	
MI2L1e	39		0.1		0.4	0.2	0.1	0.2	0.1	0.4	59.3	
MI4L1a	46.4		0.1		1.2	0.2		0.2		0.5	51.4	
MI4L1b	38.9				0.2			0.1		0.2	60.6	
MI4L2a	46.4		0.1		1			0.1		0.2	51.9	
MI5L1a	36.5				0.3	0.1			0.1		63	
MI5L1b	46.7				0.4	0.1	0.1	0.1			52.6	
MI5L1c	46.5	0.3	0.2	0.4	1.2	0.7			0.1	0.1	50.2	0.2
MI6L1a	48.2		0.1		0.1	0.2	0.1	0.5	0.1	0.1	50.5	
MI6L1b	39.3				0.3	0.1				0.2	60	
MI6L1c	46.2		0.3	0.3	0.7	0.3			0.1	0.4	51.4	0.2
MI6L2	47.5		0.1		0.4	0.1	0.2	1.1		0.2	50.2	
MI7L1a	38.5				0.1	0.1		0.1		0.1	61.2	
MI7L1b	47.5		0.2		0.2	0.1	0.1	0.2		1	50.5	
MI8L1a	37.8							0.2			62	
MI8L1b	47.5				0.4			0.1		0.3	51.6	
MI8L2a	47.2				0.2					0.1	52.2	0.2
MI8L2b	62.6		0.7	0.5	1.3		0.8		0.2	33.4	0.5	
MI9L1	47.8							0.7			51.5	
MI10L1a	46.5				0.3	0.2					53	
MI10L1b	38.6					0.1					61.4	
SI1L1a	40.1				0.1		0.5	4.2			55	
SI1L1b	43.6			0.1	0.1		1.6	18.5			36.1	
SI1L1c	55						14.8				29.8	0.3
SI1L1d	35.8						0.4				63.7	
SI1L1e	28.3				0.1						71.6	
SI1L2	49.7		1.2	4.7	13.9	0.5			1.5	0.5	27.9	

Table 5.2
Raman spectral signature of pure iron oxides and hydroxides

Magnetite Fe_3O_4	Maghemite γFe_2O_3	Hematite αFe_2O_3	Hematite * Fe_2O_3 (synthetic)	Goethite $\alpha FeOOH$	Lepidocrocite $\gamma FeOOH$
				205 (w)	
		225 (vs)	224(vs)		
		240		245 (w)	250 (vs)
310 (w)		290 (vs)	291(vs)	300 (m)	300 (w)
	380 (m)			390 (vs)	380 (m)
		405 (m)	407(m)	415	
	460 (m)	495 (w)	494(w)	480 (w)	
540(m)	510 (m)			550 (w)	525 (w)
		605 (m)	610		650 (m)
670 (vs)	670 (s)		660(w, sh)	685 (m)	
	720 (vs)				

Note: w, weak; s, strong; vs, very strong; m, medium; sh, shoulder; (the data adapted from Bell *et al*. (1997)* and Froment *et al*. (2008).

Table 5.3
EDS analysis of corrosion layers on copper artefacts from K2 and Mapungubwe (wt%)

Objects/layer	O	Na	Mg	Al	Si	P	S	Cl	K	Ca	Fe	Ni	Cu	Sn
KC1 L1	13.5				1.4			28.3					56.8	
KC1 L2	26.2				0.4			15.7					57.7	
KC1 L2a	12.1				0.2			0.3					87.4	
KC1 L3	13.3							0.2					86.5	
KC1 L3a	26.5				0.4			15.1					58	
KC1L4	27.4				0.2			15.4					57	
KC1 L4a	26.3				1.0			15			0.4		57.3	
KC1 L4b	40.5		0.4		20.2			0.3	0.7	0.5	0.1		37.3	
KC2L1	15.6							0.2					84.1	
KC2L1a	9.8			0.2			0.4	3.2					86.4	
KC2L2	16.6							23.6					59.7	
KC2L3	14.4							0.5				0.3	84.8	
KC2L4	45.5		0.6		17.5	0.3		0.2	0.8	0.9			34	
KC2L4a	28.1							15.3					56.6	
KC4L1	15.6												84.4	
KC4L1a	16.6				0.6			0.3					82.4	
KC4L2a	37.5		0.4		8.7	0.7		3.5		2.8			46.4	
KC4L2b	24.9			0.1	0.8			15.3					58.9	
KC4L2c	12.5				0.8			26.5					60.2	
KC5L1	14.1												85.9	
KC5L2	20.9				8.3		2.8	0.3		0.7			66.5	
KC5L3	38.6		0.2		17.6		0.2			0.9			42.5	
MC2L1	13.7							0.9					85.4	
MC2L1a	25.8							15					59.2	
MC2L2	13.1							0.5					86.4	
MC2L2a	11.2			0.2	0.1			27.8					60.7	
MC2L3	17.9			0.4	2.6	0.3	0.3	12.9	0.3	0.3	0.3		64.7	
MC2L3a	30.7			0.1	1	0.3	0.1	12.9		0.2			54.6	

247

Table 5.3: EDS analysis of corrosion layers on copper artefacts from K2 and Mapungubwe (continue)

Objects/layer	O	Na	Mg	Al	Si	P	S	Cl	K	Ca	Fe	Ni	Cu	Sn
MC4L1	13.6							0.3					86	
MC4L1a	15.8							25.9					58	
MC4L1b	26.3							16.3					57.4	
MC4L1c	60.6						17			20			2.4	
MC4L2	14.3				0.4			2					83.3	
MC4L2 a	28.9				0.3			15.3					55.4	
MC4L2b	30		0.2	0.6	1.1		0.3	13.7			0.6		53.4	
MC4L3	8.5				0.1			27.5					63.9	
MC7L1a	28.5				0.5		1	11.6			6.6	0.2	51.6	
MC7L1b	43.9				0.6		0.6	1.4			42.4		11	
MC7L1c	46.5				0.5			0.2		0.1	48.4		4.1	
MC7L1d	36.1				0.4			0.1			62.8		0.5	
MC7L1e	58.1		2				0.8		0.1	37	0.9		0.9	
MC7L1f	46.9						0.8	0.3		0.8	48.2		2.9	
MC7L2a	14							0.5					85.5	
MC7L2b	28.3				0.1			14.7					56.9	
MC7L2c	28.7							13					58.2	
MC7L2d	23.9				0.4		7	6.9			2.8		59	
MC7L2e	29.7			0.1			0.5	14			0.4		55.4	
MC7L2f	35.5							12.8					51.5	
MC7L2g							18.2	1.2					80.6	
MC7L2h	29.9						0.1	14					56	
MC7L2h1	44.3				0.1			1.6					53.9	
MC7L2i	17.8				0.1		10.7	3.5					67.9	
MC7L3a	25						9.5	0.7					64.8	
MC7L3b	22.6				0.4			13.5					63.5	
MC7L3c	37.9		0.2		17.4	0.2			0.2	1.5			42.6	
MC8L1	21.6			0.1	1.2		0.1	12.4					44.4	20.1
MC8L1a	15.4			0.2	1.3			19.5					47.1	16.5
MC8L1b	26.5				0.2			15.4					57.8	

248

Table5.3: EDS analysis of corrosion layers on copper artefacts from K2 and Mapungubwe (continue)

	O	Na	Mg	Al	Si	P	S	Cl	K	Ca	Fe	Ni	Cu	Sn
MC8L1c	17.1				0.5			0.9					80.5	0.8
MC8L1c	17.9				0.3			0.7					66.7	14.4
MC8L1c	16				0.2			0.5					83.2	
MC8L1d	26.5		0.1		4.5	0.3	0.6	2		1.2		0.6	64.2	
MC8L2a	28.7				0.9		0.1	0.1					57.8	12.3
MC8L2b	14				0.2			0.2					85.6	
MC8L2c	29.5				0.1		0.1	13.5		0.1			55.4	1.2
MC8L2d	32.8		0.1		11.5			4	0.1	0.6			50.8	
MC9L1	30.2							18.3					51.5	
MC9L1a	17.9				0.1			17.6					64.3	
MC9L2	15.6							1.2					83.2	
MC9L3	21.7		0.5		25.5			0.5		1			50.7	
MC9L3a	57.5	6.8		8.5	26								1.2	
MC10L1	8						0.2	3					88.7	
MC10L1a	21.8				0.1			24.4					53.7	
MC10L2	14.8				0.1			1.3					83.8	
MC10L3	9.7			0.2	0.1			31.7					58.2	
MC10L4	15.5				0.1			4.5					79.9	
MC10L4a	28.7			0.5	1.4			12	0.1				57.3	
MC11L1	14.7							0.1					85.1	
MC11L2a	36.3		0.4	0.2	13.1	3.2	0.1	0.8	0.5	2.2			43.2	
MC12L1	14.4							0.2					85.4	
MC12L2	15.3			0.1	0.4			1.2	0.1				82.9	
MC12L3	43.4			0.1		11.3		3.8	1.5	4.5			35.4	
MC12L1a	6.1			0.1				30.9					62.8	
MC12L2a	14.4							0.4					85.2	
MC12L3a	41.2		0.2	0.2	2.5	8.5		3.4	1.3	3.7	0.2		38.6	
MC12L4a	28							14.9				0.2	56.7	
SC2L1	22.6			0.1	0.5			16.2					60.5	
SC2L2	24				0.2			15.9					59.8	

249

Table 5.4.

Archaeological and pedological characteristics of soil layers from TS 1968- K2

Layer	*Depth* cm	*Coarse Sand* %	*Silt* %	*Clay*%	*Total*%	*Soil Type* [a]	*pH*	*EC* mS/m	*Resistivity* Ohm.cm	*C* %
2	20-40	74.4	17.5	0.5	92.4	Silty Sand	8.31	250	400	1.59
4	60-73	64.3	26.3	4.3	94.8	Silty Sand	9.36	429	233.1	1.87
6	86-100	73.8	20.0	0.5	94.3	Silty Sand	9.45	554	180.51	2.81
9	120-130	78.1	15.0	0.5	93.6	Silty Sand	9.37	374	267.38	0.92

Note: a; according to Unified Soil Classification System (USCS)

Table 5.5
Amount of soluble salts in soil layers of TS 1968- K2

Layer	Cl^- (mg/kg)	SO_4^{2-} (mg/kg)	CO_3^{2-} (g/kg)	PO_4^{3-} (mg/kg)
2	511.1	1123.4	20-80	1.1
4	851.0	1348.1	80-160	54.4
6	964.3	1984.7	80-160	392.5
9	732.6	1662.6	20-80	13.0

251

Table 5.6
Soil-Test Evaluation AWWA Rating-Standard C105-72

Soil characteristics	Points
Resistivity-ohm.cm	
Based on single probe at pipe depth or water-saturated Miller soil box	
< 700	10
700 to 1000	8
1000 to 1200	5
1200 to 1500	2
1500 to 2000	1
>2000	0
pH	
0 to 2	5
2 to 4	3
4 to 6.5	0
6.5 to 7.5	0
7.5 to 8.5	0
> 8.5	3
Redox Potential	
> +100 mV	0
+50 to +100 mV	3.5
0 to + 50 mV	4
Negative	5
Sulfides	
Positive	3.5
Trace	2
Negative	0
Moisture	
Poor drainage, continuously wet	2
Fair drainage, generally moist	1
Good drainage, generally dry	0

Source: Palmer 1989